UNIVERSITY OF SOUTHAMPTON

FACULTY OF NATURAL AND ENVIRONMENTAL SCIENCES

Biological Sciences

Novel Roles for the MAPK-interacting serine threonine kinases (Mnks)

by

Rebecca Stead

Thesis for the degree of Doctor of Philosophy

May 2013

UNIVERSITY OF SOUTHAMPTON

ABSTRACT

FACULTY OF NATURAL AND ENVIRONMENTAL SCIENCES
Biological Sciences

Doctor of Philosophy

Novel Roles for the MAPK-interacting serine threonine kinases (Mnks)

by Rebecca Stead

The mitogen activated protein kinase (MAPK)-interacting serine threonine kinases (Mnks) are components of the MEK/ERK and p38MAPK signalling pathways. Research has focused on the role of the Mnks in tumorigenesis, inflammatory signalling cascades and translation of inflammatory cytokines. The physiological roles of these kinases are still not well understood and their functions have yet to be fully elucidated. This prompted the work presented in this study where the roles of the Mnks have been investigated in the phenomenon of rapamycin-induced eIF4E phosphorylation and the role of the Mnks in glucose and lipid metabolism. Increased eIF4E phosphorylation has been correlated with tumorigenesis and a potential anti-cancer therapy, rapamycin, increases eIF4E phosphorylation in cancer cells. The increase in eIF4E phosphorylation is caused by mTORC1 inhibition-dependent increases in Mnk2a activity. The Mnks are enriched in tissues important for glucose metabolism and here a role for the Mnks has been established in insulin signalling. Investigation revealed that the Mnks phosphorylate IRS1 at 5 sites resulting in its stabilization by impairing its proteasome-mediated degradation. The consequence of Mnk1/2 double knockout in mice is glucose intolerance due to reduced IRS1 protein in white adipose tissue. The incidence of type 2 diabetes as a result of obesity is rising rapidly but the mechanisms responsible are as yet not fully understood. Evidence presented in a patent suggests the Mnks may play a role in lipid metabolism and insulin sensitivity. This inspired research presented here showing Mnk2-KO mice exhibit a lack of weight gain when fed high fat diets. Interestingly the Mnk2-KO mice were resistant to severe diet-induced insulin resistance. This appears to be related to a reduction in chronic inflammation usually associated with high fat diet feeding.

Contents

List of tables

List of figures

Declaration of Authorship

I, Rebecca Stead declare that the thesis entitled Novel Roles of the MAPK-interacting serine threonine kinases (Mnks) and the work presented in the thesis are both my own, and have been generated by me as the result of my own original research. I confirm that:

- this work was done wholly or mainly while in candidature for a research degree at this University;
- where any part of this thesis has previously been submitted for a degree or any other qualification at this University or any other institution, this has been clearly stated;
- where I have consulted the published work of others, this is always clearly attributed;
- where I have quoted from the work of others, the source is always given. With the exception of such quotations, this thesis is entirely my own work;
- I have acknowledged all main sources of help;
- where the thesis is based on work done by myself jointly with others, I have made clear exactly what was done by others and what I have contributed myself;
- none of this work has been published before submission.

Signed: ……..

Date:……

Acknowledgements

Firstly I would like to thank Professor Chris Proud for giving me the opportunity to study for a PhD in his lab. His support and expertise has been invaluable throughout my studies and has provided me with the knowledge and skills for my future career. I would also like to thank the Gerald Kerkut Trust and Parnell Diabetes Foundation for the funding to conduct the research presented in this thesis.

I would like to express a big thank you to all of the current and past members of the Proud lab, their help and support has got me through the good and bad times during this project. I would also like to thank the Coldwell lab for their support over the years and their willingness to always help me. I especially want to thank Noel Wortham for his readiness to help no matter what I asked and he was always happy to not just show me how to do something but to explain the science behind it. The animal work conducted during this thesis would not have been possible without the expertise provided by Felino Cagampang. Felino immediately accommodated the needs of my project and taught me vital skills that will be important in my new job. I would also like to thank Valentina Iadevaia, Claire Moore and Suzanne Brooks for their teaching and advice with a number of the methods used throughout this work. I would also like to express my thanks to Hans Schuppe who helped me with all the microscope work throughout this study and I am so grateful for being able to share in his knowledge before he passed away.

A thank you is also reserved for the various friends I have made during my studies. Lisa Perry has become one of my close friends and helped me so much with words of encouragement and support. I want to thank Sam Bolton for being an amazing friend who always wanted to know how I was and for being there for me when needed. Steph Austin has been an exceptional friend to me who has supported me and listened to all my worries and stresses. Thanks to Scott Kimber for being my friend and taxi. Many thanks to the residents of building 85 and SGH including Olivia Larsson, Ben Mulcahy, Adam Hart, Garrick Taylor, Kirstin Williamson, Kelly Hooper, Katy Stubbs, Shmma Quaraishe, Nancy Wong, Nash Matinyarare, Christine Reitmayer, Jo Bailey and Halina Mikolajek. Thanks also to Lorraine Prout for her support.

I want to thank my mum, dad and brother for their unconditional love and support without which I would not be where I am today. I also want to thank my soon to be in-laws from the Fountain family who have made me feel one of their own.

This thesis is dedicated to Tom Fountain, my soon to be husband. Without his love I would not be the person I am today. Whenever I needed to go to the lab or stay late he would always wait for me and supported me unconditionally throughout my studies. For this I am always in his debt and will always love him.

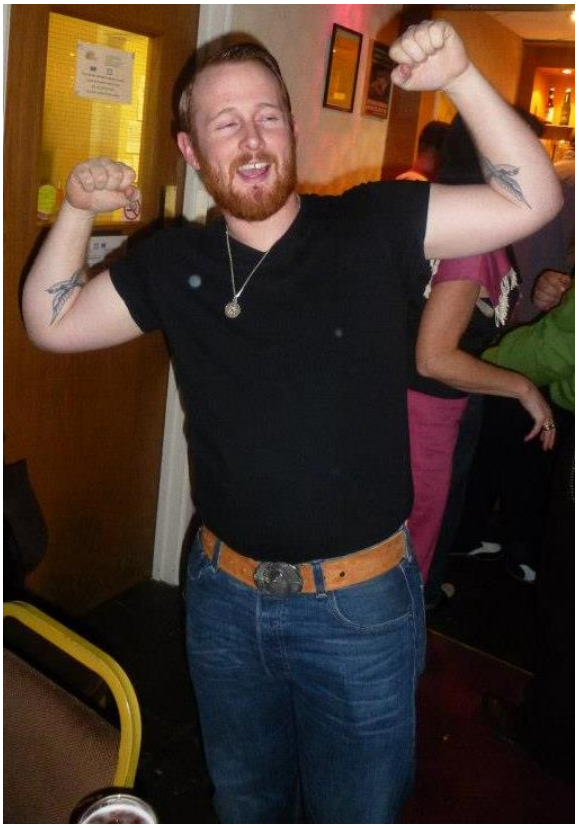

Abbreviations

β-GP: β-glycerolphosphate

β-ME: β-mercaptoethanol

2-DG: 2-Deoxyglucose

4E-BP: eIF4E-binding protein

ADP: adenosine diphosphate

AMP: adenosine monophosphate

AMPK: AMP-activated protein kinase

APS: ammonium persulphate

AS160: Akt substrate of 160kDa

ATM: adipose tissue macrophage

ATP: adenosine triphosphate

BAT: brown adipose tissue

Bcl-2: B-cell CLL/lymphoma 2

BCA: bicinchoninic acid

BSA: bovine serum albumin

cAMP: cyclic AMP

CVD: cardiovascular disease

DMEM: Dulbecco‘s modified Eagle‘s medium

DMSO: dimethyl sulphoxide

dNTPs: deoxynucleoside triphosphates

DTT: dithiothreitol

eEF: eukaryotic elongation factor

EGF: epidermal growth factor

eIF: eukaryotic initiation factor

eIF4F: eukaryotic initiation factor 4F complex

EDTA: ethylenediaminetetraacetic acid

EGTA: ethylene glycol tetraacetic acid

ER: endoplasmic reticulum

eRF: eukaryotic release factor

ERK: extracellular signal-regulated protein kinase

FBS: fetal bovine serum

FFA: free fatty acid

FGF: fibroblast growth factor

FOXO: forkhead box protein O

G6P: glucose-6-phosphate

GAP: GTPase-activating protein

GAPDH: glyceraldehyde-3-phosphate-dehydrogenase
GDP: guanosine diphosphate
GEF: guanine nucleotide exchange factor
GLUT: glucose transporter
GK: glucokinase
GPCR: G protein coupled receptor
GSK3: glycogen synthase kinase 3
GSV: glucose storage vesicle
GTP: guanosine triphosphate
GTT: glucose tolerance test
h: hours
HEK 293 cells: Human Embryonic Kidney 293 cells
hnRNP: heterogeneous nuclear ribonucleoprotein
IFNγ: interferon gamma
IGFR: insulin-like growth factor receptor
IL: interleukin
IR: insulin resistance
IRS: insulin receptor substrate
JNK: c-Jun N-terminal kinase
LPS: lipopolysaccharide
m^7GTP: 7-methyl-GTP
MAPK: mitogen-activated protein kinase
MCF7 cells: Michigan Cancer Foundation -7 cells
MCP-1: monocyte chemotactic protein-1
MEK: mitogen-activated protein kinase kinase
Met-$tRNA_i$: Methionyl tRNA specialised for initiation
min: minutes
MK: MAPK activated kinase
Mnk: mitogen-activated protein kinase-interacting kinase
mRNA: messenger RNA
MSK: MAPK stress activated kinase
mTOR: mammalian target of Rapamycin
NEFAs: non-esterified fatty acids
NES: nuclear export signal
NLS: nuclear localization signal
NK cells: natural killer cells
PABP: poly (A)-binding protein

PBS: phosphate-buffered saline

PDK: phosphatidyl -dependent kinase

PH domain: pleckstrin homology domain

PI3K: phosphatidylinositol 3-kinase

PIP_2: phosphatidylinositol -4, 5- bisphosphate

PIP_3: phosphatidylinositol -3, 4, 5- trisphosphate

PKA: protein kinase A

PKB: protein kinase B

PKC: protein kinase C

PMA: phorbol myristate acetate

PP2A: protein phosphatase 2A

PPAR: peroxisome proliferator-activated receptor

PRAS40: proline-rich Akt substrate of 40 kDa

PTEN: phosphatase and tensin homolog deleted on chromosome 10

qPCR: quantitative real time polymerase chain reaction

RANTES: regulated on activation normal T cell expressed

Raptor: regulatory associated protein of mTOR

Rheb: ras homology enriched in brain

Rictor: rapamycin-insensitive companion of mTOR

RSK: p90 ribosomal S6 kinase

RTK: receptor tyrosine kinase

S6K: p70 ribosomal protein S6 kinase

SAT: subcutaneous adipose tissue

SDS-PAGE: sodium dodecyl sulphate-polyacrylamide gel electrophoresis

sec: seconds

SOS: Son of Sevenless

T1DM: type 1 diabetes mellitus

T2DM: type 2 diabetes mellitus

TEMED: tetramethylethylenediamine

TG: triglyceride

TGN: *trans* Golgi network

TNFα: tumour necrosis factor alpha

tRNA: aminoacyl-transfer RNA

TSC1/2: tuberous sclerosis complex ½

UTP: uridine triphosphate

UTR: untranslated region

VAT: visceral adipose tissue

VEGF: vascular endothelial growth factor

WAT: white adipose tissue

Chapter 1

Introduction

1.1 Overview

Responses to external and internal changes of the extracellular and intracellular environment require a complex web of proteins that communicate changes through cascades of phosphorylation as well as various other events. The relationships shared by signalling components are very intricate and tightly controlled by proteins within the cascade as well as by other regulatory proteins. Cellular signalling is essential for cell survival and controls many aspects of cell life such as responses to pathogens, hormones, ionic changes as well as overall homeostasis. Dysfunction of cellular signalling can lead to a diverse range of conditions including autoimmune diseases, cancer and diabetes [1]. Many signalling proteins are not confined to just one pathway and very often function in several pathways creating very intricate effects of extracellular and intracellular activation or inhibition. One such group of proteins are the mitogen activated protein kinase (MAPK)-interacting serine threonine kinases (Mnks), which are the focus of this research.

1.2 Translation

1.2.1 Overview

The rate of transcription, nuclear export of mRNA, mRNA stability, rate of translation and protein degradation all affect protein levels. The rate of translation is thought to be the most important for determining the amount of protein [2]. Characteristics of the mRNA to be translated will affect its rate of translation and determine whether it is sequestered or rapidly degraded [3]. The rate of translation is also controlled by modification of proteins that direct protein synthesis, such modifications include phosphorylation, which is especially important. The signalling pathways that regulate phosphorylation of translational proteins are therefore of significant interest and their dysregulation can lead to disease. The proteins that form the translational machinery may themselves become inadequate at their role either through excessive activity or decreased/lack of activity also resulting in disease. The process of protein synthesis requires messenger RNA (mRNA), which is generated through transcription and RNA processing in the nucleus to produce a mature mRNA molecule that is exported to the cytoplasm. mRNA transport into the cytoplasm is mediated by sequences in the untranslated regions (UTR) and proteins bound to these sequences, this also governs if and when the transcript is translated [4, 5]. Assuming there is no reason for the mRNA to be sequestered, it is possible for translation to commence. Translation also requires ribosomes, which are complexes made from proteins and RNAs, consisting of two major subunits the 40S and 60S, forming an overall

80S unit [6]. There are three important steps that take place during translation: of which the first two are stringently regulated by signalling pathways.

1.2.2 Initiation

There are two types of cytoplasmic translation: cap-dependent translation and cap-independent translation; this review only covers the former. Capped mRNA contains an m^7GpppX (where X is any nucleotide), which is important for mRNA stability, nucleocytoplasmic shuttling and most importantly serves as the site where initiation factor complexes assemble in order to commence translation [7]. The initiation of translation is a highly complex process and requires a number of initiation factors (eIFs), methionine-tRNA (Met-tRNA) and the ribosomal subunits.

The 43S preinitiation complex is a prerequisite for the actual initiation of translation. This complex consists of a number of components, including: initiation factors (eIFs), Met-tRNA and the 40S subunit of the ribosome (Fig 1.1A). The Met-tRNA must bind to eIF2, which has 3 subunits; α –regulates eIF2 through phosphorylation, the β subunit binds eIF5 and the γ subunit binds Met-tRNA and GTP [8]. The factor eIF2B regulates the association between eIF2 with GTP and GDP, functioning as a guanine nucleotide exchange factor (GEF) and under periods of translation down regulation associates with phosphorylated eIF2α in an inhibitory fashion [9]. Both Met-tRNA and GTP must bind eIF2 to form the ternary complex, this then binds to the 40S subunit, again through eIF2γ and also eIF2β [9]. The factors eIF1 and eIF1A interact with the 40S subunit, eIF2 and eIF3 functioning to stabilise the interaction between the ternary complex and the rest of the preinitiation complex. eIF3 also acts as a scaffold and can bind to the 40S subunit as well as the other eIFs [9]. eIF5 is also associated with the 43S preinitiation complex and binds to the 40S subunit, eIF2β and eIF2γ [10]. The eIF4F complex is responsible for the association of the 43S preinitiation complex with the mRNA and produces the 48S initiation complex that is then ready to scan for the AUG start codon and begin protein synthesis [3, 8].

The formation of the eIF4F complex requires the association between the eIF4 factors: eIF4E, eIF4G and eIF4A (Fig. 1.1B). The initiation factor that actually binds the cap is eIF4E, whose structure resembles that of a clamp [7]. There are 4 different eIF4E forms in humans: eIF4E1 (referred to here as eIF4E), eIF4E1b, eIF4E2 (or 4E-HP) and eIF4E3 [11]. Binding to the cap requires the conserved residues: Trp56, Trp102 and Glu103 (eIF4E1 mouse). These residues are required for π-π interactions and binding to the guanine ring of the mRNA cap via hydrogen bonds, whilst arginine residues function to coordinate oxygen from the m^7GTP phosphate groups [7]. The kinetics of eIF4E-mRNA

binding is rapid (decays within ~0.1s) unless there are other binding partners bound to stabilize the interactions or eIF4E is bound to eIF4G [12].

The role of eIF4G is as a scaffold between the cap and the 40S subunit, through binding to eIF4E, eIF3 and eIF4B. There are two forms of eIF4G expressed in cells; eIF4GI and eIF4GII, which are then further differentiated as numerous isoforms [13]. The structure of eIF4G consists of numerous important domains: the N-terminal domain, which contains the poly(A) binding proteins (PABPs) binding region, eIF4E, eIF4A, mRNA and eIF3 binding sites and the C-terminus, which contains the sites for Mnk binding [14]. The ability of eIF4G to bind mRNA and PABP is important for strong cap binding and is therefore not wholly dependent on eIF4E [14]. The PABPs mediate a bridge between the poly A tail and the 5'-end of mRNA via eIF4G and eIF4B. Binding of PABPs to eIF4G enhances formation of 48S complexes through circularisation of mRNA and increased recruitment of the 40S subunit, whilst binding to eIF4B is thought to increase the association of eIF4F with the 5'-cap [3]. The binding of eIF4G to eIF3 is important to the bridging role of eIF4G between mRNA and the 43S preinitiation complex; however experiments suggest that loss of this binding does not affect overall protein synthesis but impinges on specific mRNAs resulting in an important point of control for expression of specific proteins [15]. The interaction between eIF4E and eIF4G requires the consensus sequence YXXXXLϕ (ϕ is usually L, but can be M or F) found in the N-terminus of eIF4G and the residue Trp73 in eIF4E [7]. The eIF4G/eIF4E association is thought to result in an increased affinity of eIF4E for the m^7 cap [14]. An important translational regulator can compete with eIF4G binding with eIF4E due to the presence of the eIF4E consensus sequence, these proteins are aptly named the eIF4E-binding proteins (4E-BPs). In a hypophosphorylated state 4E-BPs strongly compete with eIF4G for binding to eIF4E in order to block translation initiation. In response to various stimuli, phosphorylation of the 4E-BPs reduces the interaction with eIF4E allowing for eIF4E to bind eIF4G and promote initiation [16]. eIF4G also binds to eIF4A, which is a DEAD-box RNA helicase that is necessary to unwind any secondary structures in the 5' of the mRNA to ensure easy scanning for the AUG start codon. Binding of eIF4A to eIF4G through HEAT-domains results in its activation and the removal of secondary structures from the mRNA, which is believed to be required for the subsequent binding to the 43S preinitiation complex [14]. eIF4A requires ATP hydrolysis for rapid cycles of binding and dissociation in order to remove multiple secondary structures and also requires eIF4B, which functions to increase the affinity of eIF4A with mRNA [14]. The point at which eIF4F dissociates is unknown, i.e., whether it occurs during scanning, or, once the start codon has been recognized. It may remain associated with the cap.

Scanning for the start codon is ATP dependent, when the start codon is recognized there is a pause, that, if long, enough allows eIF5 to activate the GTPase within eIF2 (Fig. 1.1C). This then leads to dissociation of eIF2-GDP and subsequently eIF3 as well as the other initiation factors. Following this eIF4B mediates the joining of the 60S subunit to form the complete 80S ribosome [3, 8].

It must be noted that eIF4E is extremely important in initiation because it must bind to the m^7G cap, without this, cap-dependent translation cannot occur.

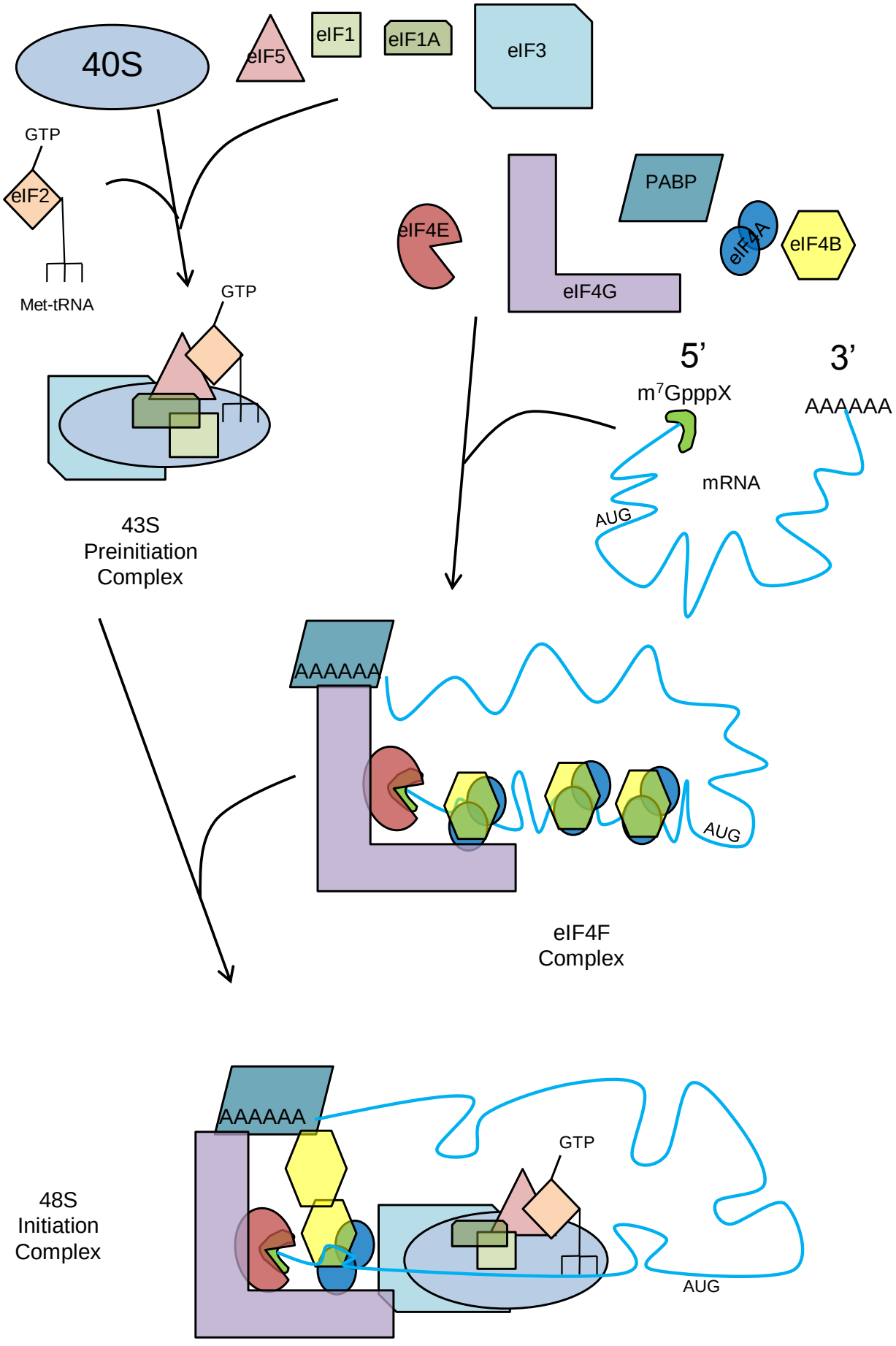
40S
eIF5
eIF1
eIF1A
eIF3
GTP
eIF2
Met-tRNA
GTP
43S
Preinitiation
Complex
eIF4E
eIF4G
PABP
eIF4A
eIF4B
5'
3'
m7GpppX
AAAAAA
mRNA
AUG
AAAAAA
AUG
eIF4F
Complex
AAAAAA
GTP
AUG
48S
Initiation
Complex

Figure 1.1 Illustration of cap-dependent translation initiation in mammals. The 43S preinitiation complex and the eIF4F complex are assembled followed by the joining of both complexes to produce the 48S initiation complex. Adapted from [17].

1.2.3 Elongation and Termination

Elongation requires a different set of proteins called the eukaryotic elongation factors (eEFs), of which there are two; eEF1 and eEF2. After initiation, Met-tRNA$_i$ is found in the peptidyl (P) site and the aminoacyl (A) site is ready for the next tRNA (Fig. 1.1D). The A-site binds to the next codon of the mRNA and shifts relative to the reading frame [17, 18]. Entry of the correct tRNA into the A site is mediated by eEF1A bound to GTP. Once the tRNA anticodon binds correctly to the mRNA codon the GTPase activity of eEF1A is activated causing a release of GDP and eEF1A to dissociate from the tRNA and ribosome. The function of eEF1B (composed of subunits; α, β and γ) is to act as a guanine nucleotide exchange factor (GEF) and recycles eEF1A-GDP back to eEF1A-GTP ready for another cycle of elongation [18, 19]. The presence of a tRNA in the A site and another in the P site, leads to the peptidyl transferase reaction. The 60S ribosome is actually an rRNA-based enzyme and thus called a ribozyme. It catalyzes the nucleophilic attack of the carbonyl group of the peptidyl-tRNA on the α-amino group of the aminoacyl-tRNA. The net result of this is that the nascent polypeptide previously bound to the P-site tRNA are now joined by a peptide bond to the newly arrived amino acid attached to the A-site tRNA. The next step is for the sequential movement of the mRNA and tRNA such that the A site is freed for the next aminoacyl-tRNA. This process is called translocation and is mediated by eEF2 bound to GTP. The hydrolysis of GTP is necessary for the movement of the mRNA relative to its interaction with the tRNA [18].

Elongation continues until a stop codon enters the A site: there are three stop codons that signal termination in mammalian cells; UAA, UAG and UGA. All three are recognised by a class I release factor (RF) eRF1, and a second class of release factors, eRF3, functions to stimulate the GTPase activity of eRF1.

The mechanism of peptide termination involves eRF1 entering the A site of the ribosome and because of its similar structure to tRNA it can recognise the stop codon in the 40S subunit and then activate the peptidyl transferase centre in the 60S subunit. However the actual recognition of stop codons and activation of hydrolysis are still elusive. It is thought that the amino acid sequence, NIKS, in the N-terminus of eRF1 acts as a recognition sequence for the stop codon, essentially like an anticodon of tRNA – it is an example of a protein mimicking RNA. The C-terminus of eRF1 is believed to bind to eRF3. The exact dynamics between eRF1 and eEF3 is not well understood [20, 21]. The overall effect is release of the new peptide from the translation machinery.

1.2.4 Control of Translation through Signalling Pathways

As previously mentioned, translation is regulated by a number of pathways; here two of the major pathways are discussed: the mammalian target of rapamycin (mTOR) and mitogen-activated protein kinase (MAPK) pathways.

The mTOR pathway includes mTORC1 and mTORC2; in this thesis, focus will be directed at mTORC1 as this is the pathway involved with translation. Both mTORC1 and mTORC2 contain the mTOR protein amongst others. The mTORC1 complex consists of the mTOR protein, Raptor, mLST8, Rheb and PRAS40, whilst mTORC2 consists of mTOR, Rictor, Sin1 and mLST8 [22]. Activation of the mTORC1 pathway occurs through hormones, growth factors, cytokines and neuropeptides, acting at their respective receptors and leading to activation of a number of cellular pathways that then alter the activity of mTORC1. A classic example of mTORC1 signalling involves its control by insulin. Activation of the insulin receptor elicits the conventional insulin receptor/IRS1/PI3K pathway (discussed in section 1.6.2, Fig. 1.6), which in turn leads to protein kinase B (PKB) activation. Full activation of PKB requires that Thr^{308} and Ser^{473} are phosphorylated [23, 24]. Activated PKB then phosphorylates Tuberous Sclerosis complex 2 (TSC2), which is found in a heterodimeric complex with TSC1; this phosphorylation leads to an inhibition of the activity of the TSC2/TSC1 complex. Under basal conditions TSC2/TSC1 is active and acts as a GTPase activating protein (GAP) towards Rheb. Rheb is a small GTPase and when TSC2/TSC1 is active Rheb associates with GDP and is inactive. When growth factor signalling (i.e. insulin) is activated the inhibition of TSC2/TSC1 in turn blocks its GAP activity towards Rheb thus shifting towards the active Rheb-GTP form [25]. The actual mechanism of Rheb activation of mTORC1 is not yet understood; however GTP must be bound to Rheb to elicit mTORC1 kinase activity. For mTORC1 to phosphorylate its substrates these targets must bind to a separate polypeptide within the mTORC1 complex called raptor [26]. The activity of mTORC1 is also reportedly controlled through another PKB substrate, PRAS40, phosphorylation by PKB leads to the dissociation of PRAS40 from the mTORC1 kinase domain resulting in removal of PRAS40's inhibitory influence [22, 25]. mTORC1 is also controlled by amino acid levels and energy status through other pathways, not described here, but details can be found in these papers [22, 25].

Downstream of mTORC1 are a number of targets related to protein synthesis. Some direct mTORC1 targets are translation factors whilst others are downstream of other mTORC1 substrates or indirectly regulated by mTORC1. A direct target of mTORC1 are

the eIF4E-binding proteins (4E-BPs), mTORC1 is capable of phosphorylating the 4E-BPs. The effect of this is the dissociation of 4E-BPs from eIF4E allowing eIF4E to bind to eIF4G and promote cap-dependent translation [25]. Addition of mTOR inhibitors blocks the dissociation of 4E-BPs and thus inhibits translation. The best known mTORC1 inhibitor is rapamycin, which is an allosteric inhibitor of mTORC1 only. Rapamycin binds to cytosolic FKBP12 and is thought to form a complex with the FBP binding region within mTORC1 although the exact mechanism of inhibition is not yet understood [27]. There are a number of mTOR ATP-competitive inhibitors (e.g. PP242) that block both mTORC1 and mTORC2 activity and strongly inhibit the dissociation of 4E-BPs from eIF4E [28]. There is extensive evidence that rapamycin does not block and in fact increases phosphorylation of eIF4E, which requires binding to eIF4G *in vivo* [29-31]. The other major targets of mTORC1 are the p70S6 kinases, S6K1 and S6K2, which are phosphorylated and activated by mTORC1 and phosphorylate substrates including the S6 ribosomal protein, eIF4B and eEF2K. The effect of S6 phosphorylation was believed to be related to TOP mRNA synthesis but has since been disproven whilst there is evidence from S6 knockout mice that suggests S6 is important for cell growth (reviewed [32]). Phosphorylation of eEF2K by S6K leads to the inhibition of eEF2K and the subsequent dephosphorylation of eEF2 resulting in its engagement in translation elongation [33]

The MAPK pathway, as discussed in section 1.3.3, encompasses a large number of cellular signalling kinases and its activation has numerous effects within the cell. Protein synthesis can be regulated by both the extracellular regulated (ERK) and p38 MAPK pathways through a number of its targets. Translational regulation through both the ERK and p38 pathways involves several of the kinases from the MAPK-activated kinase (MK) family; this includes MK2, MK3, Mnk1 and Mnk2. Studies show MK2 can regulate mRNA stability as a result of p38MAPK activation. The activation of MK2 has been shown as necessary for phosphorylation of heterogeneous nuclear ribonucleoprotein A0 (hnRNPA0) [34], PABP [35] and tristetraprolin (TTP) [36], all of these are AU rich element (ARE) binding proteins that alter the stability of TNFα (tumour necrosis factor α) mRNA. Therefore by altering the stability of mRNA the rate and efficiency of translation is changed. MK2 and MK3 regulate eEF2 kinase (eEF2K) phosphorylation. The phosphorylation of eEF2K at Ser^{377} results in the decreased activity of eEF2 kinase and thus dephosphorylation of eEF2 leading to increases in translation elongation [37].

The Mnks are also regulators of translation their role in translational control is discussed below in detail in section 1.3.6.

1.3 The MAPK –interacting serine/threonine kinases (Mnks)

1.3.1 Overview

The Mnks were discovered 15 years ago [38, 39] and have since been extensively researched in the context of tumorigenesis and inflammatory disease (reviewed [40] and see [41-44]). However, the exact physiological role of the Mnks has yet to be identified, despite the generation of Mnk knockout mice [45]. Activation of the Mnks requires stimulation of the MAPK pathway; this involves activation by a wide variety of stimuli and can instigate different divisions of MAPK signalling involving different MAPK proteins. These proteins are serine/threonine kinases i.e. they phosphorylate their substrates at serine's and threonine's, they are also themselves substrates of one another in a cascade of activation.

1.3.2 Discovery of the Mnks

The discovery of the Mnks was preceded by observations that the translation factor, eIF4E, was phosphorylated in response to hormones, growth factors, oncogenic signals, cellular stresses (i.e. TNFα, LPS, arsenite (reviewed [46])) and inhibition of phosphatases (reviewed[47]). The levels of eIF4E phosphorylation were shown to correlate with changes in the cell cycle and overall protein synthesis rates (reviewed [48] see also [49]). Initially evidence suggested that eIF4E was phosphorylated on Ser^{53} [50] and so research began to identify the kinase(s) responsible leading to suggestions that protein kinase C (PKC) and p70S6K were responsible [51]. It was later discovered that an alanine mutant of Ser^{53} was still phosphorylated to the same extent as wildtype eIF4E [52], which then led to the discovery that Ser^{209} was in fact the residue phosphorylated in eIF4E [53]. This then triggered further research to determine the kinase(s) responsible for Ser^{209} phosphorylation; this showed that although PKC was capable of eIF4E phosphorylation *in vitro* it was clear there were other kinases involved (reviewed [54]). The increases in eIF4E phosphorylation in cells treated with phorbol esters, hormones, mitogens and cells expressing transforming *ras* or *src* suggested the MAPK pathway was involved because inhibition of MEK resulted in decreased eIF4E phosphorylation [55-57]. The most obvious kinase responsible for this was ERK and experiments to determine if eIF4E was a substrate for ERK showed that this was not the case indicating a substrate of ERK was potentially the Ser^{209} eIF4E kinase [55]. A two-hybrid system was used to identify the substrate of ERK that was responsible for eIF4E phosphorylation and led to the discovery of Mnk1 and Mnk2 [38, 39, 58]. The generation of Mnk1/2-DKO mice showed that the Mnks were the only kinases responsible for *in vivo* phosphorylation of eIF4E at Ser^{209} [45].

1.3.3 Upstream Pathways – the ERK and p38MAPK cascades

The phosphorylation of eIF4E occurs in response to stimuli, which initiate a cascade that culminates in the activation of either ERK or p38MAPK. The easiest division between different MAPK cascades is their stimuli, cellular stresses such as cytokines, osmotic shock and UV radiation activate the p38 MAPKs and c-Jun N-terminal kinases (JNKs), whilst growth factors and phorbol esters stimulate the MAPKs known as ERK1 and ERK2. There are also two further MAPK groups, ERK3/4 and ERK5. There are several differences in these proteins compared to ERK1/2, JNK and p38 MAPKs in terms of their distribution, structure and understanding of their function [37]. The MAPK proteins share a general cascade of activation in response to extracellular stimuli, which has been termed the MAPKKK, MAPKK, MAPK sequence, although stimuli elicit specific responses, there is overlap between pathways (Fig. 1.2). The best examples of MAPKKK's are the MEKK's such as MEKK1, MEKK3, RAF and so forth. These kinases are the points of convergence for kinases such as ras and TRAF2 etc, which are activated by various stimuli [59, 60].

The role of MAPKKK's is to phosphorylate their substrates, which are cumulatively known as MAPKK's. Some examples of these kinases are MEK1, MEK2, MKK3, MKK6 [61]. These kinases represent a point of branching that allows the activation of specific processes dependent on the original stimuli. The MAPKK's function is to phosphorylate MAPK's such as ERK1/2 and p38MAPK [61], which phosphorylate substrates such as other protein kinases that broaden and amplify the effects of the MAPK pathway or specific targets such as transcription factors, scaffolding proteins etc.

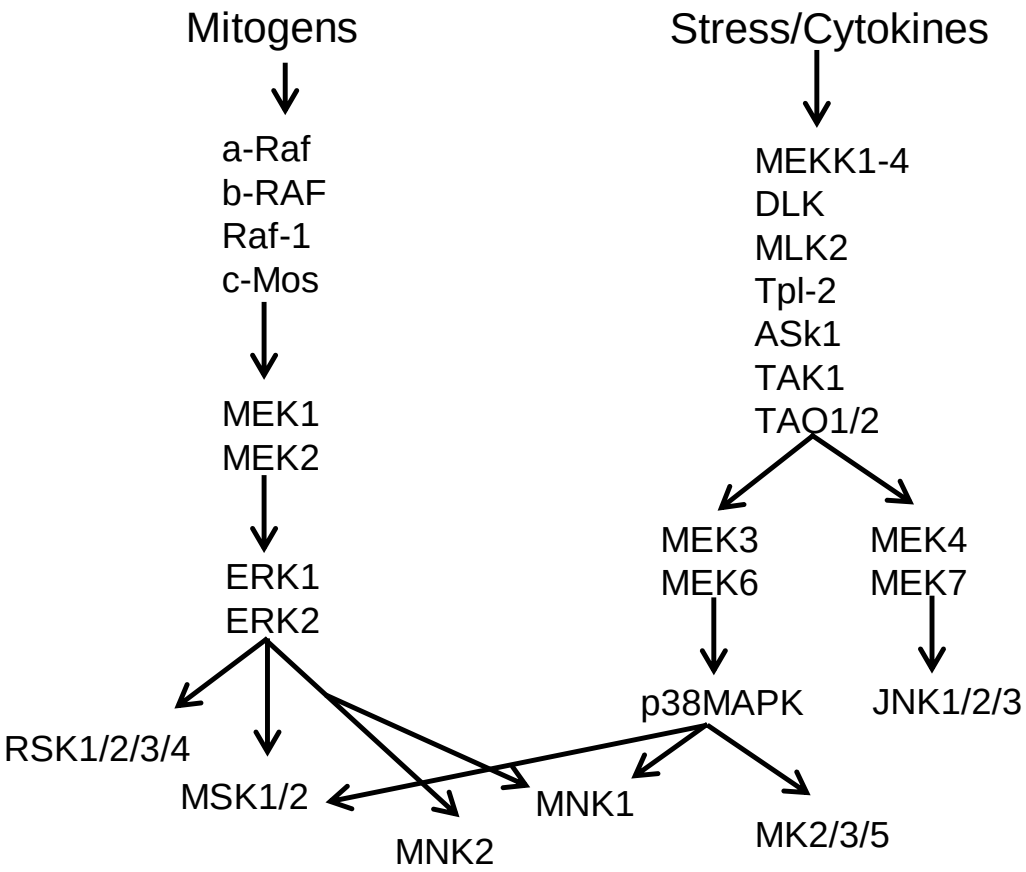

Figure. 1.2. The MAPKKK, MAPKK, MAPK pathway in the activation of ERK and p38 MAPK pathway and their downstream kinase targets, the MAPK-activated Kinases (MKs). Adapted from [37].

1.3.3.1 Ras/Raf/MEK/ERK Pathway

Mitogens can activate both GPCRs (G-protein coupled receptors) and receptor tyrosine kinases (RTKs) e.g. epidermal growth factor receptor (EGFR) and the insulin receptor. GPCRs are activated by conformational changes caused by ligand binding, which results in the exchange of GDP for GTP in the α subunit of the G-protein (heterotrimeric consisting of αβγ subunits) associated with the receptor [62]. The active α subunit can then activate numerous second messengers including phospholipase C, which in turn results in the generation of diacylglycerol (DAG) a potent activator of protein kinase C (PKC) [62]. Ligand binding to RTKs causes their dimerization and autophosphorylation, which culminates in their activation. Once active the phosphorylated tyrosine residues on RTKs present docking sites for proteins containing Src homology 2 (SH2) domains [62]. Activation of the Ras/Raf/MEK/ERK pathway involves the association of Shc with RTKs (through SH2 and phosphotyrosine binding domains (PTB)) and Grb2, which binds to a GEF called son of sevenless (SOS) [63]. The GEF activity of SOS causes the activation of the membrane bound protein Ras through the exchange of GDP to GTP [63]. Ras-GTP then recruits and activates (through a complex mechanism) Raf a serine/threonine MAPKKK. Raf is also phosphorylated and activated by PKC and functions to phosphorylate and activate the MAPKKs, MEK1 and MEK2 [63]. These kinases then go on to phosphorylate ERK1 and ERK2 on a threonine and a tyrosine residue resulting in the activation of ERK1/2, which are serine/threonine kinases [63]. There are over 100 substrates known for ERK1/2 leading to the ability of these kinases to alter cell growth, proliferation, metabolism, transcription, translation and so forth [63].

1.3.3.2 p38MAPK Pathway

In the p38 MAPK pathway, stimulation of cell surface receptors leads to activation of a variety of MAPKKKs including MEKK 1-4 and others. The MAPKKs downstream specifically for p38MAPK are MEK3 and MEK6. There is some difference between MEK3 and MEK6 such that the former is more selective for the α and β isoforms of p38 whilst the latter is non-selective for all isoforms (α, β, γ and δ). p38MAPK is activated by MEK3 and MEK6 through phosphorylation of a Thr-Gly-Tyr motif located within the activation loop [64]. Importantly the p38 MAPK pathway, as stated, overlaps with the ERK pathway in some of its targets [37]. Kinases that are substrates of MAPK's are called MAPK activated kinases (MKs) and include the MSKs (MAPK stress activated kinases); MK2, 3 and 5; RSKs (ribosomal S6 kinases) and the Mnks (MAPK interacting kinases or MAPK signal

integrating kinases). As can be seen (Fig. 1.2) Mnk1 can be activated by both ERK1/2 and p38MAPK, whilst Mnk2 is only activated by ERK1/2.

1.3.4 Structure of the Mnks

There are two human genes: MKNK1 and MKNK2 that encode 4 isoforms of the Mnks, which are alternatively spliced to produce Mnk1a and Mnk1b, Mnk2a and Mnk2b mRNAs, respectively [65, 66]. Whilst in mice MKNK1 and MKNK2 only give rise to Mnk1 (equivalent of Mnk1a) and Mnk2 (equivalent of Mnk2a). Hence forth Mnk1 and Mnk2 refer to the murine forms and human forms are described as Mnk1a, and Mnk2a. As can be seen (Fig. 1.3), there are a number of differences between the isoforms, which give rise to the differences in their localization and functions. The activity of the Mnks differs considerably wherein Mnk1 has low basal activity and is highly activated by ERK1/2 and p38MAPK and Mnk2 has high basal activity and is only minimally activated further by ERK1/2 [67, 68].

The general structure of this group of kinases involves an N-terminal polybasic region that stipulates nuclear localisation and eIF4G binding followed by a catalytic domain. In the longer isoforms, Mnk1a and Mnk2a (and murine Mnk1 and Mnk2) there is also a C-terminal MAPK binding domain, whilst Mnk1a also contains a C-terminal nuclear export signal. All isoforms possess the catalytic domain, which contains the essential features for kinase activity. The catalytic domain of most kinases is well conserved and the Mnks share some common features, which place them in the Ca^{2+}/calmodulin-dependent kinases (CaMK) group of the main Ser/Thr kinase superfamily; however, they are not dependent upon Ca^{2+}/calmodulin for activation [68]. The general structure of most protein kinases is segregated into a bilobal arrangement consisting of an N-terminus and C-terminus in-between which is a conserved ATP binding pocket [69]. Protein kinases contain a conserved sequence of DFG, which is essential for Mg^{2+}binding and as such orientation of ATP [69].

However the Mnks present a difference from other kinases here, as they do not have the conserved DFG sequence but instead have DFD (Asp^{191}, Phe^{192} and Asp^{193} for Mnk1a and Asp^{226}, Phe^{227} and Asp^{228} for Mnk2a, Fig. 1.4) [68, 69]. Preceding the DFG/D motif are a number of important conserved features; in the 3-D structure of kinases the glycine-rich loop provides an enclosure for ATP and contacts its γ-phosphate group and a conserved lysine residue (Lys^{78} for Mnk1a and Lys^{113} for Mnk2a) functions to stabilize interactions by the DFG/D motif and ATP binding [68, 70, 71].

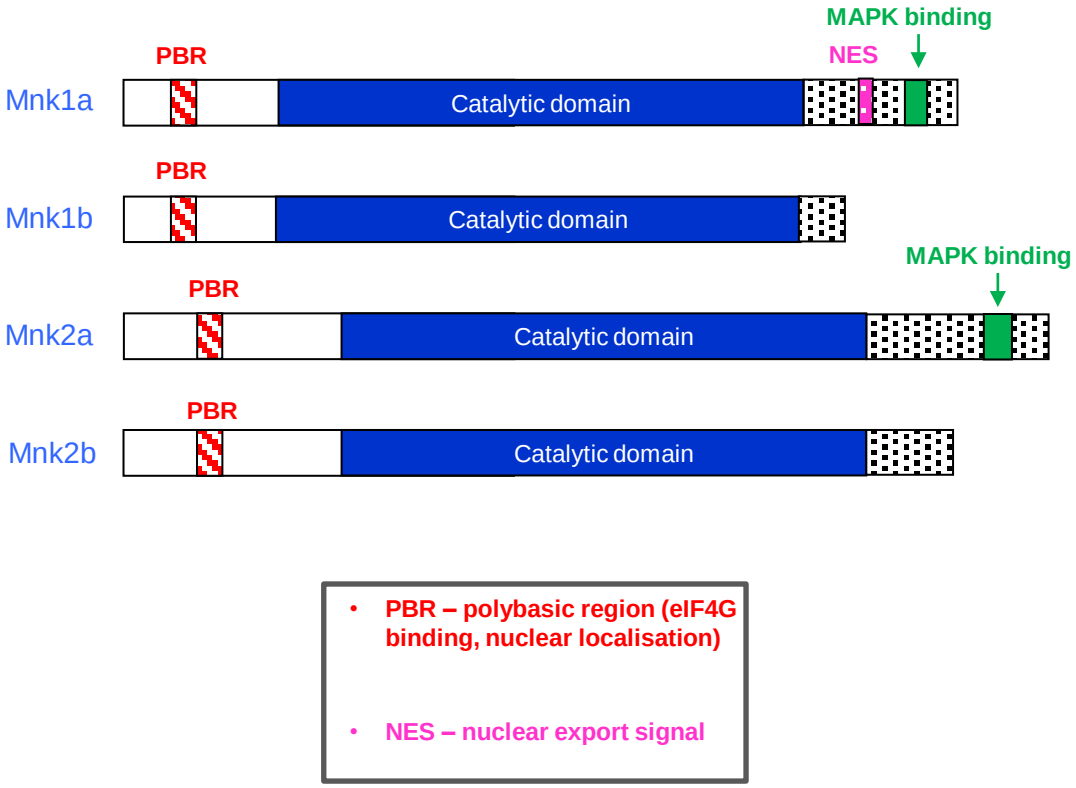

Figure. 1.3. The essential structural components of the four Mnk isoforms present in human cells. There are only two Mnks present in mice, Mnk1 and Mnk2, which correspond to human Mnk1a and Mnk2a. Adapted from [37].

The P+1 loop is a common feature of most kinases, which is necessary for substrate binding and occurs at the residue following the site of phosphorylation. In the Mnks this occurs after the second threonine of the T-loop (Fig. 1.4) i.e. Thr^{202} for Mnk1, Thr^{214} for Mnk1a and Thr^{249} for Mnk2a. Immediately after the P+1 loop is the αEF helix, which is linked to the αF helix via the αEF loop, the role of this arrangement is positioning of the APE motif, which is essential in autoinhibition and accommodation of activation segment phosphorylation residues [68, 71]. The active and inactive conformations of Mnk1a and Mnk2a show some striking differences that provide evidence for their differing levels of activity. Within the C-terminal lobe is the catalytic loop and activation segment that contains the DFD motif and APE motif. The Mnks are again different from the normal kinase convention in that their activation loop includes the αEF helix and αEF/αF loop. Usually the activation loop involves those residues undergoing reorganization, whereas in the Mnks this involves residues within this particular helical structure (Fig. 1.4) [68-70]. Another Mnk-specific feature is an insertion (residues 233-237 Mnk1a, 263-267 Mnk2a) into the αEF helix, which results in changes to the inhibitory interaction of the C-terminal lobe with the N-terminal lobe such that, instead of normal kinase intramolecular bonds, the Mnks form intermolecular pairings [70]. Residues within the αEF helix, Glu^{225} of the APE motif and Glu^{228} of insertion 2, interact with other amino acids in the αC regulatory helix, Arg^{90} and Arg^{93}. This results in positioning of the activation segment within the N-terminal lobe. An additional feature of the Mnks' autoinhibitory mechanism is the presence of a phenylalanine that has a slightly different role in each kinase but functions to block important features of the active conformation. In Mnk1a, the residue Phe^{230} (also conserved in Mnk2a) is found in the Mnk-specific insert 2 and functions to displace the DFD motif through rotation of Asp^{191} (Asp^{226} for Mnk2a) this then causes the side chain of the phenylalanine from the DFD motif (Phe^{192} for Mnk1a, Phe^{227} for Mnk2a) to occupy a hydrophobic pocket created by leucines and valines, which under active conditions is part of the ATP site [67, 68].

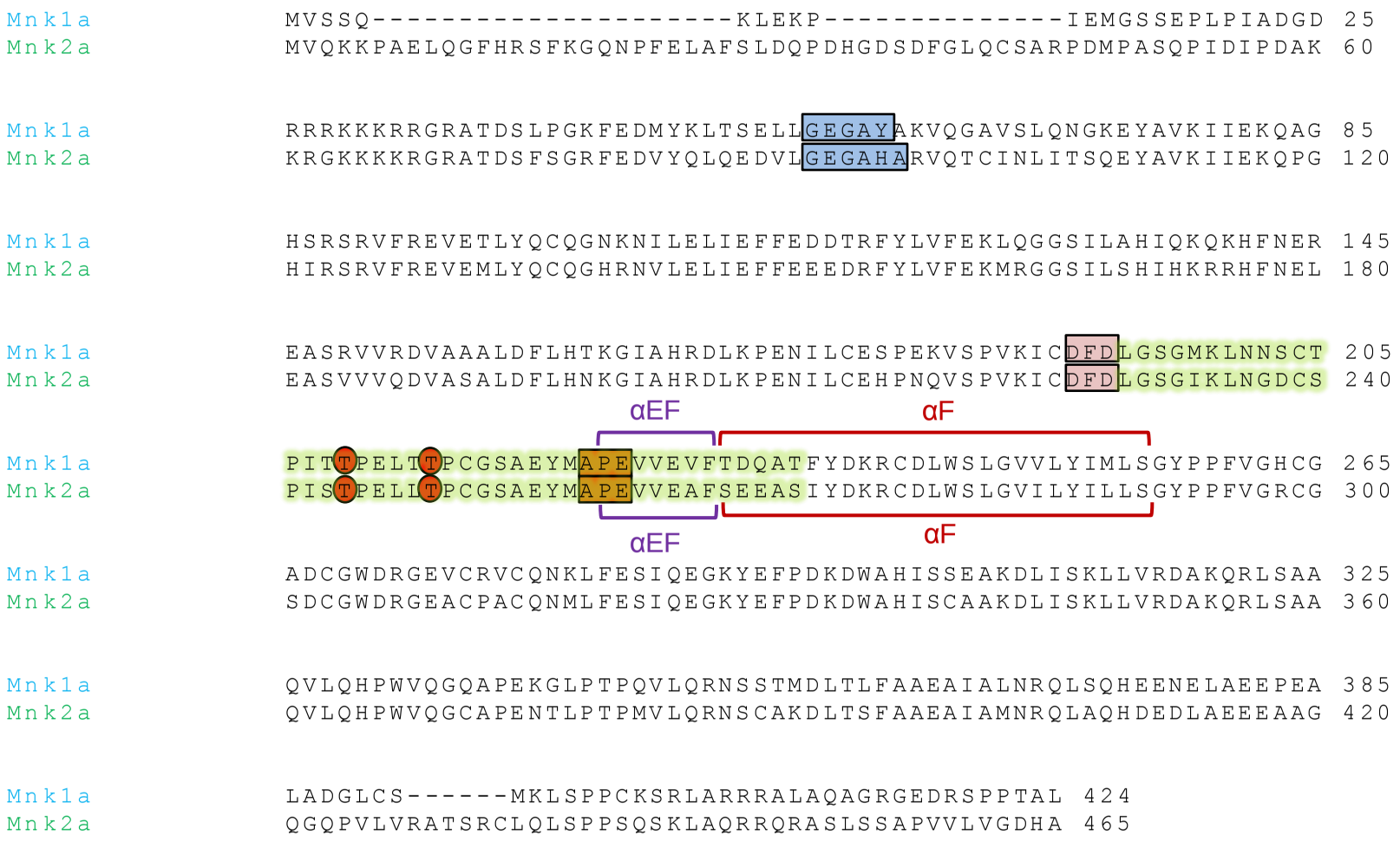
Mnk1a MVSSQ----------KLEKP----------IEMGSSEPLPIADGD 25
Mnk2a MVQKKPAELQGFHRSFKGQNPFELAFSLDQPDHGDSDFGLQCSARPDMPASQPIDIPDAK 60
Mnk1a RRRKKKRRGRATDSLPGKFEDMYKLTSELLGEGAYAKVQGAVSLQNGKEYAVKIIEKQAG 85
Mnk2a KRGKKKKRGRATDSFSGRFEDVYQLQEDVLGEGAHARVQTCINLITSQEYAVKIIEKQPG 120
Mnk1a HSRSRVFREVETLYQCQGNKNILELIEFFEDDTRFYLVFEKLQGGSILAHIQKQKHFNER 145
Mnk2a HIRSRVFREVEMLYQCQGHRNVLELIEFFEEEDRFYLVFEKMRGGSILSHIHKRRHFNEL 180
Mnk1a EASRVVRDVAAALDFLHTKGIAHRDLKPENILCESPEKVSPVKICDFDLGSGMKLNNSCT 205
Mnk2a EASVVVQDVASALDFLHNKGIAHRDLKPENILCEHPNQVSPVKICDFDLGSGIKLNGDCS 240
αEF
αF
Mnk1a PITTPELTTPCGSAEYMAPEVVEVFTDQATFYDKRCDLWSLGVVLYIMLSGYPPFVGHCG 265
Mnk2a PISTPELITPCGSAEYMAPEVVEAFSEEASIYDKRCDLWSLGVILYILLSGYPPFVGRCG 300
αEF
αF
Mnk1a ADCGWDRGEVCRVCQNKLFESIQEGKYEFPDKDWAHISSEAKDLISKLLVRDAKQRLSAA 325
Mnk2a SDCGWDRGEACPACQNMLFESIQEGKYEFPDKDWAHISCAAKDLISKLLVRDAKQRLSAA 360
Mnk1a QVLQHPWVQGQAPEKGLPTPQVLQRNSSTMDLTLFAAEAIALNRQLSQHEENELAEEPEA 385
Mnk2a QVLQHPWVQGCAPENTLPTPMVLQRNSCAKDLTSFAAEAIAMNRQLAQHDEDLAEEEAAG 420
Mnk1a LADGLCS------MKLSPPCKSRLARRRALAQAGRGEDRSPPTAL 424
Mnk2a QGQPVLVRATSRCLQLSPPSQSKLAQRRQRASLSSAPVVLVGDHA 465

Figure. 1.4. Amino acid sequence of Mnk1a and Mnk2a showing their major features. In order of feature: blue box – glycine-rich loop (GR loop), pink box DFD sequence, green highlighted residues form the activation segment, red circles are T-loop residues that are phosphorylated, orange box APE sequence, purple and burgundy brackets are α helices as labelled. Adapted from [70].

This means that in the inactive Mnk conformation the DFD motif is rotated in a fashion that forms a “DFD-out” conformation and results in occupation of the ATP site with a bulky side chain, thus blocking ATP entry. A further effect of this arrangement is that Asp^{191} becomes wedged between Glu^{94} and Lys^{78}. These two residues, along with Asp^{170}, form an ionic pair, which supports ATP binding, thus with Asp^{191} wedged between them this blocks ATP binding. One of the major differences between Mnk1a and Mnk2a is the greater affinity of Mnk2a for ATP, which is linked to the higher basal activity of Mnk2a. The residue Tyr^{60} in Mnk1a forms hydrogen bonds with the backbone carbonyl of Asp^{193} of the DFD motif and the backbone amide of Val^{227} of insert 2; this likely produces a very stable orientation of the inactive conformation [70]. In Mnk2a, Tyr^{60} is replaced with His^{95}, which cannot form these interactions, and thus this restrictive arrangement is absent. Furthermore in Mnk1a, Thr^{97} forms hydrogen bonds to Arg^{93} and Phe^{230}, in Mnk2a Tyr^{97} is replaced with Met^{132}, which again cannot form this restrictive structure. These features mean it is likely that ATP can leak into Mnk2a encouraging its activation and thus lead to a higher basal activity, whereas Mnk1a has a highly restrictive inhibitory conformation that makes this impossible [67-70, 72]. The activation of Mnk1a requires phosphorylation at a number of residues, which can occur through upstream signalling pathways or autophosphorylation, phosphorylation of Mnk2a occurs at shared sites with Mnk1a.

1.3.5 Activation of the Mnks and Isoform Differences.

T-loop phosphorylation is essential for the activity of the Mnks but there are distinct differences between isoforms, which contribute to the differing levels of activity seen in the different isoforms. Another threonine, Thr^{332} (Thr^{344} in Mnk1a and Thr^{379} in Mnk2a) is also phosphorylated in both Mnk1 and Mnk2 but has a different role in each protein. Evidence suggests the phosphorylation is not necessary for Mnk1 activity and mutations to glutamate, aspartate or alanine actually increase the basal and stimulated activity of Mnk1. It is suggested that in Mnk1 this residue plays a role in autoinhibition [58, 67]. However, in Mnk2, mutation to alanine or aspartate caused a loss of Mnk2 activity determined by its ability to phosphorylate the known Mnk substrate eIF4E, suggesting that here this residue may be constitutively phosphorylated, which along with other features may explain the difference in activity between Mnk1 and Mnk2. Other phosphorylation sites identified in Mnk2 include Thr^{403}, Ser^{27}, Ser^{399}, Ser^{401} and Ser^{173} [73].

There are other major differences between the four different Mnk isoforms that support the disparities seen in their activity. Their activity can be measured in an *in vitro* kinase assay, which involves combing large quantities of either Mnk with recombinant eIF4E and radioactive ATP, the incorporation of radioactive ATP into eIF4E can be measured to give a quantitative activity of the Mnks. As previously mentioned, Mnk1a has low basal activity

and is greatly stimulated by ERK and p38 MAPK pathways, Mnk2a has a high basal activity that is only slightly stimulated by ERK of p38MAPK (and hardly decreased by inhibitors of these pathways). The shorter isoforms also show differences, Mnk1b has a higher basal activity than Mnk1a (but lower than Mnk2a) and is only very slightly stimulated by upstream kinases, whilst Mnk2b has lower basal activity and is not greatly stimulated, although it is unclear how this isoform is activated. The most obvious difference between the isoforms is that Mnk1a and Mnk2a are both longer such that their C-terminus contains a MAPK binding motif, whilst Mnk1b and Mnk2b do not contain this C-terminus and as such lack the MAPK binding motif (Fig. 1.2). There are also differences between Mnk1a and Mnk2a in the C-terminus and catalytic domain that confer the differing MAPK binding profiles. Studies investigating these differences have identified clear sequence differences that allow Mnk2 to bind more strongly to active, phosphorylated ERK (p-ERK), whilst decreasing its affinity for p38 MAPK [39, 72]. Creation of chimeras of the murine Mnk1 and Mnk2 proteins showed that, by adding the C-terminus of Mnk2 to the N-terminus plus the catalytic domain of Mnk1, the high basal activity of Mnk2 and p-ERK binding was not quite matched. This suggests residues in the N-terminus of Mnk2 and/or catalytic domain are necessary for its higher basal activity and ability to bind p-ERK along with those in the C-terminus. Binding to p-ERK by Mnk2 also adds to the high basal activity because the area Mnk2 binds to in p-ERK causes ERK to be protected from dephosphorylation by phosphatases. This explains why Mnk2 remains active when cells are treated with MEK and p38 MAPK inhibitors [72]. There is a residue in the activation segment of Mnk2 that is required for binding to p-ERK. In Mnk2, Asp^{191} (Asp^{238} Mnk2a) has been shown to be an important residue, which in Mnk1 is replaced by Ser^{191}. Evidence shows that an S191D mutation in an Mnk1 mutant chimera protein consisting of an Mnk1 N-terminus and Mnk2 C-terminus can bind p-ERK and has a high basal activity that is not blocked by MEK and p38 inhibitors, similar to Mnk2a [72]. In Mnk1, Ser^{191} (Ser^{208} Mnk1a) is phosphorylated but is not part of the MAPK binding motif and it is not an autophosphorylation site; furthermore, its replacement with a non-phosphorylatable residue does not abolish Mnk1 activity so it is unlikely this site is necessary for activation [72].

Given the differing affinities of Mnk1 and Mnk2 for ERK and p38 MAPK, it is no surprise that their MAPK motifs are different. In Mnk1, the MAPK motif is LARRR, whilst for Mnk2 it is LAQRR [72]. Mutational studies and swapping the motifs in the proteins showed that LARRR is essential for p38 MAPK binding. Although the Gln in Mnk2 is important for ERK binding, it does not confer p-ERK binding by itself, due to the Asp^{191} residue in the

activation segment. Phosphorylation of Ser^{384} also occurs in the Mnks and is just upstream of the MAPK motif. The data show that phosphorylation of this residue negatively regulates ERK binding in Mnk1 but does not do so in Mnk2. Ser^{387} is also phosphorylated in Mnk2 (not Mnk1, where it is replaced by a Cys residue) and appears to also be very important for binding to p-ERK [72]. Other residues that have been shown of importance to the difference in binding affinities of Mnk2 include Leu^{400}, which is an alanine in Mnk1 and Arg^{398} which is also key to p-ERK binding [72].

1.3.6 Targets and Binding Partners

The Mnks phosphorylate their targets at sites that are rich in basic and serine residues [74]; however this does not always denote Mnk phosphorylation and so far all of their known targets are phosphorylated on serine residues.

1.3.6.1 eIF4E

The major shared target of all the Mnk isoforms is the translation initiation factor eIF4E. The Mnks are the major physiological kinases that target this initiation factor and function to phosphorylate this protein at $Ser^{209,}$ although there is controversy over the effect of eIF4E phosphorylation on translation initiation and thus the rate of protein synthesis. It is now generally accepted that phosphorylation causes the affinity of eIF4E for capped mRNA to decrease, however the effect this has on protein synthesis is the subject of conflicting models. The accepted model is supported by evidence that suggests the decrease in affinity allows for release of translation factors from the translation machinery resulting in rapid successive rounds of translation initiation and therefore an increase in protein synthesis [75]. This idea relies on successful binding of the 48S initiation complex to the 60S subunit before phosphorylation; however there is not yet any evidence concerning when during initiation the Mnks phosphorylate eIF4E other than that eIF4G must be bound to eIF4E. This suggests that eIF4F complex formation and binding of eIF4E to the capped mRNA must have already occurred. Opposing this model is the notion that decreasing affinity of eIF4E for capped mRNA leads to a decrease in protein synthesis [76]. However the experiments undertaken in this study, involve the overexpression of the Mnks resulting in very high levels of eIF4E phosphorylation [76]. This is turn would deplete the cellular pool of cap-binding-competent eIF4E because so much is phosphorylated leading to the observation of a decrease in the rate of protein synthesis.

There is important evidence that supports the likelihood that phosphorylation of eIF4E leads to amplified protein synthesis, such that increased phosphorylation of eIF4E in some cancers (especially lymphoma) is necessary for tumorigenesis [77-79]. One particular study used both mouse and human samples to analyse the effects of expression levels of Mnk1, eIF4E and an antiapoptotic protein, Mcl-1 in models of lymphoma. Using phosphorylation deficient eIF4E mutants (S209A), these authors showed that this lead to a decrease in tumorigenesis, which was rescued by expression of a 'phosphomimetic' mutant (S209D) of eIF4E. This supports the importance of eIF4E phosphorylation in its oncogenic ability [79]. The authors then assessed the effect of overexpression of Mnk1, which was shown to mimic the effect of eIF4E overexpression on cancer cell growth. Lymphomas where Mnk1 or eIF4E was overexpressed showed low levels of apoptosis compared with control cancer cells. Further experiments, using the S209A mutant, showed that eIF4E phosphorylation was involved in resistance to apoptosis in these cells. Using Mnk1/2 DKO cells these authors also illustrated that the Mnks were necessary for desensitization to apoptosis. One of the targets responsible for the low levels of apoptosis was identified as the antiapoptotic protein Mcl-1, which shows high levels in eIF4E and Mnk1-expressing cells. Loss of either of these components reduced Mcl-1 protein expression and increased sensitivity to apoptosis. Analysis of cells transfected with kinase-dead Mnk mutants showed that Mnk inhibition only sensitized tumorigenic cells that had deregulated translational machinery [79]. Since the Mnks have the unusual DFD motif and Mnk1/2 DKO animals present no overt phenotype, the Mnks present an excellent cancer drug target.

The importance of the Mnks and eIF4E phosphorylation has also been identified in other disease states especially inflammatory syndromes; this is not surprising given that Mnk1 is activated by p38 MAPK and ERK, which are stimulated by cytokines. The consequence of many cytokines upon their target cells is the production of inflammatory proteins that coordinate responses against challenges to the immune system. The interleukins, IL-2 and IL-15 selectively cause natural killer (NK) cell proliferation, survival and cytotoxic abilities in part through increased protein levels of a common downstream target, the transcription factor Ets1. Ets1 is important for the expression of inflammatory cytokines such as interferon γ (IFNγ) [80]. A study into the pathways that trigger this showed ERK activation results in Mnk1-dependent phosphorylation of eIF4E leading to an increase in levels of Ets1. This represents another important target in diseases where NK cells are lacking such as HIV and some cancers or where NK activity is deregulated such as autoimmune diseases [80].

The production of pro-inflammatory cytokines is also linked to the Mnk-dependent phosphorylation of eIF4E and again this presents a target for immune disorders where cytokine release is either excessive or lacking. Experiments with keratinocytes show phosphorylation of eIF4E is necessary for the production of the cytokines, TNFα, IL-1β and IL-6, thus in skin disorders where there is excessive production of these proteins the Mnks represent a sensible target for inhibition [44]. Another, similar, example shows that type I interferons (IFNs) can instigate JNK activation leading to downstream engagement of the ERK pathway, previous studies discarded JNK signalling as playing a role in Mnk activation but this was only ever aimed at direct activation of Mnk not as shown here through ERK. The data show that JAK1 is necessary for instigation of the ERK-Mnk pathway and the resulting phosphorylation of eIF4E vital to the production of the IFN-stimulated genes (Isg), Isg15 and Isg54. The Isg15 protein is necessary for NK cells proliferation whilst Isg54 is required for programmed cell death of virally infected cells. Similarly to those examples described above the Mnks again present a useful target in disease in this instance for IFN toxicities, cytopenias [81-83].

Treatments such as anisomycin can activate the p38 MAPK and ERK pathways. One of the downstream proteins induced by this treatment is the CCAAT/enhancer-binding protein homologue (CHOP). The CHOP protein is a transcription factor that induces expression of various proteins that cause the arrest of the cell cycle usually as a result of viral infection. Again activation of the Mnks and phosphorylation of eIF4E is required for the increased levels of CHOP protein expression [84].

1.3.6.2 eIF4G

Phosphorylation of eIF4E is strongly dependent on the association of eIF4E with eIF4G and the binding of the Mnks with eIF4G, as demonstrated by an eIF4G-binding deficient eIF4E mutant, whose phosphorylation is strongly impaired *in vivo* [85]. Similarly mutations to the Mnks, which block Mnk-eIF4G binding also decrease eIF4E phosphorylation *in vivo*. The interaction between the Mnks and eIF4G involves specific sequence motifs present in each protein. The N-termini of both Mnk1 and Mnk2 contain similar basic sequences, which confer binding to eIF4G. In Mnk1 KRR (residues 14-16) and KKR (residues 18-20) are both necessary as demonstrated by the loss of Mnk1-eIF4G binding when these residues are mutated to alanine [86]. The sequences in Mnk2 required for eIF4G binding are KKR (residues 60-62) and KKK (residues 65-67) as illustrated by the mutation to alanine residues [87]. Both Mnks bind to a HEAT domain in the C-terminus of eIF4G [85, 88]. HEAT domains are repeats of two antiparallel α-helical folds (HRs) found in a number of proteins and named based on the first four proteins identified to contain this structure (Huntingtin, eEF3, protein phosphatase 2A (PP2A) and mTOR) [88, 89]. The HEAT

domain that confers Mnk binding contains 4.5 HRs and within these HRs are two acidic and aromatic boxes (AA boxes) whose residues contact the K and R residues in Mnk1 and Mnk2. Both AA boxes are required for Mnk-eIF4G binding [90].

The binding of Mnks to eIF4G presents an important checkpoint in the regulation of eIF4E phosphorylation and eIF4F complex function. Formation of the eIF4F complex is linked to the phosphorylation state of the Mnks and eIF4E as demonstrated by the knockdown of PP2A, which lead to an increase in eIF4G and phosphorylated eIF4E precipitating on m^7GTP sepharose; furthermore inhibition of the Mnks lead to decreased eIF4G and phosphorylated eIF4E in an m^7GTP pulldown assay [91]. Phosphorylation of the linker sequences between HEAT domains in eIF4G controls the binding to Mnk1. Casein kinase 2-α phosphorylates eIF4G at Ser^{1239} (found in the interdomain linker between HEAT domains) and increases the phosphorylation of eIF4G by ERK1/2 at Ser^{1232}, this in turn results in changes to eIF4A/3/4B binding to eIF4G and increased Mnk1-eIF4G binding, therefore serving to regulate translation initiation [92]. Similarly phosphorylation of Ser^{1186} on eIF4G by PKCα also increases Mnk1-eIF4G binding [93].The control of translation initiation by stimulatory pathways is further linked to the phosphorylation of the T-loop in Mnk1, which has been shown to be required not only for activity but also for eIF4G binding, as shown by mutation of the Thr^{197} and Thr^{202} to alanine resulting in the reduction of Mnk1-eIF4G binding. Under non-stimulatory conditions the C-terminus of Mnk1 has unknown features that inhibit Mnk1-eIF4G binding [94]. This represents another example of the tight control of eIF4E phosphorylation by Mnk1. During apoptosis translation is downregulated through various pathways, one of which involves the modulation of Mnk1-eIF4G binding. Caspase-cleaved Pak2/gamma-PAK phosphorylates Mnk1 at Thr^{22} and Ser^{27}, which leads to a strong reduction in binding to eIF4G, which would presumably lead to reduced eIF4E phosphorylation and a decrease in translation, although the authors do not investigate this [95]. The relationship between Mnk2 and eIF4G has been far less researched than Mnk1-eIF4G but recent evidence demonstrates a complex signalling pathway that regulates eIF4G phosphorylation. The activity of Mnk2 was shown to be correlated with decreased phosphorylation of eIF4G at Ser^{1108} (a known serum induced site) in an unclear mechanism involving serine-arginine-rich kinases and was proposed to lead to decreased translation [96]. However given that Mnk2 is highly active under basal conditions and eIF4E phosphorylation is correlated with this it remains to be seen as to why Mnk2 would negatively regulate translation via eIF4G in an apparent direct contradiction to increased eIF4E phosphorylation and subsequent translation initiation.

The intricate relationships between the Mnks, eIF4G, eIF4E and translation initiation would benefit from further research especially with regards to regulation of specific subsets of mRNA.

1.3.6.3 hnRNPA1 and PSF.p54^{nrb}

The phosphorylation of eIF4E by the Mnks is one mechanism that alters the expression of some mRNAs but there is evidence that the Mnks can regulate the synthesis of other mRNAs independently of eIF4E. The mRNAs for many inflammatory cytokines, such as TNFα, contains sequences within their 3'UTRs that can exert a number of control measures upon the mRNA. One such sequence contains a high level of A and U, so these regions are called AU rich elements (AREs). The AREs can recruit a subset of proteins called ARE-BPs (ARE-binding proteins), which are then able to regulate transport from the nucleus to the cytoplasm, regulate message stability and control mRNA translation [97]. The production of TNFα is controlled by both the MEK/ERK and p38 MAPK cascades. The p38 MAPK pathway controls TNFα production through MK-2, which acts upon the ARE-BPs; TTP (tristetraprolin) [98], HuR [99] and heterogeneous nuclear ribonucleoprotein (hnRNP) A0 [100]. The former two proteins modulate TNFα mRNA stability whilst the latter has a number of nuclear functions. This model explains why stability of the mRNA changes in response to the p38 MAPK input but it does not explain how the MEK/ERK pathway control protein levels since MK-2 is not activated by ERK. The Mnks are also MKs and are downstream of ERK and so represent a potential regulator of TNFα translation. One such study showed that Mnk1 overexpression resulted in a 4-fold dose-dependent increase in a TNFα mRNA reporter construct whilst there was no similar increases in control mRNA (GAPDH) [42]. Deletion of the ARE in TNFα mRNA lead to a 50% reduction in reporter construct expression compared to full length mRNA and analysis of pulldowns of the ARE-BPs bound to TNFα showed that the Mnks could phosphorylate some of these proteins. Three of them were identified: hnRNP A0, which is already known to be phosphorylated by MK-2, JKT BP and hnRNP A1. *In vitro* experiments then confirmed that the Mnks could phosphorylate hnRNP A1, which led on to *in vivo* identification of the phosphorylation sites Ser^{192}, Ser^{310}, Ser^{311} and Ser^{312}. The next step was to assess the effect of phosphorylation of hnRNP A1 on its function, which showed this led to its decreased association with TNFα mRNA and a resulting increase in TNFα protein [42]. This was further supported by addition of the Mnk inhibitor CGP37580 that reversed these effects.

Following this new understanding that the Mnks could modulate mRNAs with AREs, interest was directed at finding other substrates of the Mnks bound to AREs. The complex PSF.p54^{nrb} was shown to precipitate on an m^7-GTP Sepharose cap resin along with Mnk,

eIF4G and eIF4E [41], which might be a result of by binding to any of these proteins or mRNA. Further experimentation using a biotinylated oligoribonucleotide showed that the PSF.p54^{nrb} complex bound to only the ARE-containing oligoribonucleotide. *In vitro* experiments then showed that the Mnks could phosphorylate PSF at Ser^{8} and Ser^{283}; interestingly Mnk2 could phosphorylate Ser^{8} much more efficiently than Mnk1 suggesting this is more likely an Mnk2 specific site. Again it was of interest to determine what effect PSF phosphorylation had on TNFα mRNA association, and addition of the Mnk inhibitor CGP57380 to activated Jurkat T cells was shown to decrease PSF binding to the TNFα mRNA. This indicates that phosphorylation of PSF.p54^{nrb} by the Mnks leads to increased binding to TNFα mRNA. The known functions of PSF-p54^{nrb} are mostly in nuclear events such as transcription, nuclear RNA processing, DNA relaxation and retention of edited mRNA and may regulate TNFα mRNA in this respect (reviewed [101]) and as such may represent a role of Mnk2a or mnk2b in the nucleus.

This provides evidence that the Mnks can control translation of a specific subset of mRNAs further providing another potential therapeutic target for disorders such as inflammatory bowel disease, rheumatoid arthritis and antigen induced septic shock where TNFα is overexpressed.

There is another example of Mnk-dependent modulation of mRNA translation, the regulation of the *c*-Jun mRNA. The authors of the study noticed that phosphorylation of eIF4E did not constitute a considerable influence of levels of c-Jun protein and suggest it is possible the Mnks are targeting a protein bound to the c-Jun mRNA at initiation thereby influencing its translation although do not investigate this further [102].

1.3.6.4 Sprouty

The other known target of the Mnks is a protein that is not involved in translation, suggesting these kinases have a translation-independent role. Signalling pathways must be regulated otherwise unchecked can lead to a multitude of problems for the cell. Signalling pathways are controlled by phosphatases, which switch off phosphate activated signalling and small proteins that are either secreted by cells or present in the cell that act as antagonists to produce inhibitory feedback loops [103]. An example of a small protein signalling antagonist is Sprouty, which functions to regulate RTK signalling. For example, it can interfere with epidermal growth factor (EGF) and fibroblast growth factor (FGF) signalling by antagonising both the receptors and Ras-dependent activation of ERK (reviewed [104]). Expression of Sprouty is regulated by signalling at the transcriptional

level but it is also evident at the posttranslational level whereby Sprouty phosphorylation on tyrosine and serine modulates its stability. Phosphorylation of the former site, $Tyr^{55,}$ leads to increased association of Sprouty with E3 ubiquitin ligase and resulting in its degradation, which leads to loss of antagonism of the signalling pathway. The phosphorylation of Ser^{112} and Ser^{121} has been shown to be Mnk-dependent. Addition of p38 MAPK and MEK/ERK inhibitors in combination abrogates the phosphorylation of these residues in Sprouty, thus since there are no MAPK motifs it is likely that the Mnks (or in some instances RSKs) are responsible because they are the only MKs activated by both p38MAPK and ERK. Furthermore, six possible Mnk sites (serine and basic rich regions) are present in Sprouty. However, the data regarding the function of serine phosphorylation of Sprouty are conflicting. In one study, serine phosphorylation was shown to have the opposite effect of tyrosine phosphorylation in that serine phosphorylation leads to an increased stability of the Sprouty protein and therefore an increased ability of Sprouty to antagonize RTK signalling [74]. Use of Mnk inhibitors and mutants that are inactive further supported this role because the loss of Mnk activity led to an increase in Sprouty degradation. Conversely, constitutively active Mnk mutants blocked Sprouty degradation. Further evidence also shows that serine phosphorylation blocks Tyr^{55} phosphorylation therefore totally blocking ubiquination and subsequent degradation of Sprouty. The authors of this paper suggest the isoform responsible is Mnk1 because it is activated by the ERK and p38MAPK pathways. Interestingly increased antagonism of RTK induced Ras-ERK activation by sprouty, may lead to the inactivation of Mnk1 in a potential negative feedback loop [74]. Another study presents contradictive data, which show Mnk2 phosphorylation of the Ser^{112} and Ser^{121} sites results in association with the E3 ubiquitin ligase Nedd4. This leads to the ubiquination and degradation of Sprouty. This would lead to a potentiation of ERK activation and fibroblast growth factor signalling [105], which may correlate with the high basal activity of Mnk2a in a positive feedback loop. When comparing these studies there is a potential that Mnk1 and Mnk2 have isoform specific effects on the same substrate and further research would benefit from experiments in Mnk1 and Mnk2 single knockout cells.

1.3.6.5 Potential Substrates

The classification of the Mnk2 gene and its splice variants arose through a yeast-two hybrid experiment using the oestrogen receptor β [66]. This data showed that Mnk2, specifically Mnk2b was able to bind to the ligand binding domain of the oestrogen receptor ERβ. The authors unfortunately did not assess whether the receptor was an Mnk2b target [66]. However the $PSF.p54^{nrb}$ complex binds to the nuclear hormone receptor family of which the oestrogen receptor is a part of and, as mentioned, the Mnks can phosphorylate this complex [41]. This would be a novel area of research regarding the functions of Mnk2.

Another reason this maybe interesting, in combination with the evidence for Sprouty regulation, comes from a patent for a specific Mnk inhibitor that shows activity against Mnks leads to increased insulin sensitivity and fatty acid synthesis [106]. Insulin signalling is an RTK induced process and the oestrogen receptor has been shown to have links to obesity. Investigation into this, using an Mnk2 knock-out animal would be of great interest.

1.4 Glucose Metabolism in Mammals

1.4.1 Overview

The absorption and endogenous production/regulation of glucose are essential for overall whole body energy homeostasis. Food and drink ingested by mammals are processed at numerous points from the mouth to the intestines. The point of entry into the body occurs in the intestines where free fatty acids, amino acids and monosaccharide's are absorbed through the enterocyte microvillus of the small intestines [107]. Both amino acids and monosaccharides (e.g., glucose) are taken up through active transport by sodium-dependent transporters. Fructose and galactose are taken up by the liver and converted into glucose, which can be released back into circulation, stored as glycogen or used to produce ATP. For the purpose of this thesis, the focus will be on glucose transport. Glucose is transported across the enterocyte membrane by both Na^+-dependent active transport (driven by the Na^+ gradient created by the Na^+/K^+ ATPase at the basal membrane of the enterocyte) and facilitated diffusion. At the apical membrane the symporter sodium/glucose cotransporter 1 (SLC5A1) binds to two Na^+ ions resulting in a conformational change that reveals a glucose binding pocket, which when bound to glucose leads to a further conformational change that leads to the release of glucose into the cytosol followed by the sodium ions [108]. Galactose is also transported across the apical membrane by SLC5A1 whilst fructose is transported by glucose transporter 5 (GLUT5). At the basal membrane, facilitated diffusion by GLUT2 transports glucose into the blood stream [109, 110]. The GLUTs form oligomeric structures, which are formed of two dimers to produce a channel through the plasma membrane allowing glucose to traverse based on the concentration gradient [111-113]. Once in the bloodstream, glucose is taken up in a tissue-specific manner and is tightly regulated by hormones.

1.4.2 Glucose Oxidation – The Krebs Cycle

Glucose entering the cell is converted to glucose-6-phosphate (G6P) by a family of hexose converting enzymes called hexokinases, of which there are 4 isoforms called hexokinase I, II III and IV. Hexokinase IV is most commonly referred to as glucokinase (GK) and is only found in the pancreas, liver, and intestines [62, 107]. The production of G6P requires one molecule of ATP and acts as an inhibitor of hexokinases therefore self-regulating the reaction [62, 107]. The fate of G6P is dependent on cell type and metabolic requirements; here we shall discuss the process of glycolysis and the subsequent generation of ATP by the Krebs cycle.

The glycolysis pathway results in the production of pyruvate, the eventual formation of ATP and the reduced form of nicotinamide adenine dinucleotide (NADH) from pyruvate during the Krebs cycle [62, 107, 114]. Glycolysis is a 10 step enzymatic process occurring in the cytosol, G6P is converted to glyceraldehyde-3-phosphate (GAP) and dihydroxyacetone phosphate (DHAP) by two enzymatic processes. DHAP is an isomer of GAP and is readily converted into GAP [62]. This means that glucose has been degraded into two molecules of GAP. The remaining 5 enzymatic reactions produce phosphoenolpyruvate (PEP), which is used by pyruvate kinase to produce one molecule of ATP and pyruvate [62, 107, 114]. Overall one glucose molecule will produce a net gain of 2 ATP, 2 NADH and 2 pyruvate molecules (since two GAP molecules are produced during the conversion of DHAP). The fate of pyruvate is varied depending on cellular requirements, for example during exercise the muscle uses pyruvate to generate lactate when oxygen is unavailable. During aerobic conditions pyruvate is fed into the Krebs cycle – also known as the tricarboxylic acid (TCA) cycle or citric acid cycle.

In order for cells to generate energy, in the form of ATP, pyruvate is oxidized in an 8 step series of reactions. This cycle is not just part of glucose catabolism but also forms a major part of fatty acid oxidation and amino acid oxidation. The generation of electron pairs in the form of NADH and flavin adenine dinucleotide ($FADH_2$) are used in the mitochondria to drive an electrochemical gradient that results in the generation of ATP. Furthermore, since this is a cyclic series of reactions and the final product oxaloacetate is both consumed at the start of the reaction and generated at the end of the reaction this process continues unless any of the products become depleted [62, 107, 114]. In the instance of glucose catabolism, the product pyruvate, generated from glycolysis, is used by the multi-enzyme complex pyruvate dehydrogenase to generate acetyl-CoA. This occurs in a complex multistep process, which overall generates CO_2 and NADH. The product acetyl-CoA can also be generated by fatty acids, which shall be discussed later. Citrate is the first product of the cycle and is produced by condensation of oxaloacetate and acetyl-CoA. The cycle

continues with conversion of citrate back to oxaloacetate, which can then be fed back into the cycle [62, 107, 114].

The NADH and $FADH_2$ produced by glycolysis and the citric acid cycle can yield up to 38 molecules of ATP during aerobic conditions from just one molecule of glucose. This process is tightly regulated by signalling pathways, substrate availability and the levels of downstream metabolites and is thus dependent on the metabolic requirements of the cell.

1.4.3 Glycogenesis and Glycogenolysis

Glycogen is a branched polymer of glucose units bound to glycogenin and can store 400 mmol of glucose as 0.01µmol of glycogen. This allows storage of vast amounts of fuel without affecting the osmolarity of a cell [115].

During glycogenesis, G6P is converted to glucose-1-phosphate (G1P) by phosphoglucomutase (with the intermediate glucose-1,6-bisphosphate), which is then used in a reaction along with uridine triphosphate (UTP). UTP provides the energy for converting G1P to uridine diphosphate (UDP)-glucose catalysed by the enzyme UDP–glucose pyrophosphorylase. The UDP-glucose is then added to a non-reducing end of a glycogen chain by glycogen synthase. This requires a glycogen chain to already be present, which is achieved by the glycosyltransferase: glycogenin, which extends a chain of glucose residues from UDP-glucose creating a basis for glycogen synthase to work from [62]. Glycogen is a branched molecule and this is achieved by the enzyme amylo-(1,4-1,6)-transglycosylase.

A reversal of glycogen synthesis occurs when there is a requirement for glucose such as fasting or exercise. This requires the activation of phosphorylase kinase, which phosphorylates and activates glycogen phosphorylase; the enzyme responsible for generating G1P from glycogen. Another enzyme, α(1-4) transglycosylase is required to ensure suitable glycogen units are available for glycogen phosphorylase to process. The subsequent G1P is converted to G6P by phosphoglucomutase in a reversal of the reaction described earlier. In the liver plasma glucose can be increased through glucose-6-phosphatase, which can convert G6P back to glucose, which will diffuse out of the hepatocytes into the circulation via GLUT2 [62]. In the muscle G6P is fed into the glycolysis pathway in order to generate energy.

1.4.4 Gluconeogenesis

Gluconeogenesis is the process of producing glucose from non-carbohydrate substrates such as lactate and glucogenic amino acids [116]. Firstly pyruvate must be converted to phosphoenylpyruvate (PEP), which requires energy in the form of ATP and GTP as well as an intermediate in the form of oxaloacetate. There are two enzymes involved; pyruvate carboxylase converts pyruvate into oxaloacetate using ATP and PEP carboxykinase (PEPCK) converts oxaloacetate into PEP using GTP [62]. It is important to note this occurs in the mitochondria and upon the formation of PEP the pathway moves into the cytosol where PEP is converted into a number of intermediates by the glycolysis enzymes but in reverse to produce fructose-1,6-bisphosphate. The next step is formation of fructose-6-phosphatase by fructose 1,6-bisphosphatase and finally the enzyme phosphoglucose isomerase converts this to G6P, which can then be converted to glucose by glucose-6 phosphatase [62]. Since only the liver and kidneys express glucose-6-phosphtase, gluconeogenesis is confined to only these tissues, with some debate about the potential for the intestines to also engage in this process [116-118].

1.4.5 Regulation of Plasma Glucose Levels

The brain uses 60-70% of the body's glucose at resting levels, which requires very careful control of resting plasma glucose through hormonal control during the fed and fasted states [114]. Glucose obtained from food is taken up by a number of tissues; the liver takes up 40%, the skeletal muscle 30%, adipose tissue 5%, kidneys 10% and the brain 15%. The fate of glucose and the mechanisms for its continuous regulation are tissue specific but are highly coordinated within the body [119].

Ingestion of a meal and the subsequent absorption of dietary sugars into the blood stream, by the intestines, leads to a rapid rise in plasma glucose from fasting levels of 5-6.1 mmol/L (normal range for human males and mice) [120] to a level below 7.8 mmol/L after 2 hours (during glucose tolerance test (GTT)) [107]. The presence of glucose in the intestinal epithelium causes the release of glucagon-like peptide-1 (GLP-1) and gastric inhibitory polypeptide (GIP), which enter the circulation and nervous system to prime the body for the increase in glucose [121].

The presence of high levels of plasma glucose after a meals leads to diffusion of glucose into the β cells in the Islets of Langerhans in the pancreas via GLUT2. Once inside the cell glucose is phosphorylated by GK to produce G6P, this is the rate limiting step for this process. The G6P is then fed into the Krebs Cycle. During glucose oxidation in the mitochondria intermediates such as malate, glutamate and citrate are released, which are

one of the stimulatory signals for exocytosis of vesicles containing insulin. Another pathway required for insulin release is the ATP:ADP ratio, which is also altered due to increased activity of the Krebs cycle. An increase in ATP and decrease in ADP results in closure of K^+ ATP sensitive channels leading to a depolarization of the cellular membrane causing the opening of voltage-gated Ca^{2+} channels and the subsequent influx of Ca^{2+}. This is required for exocytosis of vesicles containing insulin. The third pathway required for insulin release is triggered by the GLP-1 receptor (GLP-1R) and GIP receptors (GIP-R), which increases cyclic adenosine monophosphate (cAMP) levels causing the activation of protein kinase A (PKA), which also functions in vesicular exocytosis [122].

Once released, the role of insulin within the body is multifaceted and is discussed in greater detail in sections 1.2.4 and 1.6. In terms of plasma glucose regulation, insulin is required to bind to cells containing the insulin receptor particularly myocytes in the muscle, hepatocytes in the liver and adipocytes in the adipose tissue. The overall effect is to increase the uptake of glucose by these cells (discussed in section 1.6) and thus clearing plasma glucose. The fate of glucose once taken up by the liver, muscle and adipose tissue is different for each organ.

The liver is the major source of endogenous glucose under fasting conditions due to the ability of hepatocytes to store 5-8% of their weight as glycogen. After a carbohydrate rich meal, glucose reaches the liver via the hepatic portal vein where hepatocytes take up glucose in the same way as the pancreas, GLUT2 being the major isoform responsible in the livers of adults [123]. Once inside the cell glucose is phosphorylated to G6P by GK in a rate limiting fashion. G6P can then enter one of 3 pathways; glycogen synthesis (glycogenesis), the pentose phosphate pathway (to produce NADPH) or glycolysis and subsequently the citric acid cycle [62, 123]. The process of glycogenesis is stimulated by insulin, which, through the classic IRS1/PKB pathway, inactivates glycogen synthase kinase 3 (GSK3α/β) by phosphorylation of residues Ser^9 and Ser^{21}. GSK3 is responsible for inhibitory phosphorylation of glycogen synthase at Ser^{641} and Ser^{645}.The inactivation of GSK3 by insulin leads to dephosphorylation of glycogen synthase by protein phosphatase-1 and hence its activation [124-126]. G6P and glycogen are both allosteric inhibitors of glycogen synthase [126].

During fasted conditions, when the pancreas senses a reduction in plasma glucose levels to below 5mmol/L, glucagon is released from the α-cells, which binds to the glucagon receptor present on hepatocytes. Similarly adrenaline acts on β-adrenergic receptors in the pancreas to inhibit insulin secretion in situations of exercise or stress and also increases glycogenolysis in the liver and muscle [121]. This causes a signalling cascade

that generates cAMP, which activates PKA. The function of PKA is to phosphorylate and activate phosphorylase kinase and thus phosphorylate and inhibit glycogen synthase. This therefore leads to the production of glucose via glycogenolysis. Another pathway by which hepatocytes are able to increase plasma glucose during fasting is gluconeogenesis; this pathway is used when liver glycogen stores are depleted. Gluconeogenesis results in the production of glucose from pyruvate, which is produced mostly from lactate and glucogenic amino acids e.g. alanine [116]. Previously it was thought the liver was almost completely responsible for regulating fasting glucose levels. However, the evidence shows that the kidney can contribute to glucose homeostasis via gluconeogenesis and there is some debate and evidence that the intestines too may partake in gluconeogenesis [116-118].

The other major tissue in the body that regulates plasma glucose is skeletal muscle. The predominant mechanism of glucose uptake by the muscle is stimulated specifically by insulin via facilitated diffusion through GLUT4 (the specifics of the signalling pathway that occurs is discussed in section 1.6) and a small amount by GLUT1 [121]. The muscle therefore functions to replenish its glycogen stores after carbohydrate rich meals and thus clears glucose from the blood. Whilst the liver is responsible for maintaining blood glucose during fasting, the muscle uses its glycogen stores during periods of exercise in order to generate energy for muscle contraction [107]. There is no glucose-6-phosphatase in muscle [127] and so the G6P produced by the glycogen breakdown is fed into the glycolysis pathway in order to produce ATP via the Krebs cycle or through anaerobic respiration.

Adipose tissue is responsible for clearing approximately 5% of the plasma glucose after a meal and in a similar fashion to muscle expresses GLUT4 and is stimulated by insulin to take up glucose [128]. Unlike the muscle or liver, adipose tissue does not store glucose as glycogen but instead stores excess glucose as fat. This process is stimulated by insulin and is known as lipogenesis, which is discussed in detail later.

As previously mentioned, the kidneys are another point of both glucose clearance and glucose production and therefore contribute to overall whole body glucose homeostasis. Unlike the liver, the kidneys are only able to produce glucose via gluconeogenesis since they have no capacity to store glycogen. This is controlled not by glucagon but by catecholamines, growth hormone and thyroid hormone . Furthermore the kidney uses the glucogenic glutamine as a precursor (as well as lactate) whilst the liver uses alanine [119]. Consequently during fasting of a duration around 16h, the liver contributes 75-80% of the plasma glucose whilst the kidneys are responsible for 20-25% [119]. This is important when considering fasting glucose levels after this time period.

1.4.6 Type 2 Diabetes Mellitus

Diabetes mellitus is a disease classically defined as either type 1 diabetes (T1DM) or type 2 diabetes (T2DM). The difference between the types arises from the cause but both are clinically diagnosed by fasting glucose >7.0 mmol/L and glucose levels >11.1 mmol/L after 2h following an oral glucose tolerance test (OGTT) [129]. Diabetes is estimated to affect 285 million people globally [130] and of those 2.6 million have been diagnosed in the UK (2009). The prevalent form in the UK is T2DM, which accounts for 90% of cases [130]. The cost of care for diabetic patients by the NHS has risen markedly in the last 10 years. From 2000-2008 the cost of dispensed prescriptions rose from £290 million to £591 million, nearly a 50% increase [131]. In 2008 alone the cost of treatment for diabetes cost £708 million, this is almost 10% of the annual NHS diabetes budget [131]. There are, of course, other costs to the NHS; hospitalization of patients, out-patient care, complications of diabetes etc. The annual budget that covered all diabetes related costs, for 2007-2008, was £9 billion [130]. These costs are very high and will inevitably increase rapidly over the next 15 years with estimates of 4 million people to be diagnosed by 2025 [130]. The prevalence of T2DM is increasing rapidly and has been deemed a 21st century epidemic. A combination of increasingly sedentary lifestyles, obesity and an ageing population are believed to be major contributors to this trend [132].

The major difference between T1DM and T2DM is the cause of increased plasma glucose levels. T1DM is simply a result of a destruction or damage of the β cells of the pancreas, which leads to a loss of insulin release. Patients with T1DM must carefully monitor blood glucose levels and inject insulin in order to maintain their health [107]. For the purpose of this thesis, we will focus on T2DM.

The development of T2DM usually occurs after the age of 30-40 and is associated with polycystic ovary syndrome (PCOS), Cushing's syndrome, acromegaly and other genetic factors. However the major cause of T2DM is obesity and the associated metabolic syndrome and insulin resistance [107]. We shall discuss obesity and the metabolic syndrome in greater detail in the next section as well as the complex molecular mechanisms that are thought to be responsible for insulin resistance in diet-induced T2DM. Large scale, longitudinal statistical studies have established that there are distinct phases in the pathogenesis of T2DM. The first phase in the progression to T2DM is the onset of insulin resistance, which is characterised by a decrease in the sensitivity of target tissue to the actions of insulin. This is the result of an increase in inflammatory cytokines, increased plasma lipid metabolites and changes in hormonal balances that result in perturbed insulin signalling within the target tissue and consequently a reduction in

glucose uptake [62, 107, 133]. Generally during the early onset of insulin resistance there is a compensatory increase in insulin secretion, which functions to maintain normoglycaemia or impaired glucose tolerance [134]. The eventual progression to T2DM is prolonged insulin resistance resulting in substantial reductions in glucose uptake by target tissues and a reduction in insulin secretion due to β cell dysfunction or T2DM can progress simply due to a genetic predisposition towards a deficit in insulin secretion in combination with insulin resistance [134].

The current treatments available for T2DM are dependent on the stage of disease progression. Early intervention at the onset of insulin resistance can be achieved simply by lifestyle changes in terms of diet and exercise, with a reduction in caloric intake and an increase in exercise. However, when this is not appropriate or ineffective, pharmacological intervention is required. Two types of drugs are commonly prescribed to T2DM patients, metformin and thiazolidinediones (rosiglitazone and pioglitazone) [133]. Metformin functions mostly to increase the duration of insulin action, reduce liver gluconeogenesis, and increase muscular glucose uptake. The thiazolidinediones are agonists of the peroxisome proliferator-activated receptor γ (PPARγ), which is a transcriptional activator or insulin target genes including GLUT4 [133]. However the thiazolidinediones have side effects, e.g., Avandia (Rosiglitazone) can cause cardiovascular disorders [135], although the incidence of this is decreasing due to better understanding and improved patient care. Metformin has some side effects including gastrointestinal disruption (diarrhoea, nausea, vomiting), vitamin B12 deficiency and lactic acidosis [136]. It is therefore paramount to continue with research into the cause of T2DM and the resulting development of cheaper, more effective drugs.

1.5 Lipid Metabolism

1.5.1 Overview

The processing of dietary lipids is much simpler than that of glucose. Lipid globules are coated in bile salts within the intestinal lumen. The bile salts allow for enzymatic digestion by lipases to form free fatty acids and monoglycerides (with small amount of diglycerides and glycerol), which remain bound to bile salts and form micelles. Micelles are able to diffuse across the plasma membrane of the microvilli and once inside the cell are re-esterified into triglycerides. The cell then repackages triglycerides into chylomicrons or lipoproteins in order for them to be transported in the hepatic portal vein to the liver. Both the liver and adipose tissue are the major organs responsible for lipid metabolism and storage [107].

1.5.2 Lipogenesis and Fatty Acid Synthesis

The liver and adipose tissue are responsible for clearing approximately 40% and 5-10% of plasma glucose, respectively [119]. During periods of glucose levels that exceed those needed to meet ATP demand and, in the liver, glycogen storage capacity, there is an increase in acetyl-CoA levels, which are then stored as triglycerides (TGs) in the adipose tissue and sometimes in the liver [62, 107]. The process by which this occurs is called lipogenesis. Excess glucose is converted to pyruvate by glycolysis and subsequently acetyl-CoA is generated by pyruvate dehydrogenase as already described. This occurs in the mitochondria but the enzymes required for lipogenesis are found in the cytosol and the mitochondrial membrane is impermeable to acetyl-CoA so it must be converted to citrate by citrate synthase and transported across the mitochondrial membrane by the tricarboxylate transport system [62]. Once in the cytosol, citrate must be converted back into acetyl-CoA requiring the enzyme ATP-citrate lyase (ACL), which reverses the reaction catalysed by citrate synthase and requires the hydrolysis of ATP. This reaction also generates oxaloacetate, which is reduced to malate and then decarboxylated to pyruvate, which is returned to the mitochondria [62]. Acetyl-CoA in the cytosol can be used in the process of fatty acid synthesis by the enzyme acetyl-CoA carboxylase (ACC) to produce malonyl-CoA, which is the rate-limiting step of de novo fatty acid synthesis. The next step involves the multienzyme complex fatty acid synthase (FAS), which catalyzes the reaction of malonyl-CoA and acetyl-CoA with the acyl-carrier-protein (ACP), which forms part of the FAS complex [62]. A series of reactions from the acetyl-ACP and malonyl-ACP combination is repeated 7 times to produce a chain, which is hydrolysed by palmitoyl thioesterase to produce palmitate [62]. Fatty acids that are either synthesised in this fashion or obtained from the diet are stored as triglycerides (TGs, also known as triacylglycerols) in adipose tissue and in the liver. The synthesis of TGs occurs in both the ER and mitochondria. In the mitochondria, glycerol-3-phosphate acyltransferase uses fatty acids and glycerol-3-phosphate (generated by glycolysis) to produce lysophosphatidic acid. In the ER lysophosphatidic acid is generated from acyl-dihydroxyacetone by acyl-dihydroxyacetone phosphate reductase. Phosphatidic acid is produced from lysophosphatidic acid by 1-acylglycerol-3-phosphate acyltransferase and is then used to form DAG by phosphatidic acid phosphatase. Triglycerides are then formed from fatty acyl-CoAs (e.g. palmitate) combined with diacylglycerols by the enzyme diacylglycerol acyltransferase [62]. In order to prevent immediate reversal of TG synthesis, TGs are

coated in a storage molecule called perilipin (lipid droplet-associated protein), which is hormonally regulated [137].

The regulation of lipogenesis and fatty acid synthesis is tightly controlled by signalling pathways and gene expression. Insulin is the major hormone responsible for activating lipogenesis whilst glucagon deactivates lipogenesis. Other hormones fine tune fatty acid metabolism. ACC is highly controlled by phosphorylation especially phosphorylation of Ser^{79} by AMP activated protein kinase (AMPK) and Ser^{1200} by PKA, which inhibits its activity [62, 138]. ACC is also regulated by citrate and palmitate in an allosteric fashion such that citrate is activating and palmitate (and other long chain fatty acids) is inhibitory [138]. Insulin also regulates the phosphorylation of ATP citrate lyase via activation of PKB. ACL is phosphorylated at Thr^{446} and Ser^{450} by GSK3, which is inactivated by insulin leading to the dephosphorylation of ACL. In combination with phosphorylation at Ser^{454} by PKB there is an insulin-induced increase in ACL activity [139, 140]. The expression of genes involved in lipogenesis is also highly regulated by hormones, glucose and fatty acids. The major transcription factors responsible for the expression of FAS and ACC are the sterol response-element binding proteins (SREBP-1 and SREBP-2), liver X receptors and carbohydrate-responsive element-binding protein (chREBP) [138]. The presence of fatty acids within a cell regulates the activity of SREBPs. During times of low levels of fatty acids an intricate localization pathway is activated resulting in the translocation of SREBPs from the ER to the nucleus and subsequent lipogenic gene expression through an mTORC1 dependent mechanism [141].

1.5.3 Lipolysis and β Oxidation

Lipolysis occurs in three specific processes, which occur in a tissue-specific manner. As previously mentioned, triglycerides cannot enter enterocytes or in fact any type of cell. Thus, in the intestines the lipolytic enzymes gastric lipase and pancreatic lipase are responsible for the generation of free fatty acids (FFAs) that are absorbed by the intestinal epithelium. FFAs are not easily dissolved within the blood plasma and are thus transported in complex with plasma proteins (discussed later) and at their target tissues FFAs are released by lipoprotein lipase (LPL) resulting in non-esterified fatty acids (NEFAs), which are either taken up by target tissue or spill over into the blood plasma. During periods of low glucose availability, triglycerides stored in adipose tissue are used to produce free fatty acids, which can be transported in the blood to be used as energy via fatty acid oxidation.

Lipolysis within the adipocyte is a reversal of TG synthesis as described previously and requires three different enzymes. TGs are converted to DAGs by adipose tissue triglyceride lipase (ATGL), whose expression and activity is tightly regulated. The

expression of ATGL is increased by transcription factors such as PPARs and FoxO1, which are both regulated through complex signalling pathways controlled by insulin, glucocorticoids, fasting and food intake [137, 142]. Hormone sensitive lipase (HSL) is the next enzyme required for lipolysis and converts DAGs into monoacylglycerols (MGs). As with ATGL, HSL is also highly regulated in a phosphorylation and substrate dependent fashion. Activation of HSL occurs through the β-adrenergic receptor/PKA signalling pathway, PKA directly phosphorylates HSL and also phosphorylates perilipin-1, which allows HSL to associate with TGs and DAGs resulting in its full activation [137]. Insulin functions to inhibit lipolysis by activating phosphodiesterases, which deactivate PKA. The third stage in lipolysis is the hydrolysis of MGs by monoacylglycerol lipase (MGL) and the release of FFAs [137]. Both HSL and MGL are expressed ubiquitously and function at target tissues to release FFAs.

In order to generate ATP (and therefore energy) from fat, FFAs must be fed into the Krebs cycle as a result of their catabolism in a process called β-oxidation. FFAs in the cytosol are acylated by a trio of enzymes called acyl-CoA synthases to produce fatty acyl-CoAs. The fatty acyl-CoAs are attached to carnitine, via the acyl group, so they can be transported across the mitochondrial membrane by the carnitine carrier protein. Once in the mitochondria, the carnitine group is removed leaving the fatty acyl-CoA to enter the β-oxidation pathway. The fatty acyl-CoA undergoes 4 enzymatic reactions to produce β-ketoacyl-CoA, NADH and $FADH_2$ (which can be fed into the electron transport chain to generate ATP) [62]. The resulting shorter fatty acyl-CoA can then re-enter the pathway to be reduced further until just acetyl-CoA is the end product. The acetyl-CoA generated can then enter the Krebs cycle and subsequently generate ATP. In the liver, a substantial amount of acetyl-CoA is actually used to generate ketone bodies such as acetoacetate and D-β-hydroxybutyrate, which are plasma soluble and used especially by the heart, brain and muscle when glucose is unavailable [62]. Acetyl-CoA is used in a series of reactions to generate acetoacetate and acetyl-CoA. The acetoacetate generated can be further reduced to β-hydroxybutyrate by β-hydroxybutyrate dehydrogenase [62].

1.5.4 Regulation of Lipid Metabolism

Dietary fats consist mostly of triglycerides but also cholesterol (from animal fat), phospholipids and phytosterols (from plants). The composition of dietary triglycerides is dependent on their source and includes saturated FAs, monounsaturated FAs and polyunsaturated FAs. Saturated FAs are fatty acid chains with no branching and so all the carbon atoms are saturated with hydrogen, whilst monounsaturated fats have one double bond between chains and similarly polyunsaturated fats contain numerous bonding

between chains [143]. Cholesterol is an essential sterol used in the assembly of membranes, and in the synthesis of steroid based hormones and some vitamins [144]. The cholesterol found in the intestines is mostly from bile and dead mucosal cells with only a small proportion from food [145]. As previously mentioned, fats in the intestines are broken down into FAs by lipases and enter the enterocyte via passive diffusion although there is also evidence for FA transporters [146]. Within the ER, FAs are re-esterified into TGs and cholesterol is also esterified followed by packaging into chylomicrons. In the ER, apolipoprotein B-48 (apoB 48) and microsomal triglyceride transport protein (MTTP) cooperate to form chylomicrons, which undergo exocytosis into the lymphatic system and then subsequently into the bloodstream [146, 147]. When chylomicrons pass through adipose, muscle and heart tissue the enzyme lipoprotein lipase causes the release of TGs, as FFAs and MGs, from the chylomicrons leaving chylomicron remnants (CRs), which are now enriched with cholesterol [62]. At this point, apoE is donated to the CRs, which are then released back into the circulation. The FFAs and MGs released from chylomicrons are then taken up by the surrounding tissue or enter the general circulation as NEFAs [148]. Those FFAs and MGs that enter the surrounding tissue are either fed into β oxidation and subsequently the Krebs cycle or re-esterified into TGs for storage. The CRs remain in the circulation until they pass the liver where the CRs are then endocytosed and degraded to release glycerol and FAs into the cytoplasm, which can subsequently be used in β oxidation, membrane synthesis and so forth [144].

The liver is the major organ responsible for releasing lipids into the bloodstream and as such synthesises a variety of lipoproteins capable of carrying TGs and cholesterol. The largest of these is very low density lipoprotein (VLDL), which is similar to chylomicrons accept that VLDL contain apoB 100 instead of apoB 48 [143]. The hepatic pool of TG used in the formation of VLDL is believed to be derived from TGs synthesised from excess carbohydrates after a meal, which are then secreted so that the TGs can be stored in the adipose tissue [149]. VLDL also contain cholesterol and can be hydrolysed to release TGs resulting in the formation of intermediate density lipoproteins (IDL) and low density lipoproteins (LDL). Low density lipoproteins (LDL) also contain apoB 100 but contain more cholesterol compared with VLDL or chylomicrons. LDLs transport de novo-synthesized cholesterol to cells that express LDL receptors, which allows these cells to take up the cholesterol for steroid hormone biosynthesis or plasma membrane synthesis. The final lipoprotein is high density lipoprotein (HDL), which has the opposite function to the other LDLs in that HDLs transport cholesterol from the tissues to the liver. [150].

The control of whole body lipid homeostasis is regulated by substrate availability and hormones. Circulating levels of NEFAs and TGs have an impact on both intestinal and hepatic secretion of lipoproteins by increasing substrate availability such as after a meal.

Similarly glucose also increases VLDL release by increasing the cellular pool of TGs derived from lipogenesis. However periods of prolonged high NEFA and TG levels lead to hepatic ER stress and a reduction in lipoprotein secretion [151]. Insulin has been shown to decrease lipoprotein production through inhibition of FoxO1 [151]. Glucagon decreases plasma levels of TGs and FFAs by reducing TG synthesis in the liver during fasted states. The intestinal hormones GLP-1 and GIP also reduce plasma TG levels via differing mechanisms by reducing apo B expression, TG absorption or by promoting chylomicron clearance, respectively [151].

The major regulation of whole body FFAs resides in the function of adipose tissue, which is discussed below.

1.5.5 Adipokines

Adipose tissue is a dynamic organ that fluctuates in response to food intake and has been shown to be major regulator of whole body lipid and glucose homeostasis by functioning in a similar fashion to other endocrine organs. Adipose tissue is responsible for the synthesis and secretion of a number of factors that have varied effects throughout the body and are termed adipokines.

Leptin is a 16kDa hormone secreted mostly by adipose tissue (but also in small amounts from skeletal muscle, liver and intestines) and was discovered as a result of the generation of the ob/ob mouse, which is a leptin knockout that presents with severe weight gain [152]. Originally it was thought leptin was required to reduce weight gain, however it is now evident that leptin increases with weight gain and decreases with weight loss [153]. Adipose tissue secretes leptin in response to insulin, glucocorticoids, oestrogen, cytokines and feeding whilst cold exposure, fasting, exercise, testosterone, noradrenaline and adrenaline all decrease plasma leptin levels [152, 153]. The major function of leptin is the regulation of energy expenditure and food intake. Leptin receptors (Ob-R) are expressed in high concentrations in the hypothalamus, but also in low levels in other tissues such as the β-cells of the pancreas and in skeletal muscle [153]. In the hypothalamus, leptin binding to Ob-R results in the association of Janus kinases (JAKs) and subsequent activation of signal transducers and activators of transcription (STATs). This leads to changes in gene expression and results in reduction in neuropeptide Y and agouti-related protein (AGRP) and an increase in prepro-melanocortin (POMC) and cocaine- and amphetamine-regulated transcript (CART), which are either orexigenic or anorexigenic [152, 153]. Leptin can alter sympathetic stimulation of tissues through alteration of noradrenaline and as such increases uncoupling protein -1 (UCP1)

expression in brown adipose tissue [152]. This leads to increased fatty acid oxidation through the uncoupling of the proton gradient of mitochondria and thus an increase in energy expenditure [62]. Furthermore leptin also has some direct effects within peripheral tissues, for example in the skeletal muscle leptin results in the activation of AMPK and subsequently increases fatty acid oxidation [145]. In the β cells of the pancreas, leptin decreases insulin production and secretion as well as β-cell growth; the decrease in insulin output provides a feedback loop since insulin causes leptin release from adipose tissue [147].

The opposing hormone to leptin is another adipokine called adiponectin, which is solely released by adipose tissue. Adiponectin secretion is stimulated by insulin signalling and reduced by β-adrenergic signalling. The hormonal effect of adiponectin is the augmentation of insulin sensitivity in target tissues such as skeletal muscle and the liver [148, 154-156]. The structure of adiponectin is of great consequence. It can be secreted as trimers, hexamers or dodecamers. The dodecamers are termed high molecular weight (HMV) forms and the hexamers low molecular weight (LMW) forms. The HMV form of adiponectin is the most active and abundant in the plasma [157]. The expression of adiponectin mRNA is positively controlled by PPARγ and a complex of FoxO1-C/EBPα, which are regulated by ERK and GSK3 [154]. The post-translational modifications of adiponectin are also vital to its HMV formation. Retention by ER protein 44 (ERp44) is critical to HMV formation whilst the ERp44 binding partner Ero-1Lα functions to release adiponectin in a process regulated by NAD-dependent deacetylase sirtuin-1 (SIRT1) [154, 157]. The adiponectin receptor comes in two forms called AdipoR1 and AdipoR2, which are both expressed in the liver whilst AdipoR1 is expressed in the muscle and hypothalamus [148]. In the liver, adiponectin acts via AdipoR1 to activate AMPK resulting in decreased lipogenesis and gluconeogenesis whilst AdipoR2 activates PPARα leading to increased β oxidation [148]. In skeletal muscle, AdipoR1 activates AMPK leading to increased β oxidation (through ACC phosphorylation) and increased glucose uptake [157]. In the β cells of the pancreas AdipoR1 and AdipoR2 are thought to activate ERK resulting in the maintenance of β cell survival and function by increasing insulin synthesis and secretion [155]. Adiponectin receptors expressed by adipocytes have been linked to decreased TNFα and IL-6 release and also lead to increased expression of genes for proteins involved in fatty acid oxidation [155].

Two adipokines that have been identified within the last 15 years are resistin and visfatin [158, 159]. The physiological roles of these adipokines are not as clearly defined as those of leptin or adiponectin and there are some stark differences in both resistin and visfatin between mice and humans. Resistin is produced by adipocytes in mice but by adipose

tissue macrophages (ATMs) in humans. Furthermore, the control of resistin expression in response to hormones and meal status has not yet been fully elucidated. Glucose and glucocorticoids have been shown to increase resistin expression; however mRNA and protein levels are not well correlated [157, 160]. The effect of insulin is also not well characterised; studies have shown that insulin and TZD treatments can both increase and decrease resistin expression [158, 161, 162]. Resistin circulates within the plasma as trimers and hexamers, although the physiological relevance of this in not understood [157]. The function of resistin is also not well understood but has been reported to negatively regulate GLUT4 levels, activate suppressor of cytokine signalling 3 (SOCS3, which inhibits insulin signalling) and induce gluconeogenesis in the liver [160]. Resistin has also been strongly implicated in an inflammatory role, in both humans and mice resistin prolongs TNFα, IL-6 and monocyte chemoattractant protein-1 (MCP-1) production and also increases the expression of these pro-inflammatory cytokines from immune cells [160].

Similarly to resistin, visfatin is also secreted by immune cells and adipocytes and its regulation and function is not completely understood. The first study that classified visfatin as an adipokine reported that visfatin mutations result in increased plasma glucose levels and also led to insulin-mimetic effects [159]. However, this paper was later retracted [163] due to issues about visfatin and insulin receptor binding. Other studies have shown a correlation between visfatin levels and hyperglycaemia [164] and other data also showed visfatin regulates SIRT1 in β pancreatic cells leading to increased insulin synthesis and secretion [165]. Interestingly visfatin is strongly correlated with insulin resistance and T2DM but may represent a protective mechanism employed by the body [164].

Adipocytes are able to synthesise and secrete a number of cytokines such as TNFα and IL-6, although similarly to visfatin and resistin, resident immune cells of adipose tissue are responsible for the majority of plasma levels. TNFα is a 26kDa protein synthesised in response to lipopolysaccharide (LPS) and other bacterial products, IL-1, leptin, insulin and nutritional status in both adipocytes and tissue-resident T cells and macrophages [166, 167]. The longer 26kDa form of TNFα is secreted as a membrane bound form and is cleaved into a soluble 17kDa form by TNFα converting enzyme (TACE) at the plasma membrane [167]. The effects of TNFα have mostly been studied in terms of obesity and insulin resistance and so they will be discussed in the next section. Similarly to TNFα, IL-6 is also expressed by both adipocytes and adipose tissue resident macrophages. It is synthesized and released in response to both TNFα and exercise. Interestingly, IL-6 has

differing effects in muscle, adipose tissue and liver; furthermore muscle actually releases IL-6 in response to exercise. IL-6 causes increased leptin release and decreased adiponectin secretion along with decreases in LPL activity and increases in lipolysis. In skeletal muscle, IL-6 has been shown to increase glucose uptake and β oxidation [157]. However, in hepatocytes and adipocytes IL-6 leads to a reduction in insulin signalling [157].

1.5.6 Obesity and the Metabolic Syndrome

Obesity is characterised by a BMI over 30kg/m^2; in England 61.3% of adults and 30% of children are classified as obese, costing the NHS more than £5 billion per annum [168]. Obesity involves increased adiposity resulting in a substantial increase in the incidence of T2DM, cardiovascular disease (CVD), cancer and reduced life expectancy [169]. When insulin resistance, T2DM or impaired glucose tolerance occurs in combination with two of the following: high blood pressure, increased TG levels, abdominal obesity or low HDL, this is termed 'the metabolic syndrome' and its consequences include CVD or coronary heart disease (CHD) [170].

The obvious treatment for obesity is weight loss, which can be achieved through surgery, pharmacological treatment and lifestyle choice. However, the secondary diseases caused by obesity, i.e. T2DM, cardiovascular disease, etc., require anti-diabetic drugs (metformin, thiazolidinediones), statins (inhibitors of HMG-CoA reductase and therefore endogenous cholesterol production) and anti-hypertension drugs (ACE inhibitors etc). Furthermore the complications of metabolic syndrome are numerous and expensive to treat and so further research needs to be conducted in order to elucidate the relationship between obesity, T2DM and CVD, hopefully leading to cheaper more effective treatments or prophylactic measures.

Obesity is quite clearly a result of overfeeding and a lack of physical activity. There is a strong relationship between obesity and diets high in fat and refined carbohydrates (i.e. sugar). In the USA, 30% of calories from normal diets are obtained from fat, whilst those classified as obese obtain 60% of their calories from fat [171]. In the USA and UK the rise in obesity has been shown to be strongly correlated with increased caloric intake, whilst energy expenditure (i.e. physical activity) has remained fairly constant [172]. The current understanding of the complications associated with obesity is mostly closely related to visceral adiposity (VAT). This describes the fat depot found within the abdominal cavity and is more metabolically active than subcutaneous fat (SAT, fat under the skin) [173]. During the pathogenesis of obesity, the VAT undergoes major changes, which then contribute to the occurrence of T2DM and CVD. Increased fat and sugar consumption leads to the storage of TGs in adipose tissue, mostly in VAT, resulting in adipocyte

hypertrophy. Increased adipocyte size can lead to an increase in adipogenesis in order to store the excess dietary fats and increased fat deposition within the liver, muscle, pancreas, heart and kidneys [173, 174]. In turn, this leads to the two major contributors of insulin resistance/T2DM and CVD; dyslipidaemia and dysfunctional adipokine release. We shall discuss this in detail with regards to the development of T2DM.

The pathogenesis of T2DM in relation to abdominal obesity is complex and there is still much to be learned about the mechanisms involved. The current understanding suggests that insulin resistance is caused by dysregulation of adipokines in combination with increasing TG and NEFA levels. This is then followed by dysfunction of insulin secretion by β pancreatic cells, which culminates in the presentation of T2DM [175]. The current theory in the simplest terms is as follows (Fig. 1.5): increased fat intake results in T cell and macrophage activation and the expression of inflammatory cytokines and chemokines that cause phenotypic switching of adipose tissue macrophages (ATMs) and T cells to release pro-inflammatory cytokines leading to local and systemic insulin resistance. Adipose tissue dysfunction then leads to further increases in plasma FFAs and TGs along with deregulation of adipokines and cytokines, resulting in β-cell dysfunction and therefore T2DM [176-178].

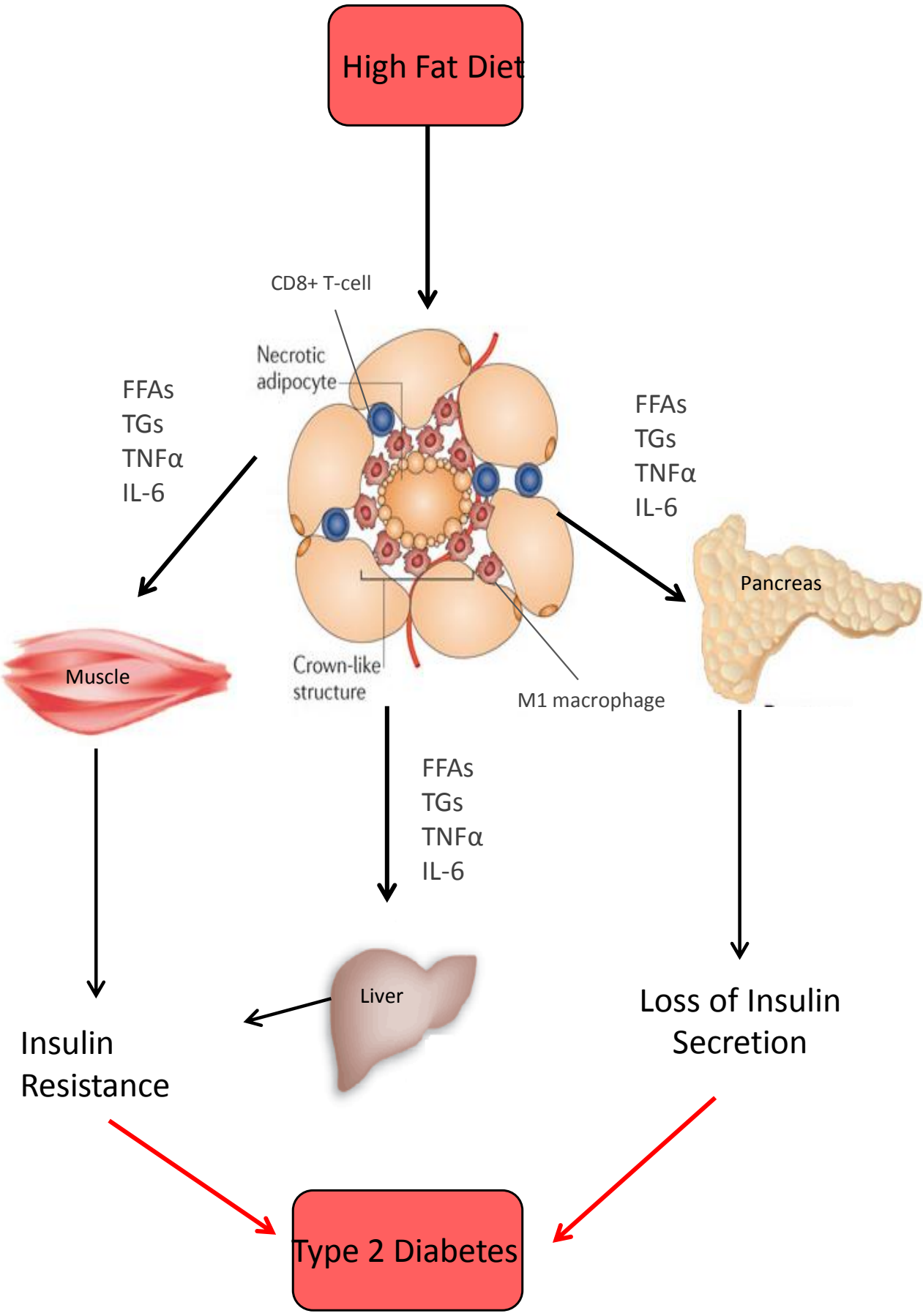
High Fat Diet
CD8+ T-cell
Necrotic adipocyte
FFAs
TGs
TNFα
IL-6
FFAs
TGs
TNFα
IL-6
Pancreas
Muscle
Crown-like structure
M1 macrophage
FFAs
TGs
TNFα
IL-6
Liver
Insulin Resistance
Loss of Insulin Secretion
Type 2 Diabetes

Figure. 1.5. Role of obesity in whole body insulin resistance. Increased release of adipokines from obese adipose tissue and resident immune cells leads to insulin resistance in the adipocyte, skeletal muscle and liver as well as β cell dysfunction and loss of insulin secretion culminating in type 2 diabetes. Adapted from [179-181].

Normal adipose tissue contains ATMs, but it also contains resident T cells of numerous lineages including Th1, Th2 and T_{reg}. Obesity causes an infiltration of both macrophages and T cells but also leads to an increase in inflammatory phenotypes of those immune cells that are already resident within the adipose tissue [177]. The activation of immune cells in response to obesity is not well understood, but is thought to involve chemokines, FFAs, hypoxia, adipocyte hypertrophy and adipokines. In lean adipose tissue, a unique population of T_{reg} cells (different to T_{reg} cells of other tissues) are present and believed to be important in maintaining insulin sensitivity of adipocytes, regulate Th1 cells and maintain the phenotype of ATMs [182]. The onset of obesity leads to a reduction in T_{reg} cells possibly due to a reduction in adiponectin and increase in leptin, which leads to an increase in $CD8^+$ and $CD4^+$ *Th1 cells* [182, 183]. Similarly the increase in FFAs, hypoxia and adipocyte hypertrophy results in recruitment of macrophages. FFAs specifically result in activation of toll like receptor 4 (TLR4) in macrophages leading to activation the of the NF-κB pathway, which is responsible for the expression of pro-inflammatory cytokines [176]. The increase in Th1 cells and CD8+ cells results in the release of IFNγ, TNFα and "regulated on activation normal T cell expressed" (RANTES), which function to recruit and polarize macrophages to an M1 phenotype. In normal lean adipose tissue macrophages are found in a mostly M2 phenotype. The M2 macrophages are activated by IL-4 and IL-13 and are characterised by the expression of IL-10, arginase I and IL-1 receptor antagonist [176, 177]. However during obesity the large increase in inflammatory cytokines and chemokines such as monocyte chemotactic protein-1 (MCP-1) leads not only to the infiltration of M1 macrophages but also to the phenotypic switching of M2 to M1 macrophages and the maintenance of a low grade chronic inflammatory state. M1 macrophages release TNFα, IL-1β, IL-6, which can then result in insulin resistance [176, 177]. The majority of M1 macrophages are found in "crown-like structures" surrounding adipocytes that are dead or dying, this then leads to further increases in FFAs and TGs in a spill over fashion [184].

The release of pro-inflammatory cytokines not only maintains ATMs and T cells but also results in local and systemic insulin resistance followed by β pancreatic cell dysfunction and the progression to T2DM. Locally within the adipocyte, TNFα causes insulin resistance by facilitating the degradation of insulin receptor substrate 1 (IRS1) and a reduction in the expression of adiponectin, GLUT4, C/EBPα and PPARγ [184]. The combination of a decrease in the inhibitory effect of insulin on lipolysis and the stimulatory effect of TNFα on lipolysis results in the increased release of FFAs from adipocytes, which can act locally on macrophages and adipocytes and also enter the circulation [185]. Furthermore, TNFα also leads to increases in IL-6, IL-1β, resistin and leptin, which all contribute to systemic insulin resistance and β pancreatic cell failure. The presence of

TNFα in the circulation results in insulin resistance in both the muscle and liver [186]. Within the skeletal muscle, TNFα causes insulin resistance in a similar fashion to adipocytes, i.e., it increases IRS1 degradation, but TNFα also suppresses fatty acid oxidation by decreasing AMPK activation resulting in accumulation of TGs, which in itself also further contributes to insulin resistance [187, 188]. Hepatic insulin resistance caused by TNFα involves activation of JNK and PKC, which phosphorylate IRS1 leading to its degradation and promotes increased gluconeogenesis and glycogenolysis [189]. The effect of IL-6 is complicated: in adipose tissue and the liver IL-6 results in insulin resistance in much the same way as TNFα does. However in the muscle IL-6 actually increases fatty acid oxidation and glucose utilization and so its contribution to whole body insulin sensitivity is complex and not yet fully understood [153]. The reduction in adiponectin seen in obesity also contributes to insulin resistance. Adiponectin (as discussed previously) enhances glucose uptake into muscle along with fatty acid oxidation. Furthermore, in the liver, adiponectin reduces gluconeogenesis [153]. Leptin resistance occurs during obesity due to the consistently high levels of leptin secreted by the enlarged adipocytes. This has been proposed to be caused by perturbed leptin signalling, decreased transport across the blood brain barrier and reduced numbers of leptin receptors (reviewed [190]). Consequently, this contributes to insulin resistance because leptin is required to reduce TG accumulation in liver and muscle [191]. Resistin has been associated with obesity and T2DM, there is some evidence of increased expression in obesity and this may lead to decreased AMPK activity resulting in changes to insulin sensitivity and glucose uptake in target tissues [157, 160]. Finally the increase in serum TGs and FFAs contribute to insulin resistance in the obese state. In the muscle increased TGs and FFAs are stored as intramyocellular TGs (IMTGs), which can contribute to insulin resistance. The intermediates of IMTGs such as ceramides have been shown to reduce PKB phosphorylation, whilst DAG, which activates several PKC isoforms, leads to down regulation of IRS1 [192]. In the liver, FFAs cause increases in DAG and, as in muscle, this leads to PKC activation and subsequent IRS1 degradation. FFAs also activate the NF-κB pathway leading to pro-inflammatory cytokine production and subsequent insulin resistance [175, 193].

Progression from insulin resistance to T2DM involves many of the above factors and their effects on β pancreatic cell function, which is seen as initial hyperinsulinemia followed by loss of insulin secretion. The cytokines produced during the chronic inflammatory state of obesity result in detrimental changes to β cell function. Pancreatic islets express TNF receptor 1(TNFR1) and TNFα binding causes a reduction in glucose-stimulated insulin secretion (GSIS) and also inhibits IL-1β action, which is required to protect β islets from

glucotoxicity [178]. In combination with IFNγ, TNFα causes apoptosis of β cells, whilst also interfering with insulin signalling within the islets, a process which is required for β cell function and regulation of insulin gene expression [178, 194]. The effects of IL-6 are protective towards islet function and insulin secretion. IL-6 receptor signalling increases insulin secretion and blocks apoptotic pathways induced by TNFα, IFNγ and IL-1β, it is therefore possible that increases in IL-6 in obesity are a protective mechanism to alleviate the impact of other inflammatory cytokines [178]. Leptin is highly upregulated in obese adipose tissue and as well as its role in insulin resistance has been linked to the dysfunction of β cells. Leptin acting through the ObRb receptor expressed on β cells, reduces insulin secretion and inhibits GSIS through a complex mechanism involving increased hyperpolarization of the cell membrane and reductions in cAMP levels [178]. Leptin also inhibits apoptosis of islets by modulation of nitric oxide through increasing FA oxidation and reducing TG storage, which in turn reduces inducible nitric oxide synthase (iNOS) expression. As previously mentioned, obesity leads to a state of leptin resistance, which occurs in islets leading to abnormal insulin secretion (hyperinsulinaemia) followed by eventual exhaustion and apoptosis of β cells during the progression of T2DM [178]. The effects of adiponectin on islets is poorly researched and not well understood. Some evidence suggests adiponectin is required for β cell function to correct abnormal insulin secretion but not through direct action upon insulin secretion pathways [178]. Similarly to the effects on insulin resistance FFAs have a strong role in β cell dysfunction in obesity related T2DM. The initial effect of FFAs is an increase in insulin secretion by modulating intracellular calcium concentration and activation of PKC; however, prolonged exposure to FFAs results in an inhibition of GSIS through changes in β oxidation, increased UCP-2 expression and modulation of K_{ATP} channels [178]. Furthermore, FFAs inhibit insulin expression and can induce apoptosis by ER stress in an NO-dependent mechanism and a reduction in anti-apoptotic factors (e.g. BCL-2) [178, 195].

Greater understanding of all of the above mechanisms of obesity induced T2DM (and CVD) will lead to cheaper, more effective treatments. However global and governmental policy on the amount of fat and cost of fatty foods would go a very long way to resolving the global epidemic of obesity and its related diseases.

1.6 Insulin Signalling

1.6.1 Overview

Insulin, as previously discussed, is synthesised by the β-cells of the islets of Langerhans within the pancreas. In response to changes in blood glucose levels, as a result of the ingestion of food and absorption of glucose by the intestines, insulin is secreted by these cells and has numerous effects upon cells that contain either insulin receptors or insulin like growth factor receptors (IGFR) [196]. The physiological effects of insulin are general anabolic effects on carbohydrate, fat and protein metabolism [196] (Fig. 1.6), but also importantly the control of protein synthesis through regulation of translation initiation and elongation, in various cell types [197].

Situations of abnormal insulin signalling can cause a number of diseases including diabetes, (and the associated consequences of T2DM such as heart disease and kidney disease), cancer, metabolic syndrome and polycystic ovary syndrome [198, 199]. Understanding the intricacies of insulin signalling is paramount to identifying novel therapeutic targets and root causes of these diseases.

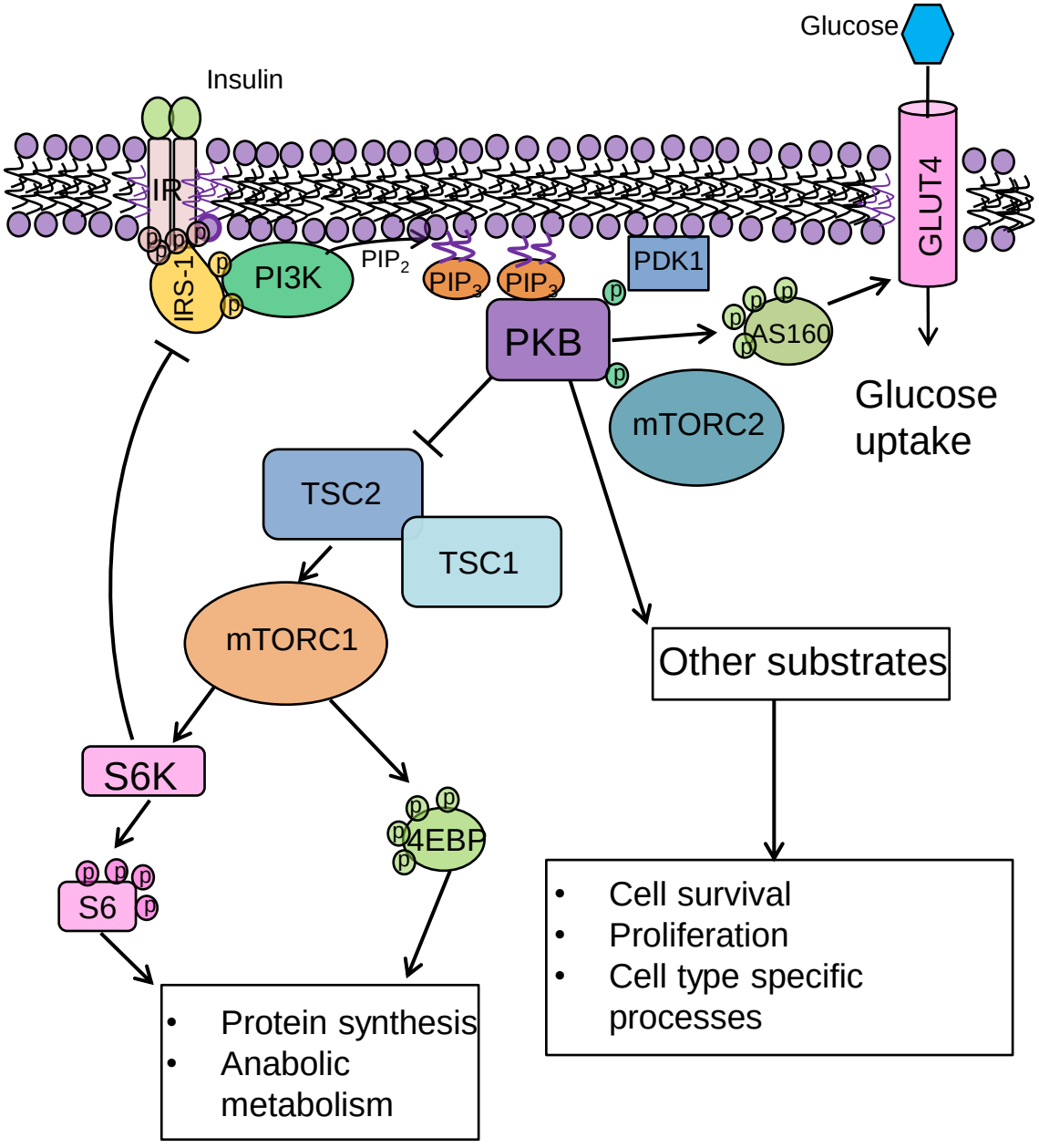

Figure. 1.6. Cellular effects of insulin. A simplified schematic of the insulin signalling cascade and the major signalling components engaged by the insulin receptor. Insulin binds to its receptor resulting in its autophosphorylation and activation. This leads to the recruitment of insulin receptor substrate 1 (IRS1), which in turn leads to the activation of phosphatidylinositol 3-kinase (PI3K). PI3K phosphorylates PIP_2 within the plasma membrane to produce PIP_3, which functions as a docking protein for protein kinase B (PKB) and phosphoinositide-dependent kinase 1 (PDK1). Both PDK1 and mTORC2

phosphorylate and activate PKB. The activation of PKB results in numerous changes to downstream signalling pathways. Abbreviations: tuberos sclerosis complex 2/1 (TSC2/1), p70 S6 kinase (S6K), eIF4E binding protein (4EBP), Akt substrate 160 (AS16)), glucose transporter 4 (GLUT4).

1.6.2 Insulin Signalling Cascade

The insulin receptor is part of the RTK family and as such shares similarities with other receptors in this group. The insulin receptor, along with the IGFR and insulin receptor-related receptor (IRR) form a subgroup within the RTK family. These receptors are all formed from four subunits arranged as dimers that consist of an α and β subunit and are distinct from class I RTK's, which only form dimers after ligand binding [196]. As the RTK name suggests these receptors have enzymatic activity and their α subunits can allosterically inhibit the β subunit until ligand binding occurs. The effect of ligand binding is complex and not fully understood, but it is known that there are two low affinity sites on each receptor monomer and binding at site 1 causes crosslinking with the ligand bound at site 2 in the other monomer [200]. This in turn causes a conformational change that removes the inhibitory influence of the α subunit towards the β subunit [196]. The dimerization of the insulin receptor causes the β subunit of one monomer to trans-phosphorylate tyrosines 1158, 1162 and 1163 of the cytoplasmic domain of the opposing monomer. The phosphorylation of these tyrosines causes a conformational change of the activation loop, which results in ATP binding and kinase activation [201]. The phosphotyrosines within the β subunit of the insulin receptor produce docking sites for essential signal-transducing proteins such as the 'insulin receptor substrates' (IRS). There are four known IRS proteins; 1,2, 3 and 4. Both IRS1 and IRS2 are ubiquitously expressed but found to be expressed at the highest levels in the liver, skeletal muscle, adipose tissue , kidney, heart, brain and spleen, whereas IRS3 is specific to rodent adipose tissue and IRS4 is only found in the brain, thymus, kidney and liver [202, 203]. Data from IRS knock-out animals shows IRS1 and IRS2 to be the important isoforms for propagation of insulin signalling in relation to glucose uptake and so we shall focus on these isoforms from now on [204, 205]. The sequences of IRS1 and IRS2 share 75% sequence homology, and share some common binding partners whilst also showing differing roles in the insulin-dependent activation of downstream pathways. The N-terminal region of both IRS1 and IRS2 contain a pleckstrin homology (PH) domain and phospho-tyrosine binding domain (PTB), which, are both required for optimal IRS1 phosphorylation by the insulin receptor. The PTB domain binds to the NPXY motif within the insulin receptor, whilst the PH domain binds to membrane lipids and in an unknown manner facilitates IRS1-insulin receptor binding and subsequent tyrosine phosphorylation of IRS1 [203]. The longer activation period of IRS1 and its ability to tightly bind Grb2 explains how IRS1 activates the MAPK pathway, which IRS2 is not capable of due to its transient activity [206]. Both IRS1 and another insulin receptor binding protein, Shc, can bind to Grb2 and SOS, which results in the activation of the Ras/Raf/MEK pathway and therefore consequently ERK (reviewed [207]). Under basal conditions both IRS1 and IRS2 are found in intracellular membranes (IM)s along with the p85α subunit of phosphatidylinositol

3-kinase (PI3K), upon insulin stimulation these proteins move to the cytosol [208] and bind to the phospho-tyrosines on the insulin receptor. This in turn leads to tyrosine phosphorylation of IRS1 at least 8 sites with potential for up to 20 [203, 208]. Numerous proteins can bind to the phosphotyrosines of IRS1/2 via SH2 domains including Grb2, SHP-2, 14-3-3 protein and most importantly PI3K. PI3K exists in various combinations of regulatory and catalytic subunits. The class I PI3Ks consist of 5 different regulatory subunits; p85α, p85β, p55α, p55γ and p50α and 4 catalytic subunits p110α, p110β, p110γ and p110δ (leukocyte specific) [203, 209]. The p85α subunit contains two SH2 domains that must both bind to Tyr^{612} and Tyr^{632} of IRS1 in order for full activation of the catalytic p110 subunit. This is achieved by allosteric changes of the p85α subunit caused by the SH2 domain binding IRS1 and removing repression of the p110 subunit and its subsequent positioning close to the plasma membrane where its substrate is located [210, 211]. Once activated, PI3K is then able to phosphorylate the membrane lipid phosphatidylinositol (4,5) bisphosphate (PIP_2) to produce phosphatidylinositol (3,4,5) trisphosphate (PIP_3), which is a crucial docking point for proteins containing PH domains [211, 212]. Two such important proteins are phosphoinositide-dependent kinase 1 (PDK1) and PKB, which bind to PIP_3 . This causes these two kinases to be in close proximity and subsequently PDK1 phosphorylates and activates PKB at Thr^{308} within the PKB T-loop, which is revealed through conformational changes following PIP_3 binding [212, 213]. There is a second site in PKB that is thought to prime PKB for Thr^{308} phosphorylation, this site is Ser^{473}; however the requirement of this site is highly debatable. The kinase responsible for the phosphorylation of Ser^{473} was until recently unknown, it has now been shown that there are (at least) two kinases responsible. Evidence shows that both DNA protein kinase (DNA-PK) and mTORC2 can both phosphorylate this site in response to DNA damage or mitogens, respectively [214]. The exact contribution of this site to the activity and selectivity of PKB is widely debated but mTORC2 dependent Ser^{473} phosphorylation is thought to be the most relevant [215]. The effect of PKB activation is a long list and encompasses cellular events including; protein synthesis, glucose uptake, transcription, cellar proliferation, angiogenesis, lipid metabolism and others [215].

1.6.3 Control of Glucose Uptake by Insulin

Insulin stimulates several signalling pathways, which, as already mentioned, have numerous different cellular functions. One such major pathway involving IRS1/PI3K/PKB has already been described above; here the specific control of glucose uptake by PKB-dependent and -independent mechanisms will be discussed.

Insulin-stimulated glucose uptake is mediated by GLUT4, which is part of a family of sugar transporters with 14 members [216]. Cellular glucose homeostasis is very intricately controlled and involves the regulation of GLUT4 localisation in the *Trans*-Golgi network (TGN). Upon insulin stimulation GLUT4 is translocated to the plasma membrane, followed by recycling into either sorting endosomes, recycling endosomes or back to the TGN. We shall discuss translocation to the plasma membrane as this is the most relevant to this study.

Under basal conditions GLUT4 can be found in a specialized storage system known as GLUT4 storage vesicles (GSVs). The definitive composition of GSVs is still an area of active research, the evidence so far indicates that GSVs contain GLUT4, insulin-regulated aminopeptidase (IRAP), sortilin, vesicle-associated membrane protein 2 (VAMP2) and lipoprotein receptor-related protein 1 (LRP1). These vesicles are retained at their point of formation, which is the TGN, the exact mechanism of GSV formation and retention is still not well understood. It is thought that multimers of GLUT4, IRAP, sortilin and LRP1 are sorted in the TGN and along with adaptor proteins, which are recruited by a GTPase, ADP-ribosylation factor 6 (ARF6), allow vesicular budding and clathrin coating to occur [216, 217]. Under basal conditions GSVs are thought to be retained in the TGN by the activity of RAB31 (a GTPase) and tether containing UBX domain for GLUT4 (TUG) [218, 219]. There are numerous other RABs that in a cell type-dependent fashion regulate GSV formation and sorting, in the muscle RAB8 and RAB14, whilst in adipocytes RAB10 are all targets of the RAB GTPase activating protein (GAP) Akt substrate 160 (AS160). GSVs are retained in the TGN in part by an inhibitory influence of AS160 on its RABs as well as through the actions of TUG and RAB31. Insulin results in a rapid translocation of GSVs to the plasma membrane and subsequent glucose uptake. This occurs by both a PKB dependent and PKB independent mechanism, PKB activated by insulin through PI3K has recently been shown to phosphorylate Akt substrate of 160kDa (AS160) [220]. There are six known PKB phosphorylation sites on AS160: Ser^{318}, Ser^{341}, Ser^{570}, Ser^{588}, Thr^{642} and Thr^{751}; however mutation of just four of them, Ser^{318}, Ser^{588}, Thr^{642}, and Thr^{751}, leads to reduced insulin-stimulated glucose uptake [220]. The link between phosphorylation and GAP activity is one of debate and so the exact mechanism of AS160 regulated GLUT4 translocation is not yet clear but it is most likely that the GAP activity of AS160 is reduced towards RABs resulting in the release of GSVs from tethering by TUG [220, 221]. AS160 is a divergent point for other insulin dependent pathways. Both PKC and AMPK regulate the binding of AS160 with 14-3-3 proteins. This interaction has been shown to be essential to GLUT4 translocation but the mechanism is again unclear [222].

In order for the GSVs to translocate to the plasma membrane there is a requirement for remodelling of the actin-cytoskeleton. For long distance translocation microtubules are

necessary whilst shorter distances requires cortical actin [216, 221]. Insulin is capable of modulating this process by altering the ATPase activity of motor proteins such as KIF3, KIF5B, MYO1C and MYO5B [216, 221, 223]. Once GSVs are close to the plasma membrane, they must be brought to the right compartment, an event which again is controlled by insulin. At exocytosis sites within the plasma membrane, there is a multimeric complex called the exocyst whose assembly is regulated by the control of the association of TC10 with EXO7 by insulin [224]. This process is independent of PKB and involves insulin receptor association with adaptor protein with PH and SH2 domains (APS), which causes insulin receptor phosphorylation of c-CBL. This leads to increased GEF activity of C3G resulting in the activation of the GTPase activity of TC10 [216]. EXO7 is constitutively associated with the plasma membrane and other exocyst components and so association with TC10 leads to its complete formation. [216, 224]. The exocyst interacts with RALA, which is found on GSVs and its activity is controlled by PKB through the RAL-GAP complex. PKB phosphorylates three sites on the RAL-GAP complex, which inhibits the complex resulting in the association of GTP with RALA, its subsequent activation and exocyst formation [225].

The final step in this process involves the dissociation of GSVs from the exocyst and fusion with the plasma membrane. Insulin activated PKC phosphorylates RALA resulting in its dissociation from the exocyst [226]. This then allows fusion through VAMP2 on GSVs and syntaxin 4 (STX4) at the plasma membrane. It is thought this may be regulated in a PKB dependent fashion but the substrates and exact mechanism is not yet known [216]. Furthermore, there is evidence the insulin receptor mediates tyrosine phosphorylation of MUNC18, which is associated with STX4 and that its dissociation from STX4 is required for GSV fusion [227].

1.6.4 The Mnks and Insulin Signalling

Data from two patents claim Mnk2 as a possible treatment target for T2DM; however they show opposing data sets using different methods [106, 228]. One patent shows mice treated with an Mnk2 inhibitor have increased insulin sensitivity and increased glucose uptake [106]. Investigation into the normal expression of Mnk2 showed high levels in the muscles and brown adipose tissue [228]. These authors generated a dominant negative Mnk2 mouse (Mnk2DN), which involved a T-loop phosphorylation mutant of Mnk2a attached to β-actin injected into mouse embryos and implanted into pseudo-pregnant females. The offspring selected for their expression of the β-actin-Mnk2 mutant.

Comparison of the Mnk2DN mice to normal WT mice showed them to have increased weights [228]. However, this evidence must be treated with caution since the overexpressed dominant-negative Mnk2 (Mnk2DN) can bind tightly to p-ERK, causing its sequestration and potentially leading to off target effects by inhibiting phosphorylation of other ERK targets. This may explain the weight gain and changes in insulin sensitivity. This evidence needs to be investigated more thoroughly and should involve the use of Mnk2 knock-out (KO) mice instead of Mnk2DN mice, which may provide a more conclusive answer. There is no other evidence available that has investigated the potential role of the Mnks in the insulin signalling pathway.

1.7 Aims of this Study

The functional roles of the Mnks are still elusive despite 15 years of research. The majority of research focuses on the effect of Mnk-dependent eIF4E phosphorylation in tumorigenesis and cytokine signalling pathways. There is evidence that eIF4E phosphorylation is increased in response to rapamycin, which may indicate a resistance mechanism involving the Mnks. This may explain the less than desirable efficacies of rapalogs in clinical trials for cancer therapy. The exact cause of rapamycin-induced eIF4E phosphorylation has yet to be established and is investigated in this study. Using a variety of approaches including inhibitors of the Mnks, Mnk knockout cells, Mnk knockout mice as well as both *in vivo* and *in vitro* methods the aim of this work is identify novel functions and substrates of the Mnks with specific relation to glucose and lipid metabolism.

Chapter 2

Methods and Materials

2.1 Chemicals, Biochemicals, Reagents and Antibodies.

The majority of chemicals used for these methods were purchased from Sigma-Aldrich, Fisher Scientific or Calbiochem. Tissue culture reagents were brought from Invitrogen. SDS-PAGE reagents were purchased from Bio-Rad including running and transfers buffers and nitrocellulose (0.45µm pore size) membrane. Antibodies can be seen in Table 2.1. Radiolabelled chemicals were brought from Perkin Elmer.

2.2 Buffers and Solutions.

All solutions and buffers were made using milliQ deionised water. The following list comprises those used throughout this thesis.

1X Phosphate Buffered Saline (PBS)

2mM KH_2PO_4, pH 7.4

10mM Na_2HPO_4

4 mM KCl

170 mM NaCl

Luria-Bertani (LB) Broth

1% (w/v) Bacto®-tyrptone pH 7.5

0.5% (w/v) Bacto®-yeast extract

0.5% (w/v) NaCl

LB Agar Plates

LB broth with 1.5% (w/v) Agar

TAE Buffer

0.1M Tris-borate pH 8.0

2mM EDTA

5X Sample Buffer

62.5 mM Tris- HCl pH 6.8

7% (w/v) SDS

20% (w/v) sucrose

0.01% (w/v) Bromophenol Blue

5% (v/v) β-mercaptoethanol

10X Running Buffer

25mM Tris

192mM Glycine

0.1% (w/v) SDS

Transfer Buffer

25mM Tris

192mM Glycine

20% (v/v) Methanol

0.02% SDS

Coomassie Blue

0.1% (w/v) Coomassie Brilliant Blue

50% (v/v) Methanol

10% (v/v) Glacial Acetic Acid

40% (v/v) H_2O

Lysis Buffer A

20mM Tris-HCl pH 8.0

100mM KCl

50% glycerol

1mM DTT

1% Triton X-100

1X protease inhibitor (PI) cocktail (Roche)

Lysis Buffer B

20mM HEPES-KOH pH 7.5

50mM β-glycerolphosphate

0.2mM EDTA

10% glycerol

1% Triton X-100

1mM DTT

1mM Na_3VO_4

1X PI cocktail

Lysis Buffer C

50mM HEPES-KOH pH7.5

50mM KCl

1mM EDTA

0.5% (v/v) Elugent

1mM DTT

1X PI cocktail

Lysis Buffer D

25mM Tris HCl pH 7.6

50 mM β-GP

50mM KCl

1% Triton X-100

1mM DTT

0.5mM Na_3VO_4

1X PI cocktail

Lysis Buffer E

50mM Tris HCl pH 7.5

1mM EDTA

1mM EGTA

50mM NaF

50mM Na_2PO_4

270mM sucrose

1% Triton X-100

1mM DTT

250µM okadaic acid

1X PI cocktail

1mM Na_3VO_4

Lysis Buffer F

20mM Tris-Hcl pH 8.0

137mM NaCl

2.7mM KCl

1mM $MgCl_2$

1mM $CaCl_2$

10% glycerol

1% Igepal

1mM DTT

0.5mM Na_3VO_4

1X PI cocktail

Lysis Buffer G

40mM HEPES-KOH pH 7.4

120mM NaCl

10mM Na_2PO_4

10mM β-glycerolphosphate

50mM NaF

0.3% (w/v) CHAPS

1mM DTT

0.5mM Na_3VO_4

1X PI cocktail

Lysis Buffer H

50mM Tris HCl pH 8.0

200mM NaCl

0.5% (w/v) SDS

5mM EDTA

0.5mg/ml proteinase K

Lysis Buffer I

20mM Tris-HCl pH 7.5

10% (w/v) SDS

5mM DTT

1X PI cocktail

Dialysis Buffer A

20mM Tris-HCl pH7.5

100mM KCl

5% glycerol

5mM β-mercaptoethanol

0.1X PI cocktail

Dialysis Buffer B

20mM HEPES-KOH pH 7.6

0.2mM EDTA

0.5mM DTT

100mM KCl

5% glycerol

0.1X PI cocktail

Column Buffer

25mM HEPES-KOH pH 7.6

100mM KCl

1mM DTT

Refolding Buffer

8M Urea

50mM HEPES-KOH Ph 7.6

50mM DTT

Refolding Dialysis Buffer

5M Urea

25mM HEPES-KOH pH 7.6

100mM KCl

Wash Buffer A

20mM HEPES-KOH pH 7.5

50mM β-glycerolphosphate

0.2mM EDTA

10% glycerol

Wash buffer B

100mM Tris-HCl pH8.0

0.5M LiCl

Wash Buffer C

10mM Tris-Hcl pH 7.6

150mM NaCl

1mM EDTA

Wash Buffer D

20mM HEPES-KOH pH 7.6

5mM $MgCl_2$

1mM DTT

Wash Buffer E

25mM HEPES-KOH pH 7.4

20mM KCl

Kinase Buffer A

50mM Tris HCl pH 7.5

0.1mM EGTA

10mM β-mercaptoethanol – washes

0.1% (v/v) β-mercaptoethanol – assay

Kinase Buffer B

20mM HEPES-KOH pH 7.5

50mM KCl

2mM $MgCl_2$

Kinase Buffer C pH 7.2

20mM β-glycerolphosphate

5mM sodium pyrophosphate

30mM NaCl

1mM DTT

Kinase Buffer D

25mM HEPES-KOH pH 7.4

20mM KCl

10mM $MgCl_2$

Kinase Buffer E

25mM HEPES-KOH pH 7.4

50mM KCl

20% Glycerol

10mM $MgCl_2$

4mM $MnCl_2$

1mM DTT

KRH Buffer

50mM HEPES-KOH, pH 7.4

136mM NaCl

4.7mM KCl

1.25mM $MgSO_4$

1.25mM $CaCl_2$

2.3 Molecular Biology.

2.3.1 Plasmids.

HA-GLUT4-GFP was a kind gift from Dr Sam Cushman. pCMV5HA-Mnk1a and pCMV5HA-Mnk2a was made by cloning the full length Mnk1a/2a PCR digest into the pCMV5 vector after Hind/Xba digest. Full length Mnk1a and Mnk2a were cloned into the pEBG6P vector or pGEX3X vector after PCR and EcoR1 digest. pGEX3X-IRS1 fragments B-E (Fig. 2.1) (B residues 21-400, C (108-516), D (516-896) and E (899-1235)) were a kind gift from Richard Lamb (University of Alberta, Canada). Serine/threonine mutants of IRS1 (Ser574Ala, Ser629Ala, Ser766Ala, Thr774Ala, Ser794Ala and S-5-A (Ser574Ala, Ser629Ala, Ser766Ala, Thr774Ala and Ser794Ala)) or Mnk2a (Ser74Ala and Ser437Ala) were produced by PCR with primers designed to produce the desired mutation (see table 2.2) using Phusion DNA polymerase (Thermo Scientific). Mammalian expression vectors for IRS1 (D) and IRS1 (S-5-A) were created by EcoR1 digestion of GST-IRS1 WT and S-5-A and insertion into a myc-tagged pCMV3c vector. pET28-eIF4E was made by cloning the full length eIF4E PCR product after Nco1-EcoR1 digest into the pET28 vector.

2.3.2 Transformation of competent E. coli.

Dependent on the vector and DNA insert either DH5α or BL-21 strains of *E. coli* were used. On ice competent bacteria and 1µg of vector DNA were mixed and left for 12min. Samples were then incubated at 37°C for 5min followed by 2min on ice. For 1h samples were incubated at 37°C with 1ml LB broth followed by centrifugation at 2,400 *g* for 5min at room temperature. All but 100µl supernatant was removed in which the pellet was resuspended and then plated onto agar plates containing the antibiotic to which the vector conferred resistance to. Plates were incubated at 37°C overnight and the following day plates were stored at 4°C until required and up to 1 month.

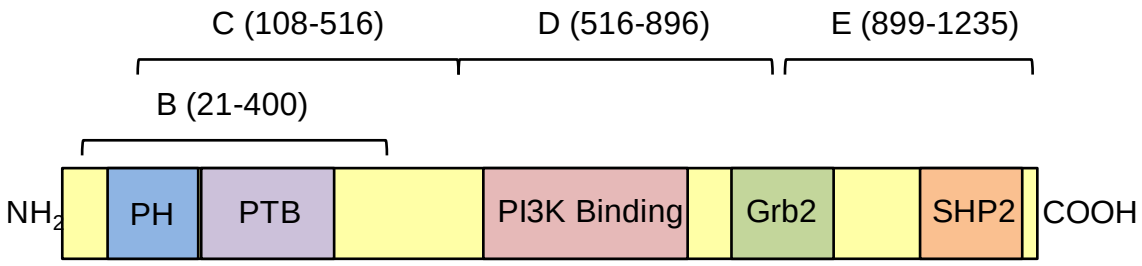

Figure 2.1. Domain structure of IRS1 and the areas covered by pGEX3X-IRS1 fragments. PH refers to Pleckstron Homology domain, PTB refers to phospho-tyrosine binding domain, Grb2 is the site for Growth factor receptor-bound protein 2 binding and SHP2 is the site for protein tyrosine phosphatase, non-receptor type 11 binding. Adapted from [229].

2.3.3 Induction, Expression and Preparation of proteins in E. coli.

Colonies containing the desired vector plus insert, from BL-21 bacteria, were grown overnight in 20ml or 50ml of LB plus antibiotic (100µg/ml ampicillin or kanamycin). The following day this was added to 200ml or 500ml LB plus antibiotic and grown until OD at 600nm is 0.5-0.7. Then 0.5-1mM IPTG was added to induce protein expression for 3 hours at 37°C. Cultures were harvested by spinning at 3,200 *g* 4°C for 15min, the pellet was lysed in 5-10ml lysis buffer A (for IRS1) or lysis buffer B (for the Mnks). Lysozyme (10mg/ml) (100µl/100ml culture) was added to samples for 30min on ice followed by sonication 6X10 sec 30% power. Soluble protein was isolated by spinning samples at 18,000 *g* 15min 4°C and then snap frozen at -80°C.

2.3.4 Purification of GST-fusion proteins.

Soluble protein from bacterial lysates and mammalian cell lysates were mixed with 0.5-1ml glutathione sepharose beads in the respective lysis buffer of the protein and rotated at 4°C for 1h. The supernatant was removed by gravitational flow through columns at 4°C and the beads washed 3X with the bed volume of lysis buffer without Triton. For bacterially expressed Mnk1/2 and IRS1 wildtype and mutant proteins, elution from the beads was achieved by adding 0.5-1ml lysis buffer (without Triton) plus 20mM glutathione creating 3-10 fractions. The fractions were subjected to SDS-PAGE and stained with Coomaisse. The fractions containing protein were pooled and dialysed for 2h for IRS1 then for both IRS1 and the Mnks dialysed overnight in 1litre of dialysis buffer A at 4°C. For Mnk1/2 produced in mammalian cells, bound fusion proteins were subjected to PreScission protease (cleaves between Gln and Gly in the sequence of LeuGluValLeuPheGln/GlyPro and therefore removes the GST tag from tagged proteins) overnight at 4°C and the following day the supernatant was collected by spinning samples at 3,200 *g* for 5min at 4°C. Protein concentration was determined and proteins stored at -80°C.

2.3.5 Solubilisation of eIF4E produced in E. coli.

Production of eIF4E was induced in bacteria as described above. Cultures were harvested by spinning at 3, 200 *g* and the pellet was lysed in lysis buffer C then vortexed thoroughly to shear cellular DNA. Lysates were then spun at 18, 000 *g* 10min 4°C and the supernatant collected and both this and the inclusion body pellet were snap frozen at -80°C. The pellet was resuspended in 20ml refolding buffer (for 200ml cultures) and dialysed against 20 volumes of refolding dialysis buffer at 4°C for 1h, after this time an

equal volume of dialysis buffer B was added to reduce both the urea and DTT concentration and left to dialyse for a further hour. Following this a volume of dialysis buffer B equal to twice the starting volume was added to further reduce the urea and DTT concentration and left for another hour. The cassette was then transferred to 1l dialysis buffer B and dialysed for a further 3 hours with the buffer changed every hour. The solution was then collected and stored overnight at 4°C.

2.3.6 Purification of eIF4E

The protein solution was mixed with 0.25-0.5ml m^7 GTP sepharose in a column and rotated at 4°C for 1h. The column was then washed with the bed volume 6 times with column buffer. eIF4E was then eluted with 10 bed volumes of column buffer with 100µM m^7GTP and a small aliquot of each fraction subjected to SDS-PAGE to determine protein containing fractions. Those fractions found to contain eIF4E were then pooled and dialysed overnight in dialysis buffer A at 4°C and the following day the protein concentration was determined and protein stored at -80°C.

2.4 Cell Biology and Protein Biochemistry

2.4.1 Mammalian Cell Culture

Prior to use, all buffers and media were warmed to 37°C. Cells were grown in an incubator kept at 37°C with 5% CO2. PC3, HEK-293 Mnk1-KO (Mnk1-KO $Mnk2^{+/+}$), Mnk2-KO ($Mnk1^{+/+}$ Mnk2-KO) and DKO (Mnk1-KO Mnk2-KO) MEF cells (a kind gift from Dr Rikiro Fukunaga, Kyoto University, Japan) were cultured in DMEM (Dulbecco's Modified Eagles Medium, GIBCO) with addition of 10% (v/v) foetal bovine serum (FBS, GIBCO), 100 µg/ml penicillin and 0.1 mg/ml streptomycin (GIBCO). Upon 80% confluence, cells were split and seeded accordingly for treatments. Briefly cells were washed twice in PBS, then 0.5-1ml 0.25% trypsin EDTA (GIBCO) was added and left to allow cells to detach. Cells were then resuspended in DMEM and seeded accordingly. 3T3-L1 cells (a kind gift from Professor Jeremy Tavaré, University of Bristol and Professor Amira Klip, University of Toronto) were cultured in DMEM (Sigma) with 10% (v/v) newborn calf serum (NCS, GIBCO), 100 µg/ml penicillin and 0.1 mg/ml streptomycin (GIBCO). Upon 80% confluence cells were split as described above and seeded accordingly. Once cells reached 100% confluence they were left to senesce for 2 days. Cells were then incubated with primary differentiation media consisting of DMEM with 10% (v/v) FBS, antibiotic, 166nM insulin, 5µM troglitazone

(PPAR agonist, Tocris), 0.25μM dexamethasone (synthetic glucocorticoid, Sigma) and 0.5mM IBMX (increases cAMP, Sigma) for 3 days, the latter 3 components induce insulin sensitizing genes leading to differentiation. Following morphological changes and lipid droplet formation cells were washed twice in PBS then incubated with secondary differentiation media consisting of DMEM with 10% (v/v) FBS, antibiotic, 166nM insulin and 5μM troglitazone, for a further 3 days. After full differentiation cells were maintained in complete DMEM until required for experiments (approx. 8 days post start of differentiation).

2.4.2 Transient Transfection of Mammalian Cells

HEK293's, PC3's, wildtype, Mnk1-KO, Mnk2-KO and DKO MEFs were transfected using the Polyethylenimine (PEI) method; 15μl of PEI (1mg/ml dissolved in 20mM HEPES pH 7.0) was mixed with 1μg of plasmid in 200μl basal DMEM and left for 15min room temperature, cells were washed twice in basal DMEM and cells were incubated with 1.5ml basal DMEM. The PEI-plasmid mix was topped up to 500μl with complete DMEM (+FBS +penn/strep) and added dropwise to cells, after 2h the media was removed and replaced with complete DMEM. Gene expression was assessed 24-48h post-transfection.

2.4.3 Gene Silencing using short interfering RNA (siRNA)

PC3's, WT MEFs and 3T3-L1 cells were transfected with Mnk1 or Mnk2 siRNA (Human Mnk1a: CAAAGAGUAUGCCGUCAAA, Mnk2a: GAACCGUUACUGUGAAUGA, Mouse Mnk1: CAUCGUGGAUUCUGACAAG, Mnk2: CCAAAGACCUCACGUCCUU all from Dharmacon, Thermo Scientific) using Dharmafect (Dharmacon, Thermo Scientific). For 6-well plates 5μl (10μM stock) siRNA was added to 195μl DMEM (no additives), in a separate tube 5μl Dharmafect reagent (formulation 3 for PC3 cells and formulation 1 for MEFs and 3T3-L1's) was mixed with 195μl DMEM (no additives) both tubes were left for 5min room temperature after this time the tubes were mixed together and left for a further 20min room temperature. For each well 1600μl DMEM (with FBS but no antibiotic) was added and mixed with the siRNA suspension and 2ml was added to each well. Gene knockdown was assessed at 48-72h post-transfection.

2.4.4 Cell Harvesting.

After treatment cells were washed 1-3 times in 1X PBS. The desired volume of ice-cold lysis buffer D for SDS-PAGE analysis, lysis buffer E for PKB assays, lysis buffer B for Mnk

assays, for PI3 kinase assays lysis buffer F or lysis buffer G for mTOR assays, was added to plates and cells scrapped from their dish into a clean microfuge tube. Lysates were centrifuged at 17, 000 *g* at 4°C for 10min. The supernatant was transferred to a new microfuge tube and lysates were either prepared for analysis or stored at -80°C. Protein concentration was determined using the Bradford method, using Bradford reagent (Bradford Laboratories Ltd, Hertfordshire, UK), absorbance was measured at a 595 nm.

2.4.5 RNA Isolation

The Trizol© method was used to isolate RNA from both cells and whole tissue as follows. For whole tissue samples 20-50mg of ground tissue was added to 0.5-1ml Trizol reagent and homogenised with a dounce homogeniser then centrifuged at 12,000 *g* for 10min at 4°C. The supernatant was then transferred to a clean microfuge tube with 200µl cholorform. To a 6cm dish of cells 1ml of Trizol was added and left for 5min at room temperature then transferred to a clean microfuge tube with 200µl cholorform. For both cell and tissue samples the trizol/chloroform mixture was vortexed until cloudy then left for 2-3min at room temperature followed by centrifugation at 12,000 *g* for 15min at 4°C. The clear aqueous layer was then transferred to a clean microfuge tube with 500µl isopropanol and mixed then left for 10min room temperature. The RNA was then precipitated by centrifugation at 12,000 *g* for 15min at 4°C. the supernatant was very carefully removed and 1ml 80% ethanol was added and the samples vortexed thoroughly followed by centrifugation at 7,500 *g* for 5min at 4°C. The ethanol was then removed and the pellet allowed to air dry for 5min followed by resuspension in an appropriate volume of nuclease free H_2O at stored at -80°C.

2.4.6 m^7GTP Sepharose Pulldowns and Immunoprecipitations

For m^7 pulldowns one part m^7GTP sepharose beads (GE Healthcare, UK) were diluted with one part Sepharose CL-4B (Sigma) allowing for 20µl per sample. The bead/Sepharose mixture was washed in 0.5ml lysis buffer A and centrifuged at 4, 700 *g* for 30 s. The supernatant was removed and 20µl of beads aliquoted per sample, 150-200µg of cell lysate was added and the mixture made up to 0.5ml with lysis buffer D. Samples were mixed at 4°C for 1h then centrifuged as previously and the supernatant removed. Samples were then washed with 0.5ml lysis buffer D twice, and centrifuged as before. For immunoprecipitations 20µl of Protein G beads (GE Healthcare) per sample, were washed in either lysis buffer B, D, E or F and centrifuged at 4, 700 *g* 30 s. The supernatant was removed and 200-500µg of cell lysate was added along with either 1µg PKB α antibody 1µg HA antibody, 1µg phospho-tyrosine antibody, mTOR kinase assays,

1µl raptor antibody or 1µl eIF4G antibody. Samples were mixed at 4°C for 1-3h and then centrifuged as previously, followed by removal of the supernatant. Samples that were immunoprecipitated for PKB were washed once in 1ml lysis buffer E with 0.5M NaCl then washed three times in 0.5ml kinase buffer A and centrifuged as previously. Samples immunoprecipitated for HA were washed once in 0.5ml wash buffer A with 1M LiCl, then twice in wash buffer A followed by once in kinase buffer B. Samples immunoprecipitated for phosphor-tyrosine were washed three times in lysis buffer D, twice in wash buffer B and once in both wash buffer C and wash buffer D. Samples immunoprecipitated for raptor were washed once in lysis buffer G, twice in lysis buffer G with 150mM NaCl and twice in wash buffer E. Samples to be analysed by SDS-PAGE were denatured at 95°C for 5 min with 10-20µl of 2X sample buffer for m^7GTP pulldowns or 40µl 5X sample buffer for immunoprecipitations. Samples were either used immediately or stored at -20°C. Samples to be used in kinase assays were kept on ice until just before the kinase reactions were started.

2.4.7 SDS Polyacrylamide Gel Electrophoresis (SDS-PAGE) and Western Blot Analysis

SDS-PAGE gels were prepared at, 10%, 12.5% or 13.5 % acrylamide (v/v) and 0.1% N,N methylene-bis-acrylamide (v/v). For proteins above 25kDa a 10% or 12.5% gel was used for those smaller a 13.5% gel was used. Samples were prepared based on desired protein concentration with 5X sample buffer and denatured for 5 min at 95°C, accept for those proteins that required purification using an m^7GTP pulldown. Samples were loaded into each lane with a prestained protein ladder (Fermentas) in one lane. Gels were run in SDS-PAGE running buffer at 180-200V for 40-60min. SDS-acrylamide gels were placed on nitrocellulose membrane laid on top of 2 sheets of 3MM Whatman filter paper, prewetted with transfer buffer, followed by a further 2 sheets of 3MM Whatman filter paper. Proteins were transferred to the membrane by wet blotting at 75V for 90min on ice. For detection of 4E-BP1 the membranes were fixed in glutaraldehyde, diluted 1:500 in PBST. After transfer the membrane was incubated with blocking buffer 5% (w/v) dried semi-skimmed milk in 1X PBS/TBS for 40 min at room temperature to prevent non – specific binding of antibody to the membrane. The membrane was then incubated with primary antibody (antibodies are described in table 2.1). Primary antibody was removed and membrane washed 3 times for 5min in PBST/TBST, membranes were then incubated with relevant secondary antibodies at a 1:20000 dilution for 40-60 min at room temperature. Excess antibody was removed by washing the membrane 3 times for 5 min

in PBST/TBST. All incubations and washes were performed with constant agitation. Antibody – Antigen complexes were detected using the Odyssey Licor scanner.

2.4.8 Confocal Microscopy

To visualise GLUT4 translocation to the plasma membrane immortal wildtype, Mnk1-KO and DKO MEFs were seeded onto coverslips 24h prior to transfection then transfected with HA-GLUT4-GFP and left for 24h. Cells were then starved of serum (DMEM without FBS) for 2h 30min and treated with 100nM insulin for 20min. Cells were washed twice with 1ml PBS then fixed with 3.7% formaldehyde for 15min at room temperature followed by 3 washes with PBS. Coverslips were then incubated with 100µl Hoechst 33342 dye (2µM) for 10min room temperature followed by X2 washes in PBS and then incubated with 100µl Alexa-Fluor 594 wheat germ agglutinin (WGA, 5µg/ml) for 10min room temperature, then washed three times in PBS. Coverslips' were mounted onto slides with Fluoromount (Sigma Aldrich) and left to dry. Slides were imaged using a Leica TCS SP2 with the multiphoton laser. HA-GLUT4-GFP expressing cells were identified down the microscope and then scanned with the multiphoton laser with excitation emissions in the 594nm range for the plasma membrane, 488nm for GFP and 760nm for nucleus. The settings were optimized and kept the same for each slide.

2.4.9 Preparation of cDNA and qPCR

cDNA was prepared using the ImProm-Reverse Transcription kit (Promega) following the manufactures method which is described here. In a clean microfuge tube 0.2-0.5µg RNA was mixed with 1µl Oligo(dT) and 1µl random primer, the reactions were heated to 70°C for 5min followed by addition of 4µl 5X reaction buffer, 4.8µl 25mM $MgCl_2$ 1µl 10mM dNTPs, 0.5µl RNasin, 1µl reverse transcriptase and made to 15µl with nuclease free H_2O. The reactions were then incubated at 25°C for 5min followed by 42°C for 60min and then 70°C 15min. This produces cDNA that was either stored at -20°C or immediately used for qPCR. Primer efficiency was determined for each primer and cDNA dilutions were produced in serial. For each sample a triplicate reaction was made containing 5µl cDNA, 4µl nuclease free H_2O, 1µl primer (see table 2.3 for sequences) and 10µl 2X Precission SYBR green master mix (PrimerDesign). 96-well plates were cycled at 95°C 10min, followed by 40 cycles of 95°C 15sec and 60°C 1min followed by a melt curve stage using the Applied Biosystems StepOne Plus qPCR machine. The average cycle threshold (CT) value of the mRNA of interest was normalised to 18S rRNA and a ΔCT value generated by expressing results as fold increase compared to a designated control.

2.4.10 In vitro Mnk Kinase Assays

15µl of HA immunoprecipitated Mnk was incubated in 25µl kinase buffer B with 1µg recombinant eIF4E, 200µM ATP and 1µCi [γ^{32}P]ATP for 10min at 30°C. The reaction was stopped by adding 5µl 4X sample buffer and denatured at 95°C for 5min. For assays with IRS1, 200ng Mnk2a (purified from HEK293 cells) was incubated with 2µg recombinant IRS1, 100µM ATP, 1µCi [γ^{32}P]ATP and made up to 20µl with kinase buffer B and left from 10-30min 30°C. The reaction was stopped by adding 5µl 4X sample buffer and denatured at 95°C for 5min. Samples were run on an SDS-PAGE gel at 200V for 1h, the gel was then stained with Coomaisse blue for 30min and then destained (40% MeOH, 10% AcOH, 50% H_2O) for 1h. Gels were dried for 1-2h at 80°C and incubated with phosphor-screen and developed with the Typhoon 700 imaging system.

2.4.11 Cyanogen Bromide Cleavage

An *in vitro* Mnk kinase assay against IRS1 was prepared as described above (section 2.4.10) except after SDS-PAGE gels were destained the fragment corresponding to IRS1 was excised and equilibrated in 70% formic acid for 30min room temperature. The gel slice was then soaked in 100mg/ml cyanogen bromide in 70% formic acid at 37°C overnight and kept away from light. The supernatant was then removed to a separate microfuge tube and the remaining sample was then dried in a speed vac followed by resuspension in 30% formic acid and incubated at 37°C for 30min. The supernatant was collected and mixed with the previous supernatant and dried in a speed vac until approximately 30µl was remaining, which was then mixed with 10µl sample buffer and 3ul 5M NaOH and boiled at 95°C 5min. samples were then loaded onto a 4-12% Novex gel and run in 1X MES running buffer (Sigma) at 170V for approximately 90min. The gel was then stained with Coomaisse blue for 30min, then destained for 2h and dried for 1-2h at 80°C and incubated with phosphor-screen and developed with the Typhoon 700 imaging system.

2.4.12 In vitro PKB Kinase Assays

15µl aliquots of immunoprecipitated proteins were incubated in 25µl kinase buffer A with 2.5µM PKI (TTYADFIASGRTGRRNAIHD, peptide inhibitor of cAMP dependent protein kinase), 30µM Crosstide peptide (GRPRTSSFAEG, includes the consesnsus sequence for PKB phosphorylation, a kind gift from Dario Alessi), 10mM magnesium acetate, 100µM ATP and 1µCi [γ-^{32}P]ATP for 20min. The reaction was stopped by removing 22µl and pipetting onto P81 Whatman phosphocellulose paper. Samples were left to air dry and

then washed three times for 5min in 0.85% phosphoric acid followed by once in methanol and allowed to air dry. Samples were counted using the Cerenkov method in the 2450 Micro beta^2 microplate counter.

2.4.13 In vitro PI3 Kinase Assays

The phosphatidylinositol (Ptdlns) substrate was prepared as followed, 3ml (10mg/ml stock in chloroform) was dried in a speed vac for approximately 30min. the dried film was then resuspended in 1ml 1% (w/v) sodium cholate in kinase buffer C and sonicated for 10min in a sonicating water bath. 20µl aliquots of immunoprecipitated proteins were incubated in 40µl kinase buffer C with 20µl Ptdlns cholate substrate and allowed to reach 37°C in a heat block. In a separate tube 39µl water, 5µl (30µM) ATP, 5µl (75mM $MgCl_2$) and 0.5µCi [γ-^{32}P]ATP were mixed and allowed to warm to 37°C. The reaction was started by adding 40µl of the ATP mix to the immunoprecipitate and left for 30min at 37°C. The reaction was stopped by adding 450µl chloroform/methanol (1:2) and vortexed thoroughly followed by storage at -20°C. The following day a Merck Kieselgel 60 20x20cm thin layer chromatography (TLC) plate was dipped into a mixture of 1:1 (v/v) methanol and 2mM EDTA and baked in an oven at 150°C until dried. A mixture of 42.9ml methanol, 30ml chloroform, 7.65ml 29.1% Ammonia and 9.45ml water was equilibrated in a chromatography tank for 90min. Samples were prepared for TLC by adding 150µl each of chloroform then 0.1M HCl and vortexed thoroughly followed by centrifugation at 2, 400 *g* 10min room temperature. The lower and interphase was transferred to a fresh tube with addition of 600µl synthetic upper phase (chloroform:0.1M HCl, 1:1 v/v) and vortexed thoroughly and centrifuged as previously. The lower phase was transferred to a fresh eppendorf and dried in a speed vac for 30-90min. the dried lipid film was then resuspended in 35µl cholorform:methanol:HCl (200:100:1 v/v) and sonicated using a sonicating water bath. 10µl of each sample was dotted onto the cooled TLC plate and allowed to dry followed by a further 10µl and allowed to dry. The TLC with samples was then placed into the equilibrated chromatography tank and left for approximately 2h or until the solvent line reached 3cm from the top of the plate. The plate was allowed to dry and then left overnight with a phosphor-screen and developed the following day using the Typhoon phosphor-imager.

2.4.14 In vitro mTOR Kinase Assays

15µl aliquots of Raptor immunoprecipitated protein was incubated in 20µl kinase buffer E with 1µg recombinant GST-4E-BP1, 100µM ATP and 1µCi [γ-^{32}P]ATP for 20min at 30°C. The reaction was stopped by adding 5µl 4X sample buffer and denatured at 95°C for 5min. Samples were run on an SDS-PAGE gel at 200V for 1h, the gel was then stained

with Commaisse blue for 30min and then destained (40% MeOH, 10% AcOH, 50% H_2O) for 1h. Gels were dried for 1-2h at 80°C and incubated with X-ray film overnight at -80°C or a phosphor-screen and developed with the Konica Minolta SRX-101A X-ograph or Typhoon 700 imaging system.

2.4.15 2-deoxyglucose Uptake Assay.

Cells were grown to 80% confluence then starved of serum overnight, for 3T3-L1 cells at 8 days post-differentiation cells were starved of serum overnight. The following morning cells were placed in serum free low glucose (1g/L) DMEM for 2h. During drug treatment cells were placed in KRH buffer and negative controls were treated with Cytochalasin B (Sigma). To start the reaction 100µl of 10X start solution: 1mM 2-deoxyglucose, 5µCi/ml [^{3}H]-2-deoxyglucose in KRH buffer, was added to the cells and placed in an incubator at 37°C for 10min. The reaction was stopped by removing the label and washing the cells three times in ice cold KRH buffer. Cells were lysed in 1ml 0.1M NaOH, protein concentration was determined using the BCA method and 250µl of sample was mixed with 2.5ml scintillation fluid (Scintisafe 2, Fisher), the radioactive incorporation was counted using the 2450 Micro beta^2 microplate counter. Samples were normalised to protein concentration and expressed as specific activity.

2.4.16 2-deoxyglucose Lipogenesis Assay.

3T3-L1 cells were differentiated and on the 8th day starved of serum overnight, the following morning cells were placed in serum free low glucose (1g/L) DMEM for 2h. During drug treatment cells were placed in KRH buffer. To start the reaction 100µl of 10X start solution: 1mM 2-deoxyglucose, 5µCi/ml [^{3}H]-2-deoxyglucose in KRH buffer, was added to the cells and placed in an incubator at 37°C for 2h. Cells were lysed in 0.8ml 0.1% SDS, protein concentration was determined using the BCA method. 0.6ml of cell lysate was mixed with 1.875ml chloroform:methanol (1:2), vortexed and left for 10min room temperature. To this 0.625ml chloroform and 0.625ml 0.5M KCl was added and samples centrifuged at 2, 400 *g* for 15min room temperature. The lowerphase was placed in a fresh microfuge tube and dried in a speed vac for 90min. The dried lipids were then resuspended in 100-200µl chloroform and counted in 2ml scintillation fluid (Ultima Gold, Perkin Elmer) using the the 2450 Micro beta^2 microplate counter. Samples were normalised to protein concentration and expressed as specific activity.

2.5 Animal Experimentation

2.5.1 Transgenic Mouse Assessment

Mnk2KO and DKO mice were bred under normal conditions from mice generously gifted by [45]. These mice were originally generated as follows; Mnk1 and Mnk2 genomic DNA clones were isolated from a mouse 129/Sv genomic DNA library using full-length mouse Mnk1 and Mnk2 cDNA probes, respectively. Vectors were created for Mnk1 and Mnk2 by inserting a neomycin resistance gene (Neo^r cassette) between the MunI site in intron 4 and the AvrII site in intron 6 of the Mnk1 gene or between the NcoI site in intron 4 and the EcoT22I site in intron 9 of the Mnk2 gene. Mouse ES cells were transfected with the Mnk1 or Mnk2 targeting vector by electroporation, and G418-resistant clones were assessed for homologous recombination by PCR. ES cells carrying the single Mnk1- or Mnk2-targeted allele were injected into BDF1 blastocysts, which were then implanted into recipient female mice. Mice with a high ES contribution were crossed to C57BL/6 females. Germ line knockout was confirmed by PCR. Single KO mice for either the Mnk1 or Mnk2 gene were generated by crossing the respective heterozygous mice. $Mnk1^{-/-}$ $Mnk2^{-/-}$ DKO mice were generated by crossing $Mnk1^{-/-}$ $Mnk2^{+/-}$ mice with $Mnk1^{+/-}$ $Mnk2^{-/-}$ mice. Mice were housed in a normal light/dark cycle and fed and watered according to Home Office regulations. Age matched C57BL/6 wildtype mice were used as controls for comparison with Mnk2KO and DKO mice [45]. To determine the genotype of mice, tail or ear samples were digested in tail lysis buffer H at 55°C overnight. Samples were centrifuged at 17, 000 *g* for 15min room temperature, equal amounts of supernatant were taken into a new eppendorf and the pellet discarded. For 100µl supernatant, 30µl 5M NaCl was added and samples left for 5mins room temperature then centrifuged at 17, 000 g for 15mins. All supernatant was taken into a new eppendorf and 100µl Isopropanol was added to samples that were then incubated at room temperature for 10min. Samples were then centrifuged for 30min at 17, 000 *g* and the supernatant discarded. Pellets were incubated in 1ml 70% ethanol (-20^{0}C) for 15min followed by centrifugation for 30min at 17, 000 *g*. Supernatant was discarded and pellet allowed to air-dry for approximately 1hr. Pellets were resuspended in 20µl MilliQ water. DNA concentration was determined using the Nanodrop spectrophotometer ND-100 (Labtech), where necessary samples were diluted to 100ng/µl. To prepare samples for PCR a master mix consisting of 0.5µl TAQ DNA polymerase (Promega), 10µl 5X buffer (Promega), 2µl dNTP, 2µl of forward and reverse primer (see table 2.4), 0.5µl 50mM $MgCl_2$ and 32µl MilliQ water was made and centrifuged at 1, 500 *g* for 30secs. 47µl of master mix was added to 3µl of sample. Samples were then subject to the following PCR (BioRad My cycler) conditions; 94^{0}C 5min, 35 cycles of; 94^{0}C 30sec, 60^{0}C 1min and 72^{0}C 1min30sec followed by 72^{0}C 10min and held at 15^{0}C ∞.

PCR products were subject to gel electrophoresis using a 2% agarose gel containing 1:20000 gel red at 100V for 50min.

2.5.2 Animal Husbandry and Diets

Mice were cared for according to the Animals (Scientific Procedures) Act 1986 as set out by the Home Office. Mice were housed in groups with no more than 6 mice in a cage and had free access to food and water. They were maintained under a 12h light/dark cycle (lights on at 07.00h). Mice were weaned at approximately 3 weeks of age and were fed rat and mouse No.1 maintenance diets (Special Diet Services, RM1, normal chow)(table 2.5). Following weaning mice were either maintained on normal chow diets or fed Special Diet Services 45% AFE fat diet (high fat diet)(table 2.5).

2.5.3 Glucose Tolerance Test

Mice are fasted for 18 hours prior to the GTT with water but no food and a DO NOT FEED card is placed in the cardholder. The following morning the mice are prepared for the glucose tolerance test: animals are weighed and the tail end numbed with lidocaine cream, the tail is nicked with a fresh razor blade by a horizontal cut of the very end, ~35 to 50 microliters of blood is very gently massaged from the tail to assess baseline blood glucose, which is measured by the glucose oxidase method using a Accu-chek glucometer, and 2 grams/kg body weight of 20% D-glucose is drawn up in a Beckton Dickenson D 29 gage 1/2" insulin syringe (one unit of D-glucose for every gram of body weight). Animals are transferred to individual cages. When all mice have been prepared the test is begun. Glucose is injected into the intraperitoneal cavity. At 15, 30, 60, 90 and 120 minutes blood glucose is sampled from the tail of each mouse by gently massaging a small drop of blood onto the glucometer strip. Glucose injections and blood glucose sampling is timed to take approximately the same amount of time per animal (i.e. 25 animals are injected in 12 minutes and blood glucose sampling of those same 25 animals should also take about 12 minutes) so that the sample times are accurate for each animal. At the end of the experiment the tips of the tail are cleaned and sprayed with Betadine and animals returned to their shared cages along with fresh food and water. Animals are checked the next day to ensure healing of the wound. This method was completed by Felino Cagampang with my assistance.

2.5.4 DEXA Scanning and Organ Removal

Mice were anaesthetised using Isoflurane or were euthanized by cervical dislocation and total blood removed by cardiac puncture. Bloods were placed in heparinised tubes and stored at 4°C until centrifugation for 10 minutes at 2, 400 *g* at 4°C. Blood glucose upon death was measured with the Accu-chek glucometer. The mice were scanned with a Skyscan 1176 in-vivo scanner with the following parameters: voltage: 50kV, current: 500µA, scan Resolution: 35.1µm, exposure time: 83ms, rotation between images: 0.5° number of images: 395. The body of the mouse was scanned in 5 separate stages, the scans from all 5 stages were then combined during reconstruction to give a single 3D volume file. Body volume, tissue volume and fat volume were calculated using the Hounsfield scale [230], these calculations were then applied to the image using the VGStudio Max software. The DEXA scanning and analysis was carried out by Stuart Lanham (University of Southampton, Human Health and Development). Following DEXA scanning mice were dissected and the left and right lobes of the liver, the heart, pancreas, spleen, right kidney and brain were dissected, weighed, and snap frozen in liquid nitrogen prior to storage at -80°C. Abdominal (surrounding epididymal and vesicular glands in males and the ovaries and uterus in females) white adipose pads as well as interscapular (between shoulder blades) brown adipose tissue (SCAPULAR) were removed, weighed and stored as above to assess offspring fat deposition. Muscles from the upper segment of the hind limbs were also dissected, weighed and stored as above. A portion of the liver, abdominal fat, left kidney, scapular fat and muscle were also fixed in 10% formalin for histology. Dissection was mostly carried out by Felino Cagampang with assistance from myself.

2.5.5 Metabolic Cage Assessment

Mice were housed in individual metabolic chambers, in which they were accustomed for at least 12h before starting the measurements. Mice had free access to food and water, and were maintained under a 12h light/dark cycle (lights on at 07.00h). The temperature in the metabolic chamber (22 ± 2°C) was stable and controlled throughout the experiment. Physical activities of the mice were monitored by an infrared photocell beam interruption method (Panlab SLU, Spain). Food intake was continuously measured using an extensiometric food weight transducer device (Panlab SLU, Spain); however this was not possible for high fat diet fed mice due to the consistency of the diet, which was not contained by the food device.

2.5.6 Tissue and Plasma Analysis

Organs were processed by grinding frozen samples to a powdered form under liquid nitrogen using a mortar and pestle. For protein isolation 20-50mg of powdered samples were mixed with 200-700µl lysis buffer I and then homogenised with a microfuge homogeniser and centrifuged at 17, 000 *g* for 20min room temperature. The supernatant was removed to a fresh microfuge tube and protein concentration was checked using the BCA method. Samples were assessed by western blotting. RNA was isolated using an adaptation of the Trizol© method. Approximately 30mg of powdered tissue was added to 1ml Trizol reagent and homogenised with a microfuge homogeniser followed by centrifugation at 12,000*g* for 10min 4°C this was followed by the rest of the protocol as above in section 2.4.5. As described above total blood was removed by cardiac puncture and placed into heparinised tubes. Samples were spun at 6000*g* for 15min 4°C and the supernatant aliquoted into fresh microfuge tubes. Samples were sent to Keith Burling (Clinical Biochemistry, Cambridge University Hospitals NHS Foundation Trust) and analysed by gas chromatography for lipid based metabolites and ELISA for insulin, leptin and cytokines.

Table 2.1 Antibodies for Western Blotting and Immunoprecipitations.

Antibody	Dilution	Supplier and Product Number (if applicable)
Phospho-eIF4E Ser^{209}	1:500	Eurogentec – custom made
eIF4E	1:1000	Cell Signalling Technology – 9742
eIF4GI	1:1000	Kind gift from Simon Morley (University of Sussex), for WB
eIF4GI	1:500	Cell signalling Technology – 8701, for IP
4E-BP1	1:1000	Raised in house
Phospho-ERK Thr^{202}/Tyr^{204}	1:1000	Cell Signalling Technology - 9101
ERK	1:1000	Cell Signalling Technology - 9102
Phospho-PKB Ser^{473}	1:2000	Cell Signalling Technology - 9271

Phospho-PKB Thr^{308}	1:1000	Cell Signalling Technology - 9275
PKB	1:2000	Cell Signalling Technology – 9272, for WB
PKBα	1µg	Dario Alessi (University of Dundee), for IP
HA	0.1µg	Roche - 11867423001
Phospho-Mnk Thr$^{197/202}$	1:1000	Cell Signalling Technology - 2111
Mnk1	1:1000	Cell Signalling Technology - 2195
Mnk2	1:1000	Sigma – M0696
Raptor	1:1000 WB 1:500 IP	Cell Signalling Technology - 2280
mTOR	1:1000 WB 1:500 IP	Raised in house
Phospho-TSC2 Thr^{1462}	1:500	Cell Signalling Technology - 3611
TSC2	1:500	Cell Signalling Technology - 3635
Phospho-PRAS40 Thr^{246}	1:1000	Cell Signalling Technology - 2640
PRAS40	1:1000	Cell Signalling Technology - 2610
Phospho-S6 Ser$^{240/244}$	1:1000	Cell Signalling Technology - 2215
S6	1:1000	Cell Signalling Technology - 2317
β-Tubulin	1:200	Santa Cruz Biotechnology – sc5274
Phospho-AS160 Thr^{642}	1:500	Cell Signalling Technology - 4288

AS160	1:500	Cell Signalling Technology - 2447
Phospho-tyrosine	1:500 IP	Santa Cruz Biotechnology – sc7020
IRS1	1:500	Cell Signalling Technology - 2382
IRβ	1:1000	Cell Signalling Technology - 3020
Myc	1:500 IP 1:2000 WB	Sigma Aldrich – M4439
p70S6K	1:1000	Cell Signalling Technology - 9202
ATP Citrate Lyase	1:1000	Cell Signalling Technology - 4332
aP2	1:1000	Cell Signalling Technology - 2120
Phospho-acetyl CoA carboxylase Ser^{79}	1:1000	Cell Signalling Technology - 3661
Acetyl CoA carboxylase	1:1000	Cell Signalling Technology - 3662
PPARγ	1:500	Cell Signalling Technology - 2430

IP denotes immunoprecipitations, WB denotes western blotting

Table 2.2 Primers for Mutagenesis.

Primer Name	Tm°	Sequence
IRS1 S574A sense	69	GGGACACAGGCACGCCGCCTTCGTGC
IRS1 S574A antisense	69	GCACGAAGGCGGCGTGCCTGTGTCCC
IRS1 S629A sense	70.4	CAGTGGCCGAAAGGGCGCTGGAGACTATATGCCC
IRS1 S629A antisense	70.4	GGGCATATAGTCTCCAGCGCCCTTTCGGCCACTG

IRS1 S766A sense	68.6	GCCTGTCCTCTCCTACTACGCATTACCAAGGTCCTTTAAG
IRS1 S766A antisense	68.6	CTTAAAGGACCTTGGTAATGCGTAGTAGGAGAGGACAGGC
IRS1 T774A sense	70.6	GATCCTTTAAGCACGCCCAGCGCCCCGG
IRS1 T774A antisense	70.6	CCGGGGCGCTGGGCGTGCTTAAAGGATC
IRS1 S794A sense	70.6	CTCCGCCTTTCCACTGCCTCTGGTCGCCTTCTC
IRS1 S794A antisense	70.6	GAGAAGGCGACCAGAGGCAGTGGAAAGGCGGAG
Mnk2a S74A sense	70.6	CGGGCCACCGACGCCTTCTCGGGCAG
Mnk2a S74A antisense	70.6	CTGCCCGAGAAGGCGTCGGTGGCCCG
Mnk2a S437A sense	69	CTGCCTGCAGCTGGCTCCACCCTCCC
Mnk2a S437A antisense	69	GGGAGGGTGGAGCCAGCTGCAGGCAG

Table 2.3 Primers for qPCR.

Primer Name	Tm°	Sequence
IRS1 sense	54.6	AGTTAGTAGAACCAAGCATTAAACAC
IRS1 antisense	55.7	TGAGGAAGAGACTGAACCATCA
ApoE sense	57	AGTGGCAAAGCAACCAACC
ApoE antisense	56.3	CTTCCGTCATAGTGTCCTCCA
UCP1 sense	55.2	GGCCTCTAGACTCAGTCCA
UCP1 antisense	56.4	TAAGCCGGCTGAGATCTTGT
PGC1α sense	55.4	GTCAACAGCAAAAGCCACAA
PGC1α antisense	56.4	TCTGGGGTCAGAGGAAGAGA
TNFα sense	57.3	CTCCAGGCGGTGCCTATG

TNFα antisense	53.8	GGGCCATAGAACTGAGAGG
IFNγ sense	56.5	TCAAGTGGCATAGATGTGGAAGAA
IFNγ antisense	55.8	TGGCTCTGCAGGATTTTCATG
MCP1 sense	57.2	GGCTGGAGAGCTACAAGAGG
MCP1 antisense	54.9	TCTTGAGCTTGGTGACAAAAAC
RANTES sense	56.3	AGCAGCAAGTGCTCCAATC
RANTES antisense	54.9	GGGAAGCGTATACAGGGTC
CD3 sense	56.4	TCCCAACCCAGACTATGAGC
CD3 antisense	56.4	GCGATGTCTCTCCTATCTGTCA
CXCR3 sense	56.5	GCCAAGCCATGTACCTTGAG
CXCR3 antisense	56.1	GGAGAGGTGCTGTTTTCCAG
Mnk2 sense	57.3	CCAGTGCCAGGGACATAGG
Mnk2 antisense	56.8	GCCACGCATCTTCTCAAACA

Table 2.4 Primers for genotyping.

Primer Name	Tm°	Sequence
Mnk1 WT sense	55.5	GACCCAGGAATGACACCTTC
Mnk1 mutant sense	65	GATTCGCAGCGCATCGCCTTCTATCG
Mnk1 antisense	58.5	GCGCAAACCACATGTGCTTT
Mnk2 WT sense	67.4	CCACATCCGCAGCAGGGTGTTCGC
Mnk2 mutant sense	64.6	GATTCGCAGCGCATCGCCTTCTATCG
Mnk2 antisense	68.4	GTCGCAGCGCTTGTCGTAGATGCTGGC

Table 2.5 Components of mouse diets used in this study.

Diet	Carbohydrate (% w/w g)	Protein (% w/w g)	Fat (% w/w g)	Fibre (% w/w g)	Energy (kcal/g)
RM1 Standard Chow	63.51	14.38	4.98	17.05	3.53
45% AFE Fat	39.8	23.0	22.6	4.6	4.54

Chapter 3

Rapamycin Induces eIF4E Phosphorylation by Increasing the Activity of Mnk2a.

3.1 Introduction

The Mnks were discovered as a result of screening for novel substrates or binding substrates of ERK. This revealed 4 different isoforms of Mnk1 and Mnk2 termed Mnk1a, Mnk1b, Mnk2a and Mnk2b [38, 39]. Humans express all Mnk isoforms whilst mice only

contain Mnk1a and Mnk2a, both of which contain a C-terminal MAPK-binding domain [38, 39]The best known substrate of the Mnks is eIF4E, which binds to the 5'-cap structure of eukaryotic mRNAs and is phosphorylated by the Mnks on Ser209 [53, 231]. eIF4E interacts with the scaffold protein eIF4G to recruit other translation factors and the 40S ribosomal subunit to the mRNA, to facilitate efficient initiation of mRNA translation. eIF4G is also required for efficient phosphorylation of eIF4E by the Mnks because the Mnks cannot bind directly to eIF4E [85]. The Mnks show differing levels of activity towards eIF4E; Mnk1a shows low basal activity, which is markedly increased by stimuli that activate MAP kinase signalling [58, 232], whereas Mnk2a shows high basal activity which is only slightly changed by activating or inhibiting ERK signalling; this likely reflects the fact that phosphorylated, active ERK can bind stably to Mnk2a but not Mnk1a, causing its continuous activation [72, 73, 87].

There is strong evidence for a role of eIF4E in tumorigenesis; e.g., levels of eIF4E are raised in many cancers (reviewed [40, 233]), whilst artificial overexpression of eIF4E in mammalian cells or in animal models leads to transformation or accelerated tumorigenesis [234, 235]. The tumorigenic mechanism may involve the increased levels of available eIF4E leading to the translation or nucleocytoplasmic transport of certain mRNAs, whose products promote cell proliferation or survival [236]. The role of eIF4E phosphorylation has yet to be conclusively identified but has been linked to the expression of subsets of specific mRNAs and as such has been recently implicated in tumorigenesis [77-79].

Rapamycin was discovered as a product of the bacterium *Streptomyces hygroscopicus* and was shown to have antifungal effects [237]. During trials of rapamycin as an antifungal it was discovered that rapamycin exhibited potent immunosuppressive effects and so has been used for immune suppression after organ transplantation [238]. Research to determine the target of rapamycin led to the discovery of the yeast homologues (TOR1, TOR2), followed by the mammalian target of rapamycin (mTOR) complex 1 and 2 [239, 240]. Rapamycin inhibits mTORC1 through an allosteric mechanism. Rapamycin binds the cytosolic protein FKBP12 and binds to the FKBP12-rapamycin binding (FBR) domain of mTOR although the exact mechanism of inhibition is still not known [241]. The availability of eIF4E is restricted by its association with eIF4E-binding proteins (4E-BPs) which block its binding to eIF4G; 4E-BPs are phosphoproteins, and their phosphorylation by the mTORC1 at specific sites causes their release from eIF4E allowing the latter to bind to eIF4G. mTORC1 is activated downstream of signalling pathways such as the ERK and protein kinase B (PKB) (reviewed [242, 243]), which include upstream components that become oncogenic (e.g, Ras, PI 3-kinase) or are regulated by tumour suppressor proteins. Thus, mTORC1 is hyperactive in many tumour

cells, favouring activation of eIF4E. This has prompted numerous studies of rapamycin and related compounds ('rapalogs') as anti-tumour agents, leading to approval of certain rapalogs in advanced renal cell carcinoma and other settings [244]. Active site-directed inhibitors of mTOR are now available; unlike rapamycin, they inhibit all mTOR's functions [28, 245, 246].

In this study the cell line PC3 have been used. This cell line was originally generated from a grade IV prostate cancer that had metastasized to the bone of a 62 year old male [247]. PC3 cells are therefore highly metastatic and exhibit characteristics such as a lack of prostate-specific membrane antigen (PSMA) [248]. There is some debate about the expression of the androgen receptor (AR) in PC3 cells with evidence providing for both positive and negative expression [249, 250], but the majority of evidence favours an AR-negative phenotype in PC3 cells [250-252]. Furthermore these cells do not express prostate-specific antigen (PSA) [250], although when used to generate xenografts in mice there is expression of PSA [253]. Another key characteristic of PC3 cells is they are PTEN null [254], which suggests aberrant PI3K/PKB signalling is a key tumorigenic pathway used by these cells. Interestingly, 50-85% of prostate cancers do show high levels of PI3K/PKB signalling [255, 256]. Evidence from PC3 cells that shows the activity of PI3K/PKB is important for in proliferation, invasion and tumour size [253, 257, 258]. Therefore mTORC1 inhibitors such as rapamycin are an attractive treatment for advanced prostate cancer and there are a number of clinical trials in progress to test their efficacy. However the current data available is disappointing [259-261].

Considering the clear links between eIF4E phosphorylation and tumorigenesis and the increasing use of rapalogs in cancer therapy, it is a major concern that rapamycin actually enhances eIF4E phosphorylation in several cell types [29, 31, 262-264]. The aim of this chapter is to gain insights into the mechanisms underlying rapamycin's ability to enhance eIF4E phosphorylation.

3.2 Results

3.2.1 Effect of Rapamycin in PC3 cells.

To investigate the effect of rapamycin on eIF4E phosphorylation the prostate cancer cell line PC3 was used. To understand if there is a role for the Mnks in the lack of efficacy of rapamycin, PC3 cells were used as a model of advanced prostate cancer.

3.2.1.1 Rapamycin-induced eIF4E phosphorylation can be blocked by inhibiting both the p110α and p110β subunits of PI3 kinase, in PC3 cells.

Numerous studies have shown rapamycin can induce eIF4E phosphorylation[31, 265, 266]. Evidence suggests this is caused by activation of PI3K. This has been postulated to occur through mTORC1 inhibition of S6K activity towards IRS1, which blocks the degradation of IRS1 and potentiates PI3K activity [31]. To further investigate the role of PI3K and its link to rapamycin-induced eIF4E phosphorylation, I studied whether specific PI3K p110 catalytic subunits are involved in this effect. Using PI3–KαVIII, TGX-221 and LY294002 to inhibit PI3K p110α, p110β and p110α, β and γ, respectively, the importance of these subunits was tested in PC3 cells that had been starved of serum (Fig. 3.1). Data from LY294002 use in previous studies is unreliable as this compound also inhibits mTOR [267]. LY294002 is an ATP-competitive inhibitor of mTOR [268] and it is possible that blocking ATP binding to mTOR combined with allosteric inhibition by rapamycin is the reason for the decrease in phosphorylation of eIF4E. PP242 is also an ATP competitive mTOR inhibitor and so fully inhibits both mTOR complexes. Thus ATP-competitive inhibition of mTORC1 may not activate the negative feedback pathway involving PI3 kinase. By using highly specific PI3 kinase inhibitors, TGX-221 and PI3-KαVIII, which only block the PI3 kinase p110β and p110α catalytic subunits, respectively, and not mTOR [269], it should be possible to determine if specific p110 subunits are involved and thus indicate whether LY294002 decreases rapamycin-induced eIF4E phosphorylation due to its ability to inhibit mTOR in a ATP-competitive manner.

The results (Fig. 3.1) indicate that PI3-KαVIII or TGX-221 did not block rapamycin-induced eIF4E phosphorylation when administered alone, but, when used in combination, produced a significant decrease in rapamycin-induced eIF4E phosphorylation (Fig. 3.1). The lack of inhibition when these compounds are used alone may be because PC3 cells express three of the four PI3 kinase p110 isoforms; α, β and γ [270]. These results suggest both the p110α and p110β subunits are necessary for rapamycin-induced eIF4E phosphorylation. This implies that particular downstream pathways may be important for rapamycin-induced eIF4E phosphorylation. This effect of LY294002 is not due to ATP-competitive inhibition of mTOR and the decrease in rapamycin-induced eIF4E phosphorylation is as result of LY294002 inhibition of the p110α and p110β subunits of PI3K.

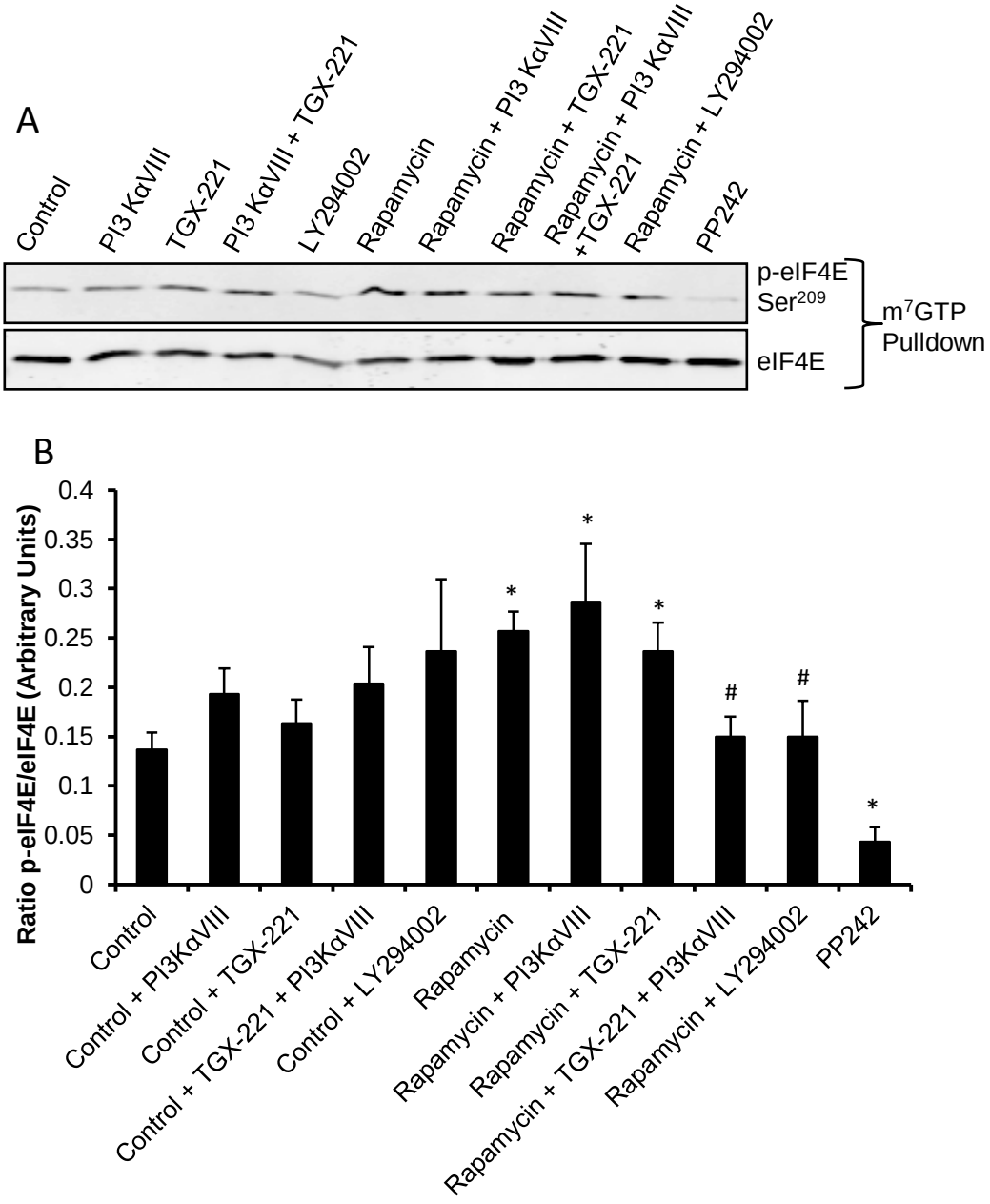

Figure 3.1. Effects of rapamycin on phosphorylation of eIF4E. A) Western blot analysis of eIF4E phosphorylated on Ser209 and total eIF4E from m^{7}GTP-Sepharose purifications from extracts of PC3 cells which had been starved of serum overnight and then treated as indicated for 2h. B) Graphical representation of the ratio of p-eIF4E to total eIF4E. Bands

were quantified by densitometry using the Licor Odyssey software. Student's t-test was used to analyse the data, * indicates $p<0.05$ compared to control, # indicates $p<0.05$ compared to rapamycin. n=3

3.2.1.2 Changes in eIF4E phosphorylation are independent of eIF4G or 4E-BP1 binding to eIF4E.

The conventional model for the effect of rapamycin on eIF4E function suggests that decreased 4E-BP1 phosphorylation leads to sequestration of eIF4E and a concomitant decrease in eIF4G binding [271, 272]. This should lead to inhibition of the phosphorylation of eIF4E as the Mnks require the scaffold function of eIF4G to phosphorylate eIF4E efficiently [85]. The data from this study appear to conflict with the model described above: rapamycin significantly increases eIF4E phosphorylation (Fig. 3.1), which is in accordance with published work [29, 31]. It was therefore important to study the effect of rapamycin on eIF4E/eIF4G binding. PC3 cells were starved of serum and treated accordingly (Fig. 3.2) followed by purification by m^7GTP precipitation. The indicate that rapamycin increases eIF4G/eIF4E binding (although not significantly as seen in Fig. 3.2). In contrast when TGX-221, PI3–KαVIII or LY294002 are used in combination with rapamycin eIF4G/eIF4E binding decreases (Fig. 3.2). The increase in eIF4G/eIF4E binding with rapamycin treatment could, in principle, explain the increase in eIF4E phosphorylation. However treatment with TGX-221 or PI3–KαVIII with rapamycin led to a decrease in eIF4G/eIF4E binding (Fig. 3.2), despite the fact that eIF4E phosphorylation was not altered by rapamycin and TGX-221 or rapamycin and PI3-KαVIII (Fig. 3.1). This suggests that eIF4G/eIF4E binding does not correlate with the levels of eIF4E phosphorylation and that changes in this parameter are not the reason for rapamycin-induced eIF4E phosphorylation. There is data that show the Mnks can phosphorylate eIF4E independently of eIF4G but, at a much slower rate [273, 274]. It is possible that inhibition of mTORC1 by rapamycin activates a pathway that allows eIF4E phosphorylation by the Mnks independently of eIF4G/eIF4E binding. This is likely to alter Mnk activity or Mnk/eIF4G binding.

As previously mentioned mTORC1 activation leads to the phosphorylation of 4E-BP1, leading to the release of eIF4E, which allows binding to eIF4G. Rapamycin would be expected to block this, resulting in less eIF4E/eIF4G binding. The data show the response to PP242 conforms to the conventional model of mTORC1 inhibition by blocking eIF4E phosphorylation, probably through a combination of decreased eIF4G binding and increased 4E-BP binding (Fig. 3.2). However, the data for rapamycin do not agree with this model since eIF4G binding is not decreased and the amount of 4E-BP1/eIF4E binding increases marginally with all treatments (Fig. 3.2). The amount of 4E-BP1 bound to eIF4E when rapamycin and PI3-KαVIII are combined (Fig. 3.2) is higher than rapamycin alone

despite eIF4E phosphorylation remaining high (Fig. 3.1). In addition, there is also a decrease in eIF4G binding (Fig. 3.2).

These data indicate that neither eIF4G/eIF4E binding nor 4E-BP1/eIF4E binding correlate with eIF4E phosphorylation.

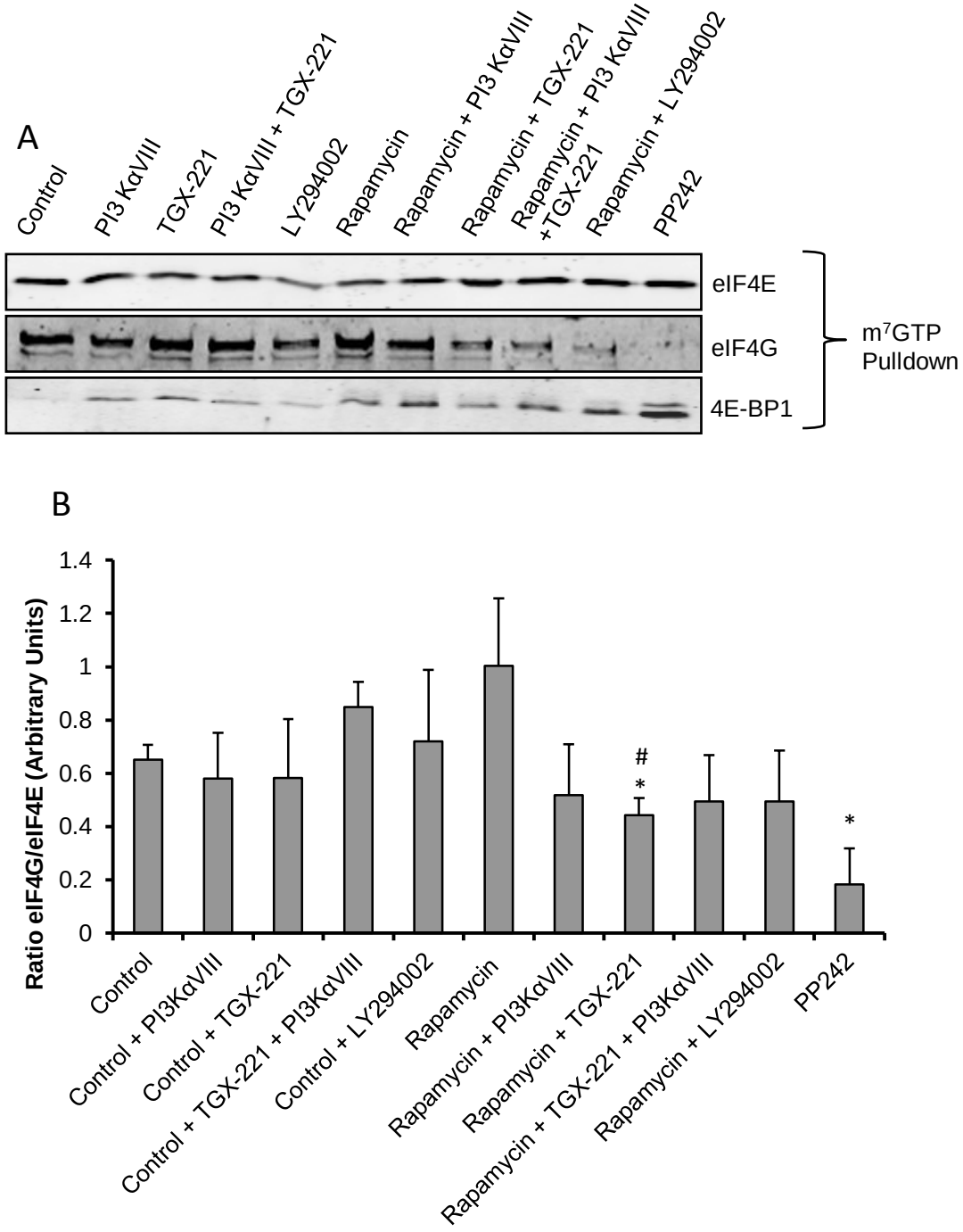

Figure 3.2. Effects of rapamycin on proteins associated with eIF4E. A) Western blot analysis of total eIF4E, total eIF4G and total 4E-BP1 from m^{7}GTP-Sepharose purifications from extracts of PC3 cells which had been starved of serum overnight and then treated as indicated for 2h. B) Graphical representation of total eIF4G to total eIF4E in material purified on m^{7}GTP-Sepharose. Bands were quantified by densitometry using the Licor Odyssey software. Student's t-test was used to analyse the data, * indicates $p<0.05$

compared to control, # indicates $p<0.05$ compared to rapamycin. n=3 for eIF4E and eIF4G and n=1 for 4E-BP1.

3.2.1.3 Increases in eIF4E phosphorylation are correlated to PKB but not ERK phosphorylation.

The pathway that links PI3K to changes in the phosphorylation of eIF4E has been partially investigated by other studies, which employed MEK inhibitors to assess whether PI3K signalling leads to the activation of ERK. One of the studies used a combination of MEK inhibitors and p38 MAPK inhibitors and reported a decrease in rapamycin-induced eIF4E phosphorylation; however they did not show these data [29]. To confirm this was the case in PC3 cells I assessed ERK phosphorylation. The data (Fig. 3.3A) show that there is a slight increase with LY294002 or rapamycin treatment but this is reduced by each of the inhibitors in combination with rapamycin and therefore does not correlate with eIF4E phosphorylation (Fig. 3.1).

The role of PKB here is less clear; while one study reports that rapamycin-induced eIF4E phosphorylation is independent of PKB [31], other authors suggest the opposite [29, 266]. It was therefore important to assess PKB phosphorylation in this study.

PKB activation requires its phosphorylation at two sites; Ser^{473} (phosphorylated by mTORC2) and Thr^{308} (phosphorylated by PDK1) [275]. Phosphorylation of the latter appears to be more important for activity towards most substrates. Phosphorylation of PKB at Thr^{308} and Ser^{473} increased with rapamycin or rapamycin in combination with PI3-KαVIII (Fig. 3.3B). TGX-221, TGX-221 and PI3-KαVIII or LY294002 decreased rapamycin-induced PKB phosphorylation at both sites. The decrease in rapamycin-induced PKB phosphorylation seen with TGX-221 (Fig. 3.3B) does not correlate with eIF4E phosphorylation (Fig. 3.1). These data make it difficult to conclude whether or not PKB is involved in rapamycin-induced eIF4E phosphorylation.

The PKB inhibitor Akti1/2 was employed to further assess the role of PKB in rapamycin-induced eIF4E phosphorylation. The data revealed that inhibition of PKB trended to block rapamycin-induced eIF4E phosphorylation (Fig. 3.4), indicative of a potential role for PKB affecting eIF4E phosphorylation. This is, however, complicated by the reduction in PKB phosphorylation seen with PMA treatment, which significantly increases eIF4E phosphorylation. Furthermore, these data conflict with the effect of TGX-221 on rapamycin-induced PKB phosphorylation and subsequent eIF4E phosphorylation, which show no correlation (Figs 3.1, 3.3B).

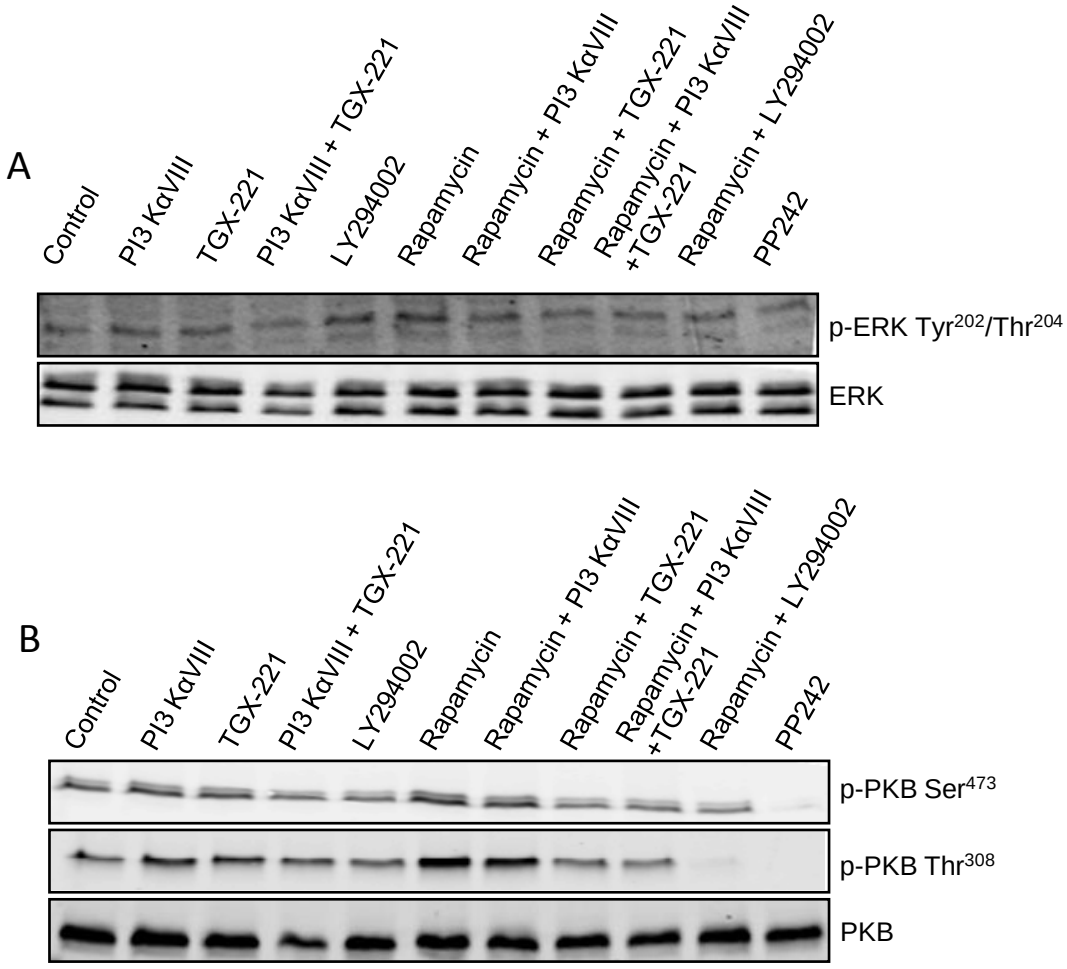

Figure 3.3. Effects of rapamycin on ERK and PKB. A) Western blot analysis phospho-ERK Thr^{202}/Tyr^{204} and total ERK of crude lysates from PC3 cells starved of serum overnight and then treated as indicated for 2h. n=1 B) Western blot analysis for phospho-PKB Ser^{473} and Thr^{308} and total PKB of crude lysates from PC3 cells starved of serum overnight and then treated as indicated for 2h. n=1.

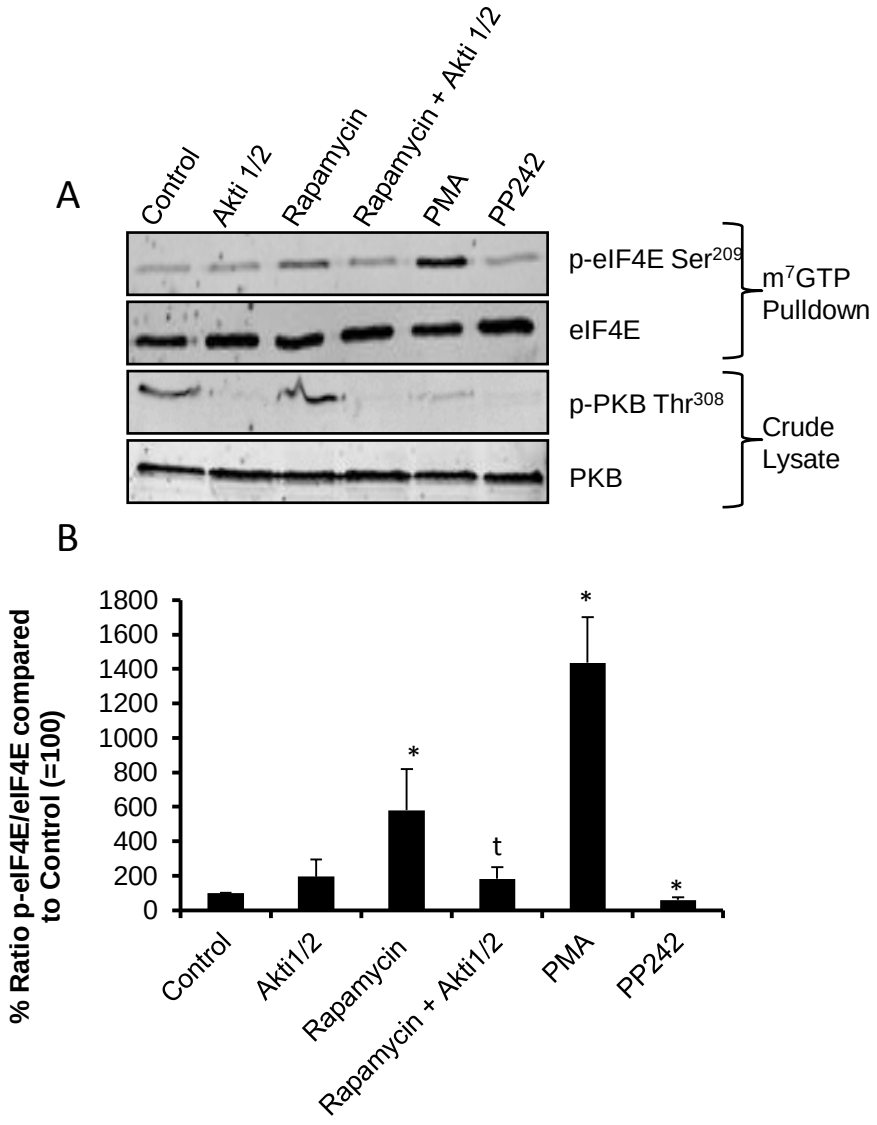

Figure 3.4 Effects of inhibition of PKB on rapamycin-induced eIF4E phosphorylation. A) Western blot analysis of p-eIF4E Ser^{209} and total eIF4E from m^{7}GTP-Sepharose purifications from extracts of PC3 cells which had been starved of serum overnight and then treated as indicated for 2h. B) Graphical representation of the ratio of p-eIF4E to total eIF4E expressed as a percentage of the control. Bands were quantified by densitometry using the Licor Odyssey software. Student's t-test was used to analyse the data, * indicates $p<0.05$ compared to control, t indicates $p<0.1$ compared to rapamycin. n=3

3.2.2 Role of the Mnks in Rapamycin-induced eIF4E phosphorylation.

The Mnks are the only kinases that are known to target eIF4E, as illustrated by the loss of eIF4E phosphorylation in Mnk1/2-DKO mice [31]. To establish if one isoform or both are responsible for rapamycin-induced eIF4E phosphorylation Mnk1 and Mnk2 single knockout cells were used. It has previously been suggested that both Mnks are responsible for this effect [31]. However in light of data just described, which show ERK does not appear to be involved, I decided to examine which of the Mnk isoforms were involved.

3.2.2.1 Rapamycin-induced phosphorylation of eIF4E is dependent on Mnk2 function but not Mnk1.

The data show that the loss of Mnk2, but not Mnk1, reduces basal eIF4E phosphorylation (Fig. 3.5). This was expected because Mnk2 has high basal activity and is not greatly activated further by ERK or p38 MAPK [72]. Knock-out of Mnk1 did not reduce rapamycin-induced eIF4E phosphorylation and rapamycin still elicits a similar increase in eIF4E phosphorylation to that seen in wildtype cells (Fig. 3.5A, C). The converse is true with the knockout of Mnk2: there is no increase in phosphorylation of eIF4E in response to rapamycin (Fig. 3.5B, C). Interestingly, PMA caused a significant decrease in eIF4E phosphorylation in Mnk1-KO cells suggesting that ERK activation inhibits Mnk2 activity, which is unexpected. This phenomenon requires further investigation.

Although the Mnk2-KO MEFs did not exhibit rapamycin-induced eIF4E phosphorylation, it was also important to determine if Mnk2 was the sole isoform responsible in PC3 cells. PC3 cells were incubated with siRNA specific to Mnk1 or Mnk2 or just Dharmafect (transfection reagent) for 48h and then serum starved followed by treatment with rapamycin or PMA. As can be seen, an efficient knockdown of either Mnk1 or Mnk2 was achieved (Fig. 3.6A). Those cells incubated with just Dharmafect or Mnk1 knockdown still showed similar levels of basal and rapamycin-induced eIF4E phosphorylation (Fig. 3.6A, B). Interestingly, Mnk1 siRNA did not lead to the decrease in eIF4E phosphorylation in response to PMA as was seen in Mnk1-KO cells (Fig. 3.5). As expected from the MEF data, PC3 cells treated with Mnk2-siRNA showed significantly lower basal eIF4E phosphorylation and no increase in response to rapamycin (Fig. 3.6).

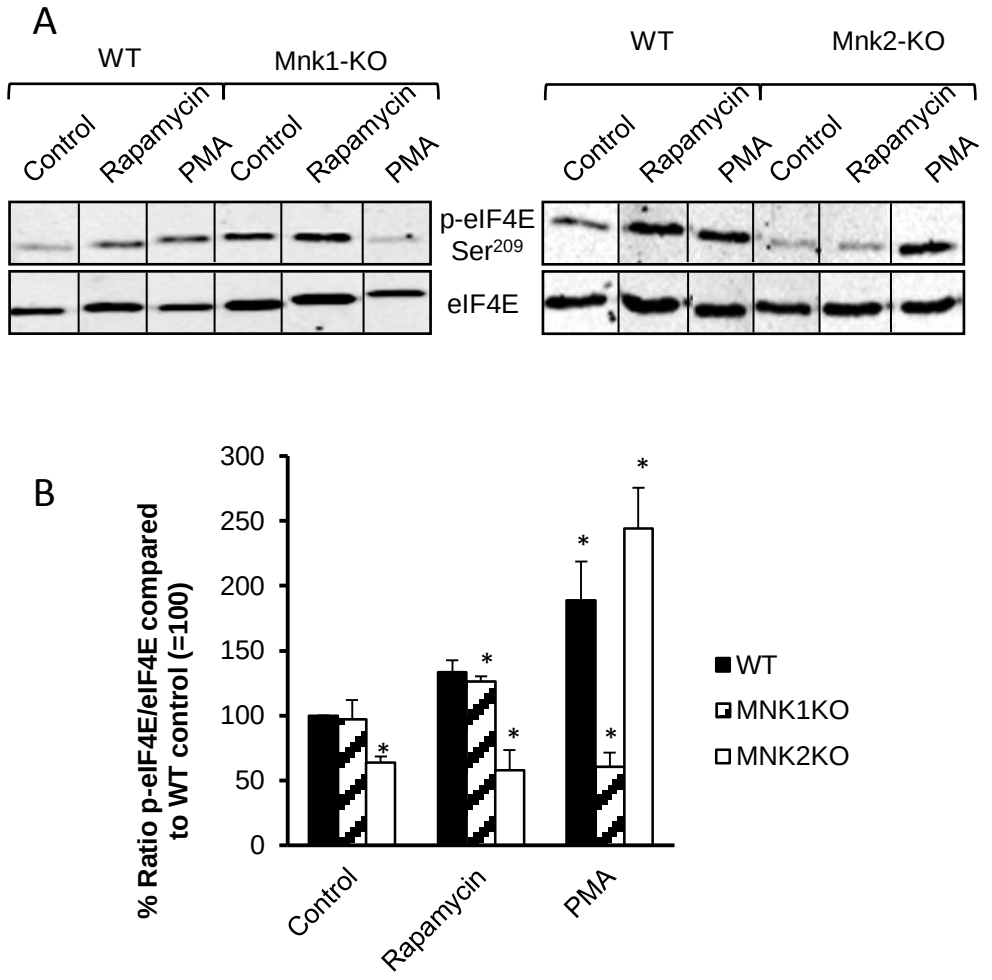

Figure 3.5 Mnk2 is required for rapamycin-induced phosphorylation of eIF4E. A) Western blot analysis of p-eIF4E and total eIF4E from m^7 GTP purifications from lysates from WT, Mnk1-KO and Mnk2-KO. Cells were starved of serum overnight then treated with 100nM rapamycin for 2h. These blots have been merged to remove unnecessary lanes as indicated from the vertical lines. B) Graphical representation of the ratio of p-eIF4E/eIF4E expressed as a % of untreated WT cells. Intensities were quantified by densitometry using the Licor Odyssey software. Student's t-test was used to analyse the data, * indicates $p<0.05$ compared to WT control.

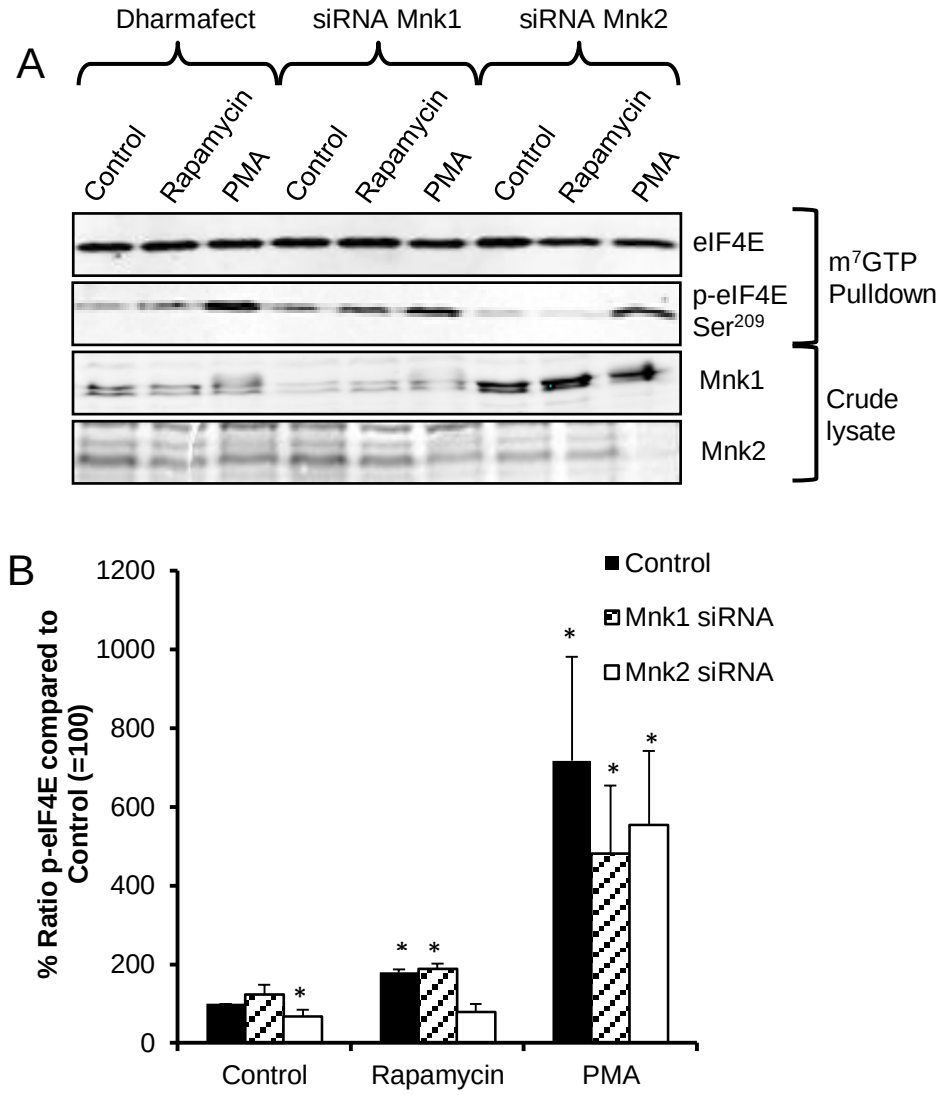

Figure 3.6 Mnk2 is required for rapamycin-induced phosphorylation of eIF4E. A) PC3 cells treated with transfection reagent alone or with Mnk1 or Mnk2 siRNA for 48h followed by overnight serum starvation and subsequent treatment with 100nM rapamycin or 0.5µM PMA for 2h. B) Graphical representation of the ratio of p-eIF4E/total eIF4E expressed as % of those for control cells. Bands were quantified using the Licor Odyssey software. Student's t-test was used to analyse the data, * indicates $p<0.05$ compared to control.

3.2.2.2 eIF4G/eIF4E binding is affected by the loss of either of the Mnks.

The data described above show that the effects of rapamycin and combinations of PI3 kinase inhibitors on eIF4E/eIF4G binding do not correlate with levels of eIF4E phosphorylation (Figs. 3.1, 3.2). However eIF4G/eIF4E binding has not been previously assessed in Mnk1-KO and Mnk2-KO cells.

The loss of Mnk1 had an overall inhibitory effect on eIF4E/eIF4G binding, which is further decreased by the addition of rapamycin, an effect also seen in the wildtype cells (Fig. 3.7). In Mnk2-KO cells, there was a significant increase in eIF4G/eIF4E binding. This could be a compensatory mechanism employed by the cell to rescue the loss of basal eIF4E phosphorylation by promoting Mnk1-dependent phosphorylation of eIF4E. Another possible explanation is that Mnk2 negatively regulates eIF4G/eIF4E binding, while Mnk1 positively regulates it.

In PC3 cells, rapamycin caused an increase in eIF4G/eIF4E binding and increased eIF4E phosphorylation (Figs. 3.1, 3.2). However, in PC3 cells, eIF4E phosphorylation does not correlate with eIF4G/eIF4E binding, as demonstrated by the addition of the individual PI3 kinase inhibitors, which decreased eIF4G/eIF4E binding but did not affect rapamycin-induced eIF4E phosphorylation (Figs. 3.1, 3.2). Similarly to PC3 cells, it is likely that in MEFs eIF4G/eIF4E binding is not important in rapamycin-induced eIF4E phosphorylation. In summary these data do show that the Mnks have an effect on eIF4G/eIF4E binding, which is interesting, but does not explain rapamycin-induced eIF4E phosphorylation.

It therefore still remains to be determined as to how rapamycin increases eIF4E phosphorylation, whether there is a change in Mnk2/eIF4G binding or an increase in Mnk2 activity.

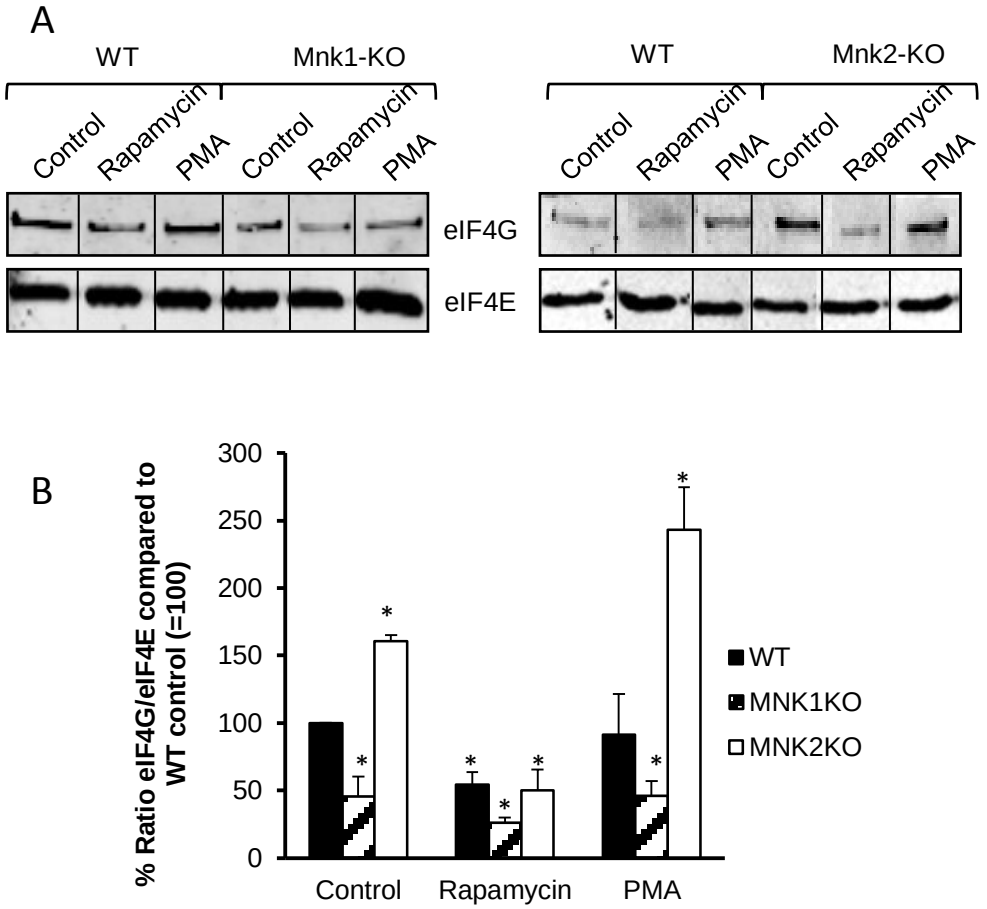

Figure 3.7 Loss of the Mnks alters eIF4G-eIF4E binding. A) Western blot analysis of total eIF4G and total eIF4E from m^7 GTP purifications from lysates from WT, Mnk1-KO and Mnk2-KO. Cells were starved of serum overnight then treated with 100nM rapamycin for 2h. These blots have been merged to remove unnecessary lanes. B) Graphical representation of the ratio of eIF4G/eIF4E expressed as a % of untreated WT cells. Intensities were quantified by densitometry using the Licor Odyssey software. Student's t-test was used to analyse the data, * indicates $p<0.05$ compared to WT control.

3.2.2.3 mTORC1 inhibition increases the activity of Mnk2a independently of T-loop phosphorylation.

The evidence presented so far has shown that Mnk2a is the isoform required for rapamycin-induced eIF4E phosphorylation (Figs. 3.5, 3.6). Since the activity of Mnk2a is dependent on its T-loop phosphorylation, it was important to assess if this was increased by rapamycin treatment and, if so, it was affected by inhibiting PI3K or PKB. PC3 cells were transfected with a vector encoding HA-tagged Mnk2a and treated as shown (Fig. 3.8). The overexpressed Mnk2a was immunoprecipitated by the HA tag and processed by western blot analysis for phosphorylation using an antibody against the T-loop. This showed that rapamycin did not increase T-loop phosphorylation indicating that a different mechanism is responsible for Mnk2a dependent rapamycin-induced eIF4E phosphorylation (Fig. 3.8). Furthermore, the addition of Akti1/2 trended towards a decrease in T-loop phosphorylation when combined with rapamycin despite no increase in T-loop phosphorylation seen with rapamycin (Fig. 3.8). This implies that PKB inhibition causes a decrease in rapamycin-induced eIF4E phosphorylation because of decreased Mnk2a T-loop phosphorylation and not by blocking the actual mechanism through which rapamycin induces eIF4E phosphorylation.

To determine whether rapamycin caused an increase in Mnk2a activity, PC3 cells overexpressing HA-tagged Mnk2 were lysed, HA-Mnk2a was immunoprecipitated and its activity assayed against recombinant eIF4E (Fig. 3.9A, B). Rapamycin markedly enhanced the activity of Mnk2a both in autophosphorylation, as indicated by the ratio of incorporated ^{32}P compared to immunoprecipitated levels of HA-Mnk2a (Fig. 3.9B), and against eIF4E (Fig. 3.9A). Interestingly, PP242 also enhanced Mnk2a activity (Fig. 3.9A, B), which indicates that inhibition of mTORC1 leads to increased Mnk2a activity. PP242 does not increase eIF4E phosphorylation *in vivo* probably because it also decreases eIF4G/eIF4E and increases 4E-BP1/eIF4E binding (Fig. 3.1, 3.2). However, this is important when considering mTOR inhibitors for cancer therapy because it is possible increased Mnk2 activity will influence other Mnk substrates, potentially in a detrimental fashion. As shown previously (Fig. 3.8), neither rapamycin nor PP242 increased Mnk2a T-loop phosphorylation (Fig. 3.9A, C). Thus, rapamycin enhances Mnk2a activity independently of changes in T-loop phosphorylation.

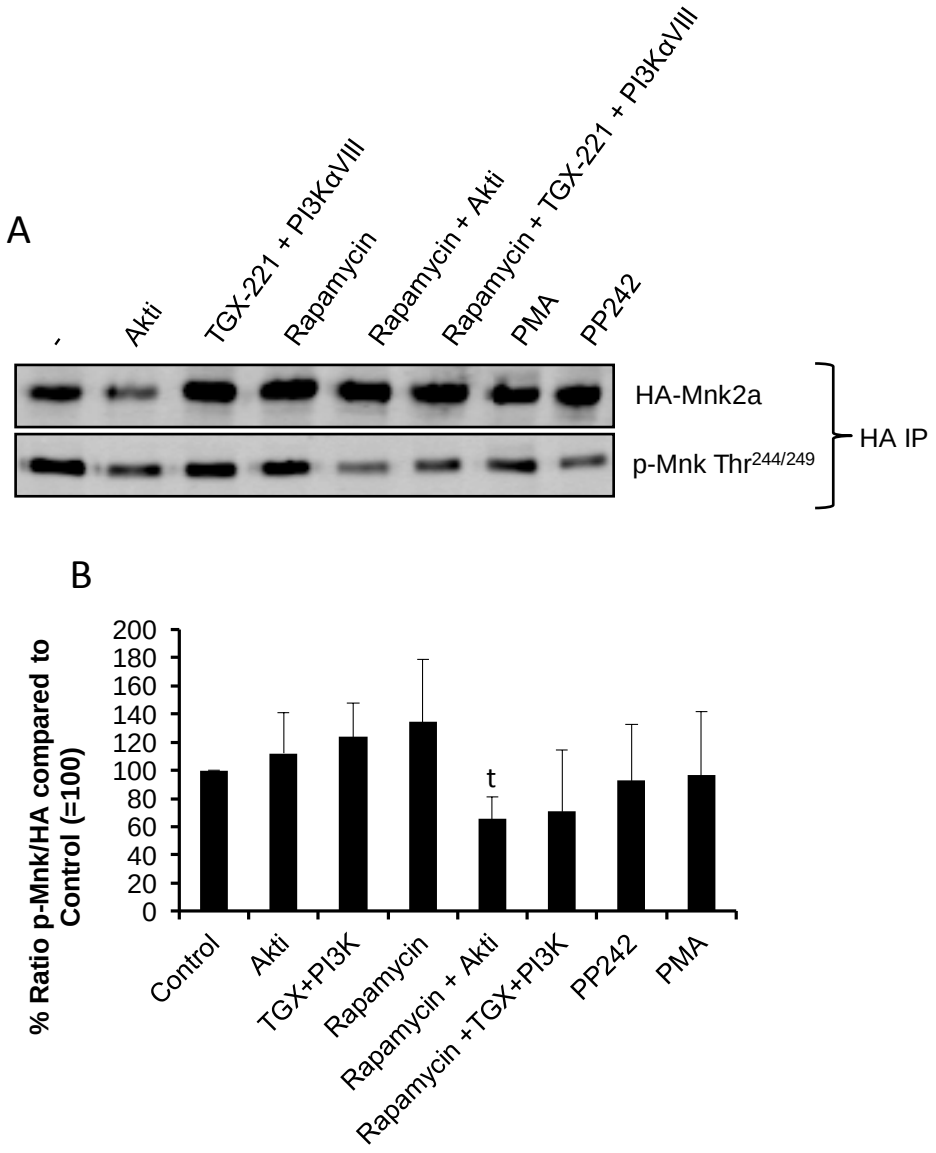

Figure 3.8 Effects of rapamycin on Mnk2 phosphorylation. A) Western blot analysis of p-Mnk2 and HA input from HA immunoprecipitates from extracts of PC3 cells PC3 cells transfected with a vector for HA-Mnk2a, left for 48h, starved of serum overnight and then treated as indicated for 2h. B) Graphical representation of the ratio of p-Mnk to HA expressed as a percentage of the control. Bands were quantified by densitometry using the Licor Odyssey software. Student's t-test was used to analyse the data, t indicates $p<0.1$ compared to rapamycin. n=3

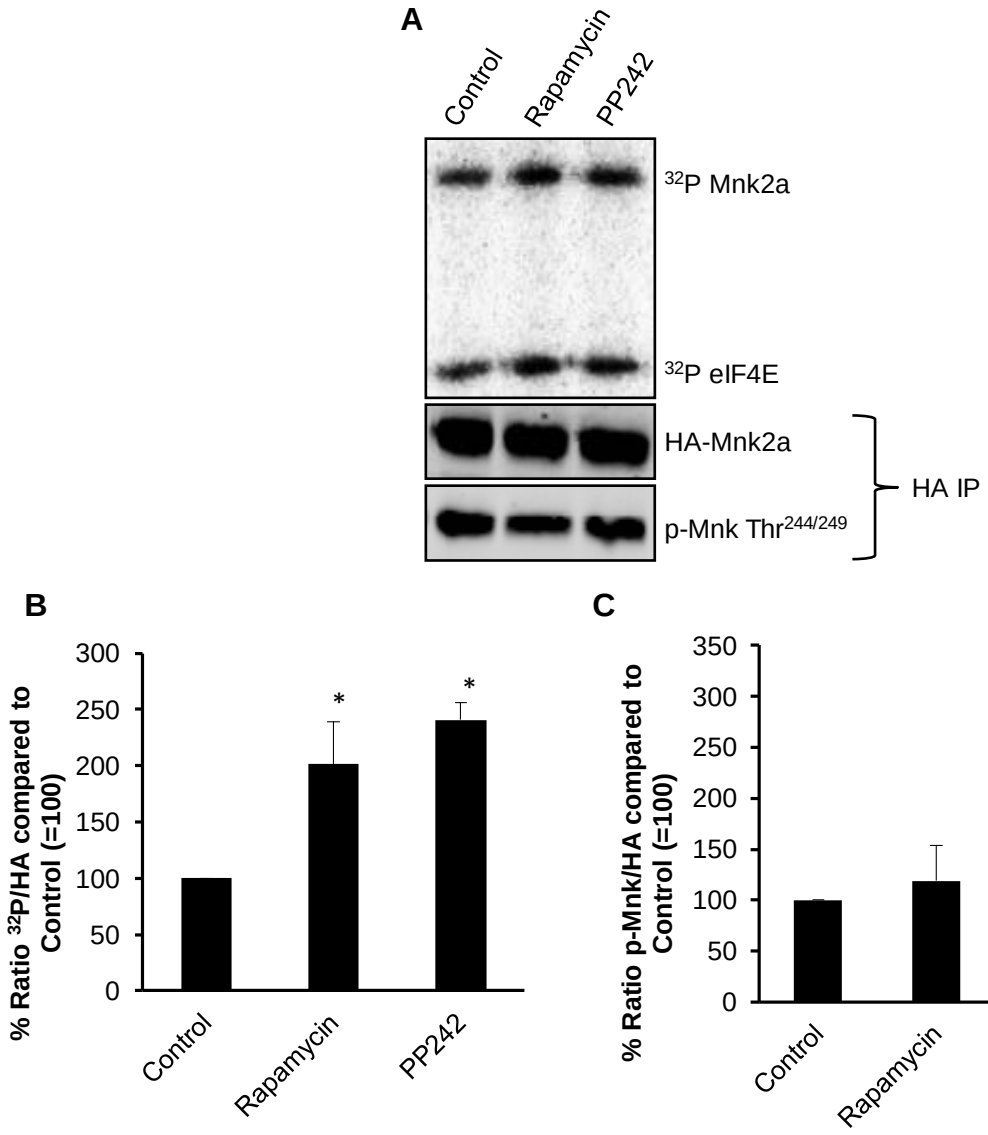

Figure. 3.9 Mnk2 activity increases in response to mTORC1 inhibition. A) PC3 cells transfected with a vector for HA-Mnk2a, left for 48h, starved of serum overnight and then treated with 100nM rapamycin, or 1µM PP242 for 2h. After immunoprecipitation with anti-HA, an *in vitro* kinase assay was performed for the activity of HA-Mnk2a against recombinant eIF4E (Mnk2a also undergoes phosphorylation in the assay, as indicated). The lower part shows western blots of cell lysates using anti-HA and p-Mnk antisera. B) Graphical representation of ^{32}P incorporation Mnk2a normalised to HA input. Bands were quantified by densitometry using ImageJ and the Licor Odyssey software, respectively. n= 4 C) Graphical representation of p-Mnk2a normalised to HA input. Bands were quantified by densitometry using the Licor Odyssey software. In B, C, Student's t-test was used to analyse the data, * indicates $p<0.05$ compared to control.

3.2.2.4 Rapamycin increases Mnk2a activity through changes to one site in Mnk2a.

The levels of autophosphorylation of Mnk2a increased with rapamycin treatment indicating that despite no changes to T-loop phosphorylation there was likely a change in phosphorylation of another site (Fig. 3.9A, C). Mnk2a from control or rapamycin-treated cells was analysed by mass spectrometry (kindly completed by Andrew Bottrill, University of Leicester). This revealed changes in the phosphorylation of two residues, Ser74 and Ser437 (data not shown). To determine if either of these sites was required for the rapamycin-induced activation of Mnk2a, mutants in which Ser^{74} or Ser^{437} was changed to alanine. The effects of rapamycin on Mnk2a [S74A] and Mnk2a[S437A] in parallel with wildtype Mnk2a were then examined. Mnk2a [S74A] phosphorylation still increased in response to rapamycin (Fig. 3.10A). The Mnk2a[S437A] mutant showed higher basal activity, in autophosphorylation and against eIF4E, than WT Mnk2a. Importantly, Mnk2a [S437A] autophosphorylation was not further increased by rapamycin (Fig. 3.10B, C). This suggests that Mnk2a is normally phosphorylated at this site impairing Mnk2a activity whereas rapamycin causes its dephosphorylation and a subsequent increase in activity. It is possible that mTORC1 inhibition may result in the activation of a phosphatase that specifically dephosphorylates Ser^{437} on Mnk2a or that mTORC1 is responsible for the phosphorylation of this site.

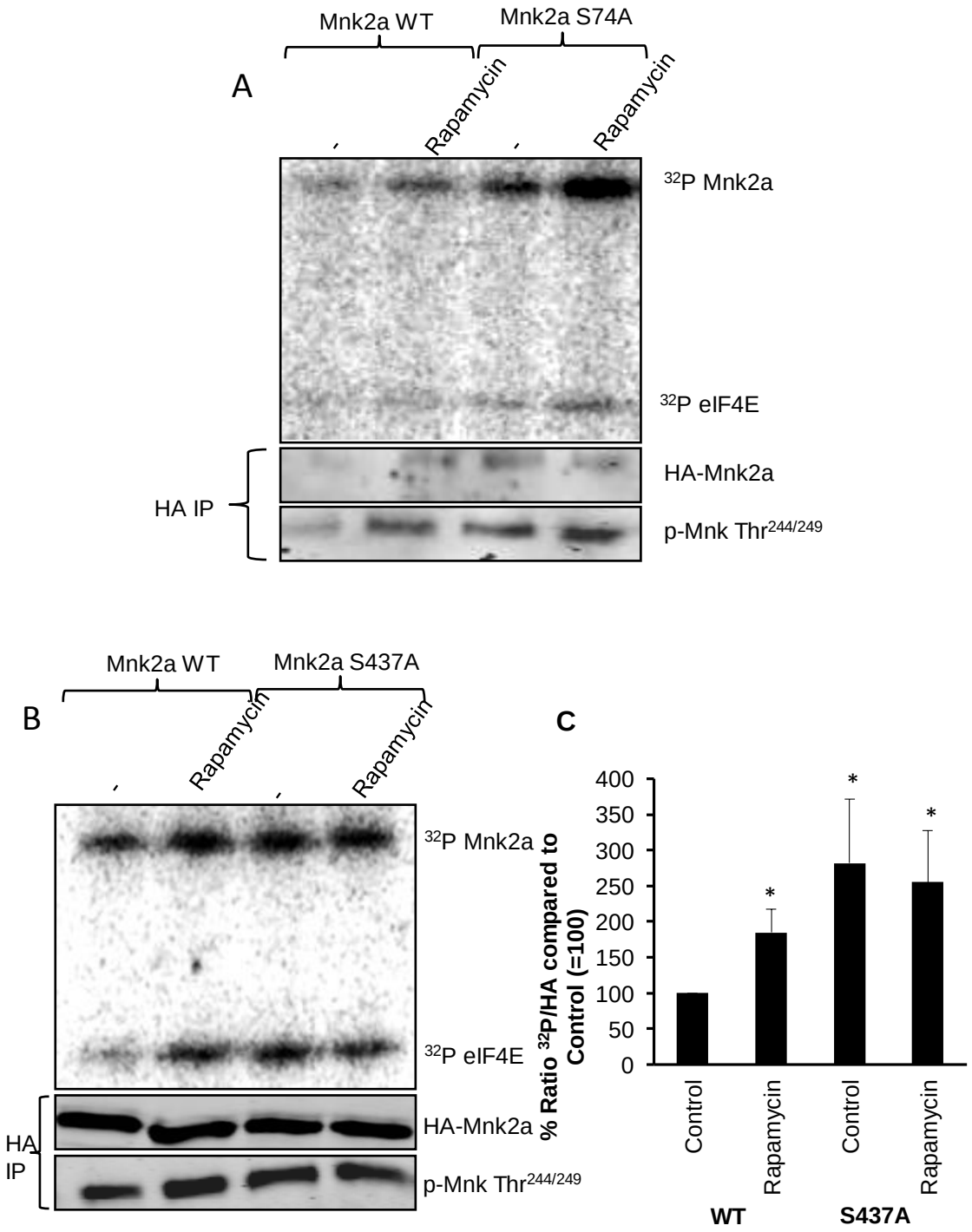

Figure 3.10 Rapamycin increases Mnk2a activity through one site Ser437. A) PC3 cells transfected with a vector for HA-Mnk2a or a S74A mutant and treated with 100nM rapamycin for 2h. After HA immunoprecipitation, Mnk activity was assayed; the figure shows an autoradiograph of the stained gel. Western blots of HA input and p-Mnk are shown below the main panel. B) PC3 cells transfected with a vector for HA-Mnk2a or a S437A mutant and treated with 100nM rapamycin for 2h. After HA immunoprecipitation, Mnk activity was assayed; the figure shows an autoradiograph of the stained gel. Western blots of HA input and p-Mnk are shown below the main panel. C) Graphical representation

of ^{32}P incorporation into Mnk2a or Mnk2a[Ser437Ala] normalised to HA input. Bands were quantified by densitometry using ImageJ and the Licor Odyssey software, respectively. Student's t-test was used to analyse the data, * indicates $p<0.05$ compared to WT control.

3.2.3 mTORC1 inhibition increases eIF4G/Mnk2 binding but not p-ERK/Mnk2 binding.

Evidence presented here has shown that Mnk2a activity increases with rapamycin and PP242 treatment in a mechanism dependent on the phosphorylation of Ser^{437} (Fig. 3.10B, C). These data were assessed *in vitro* and in the absence of eIF4G resulting in a requirement for excess Mnk2a and eIF4E. *In vivo*, Mnk2a requires eIF4G to act as a scaffold in order to efficiently phosphorylate eIF4E [72]. It was therefore important to test if mTOR inhibitors had any effect on the interaction between Mnk2a and eIF4G. HA-tagged Mnk2a was overexpressed in PC3 cells, which were treated either with rapamycin or PP242. Cells were then lysed in a low salt buffer in order to retain Mnk2/eIF4G binding, which is mediated by three lysines in the N-terminus of Mnk2a [87]. Endogenous eIF4G was immunoprecipitated and then HA-Mnk2a binding was assessed by blotting for the HA tag on Mnk2a. This revealed that rapamycin and PP242 each caused a significant increase in eIF4G-Mnk2a binding (fig. 3.11A, B).

Ser^{437} is next to the MAPK binding site (Table 3.1) in Mnk2a raising the possibility that this site may alter p-ERK/Mnk2 binding, which is thought to be important for the high basal activity of Mnk2 [72]. In order to test if rapamycin or PP242 changes in p-ERK/Mnk2 binding, within the context of the complex of Mnk2 and eIF4G, eIF4G immunoprecipitations were probed for p-ERK. This revealed that there was no discernible change in p-ERK/Mnk2 binding (Fig. 3.11A, C). Immunoprecipitates of HA-Mnk2a were also probed for p-ERK but no p-ERK was seen (data not shown) presumably because these samples were washed in LiCl, which would disrupt p-ERK/Mnk2 binding, further indicating that rapamycin and the site Ser^{437} do not alter p-ERK/Mnk2 binding. The role of Ser^{437} may be linked to a conformational change in the N-terminus of Mnk2 altering its activity as was demonstrated for other sites in the C-terminus [72].

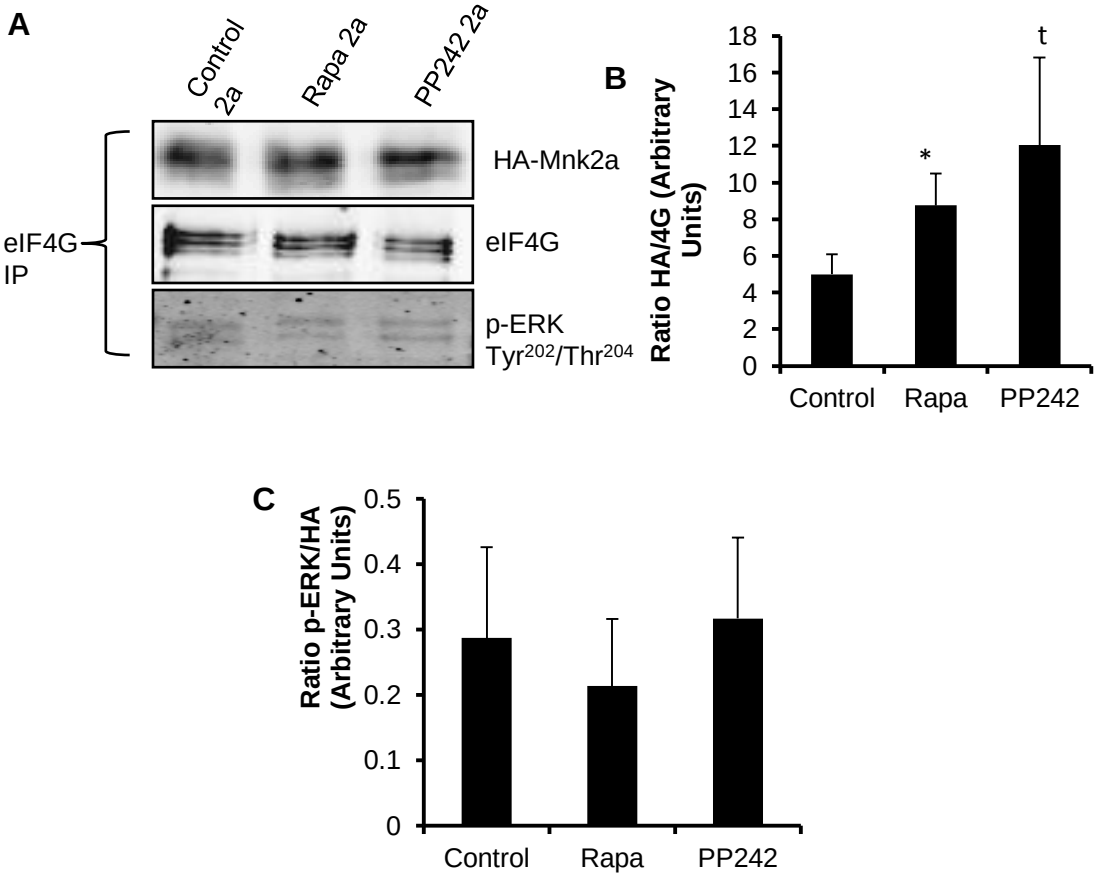

Figure 3.11 Effect of rapamycin on Mnk2-eIF4G-p-ERK binding. A) Western blot analysis of HA-Mnk2a binding to phospho-ERK Thr^{202}/Tyr^{204} and endogenous immunoprecipitated eIF4G. B) Graphical representation of the ratio HA-Mnk2a to eIF4G input. Bands were quantified by densitometry using the Licor Odyssey software. Student's t-test was used to analyse the data, * indicates $p<0.05$ compared to control, t indicates $p<0.1$ compared to control. C) Graphical representation of the ratio HA-Mnk2a to p-ERK. Bands were quantified by densitometry using the Licor Odyssey software.

Human Mnk2a

```
  1 MVQKKPAELQGFHRSFKGQNPFELAFSLDQPDHGDSDFGLQCSARPDMPASQPIDIPDAK
 61 KRGKKKKRGRATDSFSGRFEDVYQLQEDVLGEGAHARVQTCINLITSQEYAVKIIEKQPG
121 HIRSRVFREVEMLYQCQGHRNVLELIEFFEEEDRFYLVFEKMRGGSILSHIHKRRHFNEL
181 EASVVVQDVASALDFLHNKGIAHRDLKPENILCEHPNQVSPVKICDFDLGSGIKLNGDCS
241 PISTPELLTPCGSAEYMAPEVVEAFSEEASIYDKRCDLWSLGVILYILLSGYPPFVGRCG
301 SDCGWDRGEACPACQNMLFESIQEGKYEFPDKDWAHISCAAKDLISKLLVRDAKQRLSAA
361 QVLQHPWVQGCAPENTLPTPMVLQRNSCAKDLTSFAAEAIAMNRQLAQHDEDLAEEEAAG
421  QGQPVLVRATSRCLQLSPPSQSKLAQRRQRASLSSAPVVLVGDHA
```

Mouse Mnk2

```
  1 MVQKRTAELQGFHRSFKGQNPFELAFSLDLAQHRDSDFSPQCEARPDMPSSQPIDIPDAK
 61 KRGRKKKRCRATDSFSGRFEDVYQLQEDVLGEGAHARVQTCVNLITNQEYAVKIIEKQLG
121 HIRSRVFREVEMLYQCQGHRNVLELIEFFEEEDRFYLVFEKMRGGSILSHIHRRRHFNEL
181 EASVVVQDVASALDFLHNKGIAHRDLKPENILCEHPNQVSPVKICDFDLGSGIKLNGDCS
241 PISTPELLTPCGSAEYMAPEVVEAFSEEASIYDKRCDLWSLGVILYILLSGYPPFVGHCG
301 SDCGWDRGEACPACQNMLFESIQEGKYEFPDKDWSHISFAAKDLISKLLVRDAKQRLSAA
361 VLQHPWVQGCAPENTLPTPLVLQRNSCAKDLTSFAAEAIAMNRQLAQCEEDAGQDQPVV
421 IRATSRCLQLSPPSQSKLAQRRQRASLSATPVVLVGDRA
```

Table 3.1. Sequences of human and mouse Mnk2. The residues whose phosphorylation was altered by rapamycin are highlighted in red and the MAP kinase-binding motif is highlighted in green. The threonine residues in the activation loop that are phosphorylated by MAP kinases are shown in blue.

3.2.4 Mnk2 positively regulates mTORC1 activity.

Here it has been shown that rapamycin is able to induce eIF4E phosphorylation as a result of changes in phosphorylation of a potential regulatory site Ser^{437} in Mnk2a, leading to increased activity of Mnk2a. Furthermore, rapamycin also increases Mnk2/eIF4G binding, which may also contribute to the increased phosphorylation of eIF4E seen in the cell. Attempts to determine the mechanism by which this occurs have been complex, PI3K appears to have a role whilst PKB is not involved. Research published last year showed that Mnk2 regulated the phosphorylation of Ser^{1108} on eIF4G in a mechanism related to serine-arginine-rich kinases (SRPK) and to mTORC1 activity [96]. The data presented in this article showed that Mnk2 is upstream of SRPK1 and suggest SPRK1 may phosphorylate Ser^{1108} (although they show no direct evidence for this). The phosphorylation of Ser^{1108} is decreased by rapamycin and alleviated by the knockdown of Mnk2, which suggests rapamycin causes an alteration to Mnk2 activity and therefore towards SRPK1 [96]. This represents a similar situation seen with rapamycin-induced eIF4E phosphorylation. During investigations into the mechanism of eIF4G phosphorylation the authors reported reduced p70S6K1 phosphorylation in the presence of Mnk2 overexpression. This would indicate that Mnk2 has an inhibitory influence on mTORC1 activity, which the authors suggest was due to an association between Mnk2 and raptor [96]. To determine if this was related to the increase in Mnk2 activity presented here, HA-tagged Mnk2a was overexpressed followed by either mTOR (mTORC1 and mTORC2), raptor or HA immunoprecipitation and western blotting for raptor and HA. This revealed that Mnk2a was associated with raptor, and thus mTOR, as judged by the presence of HA-Mnk2a in both mTOR and raptor immunoprecipitates and the presence of raptor in HA immunoprecipitates (Fig. 3.12A). To determine if Mnk2 affected mTORC1 activity as suggested by the reduction in p70S6K1 phosphorylation shown in [96], active purified Mnk2a was added to an mTORC1 kinase assay with 4E-BP1 as the substrate. This showed that Mnk2a actually enhanced mTORC1 activity towards 4E-BP1 (Fig. 3.12B), which is contrary to what was expected based on the available literature [96]. These data also do not help the understanding of the mechanism underlying rapamycin-induced increases in Mnk2 activity. This finding may represent a possible feedback mechanism of mTORC1 activity. Mnk2a activity is increased through reduced phosphorylation of Ser437 by mTORC1 inhibition resulting in increased Mnk2a activity. Mnk2a may then phosphorylate raptor and restore mTORC1 activity. This needs to be repeated and investigated further to determine if in fact raptor is a substrate of Mnk2.

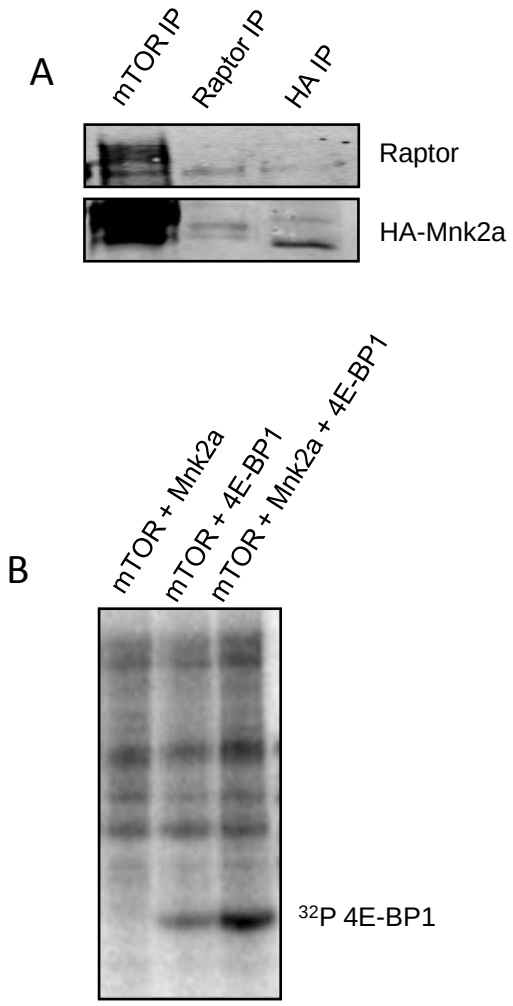

Figure 3.12 Effect of Mnk2 on mTORC1 activity. A) Extracts of HEK-293 cells expressing HA-Mnk2a were immunoprecipitated with anti-mTOR, Raptor or HA, run on SDS-PA gels and blotted for Raptor or HA overnight. n=1. B) PC3 cell extracts were immunoprecipitated for Raptor and then incubated with 1µg recombinant GST-4E-BP1, +/- 200ng Mnk2a, 100µM ATP and 1µCi [γ-^{32}P]ATP for 20min at 30°C. Samples were subjected to SDS-PAGE and then incubated with a phospho-imager screen overnight. n=1

3.3 Discussion

The deregulation of the PI3 kinase/PKB pathway is a common event in many cancers and leads to an aggressive phenotype. It is important to understand the signalling events that lead to this. Indeed, this is central to the production of effective and non-toxic therapies. It is widely agreed that the Mnks are a viable drug target because Mnk1/2 DKO mice do not show an overt phenotype [45]. Furthermore, animal models of lymphoma and glioblastoma, treated with Mnk inhibitors or knockout of the Mnks, show significantly better prognosis and resistance to recurring tumours [78]. However, it remains to be clearly established the mRNAs whose translation is altered by eIF4E phosphorylation.

Some of the data presented here agree with published findings; i) rapamycin does increase phosphorylation of eIF4E, ii) this effect appears independent of changes in binding of eIF4G and 4E-BP1 to eIF4E; iii) changes in phosphorylation of ERK is not involved in rapamycin-induced eIF4E phosphorylation. Previous studies have shown that rapamycin can increase phosphorylation of eIF4E in a PI3 kinase-dependent fashion [29, 31]. In both reports, the authors suggest this pathway is independent of changes in ERK. However, they disagree on the role of PKB. Those studies used different cancer cell lines, which could explain the differences seen. In agreement with previous work, this study shows eIF4E phosphorylation increases in PC3 prostate cancer cells when treated with rapamycin, an effect that is reduced when the PI3 kinase inhibitor LY294002 is added in combination with rapamycin. This correlates with data that show the loss of the regulatory p85α subunit of PI3 kinase also blocks rapamycin-induced eIF4E phosphorylation [31]. Rapamycin-induced eIF4E phosphorylation is also decreased with a combination of the PI3 kinase p110β inhibitor TGX-221 and the p110α inhibitor PI3-KαVIII. This suggests that both the p110α and p110β isoforms of PI3K are responsible for the effect of rapamycin probably because PC3 cells express three of the p110 isoforms: α, β and γ [270]. Since TGX-221 only inhibits the β isoform and PI3-KαVIII only inhibits the α isoform, it is possible that the other isoform can compensate when one is inhibited. These data also suggest the p110γ isoform is not involved, which may be because its expression is much lower than the other isoforms in PC3 cells and therefore cannot compensate when both p110α and p110β are inhibited [270].

The mechanism by which rapamycin leads to increased eIF4E phosphorylation was not understood and it was therefore of interest to determine how this occurs. Evidence presented here shows that rapamycin increases eIF4G/eIF4E binding, although not significantly, whilst slightly increasing 4E-BP1/eIF4E binding. This does not follow the conventional model such that it would be expected rapamycin would have a similar affect

as that seen with PP242. The data for PP242 are in line with expectations, by showing a decrease in eIF4G/eIF4E binding, an increase in 4E-BP1/eIF4E binding and decreased eIF4E phosphorylation. However, the data presented here show the combination of rapamycin and TGX-221 significantly decreases eIF4G/eIF4E binding and increases 4E-BP1/eIF4E binding without affecting rapamycin-induced eIF4E phosphorylation. Furthermore, LY294002 does not significantly decrease eIF4G binding to eIF4E but doe cause a decrease in eIF4E phosphorylation. This would suggest the changes in eIF4G/eIF4E and 4E-BP1/eIF4E binding do not explain the changes in eIF4E phosphorylation. Some interesting data came from assessing the eIF4G/eIF4E binding in Mnk single KO cells. The single KO of Mnk1 leads to a significant decrease in eIF4G/eIF4E binding whereas loss of Mnk2 results in the opposite, increased eIF4G/eIF4E binding. It is possible that Mnk2 negatively regulates eIF4G/eIF4E binding, whilst Mnk1 positively regulates binding. In the wildtype and single Mnk-KO cells rapamycin causes a decrease in eIF4G/eIF4E binding, whereas in PC3 cells there is an increase. The decrease in eIF4G/eIF4E binding in wildtype MEFs in response to rapamycin is in line with the model that mTORC1 inhibition increases 4E-BP1/eIF4E binding, therefore resulting in a dissociation of eIF4G from eIF4E [271, 272]. PC3 cells are cancer cells so will exhibit characteristics that differ from normal cells; increased eIF4G/eIF4E binding in response to rapamycin could be a resistance mechanism to overcome mTORC1 inhibition.

The role of PKB in rapamycin-induced eIF4E phosphorylation is not clear based on the available literature. The PTEN null status of PC3 cells is associated with low basal levels of eIF4E phosphorylation whilst DU145 prostate cancer cells express PTEN and show high levels of basal eIF4E phosphorylation[29]. This suggests that inhibiting PKB leads to increased eIF4E phosphorylation. Published data show PKB knockdown, by siRNA, increases eIF4E phosphorylation in apparent contradiction to the evidence that knockout of the regulatory p85α PI3 kinase subunit decreases eIF4E phosphorylation [31]. In contrast to this there is evidence, in MCF7 cells and DU145 cells, that rapamycin promotes activation of PKB, as illustrated by measurements of PKB activity[29]. The authors of this study [29] also suggest the p70S6K and IRS1 feedback loop is responsible for stimulation of PI3 kinase [266]. In some instances, the evidence in this study conflicts with previous work, which has shown rapamycin-induced eIF4E phosphorylation is related to PKB activation [266]. This report implies that PKB does not have a role in the increased phosphorylation of eIF4E seen in response to rapamycin. The data here show phosphorylation of Ser^{473} and Thr^{308} increases with rapamycin treatment; however rapamycin combined with TGX-221 results in a decrease in Ser^{473} and Thr^{308} phosphorylation whilst this is not the case for eIF4E phosphorylation. To further investigate this an inhibitor of PKB was employed, Akti1/2, which blocked rapamycin-

induced eIF4E phosphorylation; however PMA also decreased Thr^{308} phosphorylation without a concomitant decrease in eIF4E phosphorylation. Phosphorylation of the T-loop in Mnk2a does not increase with rapamycin but when combined with Akti1/2 there is a trend towards decreased T-loop phosphorylation. This suggests that the decreased eIF4E phosphorylation in cells treated with rapamycin and Akti1/2 is caused by reduced Mnk2 T-loop phosphorylation and is not related to the mechanism by which rapamycin increases Mnk2 activity. Therefore, in PC3 cells, there is more evidence to support a role for PKB in rapamycin-induced eIF4E phosphorylation.

From earlier studies and data presented in this report, it seems there is little evidence for changes to ERK in the phenomenon of rapamycin-induced eIF4E phosphorylation. Interestingly, this supports the idea that Mnk1 is not involved, since this is the isoform activated by ERK. One report indicates the p38MAPK pathway is involved and suggests both ERK and p38MAPK must be inhibited but they do not show the data [29]. Further supporting this are published data from Mnk1-KO, Mnk2-KO and DKO MEFs, which show both isoforms must be lost to block rapamycin-induced eIF4E phosphorylation [31], this is not surprising since the Mnks are the only eIF4E kinases [45]. This is hard to explain because Mnk1 has very low basal activity whilst Mnk2 has high basal activity; if Mnk1 alone was responsible then eIF4E phosphorylation in response to rapamycin would require either ERK or p38MAPK activation, which has not been shown to occur. The data here clearly show that Mnk2 is responsible for the increased phosphorylation of eIF4E in response to rapamycin because, as demonstrated, rapamycin does not induce eIF4E phosphorylation in Mnk2-KO cells, whilst in the wildtype cells and Mnk1-KO cells rapamycin elicits a similar response to that seen with PMA. A similar effect is seen in PC3 cells treated with siRNA against either Mnk1 or Mnk2 where the data show that only the knockdown of Mnk2 prevents rapamycin-induced eIF4E phosphorylation.

The mechanism by which rapamycin increases eIF4E phosphorylation is related to an increase in Mnk2a activity likely caused by decreased phosphorylation of Ser^{437}. This site is next to the MAP kinase-binding motif but it seems that changes in Mnk2a activity are not due to alterations in the phosphorylation of the T-loop by ERK, because rapamycin does not affect T-loop phosphorylation and there is no change in p-ERK/Mnk2 binding in response to mTORC1 inhibition. Dephosphorylation of Ser^{437} may alter the overall conformation of Mnk2a leading to higher intrinsic activity, since the C-terminus of Mnk2a alters the accessibility of the N-terminus of the protein [72]. The basis of the effect of this site on Mnk2a activity requires further investigation. The nature of the pathway that may result in dephosphorylation of Ser^{437} in response to rapamycin also requires future experiments, perhaps in relation to phosphatase activity. Mnk2 activity is linked to

eIF4G/Mnk2 binding and here rapamycin and PP242 result in increased eIF4G/Mnk2 binding. However, it has been shown that kinase dead Mnk2 showed greater association with eIF4G suggesting that Mnk2 activity is inversely correlated with eIF4G binding [72]. This is clearly not the situation here and the increased phosphorylation of eIF4E in response to rapamycin is associated with increased Mnk2 activity and Mnk2/eIF4G binding.

Interestingly, it also appears that raptor is a substrate for Mnk2a as there is an association between Mnk2a and raptor along with increased activity towards 4E-BP1 in the presence of Mnk2. These data do need repeating but may represent a novel feedback mechanism of mTORC1 activity in response to its inhibition. mTORC1 inhibition results in increased Mnk2a activity, which may result in increased phosphorylation of raptor and Mnk2a-dependent increases in mTORC1 activity. This is not a desirable situation when considering the use of rapalogs as anti-cancer agents.

These data further support the potential value of combined mTORC1 and Mnk inhibition in those cancers that do not respond well to inhibition of mTOR alone. The data presented here represents a potential resistance mechanism employed by cancers in response to mTOR inhibitors.

Chapter 4

The Mnks Regulate Insulin Signalling.

4.1 Introduction

The roles of the Mnks are still poorly understood even 15 years since their discovery and only a few substrates, other than eIF4E have been identified [41, 42, 74]. The research conducted on the Mnks has mostly focused on their tumorigenic potential in relation to eIF4E phosphorylation (reviewed [40, 79, 276]) [77, 78, 262, 277-279]. Other data available for the Mnks concerns their regulation of inflammatory signalling pathways and the expression of inflammatory cytokines [41-44, 81, 280-283].

The roles of the Mnks in other physiological systems has not yet been investigated within the literature but there are a couple of patents linking the Mnks to glucose and lipid metabolism [106, 228]. The evidence presented in one of these patents suggested that Mnk inhibitors caused an improved glucose profile. Treatment of WT mice with an Mnk2 inhibitor reduced blood glucose levels over 12 days of treatment [106]. The Mnk2 inhibitor (termed compound 15) was presented with little evidence to show its specificity and there are currently no other Mnk2 specific inhibitors available. Compound 15 also showed a similar efficacy in an insulin tolerance test compared to the PPARγ agonist rosiglitazone [106], which is being phased out as an antidiabetic drug [284]. The other data within this patent show compound 15 causes an increase in pancreatic insulin, although plasma insulin levels did not change [106]. Data from the other patent relating to the Mnks is more concerned with the treatment of obesity; however the authors did present expression data for the Mnks [228]. This revealed that Mnk1 is highly expressed in the lungs, spleen and muscle whilst Mnk2 is highly expressed in both white and brown adipose tissue and skeletal muscle [228]. When considering the data from both patents, it is clear there may be a role for the Mnks in glucose metabolism since Mnk inhibitors have a beneficial effect on insulin sensitivity and both Mnks are expressed in tissues related to glucose metabolism.

The aim of this chapter was to investigate whether the Mnks do indeed have a role in glucose metabolism and insulin signalling and if so to establish the mechanism by which the Mnks may do so.

4.2 Results

4.2.1 The Mnks are enriched in tissues related to glucose metabolism.

The expression of the Mnks has previously been shown by northern blot analysis to be ubiquitous and levels of both Mnks were highest in skeletal muscle [39]. However this panel did not include many tissues related to glucose metabolism so it was important to use a panel of tissues that included the pancreas and fat deposits. The expression of Mnk1 protein is greatest in the pancreas with high levels in the skeletal muscle, spleen and abdominal adipose when compared to the brain (Fig. 4.1A). Interestingly there are band shifts for Mnk1 in some tissues, this may denote altered phosphorylation states or isoforms and would be of interest to research further. The loading control GAPDH does show reduced expression in the pancreas and this was observed consistently across each mouse (n=3). Unfortunately, the only specific antibody available for Mnk2 does not work in tissue samples and so, instead, qPCR was used to assess the mRNA levels of Mnk2. Interestingly the expression of Mnk2 mRNA is almost non-existent in the pancreas (Fig. 4.1B), whilst the converse is true for Mnk1, which suggests Mnk1 has a key role in the pancreas. The expression of Mnk2 mRNA is greatest in abdominal adipose and scapular adipose with high levels also observed in the kidney (Fig. 4.1B). This would indicate that Mnk2 may have some important role in adipose tissue. The presence of both Mnks in tissues related to glucose metabolism would indicate the potential for a role of the Mnks in signalling pathways related to metabolism.

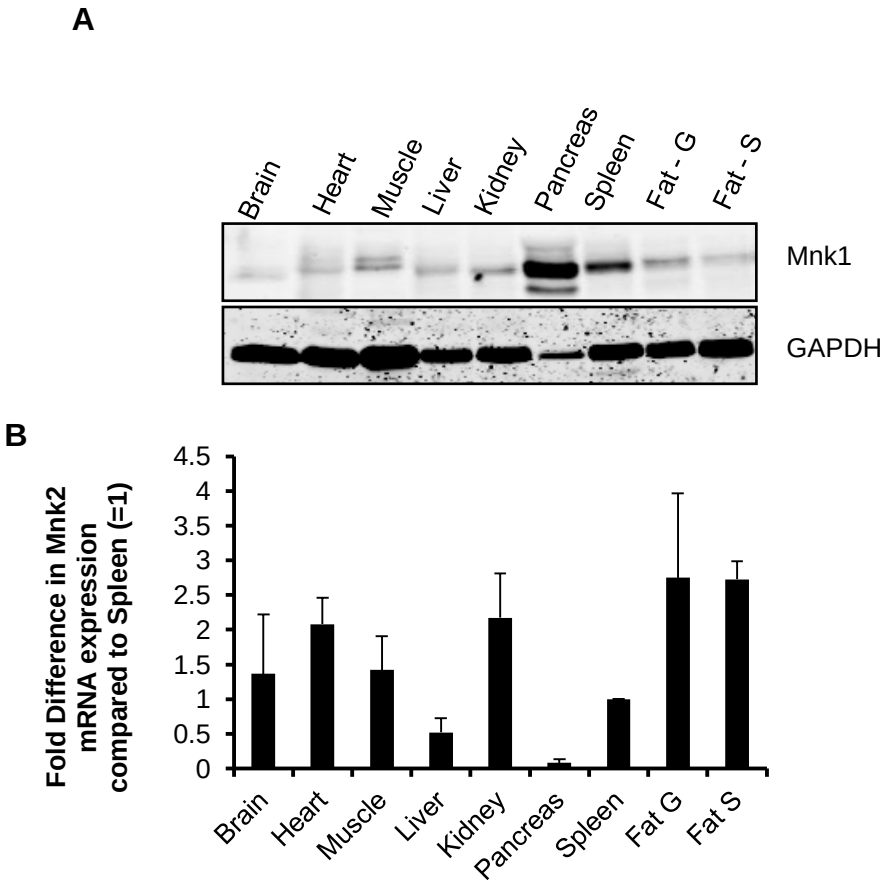

Figure 4.1. Expression of Mnk1 and Mnk2 in different mouse tissues. A) Western Blot analysis for Mnk1 in various tissues; 40µg of protein from each tissue were analysed. Fat-G and Fat-S represent abdominal adipose and scapular adipose respectively. GAPDH was used as a loading control. B) RT-qPCR analysis for Mnk2 mRNA levels; data are normalised to 18S mRNA and compared to levels in the spleen.

4.2.2 PKB phosphorylation and activity is regulated by the Mnks.

The data presented in patents related to the Mnks suggests they may play a role in insulin sensitivity [106, 228]. Furthermore there are high levels of the Mnks in insulin responsive tissues; however the data presented in these patents were conflicting as to whether Mnks play a positive or negative role in glucose metabolism. One of the most important targets of insulin signalling and a major starting point of multiple anabolic pathways is PKB, which is activated through phosphorylation at two sites; Ser^{473} and Thr^{308} [24]. It is an essential step in the initiation of glucose uptake by the cell and so represents a good indicator of insulin sensitivity [285].

The knockout of Mnk1 leads to a considerable impairment in the insulin induced phosphorylation of both sites (Ser^{473} and Thr^{308}), in PKB, compared to WT MEFs (Fig. 4.2A). In Mnk1-KO cells, there is overall reduction in phosphorylation of the site Ser^{473}, whereas the Thr^{308} shows delayed as well as lower phosphorylation compared to WT cells (Fig. 4.2A). The impairment is especially evident during insulin stimulation between 5-20min. These data suggest that Mnk1 has a positive effect on PKB phosphorylation, which in turn has a positive effect on PKB activity. The effect of insulin on PKB activity in Mnk1-KO MEFs was significantly lower at the 15min time point and there was a trend towards lower activity of PKB at 30min but returned to near normal levels after 45min (Fig. 4.2B). This is consistent with phosphorylation of the Thr^{308} site (the most important one for PKB activity [286]). This indicates that Mnk1 function is required for efficient activation of PKB following stimulation by insulin but is not required for generating a full response to insulin.

The Mnk2-KO MEFs show a difference at both phosphorylation sites compared to the WT MEFs after insulin stimulation but are not different at basal levels (Fig. 4.2C). Both phosphorylation sites exhibit a major deficit in the response to insulin in Mnk2-KO MEFs (Fig. 4.2C). These data suggest that Mnk2 is necessary for normal and efficient phosphorylation of PKB. Consistent with this the loss of Mnk2 significantly reduced the activity of PKB at all-time points investigated (Fig. 4.2D).

The differing effect of Mnk1 vs Mnk2 knockout is likely due to their differing activities; Mnk2 has higher levels of activity than Mnk1 [72] and so Mnk2 knockout has a greater effect on PKB phosphorylation and activity. Based on this evidence it was important to assess PKB phosphorylation in Mnk1/2DKO MEFs. The DKO MEFs show significantly lower levels of insulin-stimulated phosphorylation at both sites compared to the WT MEFs

and exhibit lower basal levels for the Ser^{473} site (Fig. 4.2E). Phosphorylation of the Ser^{473} site is lower at all time-points after insulin stimulation, which is expected because loss of just Mnk1 or Mnk2 results in decreased phosphorylation at this site (Fig. 4.2A, C). The results for Thr^{308} phosphorylation indicate lower basal levels and an inability to increase phosphorylation to similar levels as in the WT cells at the later time points after insulin stimulation (Fig. 4.2E). This is again expected because loss of Mnk2 had a strong effect on Thr^{308} phosphorylation (Fig. 4.2C), whilst loss of Mnk1 only affects the early levels of phosphorylation after insulin stimulation (Fig. 4.2A).

The PKB activity data show a significant reduction in PKB activation, whereby the DKO cells exhibit 65% lower activity than the WT cells (Fig. 4.2F). This suggests that, in the Mnk2-KO cells, Mnk1 does not rescue PKB activity, whereas the loss of Mnk1 may be rescued by Mnk2 to some extent. Consistent with this the loss of both Mnks means there is no remaining Mnk to compensate and in DKO cells the levels of activity are the lowest when compared to the WT cells, although the reduction in activity is very similar to that in Mnk2-KO cells indicating Mnk2 is the predominant isoform required for normal PKB activation in response to insulin.

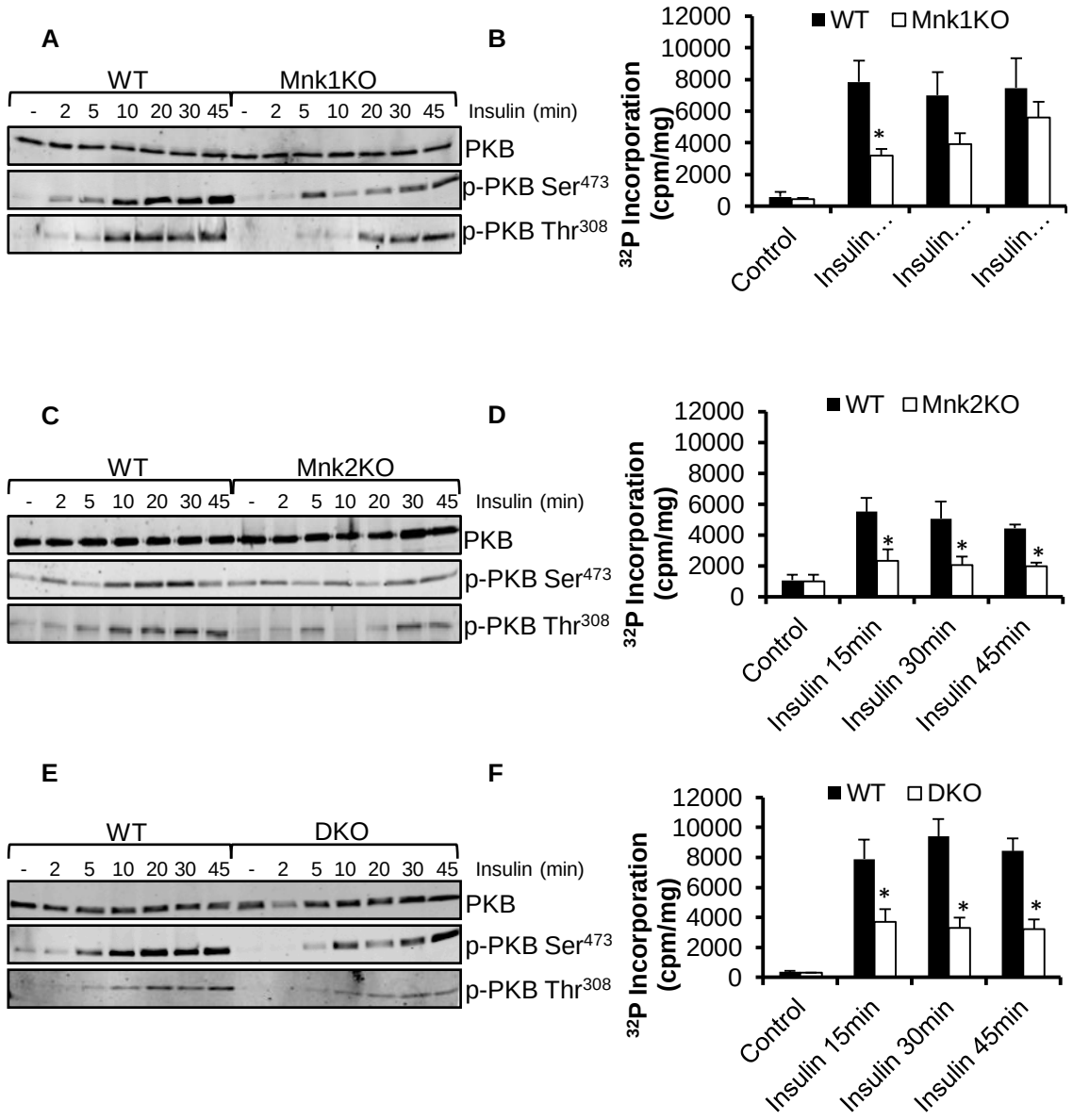

Figure. 4.2. Effects of insulin on PKB phosphorylation and activity in WT and Mnk knockout MEFs. A) Western blot analysis of total PKB, p-PKB Ser^{473} and p-PKB Thr^{308} over 45 min of insulin treatment in immortalised WT and Mnk1KO cells B) Effect of insulin on PKB activity over 45 min in immortalised WT and Mnk1KO MEFs. Cellular extracts were subjected to immunoprecipitation using an anti-PKBα antibody for 1h followed by incubation with Crosstide peptide and 1µCi [γ-^{32}P]ATP. Radioactivity was measured using the Čerenkov method. Student's t-test was used to analyse significance by comparison of each respective time point for WT and Mnk knock-out. * indicates significance at $p<0.05$. C) Western blot analysis of total PKB, p-PKB Ser^{473} and p-PKB Thr^{308} over 45 min of insulin treatment in primary WT and Mnk2KO cells. D) Effect of insulin on PKB activity

over 45 min in primary WT and Mnk2KO MEFs. Cellular extracts were analysed as described in B. Student's t-test was used to analyse significance by comparison of each respective time point for WT and Mnk knock-out. * indicates significance at $p<0.05$. E) Western blot analysis of total PKB, p-PKB Ser^{473} and p-PKB Thr^{308} over 45 min of insulin treatment in immortalised WT and Mnk1/2DKO cells F) Effect of insulin on PKB activity over 45 min in immortalised WT and Mnk1/2DKO MEFs. Cellular extracts were analysed as described in B. Student's t-test was used to analyse significance by comparison of each respective time point for WT and Mnk knock-out. * indicates significance at $p<0.05$.

4.2.3 Assessment of components of the insulin signalling cascade.

The effect of insulin involves numerous downstream pathways that control glucose uptake, cell survival, cell cycle progression, protein synthesis and other processes (as discussed in Chapter 1, sections 1.5.3 and 1.6.4). As discussed in the previous section, knockout of the Mnks results in a reduction in insulin-induced PKB phosphorylation and activation, which suggests that signalling downstream of PKB should also be affected. It was therefore important to study the contribution of each Mnk alone and of both to targets of PKB signalling.

4.2.3.1 Mnk1 knockout alters downstream PKB signalling.

A major downstream pathway activated by PKB is the mTORC1 pathway. The tuberous sclerosis complex (TSC1/2), which inhibits mTORC1 signalling is phosphorylated at Ser^{939} and Thr^{1462} (TSC2) and inactivated by PKB leading to mTORC1 stimulation [287, 288]. Other controversial evidence shows that PKB can control mTORC1 activation by phosphorylation of PRAS40 at Thr^{246}, which results in further phosphorylation by mTORC1 at Ser^{183} and Ser^{221} This leads to the dissociation of PRAS40 from mTORC1 and the subsequent removal of the inhibitory influence of PRAS40 [22, 25, 289]. Once activated, mTORC1 has numerous substrates one of which is 4E-BP1. mTORC1 phosphorylates a number of sites on 4E-BP1 including Thr^{37} and Thr^{46}, which are priming sites for Ser^{65} and Thr^{70} [290]. Insulin stimulation results in the phosphorylation of Ser^{65} and Thr^{70} by mTORC1. mTORC1 also phosphorylates S6 kinase (S6K), of which there are four isoforms; p70S6K α1 & α2 and p70S6K β1 & β2 [291], where the former are known as S6K1 and the latter S6K2. Activation of S6Ks occurs through their phosphorylation by mTORC1. This leads to phosphorylation of S6K substrates, which include the ribosomal protein S6 whose phosphorylation at $Ser^{240/244}$ acts as a readout of S6K activity.

The data show changes in the pattern of insulin-stimulated TSC2 phosphorylation at Thr^{1462} in Mnk1-KO cells. There are early increases in phosphorylation in Mnk1-KO MEFs, which occurs as rapidly as 2-5min after insulin stimulation, whilst in WT cells phosphorylation is lower in comparison (Fig. 4.3A). In WT cells the highest levels of phosphorylation occur at 20-30min, which is not seen in Mnk1-KO cells where the phosphorylation is lower. This suggests the lower insulin-induced PKB activity in Mnk1-KO cells has an effect on the pattern of TSC2 phosphorylation by PKB.

Insulin rapidly induces phosphorylation of PRAS40 on Thr^{246} with phosphorylation being seen by 2min of insulin treatment and being sustained for all times looked at in WT cells (Fig. 4.3A). This is not the case in Mnk1-KO cells where there is distinctly lower levels of phosphorylation in response to insulin, which would suggest that the deficit in early PKB activity has a major effect on PRAS40 phosphorylation.

The total 4E-BP1 blot (Fig. 4.3A) shows three bands, which indicate the extent of 4E-BP1 phosphorylation, the lowest, α, band contains unphosphorylated 4E-BP1, the middle, β, band contains 4E-BP1 phosphorylated at Thr^{36}, Thr^{45} and Thr^{69} (humans Thr^{37} and Thr^{46} Thr^{70}) whilst the highest, γ, band contains 4E-BP1 phosphorylated at all four sites (i.e. including Ser^{64} in humans Ser^{65}). In serum starved WT MEFs, all of the 4E-BP1 is found in the β and γ forms and after 10min of insulin treatment the majority of 4E-BP1 is found in the most phosphorylated γ form (Fig. 4.3A). This is consistent with the behaviour of the Ser^{64} site, which shows increased phosphorylation between 10-20min after insulin treatment (fig 4.3A). In Mnk1-KO cells there is more 4E-BP1 in the lowest α form basally and up until 10min after insulin treatment after which an increased proportion is in the γ form (Fig. 4.3A).

The phosphorylation of S6 on $Ser^{240/244}$ acts as a readout of S6K activity and therefore mTORC1 activation. The results show no obvious difference between WT and Mnk1-KO cells, with S6 phosphorylation increasing 20min after insulin stimulation in both types of cell (Fig. 4.3A). These data overall indicate the altered TSC2 phosphorylation and lower insulin-induced PRAS40 phosphorylation only affects 4E-BP1 and not S6K/S6 in Mnk1-KO cells.

To determine if the knockout of the Mnks affected other insulin-stimulated pathways the phosphorylation of ERK was assessed. There is a slight temporal shift in phosphorylation of ERK in Mnk1-KO MEFs (Fig. 4.3B) with a peak activation of 5min compared with 10min in WT cells.

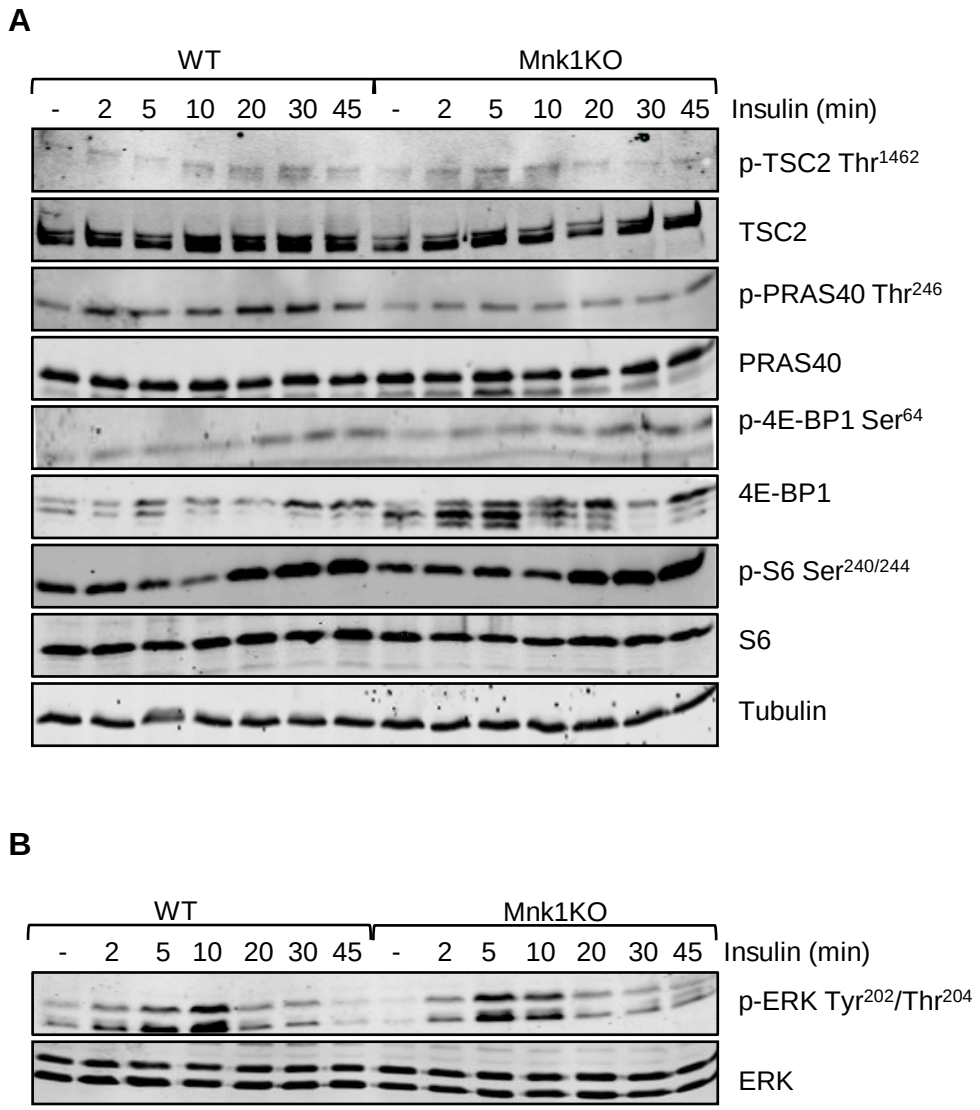

Figure. 4.3. Effect of insulin on the phosphorylation of selected proteins in immortalised WT and Mnk1KO cells. Cells were seeded in 6 cm plates and at 70-80% confluence were starved of serum overnight, followed by treatment with insulin for the times indicated. A) Western blot analysis for total TSC2 and p-TSC2 Thr^{1462} and total PRAS40 and p-PRAS40 Thr^{246}, total 4E-BP1, p-4E-BP1 Ser^{64} total S6 and p-S6 Ser$^{240/244}$. B) Western blot analysis for total ERK and p-ERK Tyr^{202}/Thr^{204}.

4.2.3.2 Mnk2KO has specific effects on downstream PKB signalling.

The insulin-stimulated activity of PKB was 60% lower in Mnk2-KO cells compared with WT (Fig. 4.2D) and so it was expected downstream signalling might be affected.

Mnk2-KO had a clear effect on TSC2 phosphorylation, with these cells showing a reduction in insulin-stimulated phosphorylation compared with WT MEFs (Fig. 4.4A). A similar effect of Mnk2-KO was seen for insulin-stimulated PRAS40 phosphorylation, a clear reduction being observed in the knockout cells (Fig. 4.4A).

The deficit in PKB activation and phosphorylation of it substrates TSC2 and PRAS40 suggests that there should also be a reduction in phosphorylation in downstream mTORC1 substrates. This was not the case for 4E-BP1 phosphorylation, which showed a rapid increase in the proportion of the γ band in Mnk2-KO cells in response to insulin; this was also reflected in the phosphorylation of the Ser^{64}, which showed slightly elevated phosphorylation in response to insulin in the Mnk2-KO cells when compared to WT cells (Fig. 4.4A). Interestingly there was some effect of Mnk2-KO on S6 phosphorylation. In Mnk2-KO cells, there were reduced levels of S6 phosphorylation at basal levels as well as a delay in its peak phosphorylation (Fig. 4.4A). In WT cells, S6 phosphorylation began to increase 10min after insulin stimulation whilst this did not occur until 30min in the Mnk2-KO cells.

These data indicate that Mnk1 and Mnk2 have differing roles in the regulation of downstream mTORC1 signalling where Mnk1 only affects insulin-induced 4E-BP1 phosphorylation and Mnk2 only affects S6 phosphorylation.

Because Mnk2 can bind to phosphorylated ERK, which is thought to play a role in the high basal activity of Mnk2 [72], ERK phosphorylation was therefore also examined. Peak ERK phosphorylation was shifted from 5/10min to 10min in Mnk2-KO cells and was slightly lower (Fig. 4.4B).

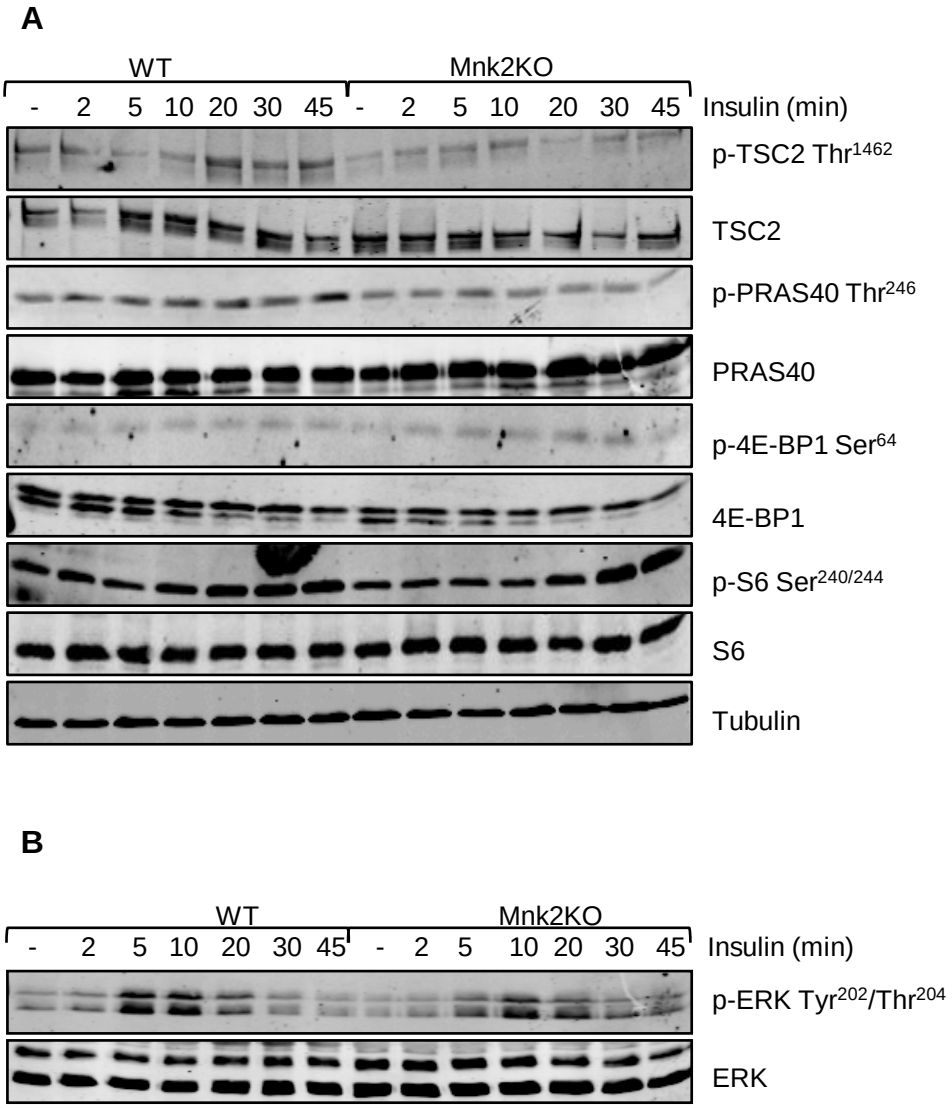

Figure. 4.4. Effect of insulin on the phosphorylation of selected proteins in primary WT and Mnk2KO cells. Cells were seeded in 6 cm plates and at 70-80% confluence were starved of serum overnight, followed by treatment with insulin for the times indicated. A) Western blot analysis for total TSC2 and p-TSC2 Thr^{1462} and total PRAS40 and p-PRAS40 Thr^{246}, total 4E-BP1, p-4E-BP1 Ser^{64} total S6 and p-S6 Ser$^{240/244}$. B) Western blot analysis for total ERK and p-ERK Tyr^{202}/Thr^{204}.

4.2.3.3 Knockout of both Mnks greatly reduces downstream PKB signalling.

The insulin-induced activation of PKB in Mnk1/2-DKO cells was slightly lower (Fig. 4.2E) than the levels seen in Mnk2-KO cells compared to WT cells (Fig. 4.2D). This suggests that there would be an effect on PKB substrates TSC2 and PRAS40, which was the case with Mnk2-KO (Fig. 4.4A) but not so much Mnk1-KO (Fig. 4.3A). Loss of both Mnks led to a reduction in the phosphorylation of TSC2 and PRAS40 in response to insulin (Fig. 4.5A). The knockout of either Mnk1 or Mnk2 had less effect on downstream mTORC1 substrates S6 and 4E-BP1 (figs. 4.3A, 4.4A), which appears to be an isoform specific effect. Therefore it was important to assess these proteins in Mnk1/2-DKO cells. This revealed that loss of both Mnks has a clear effect on both 4E-BP1 phosphorylation and S6 phosphorylation (Fig. 4.5A). There was distinctly lower insulin-stimulated phosphorylation of Ser^{64} on 4E-BP1 in Mnk1/2-DKO cells, which was reflected in the reduced levels of the γ species of total 4E-BP1. Similarly, S6 phosphorylation was lower at all time points in Mnk1/2DKO cells compared with WT cells.

These data suggest the knockout of both Mnks cause such a sufficient reduction in PKB activation in response to insulin, which culminates in a reduction in direct PKB substrates and mTORC1 signalling.

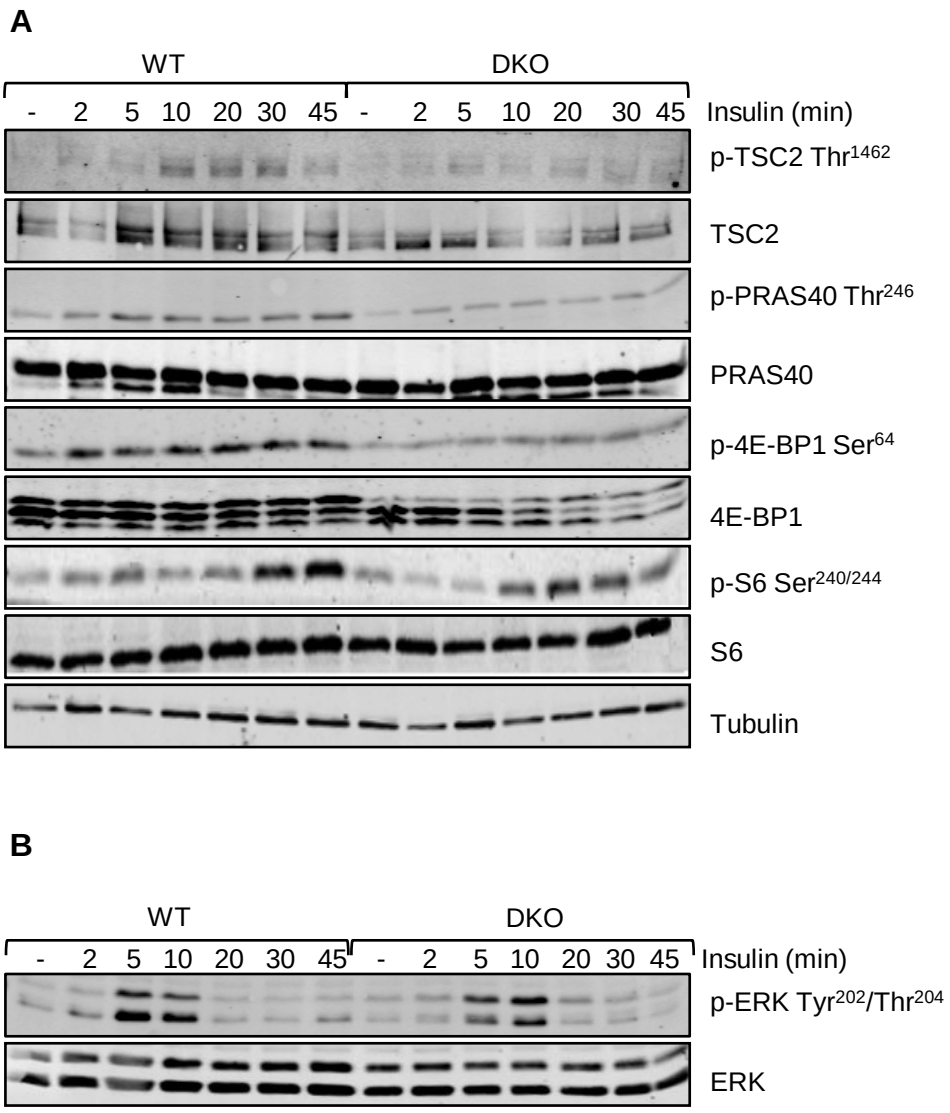

Figure. 4.5. Effect of insulin on the phosphorylation of selected proteins in immortalised WT and Mnk1/2DKO cells. Cells were seeded in 6 cm plates and at 70-80% confluence were starved of serum overnight, followed by treatment with insulin for the times indicated. A) Western blot analysis for total TSC2 and p-TSC2 Thr^{1462} and total PRAS40 and p-PRAS40 Thr^{246}, total 4E-BP1, p-4E-BP1 Ser^{64} total S6 and p-S6 Ser$^{240/244}$. B) Western blot analysis for total ERK and p-ERK Tyr^{202}/Thr^{204}.

4.2.4 Investigations into glucose uptake in Mnk-KO cells.

One of the major effects of insulin is glucose uptake, which is controlled by both PKB dependent and independent pathways. The data already shown suggest that knockout of Mnk1, Mnk2 or loss of both Mnks has a detrimental effect on insulin-stimulated PKB activation. Therefore it was important to see if Mnk knockout has an effect on insulin-induced glucose uptake. In order to investigate this three different methods were used, AS160 phosphorylation, GLUT4 translocation visualized by confocal microscopy and radioactive glucose uptake. As discussed in Chapter 1, section 1.5.3, AS160 is essential for insulin-stimulated glucose uptake and requires phosphorylation on numerous sites by PKB [220, 292], therefore this was a key target to look at in Mnk knockout cells. To visualize the effect of Mnk knockout on GLUT4 translocation cells were transfected with GFP-tagged GLUT4 and stained for the plasma membrane then confocal microscopy was used to look for any merging of GLUT4 with the plasma membrane. Finally using radioactively labelled 2-deoxyglucose the uptake of glucose into cells generated a quantitative assessment of the effect of Mnk knockout.

Analysis of AS160 phosphorylation showed that Mnk1-KO led to a reduction in insulin-stimulated phosphorylation of the PKB site Thr^{642} at all times (Fig. 4.6A). This suggests that AS160 phosphorylation is a rapid event in insulin signalling. Knockout of Mnk2 led to reduced insulin-stimulated phosphorylation at the 10-45min time points although total AS160 at 2-5min appeared slightly elevated (Fig. 4.7A). In WT MEFs there was an increase in AS160 phosphorylation from 10min that was sustained up until 45min.

Following this GLUT4 translocation was assessed in unstimulated and insulin-stimulated WT, Mnk1-KO, Mnk2-KO and Mnk1/2-DKO MEFs. This revealed that under basal conditions, GLUT4 resides around the nucleus in all cell types (Figs. 4.6B, 4.7B & 4.8B), which indicates its localization within the *trans* Golgi network (TGN) [293, 294]. Insulin stimulation leads to GLUT4 becoming dispersed throughout the WT cell, with some yellowing at points around the plasma membrane, presumably indicative of insertion into the membrane (Fig. 4.6B, 4.7B & 4.8B). However, this was not the case in Mnk1-KO cells where GLUT4 remained in the TGN (Fig. 4.6B). In Mnk2-KO cells GLUT4 does disperse throughout the cell but the amount localizing with the plasma membrane is low in comparison to WT cells (Fig. 4.7B). The Mnk1/2-DKO cells exhibit no yellow after insulin stimulation where it appears the GLUT4 is still in vesicles in the TGN (Fig. 4.8B).

The uptake of radioactive glucose into cells was then measured. Mnk1-KO, Mnk2-KO or Mnk1/2-DKO had no significant effect on basal glucose uptake (Figs. 4. 6C, 4.7B & 4.8C). In WT cells insulin caused a significant increase in glucose uptake, which was not seen

with insulin treatment in Mnk1-KO, Mnk2-KO or Mnk1/2-DKO cells (Figs. 4.6C, 4.7C & 4.8C). These data probably reflect the reduced insulin-stimulated PKB activation of Mnk-KO cells (Figs. 4.2B, D & F).

.

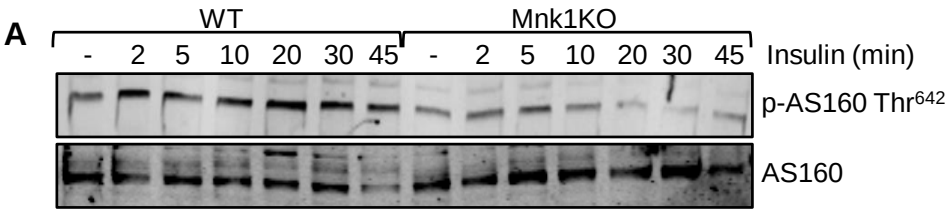
A
WT
Mnk1KO
- 2 5 10 20 30 45 - 2 5 10 20 30 45
Insulin (min)
p-AS160 Thr642
AS160

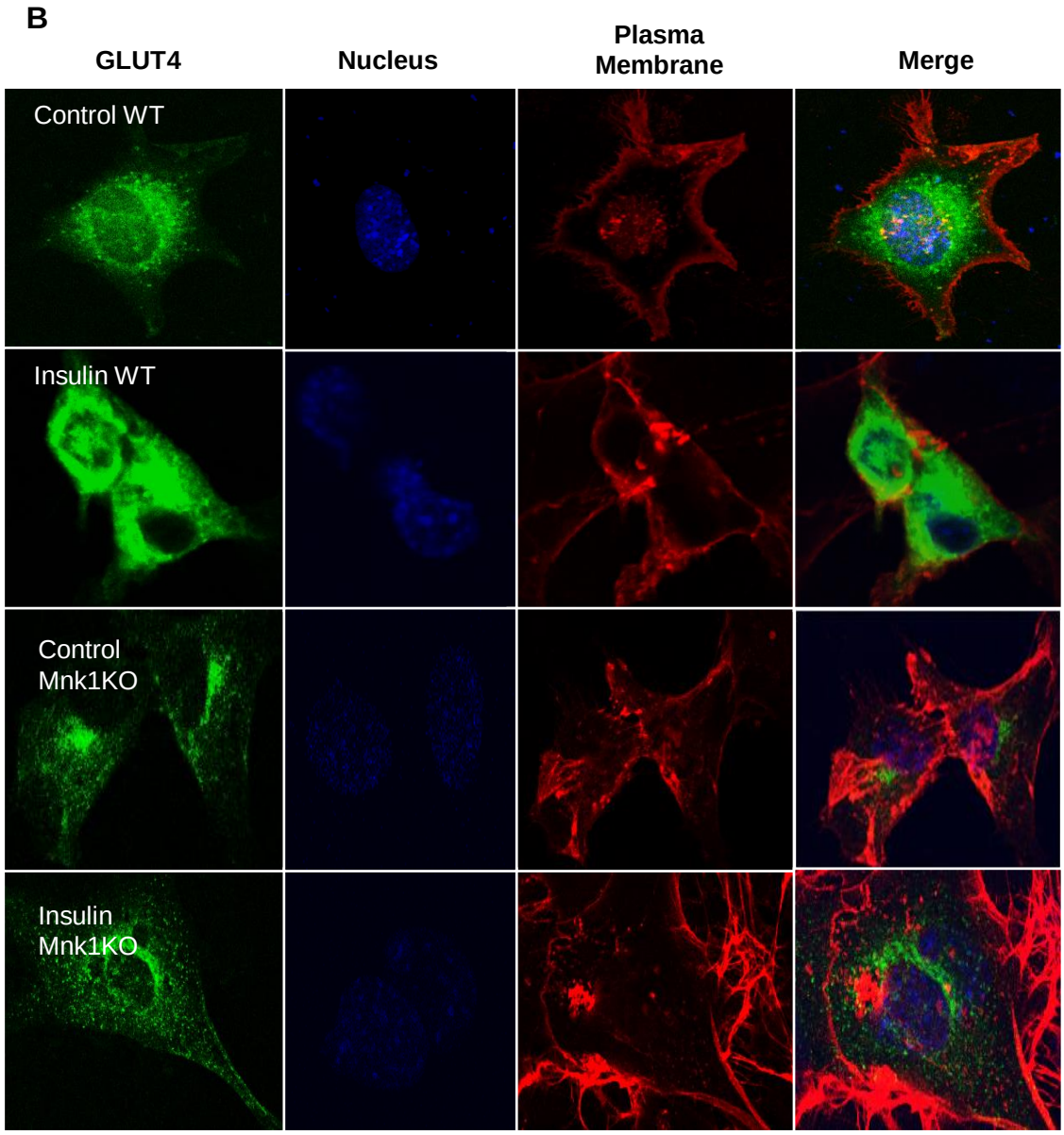
B
GLUT4
Nucleus
Plasma Membrane
Merge
Control WT
Insulin WT
Control Mnk1KO
Insulin Mnk1KO

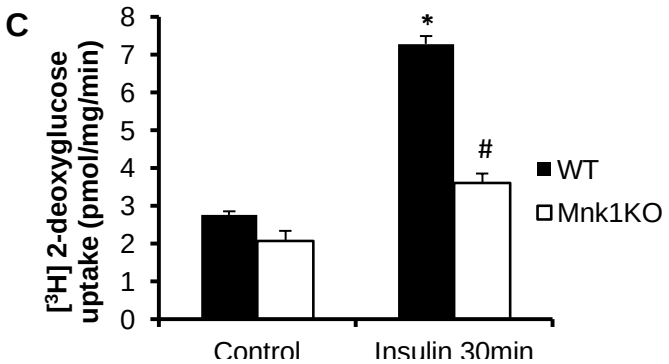
C
[3H] 2-deoxyglucose uptake (pmol/mg/min)
0
1
2
3
4
5
6
7
8
*
#
WT
Mnk1KO
Control
Insulin 30min

Figure 4.6. Effect of insulin on glucose transport into WT and Mnk1KO cells. A) Western blot analysis of phospho-AS160 Thr^{642} and total AS160. B) Effect of insulin (20 min) on the translocation of HA-GLUT4-GFP to the membrane in immortalised WT and Mnk1KO MEFs. The plasma membrane was stained with WGA tagged to Alexa-Fluor 594 and the nucleus with DAPI. Images were captured with a confocal microscope. C) Effect of insulin on [^{3}H] 2-deoxyglucose uptake into immortalised WT and Mnk1KO MEFs. Glucose transport was assessed as described in the research design and methods Student's t-test was used to analyse significance, * indicates significance at $p<0.05$ by comparison of insulin treated vs. non-treated and # indicates significance at $p<0.05$ for WT vs. Mnk1-KO.

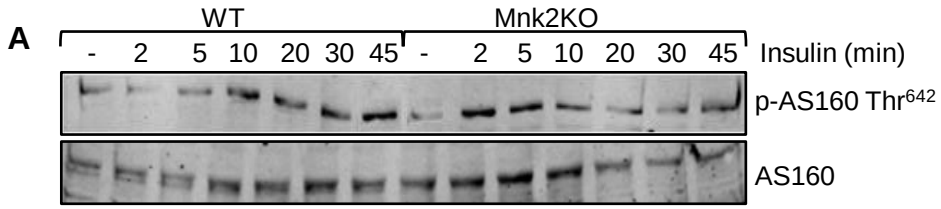
A
WT
Mnk2KO
- 2 5 10 20 30 45 - 2 5 10 20 30 45
Insulin (min)
p-AS160 Thr642
AS160

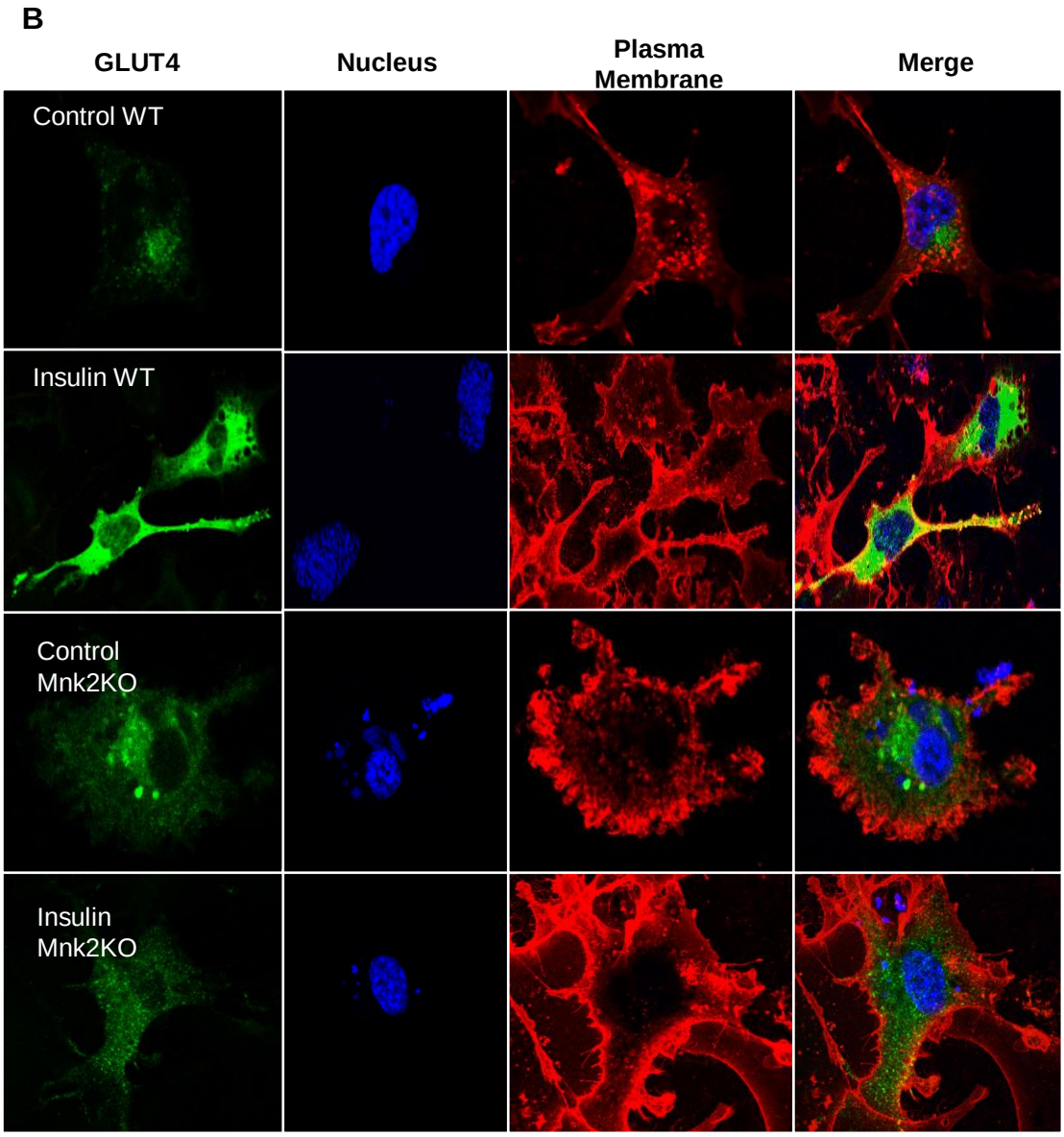
B
GLUT4
Nucleus
Plasma Membrane
Merge
Control WT
Insulin WT
Control Mnk2KO
Insulin Mnk2KO

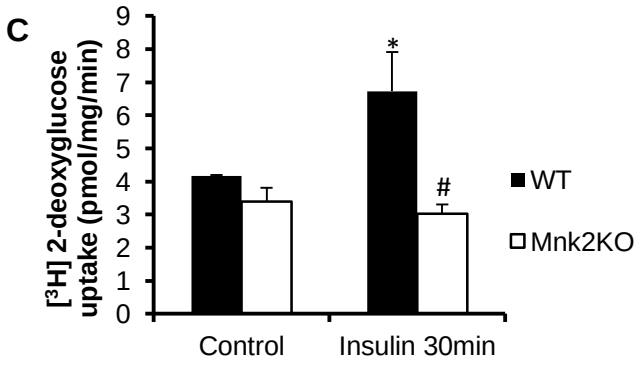
C
[3H] 2-deoxyglucose uptake (pmol/mg/min)
0 1 2 3 4 5 6 7 8 9
*
#
WT
Mnk2KO
Control
Insulin 30min

Figure 4.7. Effect of insulin on glucose transport into WT and Mnk2KO cells. A) Western blot analysis of phospho-AS160 Thr^{642} and total AS160. B) Effect of insulin (20 min) on the translocation of HA-GLUT4-GFP to the membrane in primary WT and Mnk2KO MEFs. The plasma membrane was stained with WGA tagged to Alexa-Fluor 594 and the nucleus with DAPI. Images were captured with a confocal microscope. C) Effect of insulin on [^{3}H] 2-deoxyglucose uptake into primary WT and Mnk2KO MEFs. Glucose transport was assessed as described in the research design and methods Student's t-test was used to analyse significance, * indicates significance at $p<0.05$ by comparison of insulin treated vs. non-treated and # indicates significance at $p<0.05$ for WT vs. DKO.

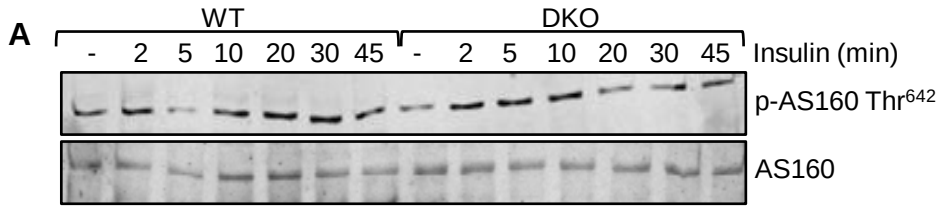
A
WT
DKO
- 2 5 10 20 30 45 - 2 5 10 20 30 45
Insulin (min)
p-AS160 Thr642
AS160

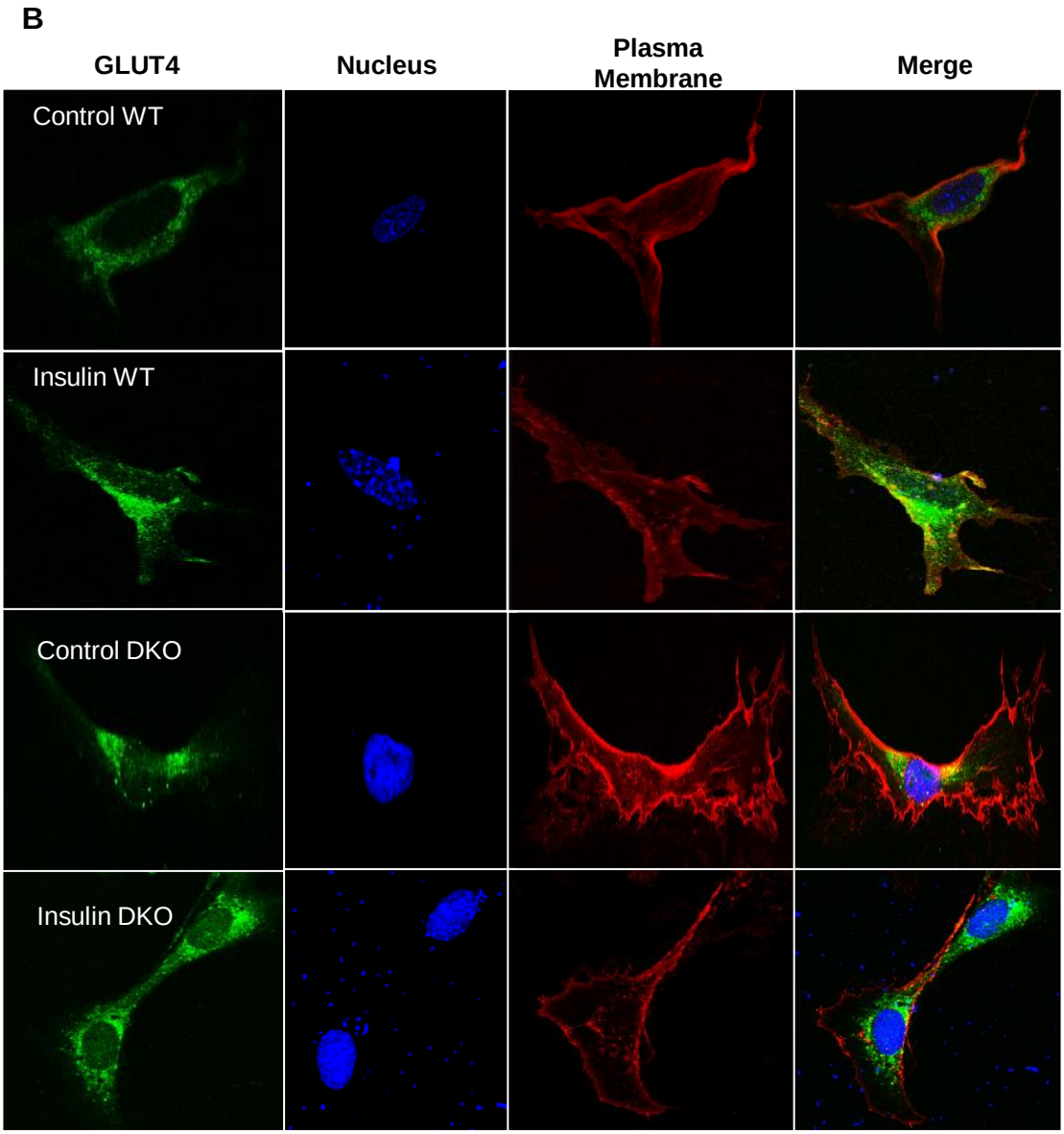
B
GLUT4
Nucleus
Plasma Membrane
Merge
Control WT
Insulin WT
Control DKO
Insulin DKO

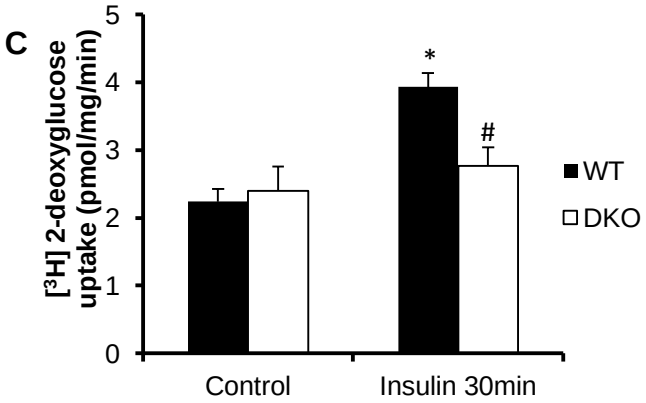
C
[3H] 2-deoxyglucose uptake (pmol/mg/min)
0
1
2
3
4
5
*
#
WT
DKO
Control
Insulin 30min

Figure 4.8. Effect of insulin on glucose transport into WT and Mnk1/2DKO cells. A) Western blot analysis of phospho-AS160 Thr^{642} and total AS160. B) Effect of insulin (20 min) on the translocation of HA-GLUT4-GFP to the membrane in immortalised WT and DKO MEFs. The plasma membrane was stained with WGA tagged to Alexa-Fluor 594 and the nucleus with DAPI. Images were captured with a confocal microscope. C) Effect of insulin on [^{3}H] 2-deoxyglucose uptake into immortalised WT and Mnk1/2-DKO MEFs. Glucose transport was assessed as described in the research design and methods Student's t-test was used to analyse significance, * indicates significance at $p<0.05$ by comparison of insulin treated vs. non-treated and # indicates significance at $p<0.05$ for WT vs. DKO.

4.2.5 Knockout of the Mnks causes perturbed PI3K activation.

The data so far indicate that the Mnks positively regulate insulin signalling by acting either directly at the level of PKB or somewhere upstream. In order to identify the mechanism(s) by which the Mnks control insulin signalling, it was important to assess PI3K activity, since PI3K is activated in response to insulin and results in the production of PIP_3, which is required for PKB activation [212, 213]. In order to measure PI3K activity, PI3K was immunoprecipitated using a pan phospho-tyrosine antibody followed by incubation with a phosphatidylinositol substrate and [γ-^{32}P] ATP. The reaction products were assessed by thin layer chromatography.

The insulin-stimulated activity of PI3K in Mnk1-KO cells was not significantly different from WT cells (Fig. 4.9A, B), which does not correlate with the lower PKB activity at only 15min (Fig. 4.2B). However, the error between samples is large and so makes it difficult to discern any effect.

The data for Mnk2-KO cells is made complicated because there is significantly higher activity at basal levels when compared to WT cells. Insulin stimulation resulted in a decrease in PI3K activity in Mnk2-KO cells compared with an increase in activity in WT cells (Fig. 4.9C, D). The activity of PI3K in WT and Mnk2-KO cells 15min after insulin treatment (Fig. 4.9C, D) correlates with PKB activity (Fig. 4.2D). The difference in basal PI3K activity between WT and Mnk2-KO cells does not correlate with PKB activity and it is not clear why this is observed.

The complexity of the data from single Mnk1 and Mnk2 knockout cells meant it was imperative to investigate Mnk1/2-DKO cells in order to determine if the Mnks regulated signalling upstream of PKB or between PI3K and PKB. The results show a significant defect in PI3K activation in response to insulin in Mnk1/2-DKO cells (Fig. 4.9E, F). This implies that the Mnks either act upstream of PI3K or on PI3K itself.

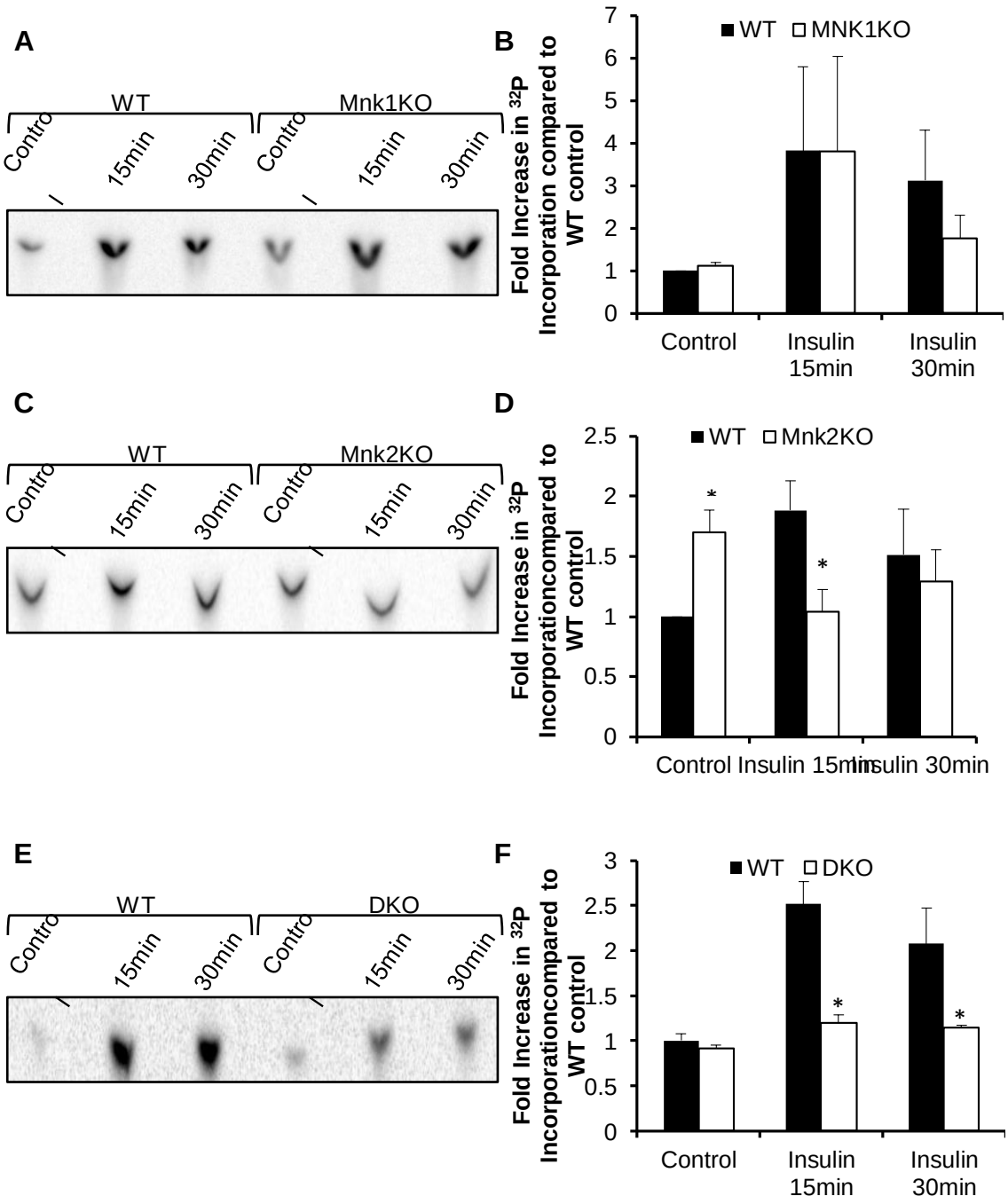

Figure 4.9. Insulin signalling is deficient in WT and Mnk-KO cells. Cells were starved of serum for 150 min and treated with insulin for the time shown followed by immunoprecipitation for phospho-tyrosine and then incorporation of [γ-^{32}P]ATP into phosphatidylinositol. Densitometry of the phosphorimage of the TLC plate was corrected for background radioactivity and normalised for protein input. A) Effects of insulin on PI3-kinase activity in WT and Mnk1KO MEFs. B) Graphs summarising data from triplicate PI3-kinase assay experiments. Data are given as fold incorporation of radioactivity compared to WT control and normalised to protein input, n = 3. Student's t-test was used to analyse

significance, * indicates significance at $p<0.05$ for WT vs. Mnk1KO at each respective time point. C) Effects of insulin on PI 3-kinase activity in WT and Mnk2KO MEFs. D) Graphs summarising data from triplicate PI3K assay experiments. Data are given as fold incorporation of radioactivity compared to WT control and normalised to protein input, n = 3. Student's t-test was used to analyse significance, * indicates significance at $p<0.05$ for WT vs. Mnk2KO at each respective time point. E) Effects of insulin on PI 3-kinase activity in WT and MNK1/2-DKO MEFs. F) Graphs summarising data from triplicate PI3K assay experiments. Data are given as fold incorporation of radioactivity compared to WT control and normalised to protein input, n = 3. Student's t-test was used to analyse significance, * indicates significance at $p<0.05$ for WT vs. MNK1/2-DKO at each respective time point.

4.2.6 Effects of Mnk Inhibitors on 3T3-L1 Cells.

Evidence presented so far from MEFs indicates that the Mnks have a potent role in the regulation of insulin signalling and are therefore required for insulin-stimulated glucose uptake. To determine if the Mnks also play a role in highly insulin-responsive cells, Mnk inhibitors were employed. The best known Mnk inhibitor is CGP57380 and affects both Mnks [76]. It does however inhibit a number of other kinases (PIM3, BRSK2 and CK1δ) [295] and so a new, more specific inhibitor called compound E (from Janssen) was also used. As previously shown the Mnks are highly expressed in abdominal adipose and so the adipocyte cell line 3T3-L1 was employed.

4.2.6.1 Mnk expression in 3T3-L1 cells.

In order to assess if the Mnks are also expressed in 3T3-L1 cells, preadipocyte 3T3-L1 cells were incubated in differentiation media (as described Chapter 2, section 2.4.1) for the times shown or left undifferentiated. Western blot analysis showed that both Mnk1 and Mnk2 were rapidly induced by 24h (Fig. 4.10). Levels peaked at day 7 of differentiation and were slightly greater than those seen in MEFs and so cells were used on the 7^{th} or 8^{th} day after differentiation began.

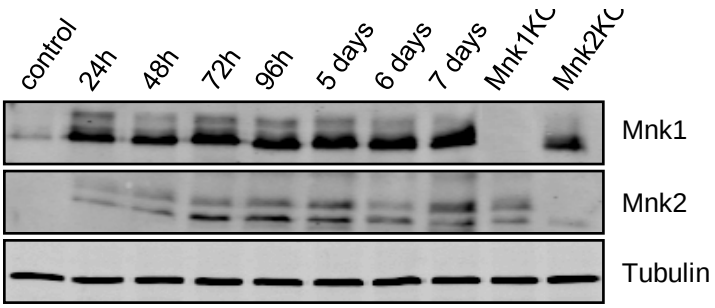

Figure 4.10. Expression of Mnk1 and Mnk2 in differentiated 3T3-L1 cells. Western Blot analysis for Mnk1 and Mnk2, cells were incubated in differentiation medium for the time indicated, control cells were undifferentiated and kept in maintenance medium. Mnk1KO and Mnk2KO are samples from knockout MEFs.

4.2.6.2 Effect of Mnk inhibition on PKB and PI3K activity.

Data from Mnk knockout cells revealed that loss of the Mnks leads to a reduction in insulin-stimulated PKB and PI3K activity. Western blot analysis of PKB phosphorylation revealed that treating cells with CGP57380 decreased the initial insulin-induced phosphorylation of Ser^{473} whilst after 20min levels were similar between samples (Fig. 4.11A). The phosphorylation of PKB at Thr^{308} was reduced at 5min and 20min after insulin stimulation in samples from CGP57380 treated cells. Insulin increased PKB activity around 12 fold at both 15min and 30min (Fig. 4.11B). This effect was significantly reduced in cells treated with compound E at the 30min time point, whilst CGP57380 reduced insulin-stimulated PKB activity at both the 15min and 30min time points (Fig. 4.11B). Compound E also exhibited a trend towards reduced PI3K activity in response to insulin whilst CGP57380 only had a marginal effect (Fig. 4.11C, D).

This data indicated that Mnk inhibition had a negative effect on insulin stimulated signalling particularly in the case of PKB. Importantly this supports the conclusion that the Mnks promote acute effects of insulin.

Inhibition of the Mnks has shown a negative effect on insulin-induced PKB activation, it was therefore relevant to study downstream targets of PKB. CGP57380 had little effect on TSC2 phosphorylation in response to insulin, although this was decreased at the 5min and 10min time points (Fig. 4.12A). A similar pattern was seen for PRAS40 with lower insulin-stimulated phosphorylation at 5min and 30min in the presence of CGP57380. Interestingly S6 phosphorylation was already high at basal levels and did not increase much with insulin treatment; however CGP57380 reduced S6 phosphorylation 5min and 10min after insulin treatment as well as under basal conditions (Fig. 4.12A). This makes the data hard to interpret, it is possible this observation is an off target effect of CGP57380 on S6K. The 4E-BP1 data shows CGP57380 reduces the shift from the β to γ form at 5min after insulin treatment as well as reduced Ser^{64} phosphorylation at 20 and 30min (Fig. 4.12A). These data indicate inhibition of the Mnks does have some effect on pathways downstream of PKB.

In Mnk knockout cells there was a shift in the temporal peak phosphorylation of ERK. This was also evident in insulin and CGP57380 treated cells with a peak in phosphorylation at 10min as opposed to a peak at 5min in just insulin treated cells (Fig. 4.12B).

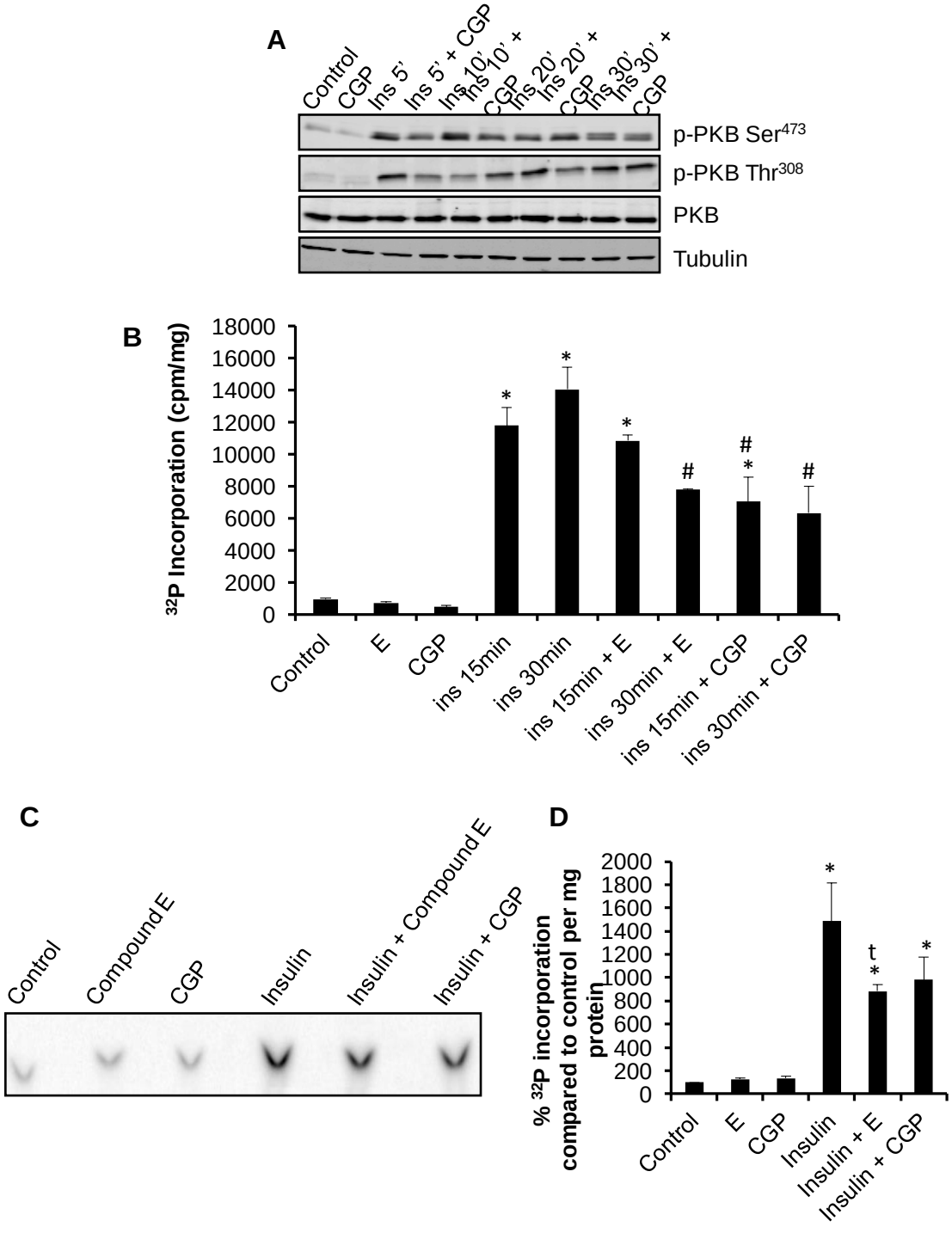

Figure. 4.11. Insulin signalling is decreased in 3T3-L1 cells treated with Mnk inhibitors. Cells were starved of serum for 150 min and pre-treated with 3µM compound E or 50µM CGP57380 for 30min followed by insulin for the time shown. A) Western blot analysis of total PKB, p-PKB Ser^{473} and p-PKB Thr^{308}. B) Effect of insulin on PKB activity over 30 min. Cellular extracts were subjected to immunoprecipitation using an anti-PKBα antibody for 1h followed by incubation with Crosstide peptide and 1µCi [γ-^{32}P]ATP. Radioactivity was measured using the Čerenkov method. Student's t-test was used to analyse significance *

indicates significance at $p<0.05$ compared to control, # indicates significance $p<0.05$ compared to insulin treated. C) Measurement of PI3K activity, cell extracts were immunoprecipitated for phospho-tyrosine and then incubated with [γ-^{32}P]ATP and phosphatidylinositol. Densitometry of the phosphorimage of the TLC plate was corrected for background radioactivity and normalised for protein input. D) Graphs summarising data from triplicate PI3K assay experiments. Data are given as fold incorporation of radioactivity compared to WT control and normalised to protein input, n = 3. Student's t-test was used to analyse significance, * indicates significance at $p<0.05$ compared to control, t indicates $p<0.1$ compared with insulin treated.

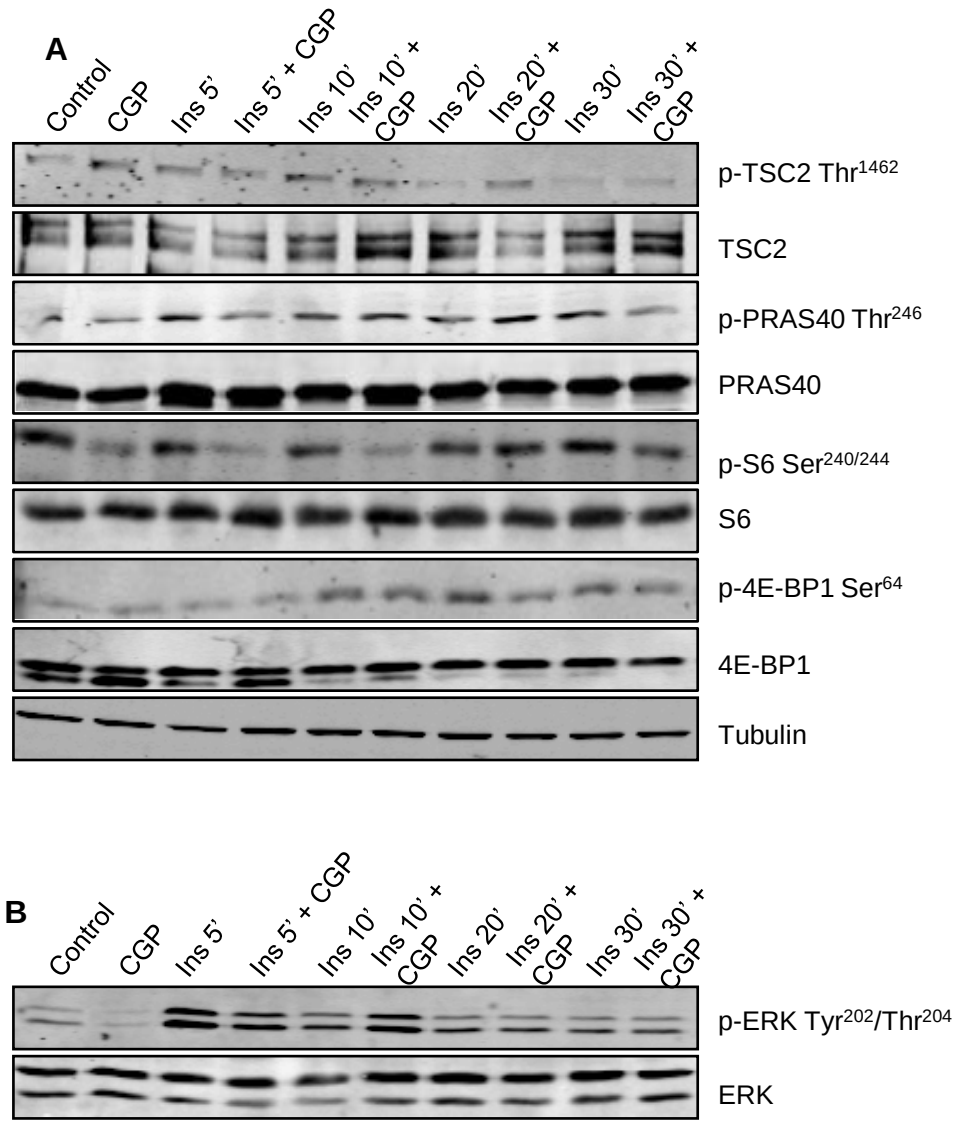

Figure. 4.12. Effect of insulin on the phosphorylation of selected proteins in fully differentiated 3T3-L1 cells. Cells were starved of serum overnight, followed by treatment with insulin for the times indicated. A) Western blot analysis for total TSC2 and p-TSC2 Thr^{1462} and total PRAS40 and p-PRAS40 Thr^{246}, total S6, p-S6 Ser$^{240/244}$, total 4E-BP1 and p-4E-BP1 Ser^{64}. B) Western blot analysis for total ERK and p-ERK Tyr^{202}/Thr^{204}.

4.2.6.3 Inhibition of the Mnks leads to a decrease in insulin-stimulated glucose uptake and lipogenesis.

In MEFs, knockout of either Mnk1 or Mnk2 led to impaired insulin-stimulated glucose uptake and AS160 phosphorylation. In differentiated 3T3-L1 cells, CGP57380 led to a decrease in insulin-stimulated AS160 phosphorylation at the 5min and 10min time points (Fig. 4.13A). Consistent with this Mnk inhibition also led to a significant reduction in insulin-dependent glucose uptake, without affecting basal levels (Fig. 4.13B).

To further assess the impact of Mnk inhibition on insulin signalling the method for glucose uptake was adapted to isolate total lipids in order to measure lipogenesis. Cells were labelled with radioactive glucose for 2h followed by extraction of total lipids in a similar method to that used in the PI3K assay (method fully described in Chapter 2, section 2.4.16). This revealed that compound E significantly decreased basal lipogenesis, an effect which was not seen with CGP57380 (Fig. 4.13C). Since compound E is a more specific Mnk inhibitor, it is possible that the Mnks do play a role in basal lipogenesis or lipolysis. Inhibition of the Mnks with either inhibitor did significantly reduce insulin-stimulated lipogenesis (Fig. 4.13C). This effect may be a consequence of reduced glucose uptake and/or a result of decreased insulin signalling to lipogenic enzymes.

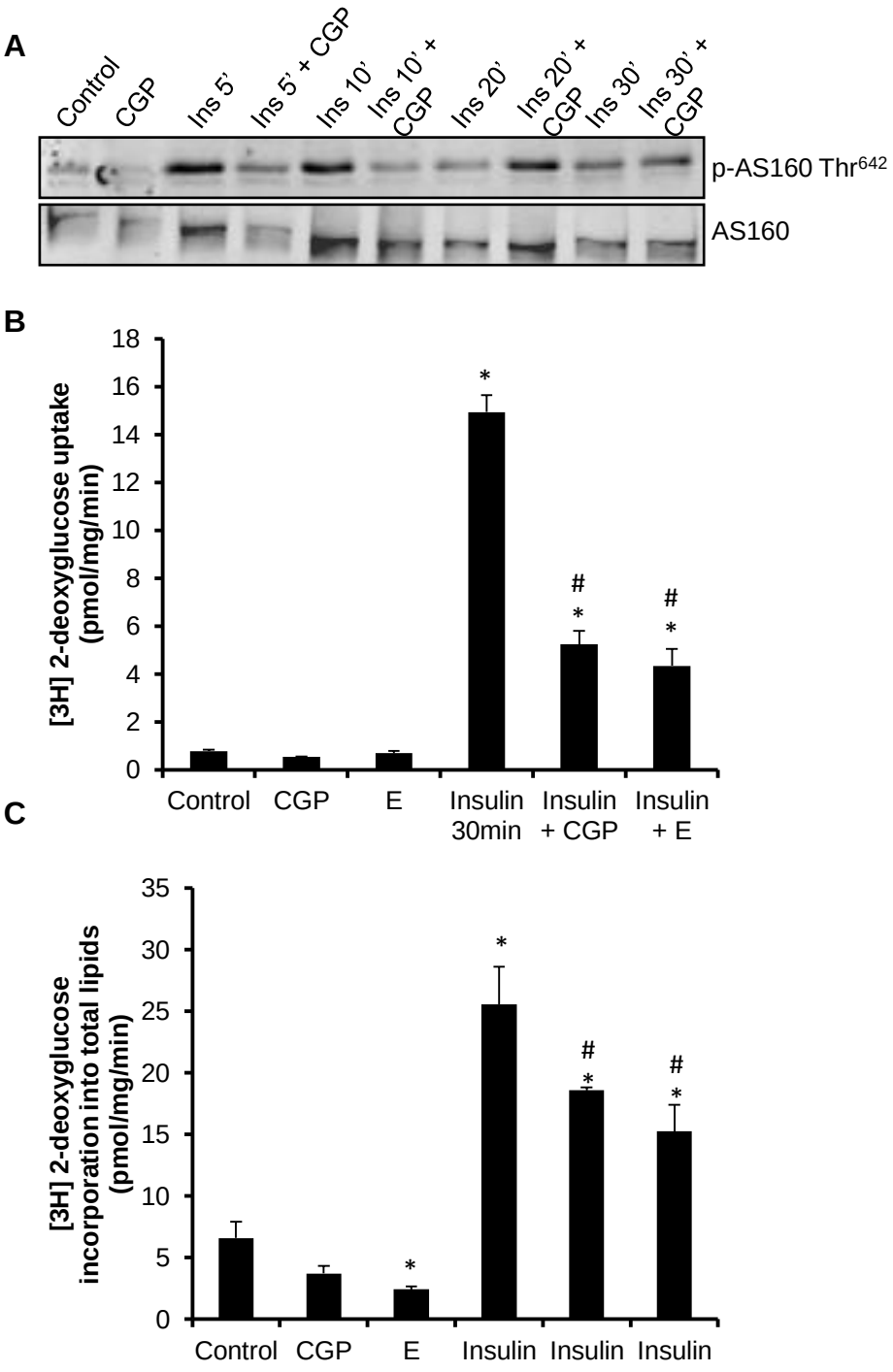

Figure 4.13. Effect of Mnk inhibitors on insulin-stimulated glucose transport in fully differentiated 3T3-L1 cells. A) Western blot analysis of phospho-AS160 Thr^{642} and total AS160. B) Effect of Mnk inhibition on insulin-stimulated [^{3}H]2-deoxyglucose uptake. Glucose transport was assessed as described in the research design and methods Student's t-test was used to analyse significance, * indicates significance at $p<0.05$

compared to control and # indicates significance at $p<0.05$ for insulin treated vs insulin treated + Mnk inhibitor. C) Effect of Mnk inhibition on insulin-stimulated lipogenesis. Cells were treated as previously and incubated with [^{3}H]2-deoxyglucose for 2h followed by total lipid isolation. Radioactive incorporation was assessed by scintillation counting. Student's t-test was used to analyse significance, * indicates significance at $p<0.05$ compared to control and # indicates significance at $p<0.05$ for insulin treated vs insulin treated + Mnk inhibitor.

4.2.7 Investigations into the mechanism by which the Mnks regulate insulin signalling.

Data so far suggest that the regulation of the insulin signalling pathway by the Mnks may involve: direct modulation of PI3K, alteration of protein or lipid phosphatases, IRS1 or the insulin receptor. Short-term Mnk inhibition led to decreased activation of PI3K and PKB as well as reduced glucose uptake, which suggests the Mnks act upon a target within the pathway in a mechanism dependent on their kinase activity. The most obvious potential target was insulin receptor substrate 1 (IRS1) because this protein is a major regulator of insulin signalling and is tightly controlled by serine/threonine phosphorylation (reviewed [229]).

4.2.7.1 IRS1 levels are lower in knockout cells and in response to inhibition of the Mnks.

In order to study this, the levels of IRS1 or the insulin receptor β (IRβ) were determined by western blot in WT MEFs, knockout MEFs and WT MEFs including cells treated with Mnk inhibitors or siRNA directed against the Mnks. This revealed that the levels of IRS1 were decreased in response Mnk inhibitors and siRNA knockdown of the Mnks. Considerably lower levels were also evident in Mnk knockout MEFs (Fig. 4.14A). The levels of IRβ were actually increased in knockout MEFs but slightly decreased in Mnk2 siRNA treated MEFs. This disparity might be caused by a compensation mechanism in Mnk knockout MEFs that is not triggered by short term depletion as with siRNA. These data indicate that the Mnks can regulate IRS1 protein levels.

Changes in the level of any protein can be a consequence of differences in transcription, mRNA stability, and protein synthesis or protein stability. The levels of IRS1 mRNA were therefore assessed by qPCR. This showed that compound E significantly increased IRS1 mRNA levels whilst Mnk2 knockout or Mnk2 knockdown with siRNA caused significant decreases in IRS1 mRNA (Fig. 4.14B). Similarly Mnk1/2-DKO cells showed significant reductions in IRS1 mRNA.

These data suggest dual regulation of IRS1 at both the protein and mRNA levels. However the major effect appears to be at the protein level. This is supported by evidence that Mnk inhibitors and Mnk1 knockout both decrease protein levels but have little effect on mRNA levels. Furthermore Mnk2 knockout or knockdown led to bigger decreases in IRS1 protein than mRNA levels.

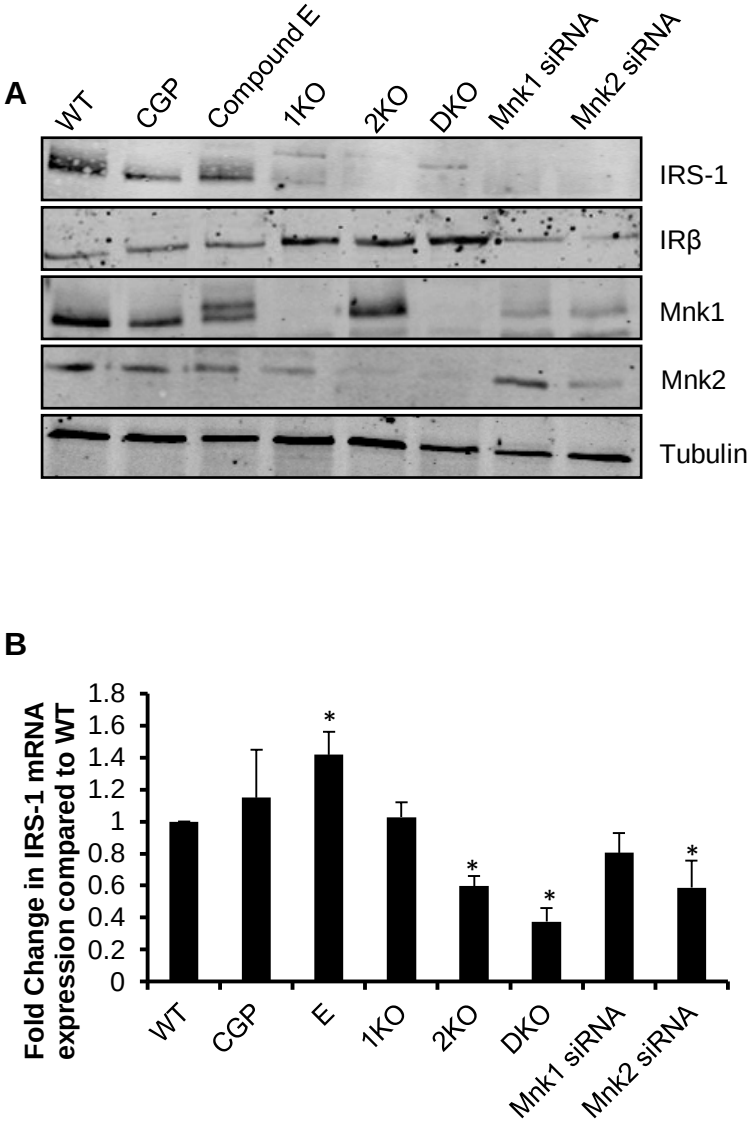

Figure. 4.14 Regulation of IRS1 by the Mnks A) Western blot analysis of WT, Mnk1-KO, Mnk2-KO, Mnk1/2-DKO MEFs and WT MEFs treated with CGP57380 (50μM, 45min), compound E (3μM, 45min) or 15nM Mnk1 or Mnk2 siRNA (24h). Blots were probed for IRS1, IRβ, Mnk1, Mnk2 and tubulin as a loading control. B) qPCR analysis of IRS1 mRNA levels using qPCR with results normalised to 18S rRNA and expressed as a fold difference in expression compared to untreated WT MEFs.

4.2.7.2 IRS1 is phosphorylated and stabilized by the Mnks.

The western blot data indicate that the Mnks can regulate IRS1 at the protein level. Because the Mnks are serine/threonine kinases it was possible that they phosphorylate IRS1. Since full length IRS1 is difficult to express, fragments of IRS1 were expressed and purified in *E. coli*. These fragments correspond to: residues 21-400 (B), 108-516 (C), 516-896 (D) and 899-1235 (E). As can been seen (Fig. 4.15A) both Mnk1 and Mnk2 can phosphorylate fragments C and D of IRS1 *in vitro*. To determine whether this was a specific effect of the Mnks, Mnk inhibitors were added to the assay and showed that phosphorylation of fragment C was likely due to a contaminating kinase but fragment D was specifically phosphorylated by both Mnks with Mnk2 having the greatest activity towards IRS1 (D) (Fig. 4.15B).

In order to identify the site/sites phosphorylated by the Mnks, the experiment was conducted as previously but the band corresponding to fragment D was excised from the gel and subjected to cyanogen bromide cleavage. The resulting cleaved product was then run on a 4-12% gel to determine which fragments were phosphorylated by the Mnks. This revealed that out of a possible 7 sites (predicted by determining the cleavage sites that would be excised by cyanogen bromide based on methionine in the fragment) that there were sites in the largest cleavage fragment and the two smallest (Fig. 4.15C).

There is no general consensus sequence used by the Mnks but there is a requirement for basic residues and they appear to prefer serine [39, 41, 74]. Based on this, a number of possible sites were identified and serine to alanine mutants were generated and then assayed to determine if these were Mnk sites. This revealed that there were 5 sites phosphorylated by both Mnks: Ser^{574}, Ser^{629}, Ser^{766}, Thr^{774} and Ser^{794}. Following this a mutant where all 5 sites were mutated to alanine was generated. This did not undergo Mnk-catalysed phosphorylation (Fig. 4.15D).

These data show that the Mnks can phosphorylate IRS1 at 5 sites in the fragment of IRS1 that is important for PI3K binding [210]. The effect of this phosphorylation required further investigation.

Serine/threonine phosphorylation of IRS1 can alter its stability, although this is usually in a negative fashion [229], which was not expected to be the case with the Mnks since inhibition or knockout/knockdown of the Mnks reduces IRS1 levels (Fig. 4.14A). To test whether Mnk inhibition caused proteasomal degradation of IRS1 cells were treated with CGP57380 or compound E after 45min of treatment with MG132. The compound MG132 is a proteasome inhibitor and was expected to block the degradation of IRS1 by the

proteasome [296]. The data showed that Mnk inhibition caused degradation of IRS1, which was prevented MG132 treatment (Fig. 4.16A). This suggests that Mnk phosphorylation was important for the stability of IRS1. To study this further a construct containing WT or the S-5-A mutant of IRS1 fragment D was created with a myc tag. This was then expressed in HEK293 cells with or without MG132 treatment. The data showed that the mutant fragment was expressed at lower levels than the WT and this difference was rescued by MG132 treatment (Fig. 4.16B). This implies that the Mnks regulate insulin signalling through stabilization of IRS1.

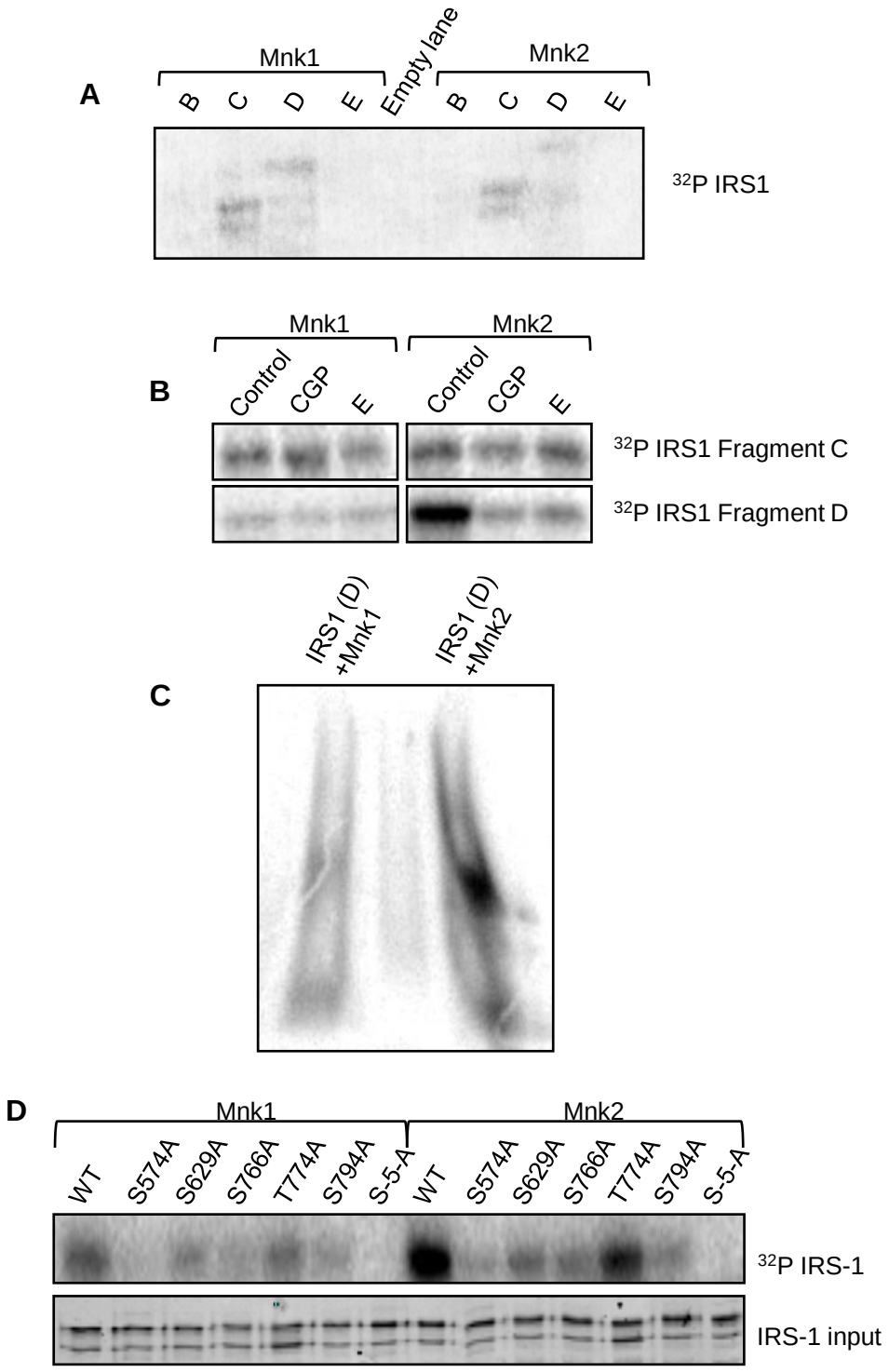

Figure. 4.15. A) *In vitro* phosphorylation of IRS1 fragments B (residues 21-400), C (108-516), D (516-896) and E (899-1235. 2 μg IRS1 were incubated with HA immunoprecipitated Mnk1a or Mnk2a with 100μM ATP and 0.1μCi [γ-^{32}P]ATP for 20min. Samples were subjected to SDS-PAGE and the gels exposed to phosphor-screens. B)) *In vitro* phosphorylation of IRS1. 2 μg IRS1, was incubated with 200ng Mnk1a or Mnk2a with

or without 20nM CGP57380 or 3nM compound E with 100µM ATP and 0.1µCi [γ-^{32}P]ATP for 20min. Samples were subjected to SDS-PAGE and the gels exposed to phosphor-screens. C) *In vitro* phosphorylation of IRS1 fragment D followed by cyanogen bromide cleavage. Samples were subjected to SDS-PAGE using 4-12% gels and then exposed to phosphor-screens. D) *In vitro* phosphorylation of IRS1. IRS1 2 µg WT, S574A, S629A, S766A, T774A, S794A and S-5-A fragments were incubated with Mnk2a with 100µM ATP and 0.1µCi [γ-^{32}P]ATP for 20min. Samples were subjected to SDS-PAGE and the gels exposed to phosphor-screens.

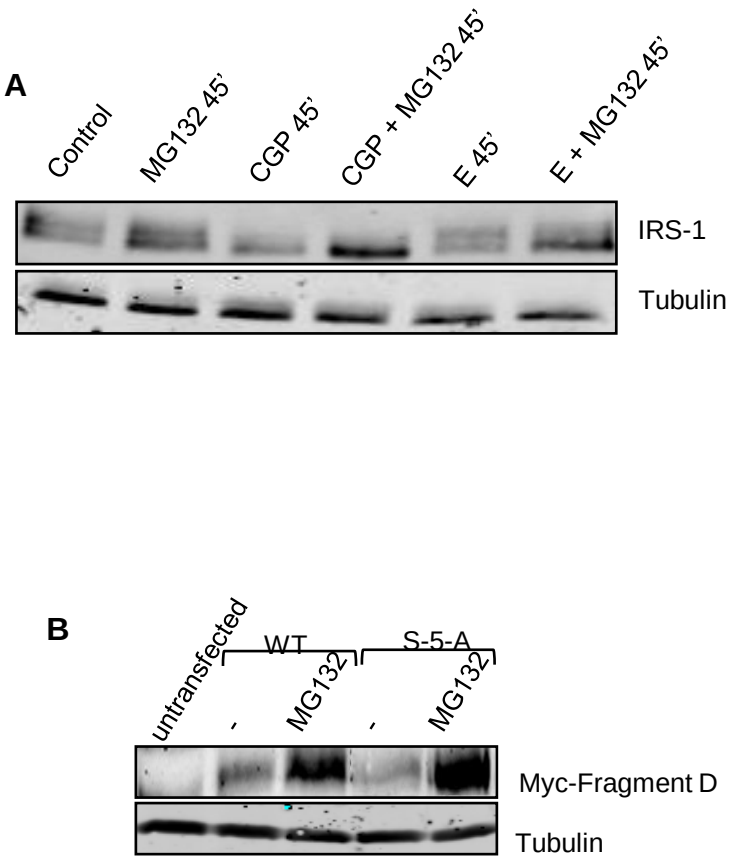

Figure. 4.16 Stability of IRS1. A) WT MEFs were treated with MG132 (10μM) for 45 min prior to treatment with or without 45 min CGP57380 (50μM) or Compound E (3μM) and analysed for IRS1 by western blotting. B) HEK293 cells were transfected with expression vectors encoding either the WT or S5A mutant IRS1, equipped with a myc-tag, using the PEI method. After 48h, cells were treated with or without 10μM MG132 for 3h and lysates were then analysed by western blot for myc- IRS1 expression. n=1.

4.2.8 Analysis of Mnk1/2-DKO mice.

To determine if the Mnks play a role in whole body insulin sensitivity, it was imperative to analyse Mnk1/2-DKO mice as this would give a clear indication as to whether the effect the Mnks have on IRS1 can lead to insulin resistance.

4.2.8.1 Phenotypic investigations of DKO mice.

The Mnk1/2-DKO mice have previously been reported to show no overt phenotype, however the authors did not show data about the weight of these mice or any differences in organ mass [45]. Here we have assessed 17 week old WT and Mnk1/2-DKO mice. Upon death, the mice were weighed and the organs dissected, weighed and snap frozen. This showed that Mnk1/2-DKO mice weigh significantly less than their age-matched counterparts (Fig. 4.17A). This is perhaps not surprising because the Mnks have been linked to tumorigenesis [77, 78, 277, 278] and so clearly have some role in growth, whether this is related to eIF4E phosphorylation or IGF1 signalling remains to be determined. Mnk1/2-DKO mice have hearts that trend towards having greater mass (Fig. 4.17B). This may be important because both Mnks were shown to be expressed to moderate levels in the heart (Fig. 4.1) These effects may be important with regards to cardiac hypertrophy. There were no distinct differences in the left lobe of the liver, either abdominal adipose or scapular depots or the skeletal muscle (Fig. 4.17. C, E, F, G). The right lobe of the liver was in fact significantly larger in Mnk1/2-DKO mice (Fig. 4.17D), which was not expected given that neither Mnk1 nor Mnk2 is expressed in the livers at levels seen in other tissues.

These data indicate there is a role for the Mnks in the overall growth of an animal.

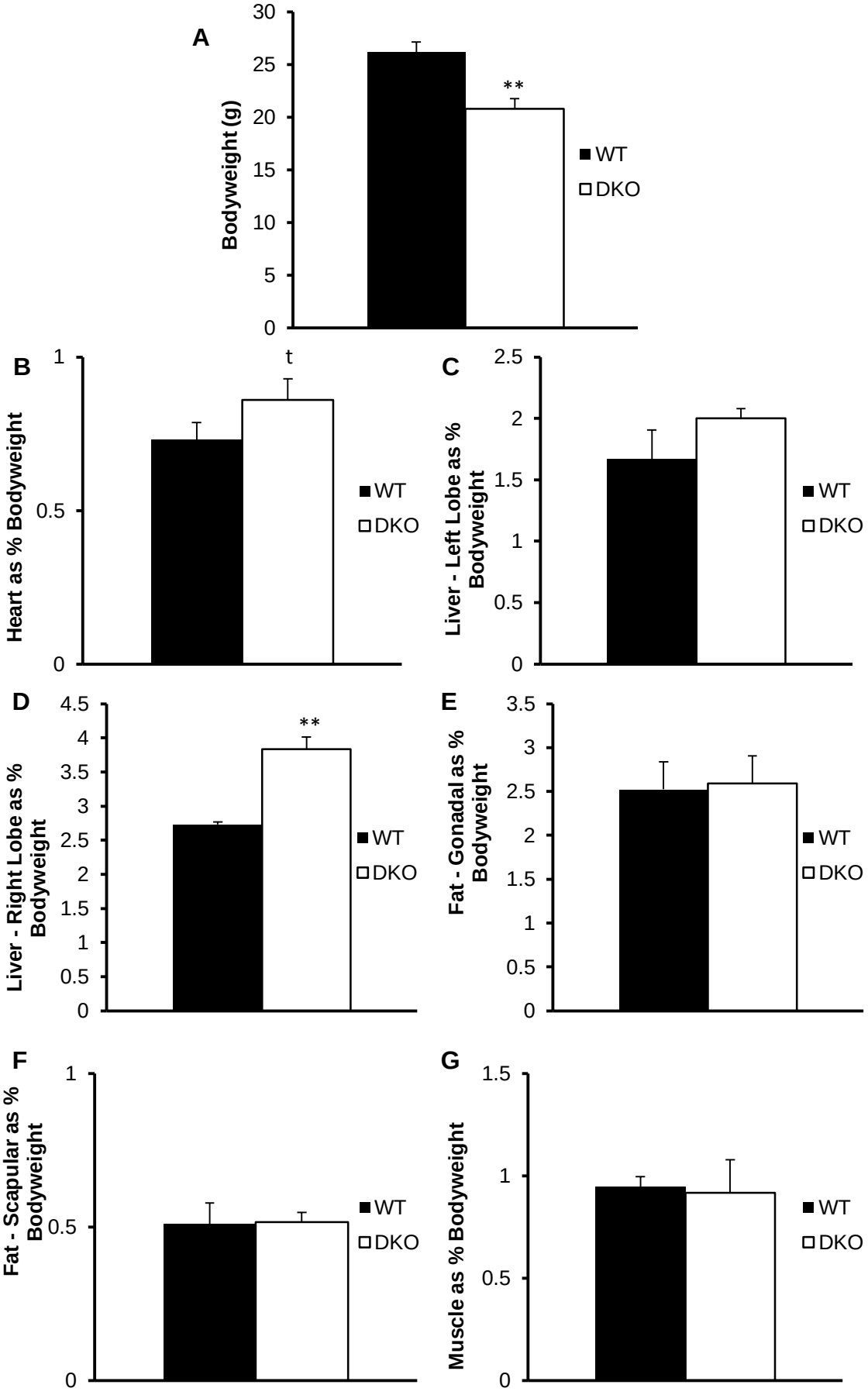
A
Bodyweight (g)
30
25
20
15
10
5
0
**
WT
DKO
B
Heart as % Bodyweight
1
0.5
0
t
WT
DKO
C
Liver - Left Lobe as % Bodyweight
2.5
2
1.5
1
0.5
0
WT
DKO
D
Liver - Right Lobe as % Bodyweight
4.5
4
3.5
3
2.5
2
1.5
1
0.5
0
**
WT
DKO
E
Fat - Gonadal as % Bodyweight
3.5
3
2.5
2
1.5
1
0.5
0
WT
DKO
F
Fat - Scapular as % Bodyweight
1
0.5
0
WT
DKO
G
Muscle as % Bodyweight
1.5
1
0.5
0
WT
DKO

Figure 4.17. Organ weight data for male WT C57/BL6 and MNK1/2DKO mice fed normal chow diets. N=4 for both groups. A) Bodyweight of 17 week old mice. Students' t-test was used to analyse the data ** indicates $p<0.01$ compared to WT B) Weight of heart expressed as a % of bodyweight, Students' t-test was used to analyse the data t indicates $p<0.1$ compared to WT. C) Weight of the left lobe of the liver expressed as a % of bodyweight. D) Weight of the right lobe of the liver expressed as a % of bodyweight, Students' t-test was used to analyse the data ** indicates $p<0.01$ compared to WT. E) Weight of the abdominal adipose expressed as a % of bodyweight. F) Weight of the scapular adipose expressed as a % of bodyweight. G) Weight of the gastrocnemius skeletal muscle expressed as a % of bodyweight.

4.2.8.2 Biochemical analysis of IRS1 levels in DKO mice.

Using qPCR the levels of IRS1 mRNA were determined in abdominal fat and skeletal muscle from WT and Mnk1/2-DKO mice, this showed that surprisingly there was increased expression of IRS1 mRNA in the abdominal adipose of Mnk1/2-DKO mice and no difference in skeletal muscle (Fig. 4.18A, B). This is contrary to the evidence from MEFs where IRS1 mRNA levels were much lower (Fig. 4.14B). The simple explanation for this is that full grown animals are able to compensate for reductions in mRNA levels where as embryonic cells have yet to develop this. The data presented previously showed that the Mnks regulate of IRS1 at the protein level by maintaining IRS1 stability (Fig. 4.16). Therefore the muscle and adipose were the strongest contenders for any difference since these were the tissues where both the Mnks and IRS1 are highly expressed. The abdominal adipose did show reduced levels of IRS1 in the Mnk1/2-DKO mice (Fig. 4.18C). Assessment of muscle levels of IRS1 show a very slight difference between WT and Mnk1/2-DKO mice, with lower levels in the latter (Fig. 4.18D).

Mnk1/2-DKO appears to have an effect on IRS1 only in the abdominal adipose, which is consistent with the fact that both Mnks are expressed in this tissue; however these data must be viewed with caution and studies on more mice are required to assess if this is indeed the case.

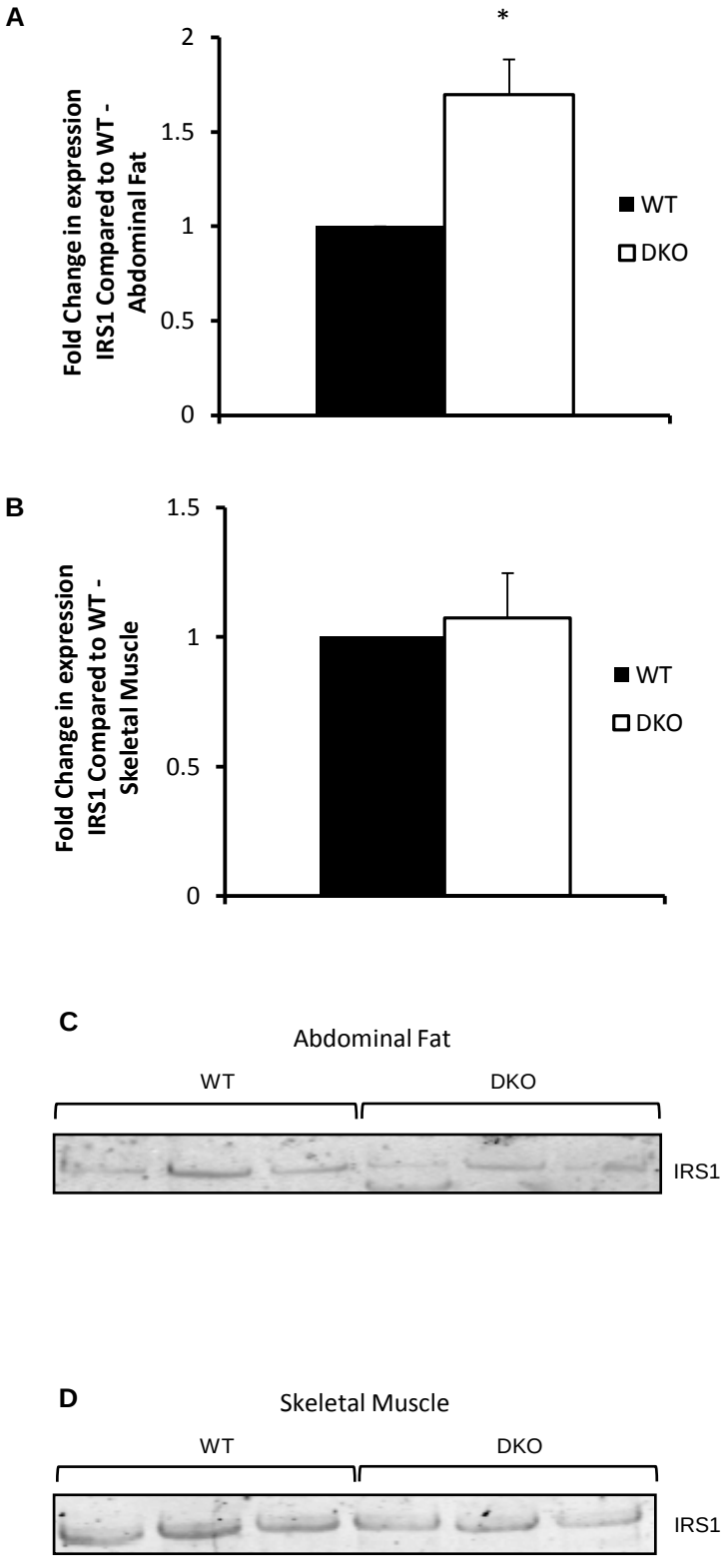

Figure. 4.18. Mnk1/2-DKO exhibit changes in IRS1 expression. A) qPCR analysis of IRS1 mRNA levels in abdominal fat using qPCR with results normalised to 18S rRNA and expressed as fold difference in expression compared to WT (n=3 different animals). B) qPCR analysis of IRS1 mRNA levels in skeletal muscle using qPCR with results normalised to 18S rRNA and expressed as fold difference in expression compared to WT

(n=3 different animals). C) Western blot analysis of IRS1 protein levels in WT and Mnk1/2-DKO mice from abdominal adipose (n=3 different animals). D) Western blot analysis of IRS1 protein levels in WT and Mnk1/2-DKO mice from skeletal muscle (n=3 different animals).

4.2.8.3 Mnk1/2-DKO mice exhibit glucose intolerance.

The data in this chapter have illustrated that the Mnks have a role in the regulation of IRS1 stability, which may explain the deficit in insulin-stimulated glucose uptake in cells lacking the Mnks.

To determine if Mnk1/2-DKO mice exhibit any differences in glucose metabolism, 16 week-old mice were subjected to a glucose tolerance test (GTT). Mice were fasted overnight and then the following day basal glucose levels were measured and mice were injected with glucose and tested at set time points thereafter (as described Chapter 2, section 2.5.3). This revealed that Mnk1/2-DKO mice show impaired glucose tolerance (Fig. 4.19A, B). Loss of both Mnks causes much slower glucose clearance as illustrated by persistent high levels of glucose at 30 and 60 min after glucose injection (Fig. 4.19A). The consequence of this effect is a significant increase in the area under the curve (AUC) in Mnk1/2-DKO mice (Fig. 4.19B).

Thus, importantly, Mnks do play a role in glucose homeostasis and presumably insulin action *in vivo*.

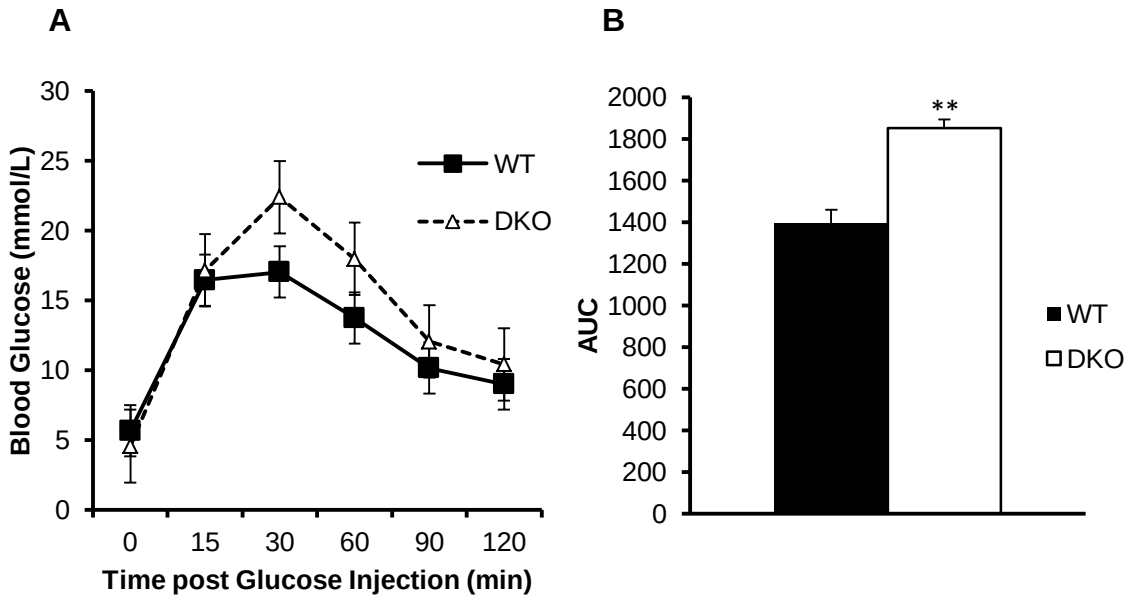

Figure. 4.19. Mnk1/2-DKO exhibit impaired glucose tolerance. A) Glucose tolerance tests for WT and Mnk1/2-DKO mice, n=5 for each WT and Mnk1/2-DKO. B) Area-under-the-curve (AUC) for glucose tolerance tests calculated using the trapezoid rule. Student's t-test was used to analyse the data; ** indicates $p>0.01$ compared to WT mice.

4.3 Discussion

Very little is known about the physiological roles of the Mnks and their substrates with most research having focused on cancer and inflammatory diseases [40, 41, 43, 44, 79, 276, 281]. The aim of this Chapter was to determine if the Mnks had any role in glucose metabolism and insulin signalling and, if so, the mechanism by which this occurred. The data shown in one patent suggested that Mnk inhibition resulted in improved insulin sensitivity [106] and so formed the trigger for the investigations described here, which were carried out using Mnk knockout cells and mice. Surprisingly, the opposite of the claims made in the patent were found here showing that the Mnks are required for normal insulin signalling and that knockout actually leads to defective glucose tolerance.

The expression of the Mnks in different mouse tissues has previously been studied at the mRNA level [39, 228]. Here, the protein levels of Mnk1 and Mnk2 mRNA were examined in an expanded tissue panel. This revealed that Mnk1 was highly expressed in the pancreas and spleen, with high levels in the muscle and white adipose tissue. Mnk2 was the most highly expressed in white and brown adipose tissue and also in the kidney, muscle and heart. This suggests a role for the Mnks in tissues related to insulin signalling and glucose metabolism. To further investigate this, Mnk knockout cells were assessed for insulin-stimulated PKB activity and downstream signalling. In view of the expectation that there would be enhanced signalling in Mnk knockout cells due to the data presented with regards to Mnk inhibition and increased insulin sensitivity [106]. In contrast, the results indicated the opposite showing that knockout of Mnk2 led to a significant decrease in insulin-induced PKB activity, whilst knockout of Mnk1 had less effect and a combined knockout of both Mnk1 and Mnk2 had the most deleterious effect. These changes in PKB activation indicated probable changes in pathways downstream of PKB. This was the case for both TSC2 and PRAS40, whose phosphorylation was decreased in all knockout cells assessed. The effects on S6 and 4E-BP1 were not as clear; knockout of Mnk1 had no effect on insulin-induced S6 phosphorylation consistent with the mild effect on PKB activity and TSC2 phosphorylation, but interestingly led to reduced insulin-stimulation of 4E-BP1 phosphorylation. In Mnk2-KO cells S6 phosphorylation was delayed whilst 4E-BP1 phosphorylation was actually increased. The cause for this is not clear and could be related to the ability of Mnk2 to bind to raptor [96]; however in Chapter 3 I showed that the presence of Mnk2 in mTORC1 kinase assays increased 4E-BP1 *in vitro* phosphorylation and so Mnk2 knockout would be expected to reduce 4E-BP1 phosphorylation. These data suggest Mnk1 and Mnk2 have different effects on mTORC1 signalling, potentially downstream of PKB and not as a consequence of changes to IRS1 stability. It would be important to assess whether 4E-BP1 and S6K/S6 are direct substrates of the Mnks. The combined knock-out of Mnk1 and Mnk2 follows expectations of reduced mTORC1

signalling caused by reduced insulin-stimulated PKB activation. Using inhibitors of the Mnks further supported this evidence whereby insulin-induced PKB activation and phosphorylation as well as downstream mTORC1 signalling was affected in an adverse fashion.

In both Mnk knockout cells and cells treated with Mnk inhibitors there was a loss of insulin-stimulated glucose uptake, consistent with the reduced insulin-induced PKB activation. This again is contrary to what was expected based on the evidence presented in the patent [106]. This is a major finding in relation to the role of the Mnks and is clear evidence that the Mnks function to regulate insulin signalling. The mechanism by which the Mnks exert this is likely related to the evidence presented here showing that the Mnks can phosphorylate and stabilize IRS1. The majority of evidence has shown that the serine/threonine phosphorylation of IRS1 impairs insulin signalling, e.g. as a negative feedback mechanism [229]. The Mnks can phosphorylate five sites in IRS1: Ser^{574}, Ser^{629}, Ser^{766}, Thr^{774} and Ser^{794} Ser^{574}. Of these sites, only Ser^{629} and Ser^{794} have previously been described [297, 298]. Ser^{794} is phosphorylated by AMPK, which has been shown to enhance insulin signalling in C2C12 muscle cells, while in white adipose tissue it actually leads to impaired insulin signalling [299]. Phosphorylation of Ser^{574}, in combination with Ser^{307} and Ser^{323}, by PKCδ has been shown to decrease tyrosine phosphorylation of IRS1 and impair IRS1 function [297]. The Mnks do not phosphorylate Ser^{307} which may be a critical inhibitory site targeted by numerous kinases as the phosphorylation of Ser^{307} disrupts insulin receptor binding [229, 300]. PKB is able to phosphorylate Ser^{629}, which enhances IRS1 function by decreasing the phosphorylation at Ser^{636}, an inhibitory site [298]. The Mnks can phosphorylate multiple sites in IRS1, which appears to stabilise IRS1 as illustrated by the recovery of IRS1 levels in cells treated with CGP57380 and MG132. It is possible Mnk-mediated phosphorylation of IRS1 protects IRS1 from ubiquitination and thus subsequent proteasomal degradation. The mechanism by which Mnk mediated phosphorylation protects IRS1 from degradation will be the subject of further research. One such line of inquiry would be to investigate SOCS-1 and SOCS-3-dependent ubiquitination of IRS1, which has been shown to be important [301-303] in relation to tyrosine phosphorylation of IRS1 and might be regulated by Mnk-mediated phosphorylation. Similarly to the phosphorylation of IRS1 on Ser^{629} by PKB, phosphorylation by Mnk2 may block phosphorylation of sites such as Ser^{307}, Ser^{312}, Ser^{527} and Ser^{636}, which have been linked to ubiquitination of IRS1 [304-306]. Mnk2 also appears to modulate the level of expression of the IRS1 mRNA, but this is secondary in magnitude to regulation of IRS1 protein and probably of lesser importance. Given that the Mnks are

known to regulate mRNA translation, it is possible Mnk2 may regulate IRS1 message levels through altering the rate of translation or the stability of IRS1 mRNA.

It appears that knocking out the Mnks leads to perturbed glucose tolerance as illustrated in Mnk1/2-DKO mice whose GTT shows a shift towards insulin resistance. This may be attributed to the reduced levels of IRS1 seen in abdominal adipose tissue. Further lines of investigation would involve assessing individual Mnk1 and Mnk2 single knockout mice to determine the individual contributions of each isoform. It would also be important to determine insulin levels in Mnk1/2-DKO mice because this may also be the cause of glucose intolerance and especially because there are high levels of Mnk1 in the pancreas suggesting a role for Mnk1 in this tissue.

These data indicate that activation of the Mnks may be an option in T2DM. There is huge effort and investment into the causes and treatment of T2DM. A broad range of treatments are currently available to slow the progression of T2DM; however, the exact mechanism behind the development of T2DM remains unclear and so more work needs to be done. Furthermore, some of the drugs used have side effects e.g. Avandia (Rosiglitazone), which can cause cardiovascular disorders [135], although the incidence of this is decreasing due to better understanding and patient care. T2DM is a disease whereby there is defective insulin signalling that results in glucose intolerance and the eventual inability of an individual to control their blood glucose levels. The deficiency in insulin signalling that causes T2DM results in the inability of insulin target tissues to respond to insulin and facilitate glucose uptake. The identification of the component(s) of the pathway from insulin receptor to glucose transport that are affected in T2DM is key to developing better treatments. Further studies into the expression of the Mnks in T2DM patients may prove interesting if there are reduced levels or if there are mutations within the Mnk genes that contribute to T2DM development.

In conclusion, these data reveal a novel role for the Mnks in the control of insulin signalling likely via a mechanism involving the phosphorylation and stabilization of IRS1. The effect of Mnk1/2 double knockout is glucose intolerance and this may be important when considering future drug treatments for T2DM.

Chapter 5

Mnk2 Knock-out Animals Exhibit a Novel Lipid and Glucose Metabolic Profile, and are Protected from Diet-induced Type 2 Diabetes and Weight Gain.

5.1 Introduction

The data described in Chapter 4 illustrated that the loss of either Mnk1 or Mnk2 or both the Mnks leads to a marked impairment in insulin signalling, indicative of intracellular insulin resistance. Furthermore data from Mnk1/2-DKO mice show that there is some degree of insulin resistance but only abdominal adipose shows decreased levels of IRS1 protein. The tissue expression profile of the Mnks shows high levels of expression of Mnk2 in scapular and abdominal adipose. It was therefore important to examine Mnk2-KO mice to see if they too show perturbed glucose homeostasis.

A number of patents have been filed that suggest a link between Mnk2 and diseases related to glucose and lipid homeostasis [106, 228]. Evidence from one of these patents shows a similar tissue expression profile of the Mnks as is shown in Chapter 4 (Fig. 4.1) as well as increased expression during 3T3-L1 cell differentiation [228] (Fig. 4.10). The authors also assessed the expression of Mnk2 in the *ob/ob* mouse, revealing a clear decrease compared with fasted WT mice. They also generated an Mnk2 dominant-negative mouse (MNK2DN), which represents a loss of function of Mnk2. A major problem with the dominant-negative model is that the non-functional Mnk2 that is expressed may still be able to bind p-ERK resulting in impaired ERK signalling and therefore any conclusions made from this model must be viewed with caution. This is because dominant negative expression of genes leads to expression of a non-functional protein product, which interferes with upstream signalling whereas knock-out of genes abolishes the expression of protein products [307]. The weight of the MNK2DN mouse is increased compared with WT mice whilst the overexpression of Mnk2 in cells leads to decreased TG storage, decreased FA transport and reduced insulin-stimulated lipogenesis [228]. This suggests that Mnk2 functions to reduce fat storage and maintain a lean bodyweight indicating that treatment with an Mnk homologue would benefit patients with lipid disorders, e.g., obesity. However, the data in Chapter 4 showed a decrease in insulin-dependent lipogenesis when differentiated 3T3-L1 cells were pre-treated with Mnk inhibitors (Fig. 4.13C). Information from a different patent shows the opposite with regard to bodyweight [106], treatment with an Mnk inhibitor called compound 15 reduced bodyweight in a similar fashion to the PPARγ agonist rosiglitazone [106]. Furthermore, this patent shows that Mnk inhibitors have the ability to lower blood glucose, increase insulin sensitivity and pancreatic insulin whilst reducing plasma triglyceride and NEFAs [228]. However, the data in Chapter 4 showed that Mnk inhibitors and Mnk knockout both lead to decreased IRS1 levels and loss of insulin-stimulated glucose uptake (Figs. 4.16, 4.6-4.8, 4.13B respectively), which suggests Mnk2 knockout mice may present with insulin resistance.

Neither of the patents discussed above tested the effect of Mnk inhibition in mice fed high fat diets, which given their claims would have been advisable. The evidence presented in either patent has not been published in peer-reviewed journals indicating that the data is either incomplete or has not been replicated. The use of the *ob/ob* mouse is also problematic (as discussed in Chapter 1, section 1.5.5), since leptin levels rise in obesity and a subsequent development of leptin resistance occurs [178]. Furthermore, the use of an MNK2DN mouse could cause unwanted side effects by altering the function of mnk2 substrates or binding partners (e.g. ERK) in an off target mechanism that is not relevant physiologically.

In Chapter 1 (section 1.5) the factors related to diet-induced obesity and T2DM were established with regard to lipid homeostasis and adipokines and their effects on the progression to T2DM. The current understanding simply suggests that the increase in dietary fat is stored in adipose tissue, which enters into a hypertrophic state resulting in low grade chronic inflammation and the increase in circulating inflammatory factors, adipokines, TGs and NEFAs (as discussed in Chapter 1, section 1.5.6). These factors account for both early stage insulin resistance and the subsequent dysfunction of β pancreatic cells culminating in a reduction in insulin secretion and the presentation of full blown T2DM [175].

The aim of this Chapter was to establish whether Mnk2-KO mice exhibit any discernible phenotype when compared with age-matched WT mice. This Chapter also investigates whether Mnk2-KO mice show differences in glucose and lipid homeostasis and if they presented with insulin resistance. Furthermore, these experiments were designed to establish if feeding Mnk2-KO mice a high-fat diet led to any differences in development of diet-induced obesity or T2DM.

5.2 Results

5.2.1 Phenotypic analysis of Mnk2 knockout mice.

Mnk2-KO mice were bred from homozygous Mnk1 WT, homozygous Mnk2 knockout parents and were age-matched with Mnk1/2 WT C57BL/6 mice and fed either normal lab chow diets or 45% fat diets post weaning (approximately 3 weeks of age), as described in Chapter 2, section 2.5.2. Both male and female Mnk2-KO mice exhibited no visible defects in growth, coat colour/shine or alertness but appeared somewhat more docile than WT counterparts.

Monitoring weight gain is a simple effective method of determining whether a drug or genetic knockout has an effect on a whole animal. Mice were weighed before allocation to diet groups and were then weighed once a week for a total of 12 weeks. The data in Chapter 4 showed that male 17 week old Mnk1/2-DKO mice weighed significantly less than age matched WT mice (Fig. 4.17A), which was not assessed in the original paper describing these mice, where organ size was described as showing no difference, similar to the data shown in Chapter 4 (Fig. 4.17) [45]. The authors of this paper did not assess the organ size or weight of Mnk2-KO mice and as such it was of interest to do so in this study.

The initial post-weaning weights of male WT and Mnk2-KO mice showed some variability of 2-3g. WT males placed on the high fat diet initially weighed slightly more than all other groups but within one week there was no difference between the groups (Fig. 5.1A). At week 5, there were clear differences between experimental groups, Mnk2-KO mice on both the normal chow and high fat diets gained weight much more slowly than WT mice on either diet (Fig. 5.1A). At week 9, WT mice on the high fat diet weighed significantly more than WT mice on normal chow diets or Mnk2-KO mice fed a high fat diet. The WT high fat fed males continue to gain significantly more weight than WT mice on normal diets as is expected from this diet (Fig. 5.1A). Mnk2-KO mice on normal chow diets begin to show significantly less weight gain than WT mice on normal diets at week 9-10 and, very interestingly, Mnk2-KO mice fed a high fat diet show no difference to their normal diet fed counterparts (Fig. 5.1A). The weights of mice at week 12 illustrate clearly that WT mice fed high fat diets are significantly heavier (as expected), interestingly Mnk2-KO mice fed high fat diets or normal chow diets are similar in weight and significantly lighter than WT mice fed either diet (Fig. 5.1C).

Female mice from the same litters as the male mice were also fed either normal chow diets or high fat diets at the same time as male mice for 12 weeks. The WT female mice show a similar pattern to the male mice when comparing chow-fed to high fat fed groups.

However it was not until week 10 that there was a significant difference between normal and high fat groups (Fig. 5.1B). Female Mnk2-KO mice do not show the same phenotype in this regard as their male counterparts and gained a large amount of weight on the high fat diet, beginning to gain this weight as early as 6 weeks after the start of high fat feeding (Fig. 5.1B). Furthermore at 12 weeks Mnk2-KO female mice weigh more on both the normal chow diets and high fat diet than WT mice (Fig. 5.1D). However it must be noted that upon death two of the WT females on chow diets exhibited severe kidney cancer and so this data must be taken with caution.

These data show a clear sex difference between Mnk2-KO mice. In male Mnk2-KO mice the loss of Mnk2 results in reduced bodyweight whilst in female Mnk2-KO mice there is an increase in bodyweight. Therefore, further investigation was required.

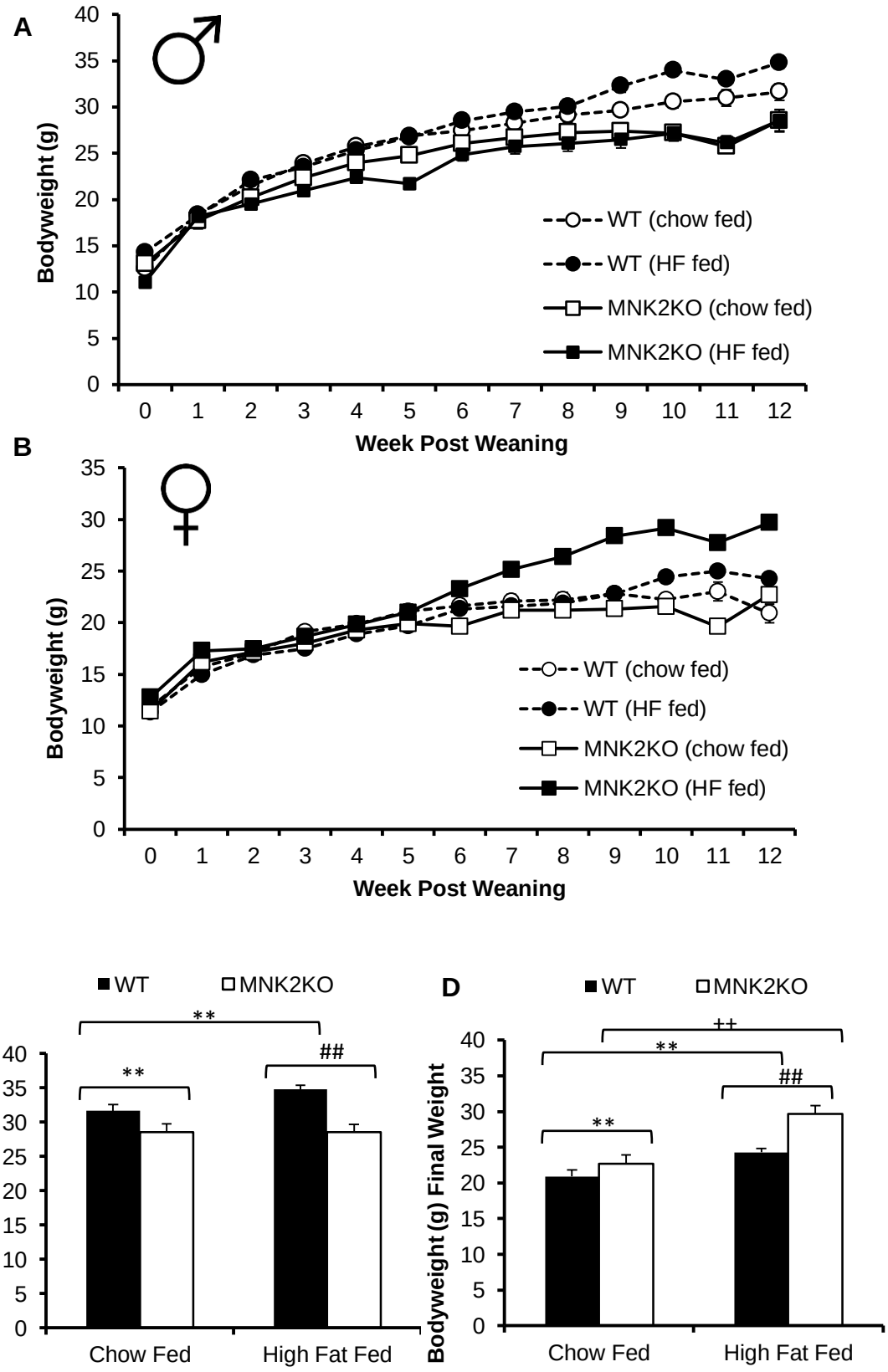

Figure 5.1. Bodyweight data for WT C57/BL6 and MNK2KO mice fed either normal chow diets or high fat (45% fat) diets. n=5 for each group A) Bodyweight across 12 weeks of feeding post-weaning in male mice. B) Bodyweig ht across 12 weeks of feeding post-weaning in female mice. C) Final Bodyweights of male mice, Students' t-test was used to

analyse the data ** indicates p<0.01 compared to WT chow fed, ## indicates p<0.01 compared to WT high fat fed. These data are from n=5 mice in each experimental group. D) Final Bodyweights of female mice, Students' t-test was used to analyse the data ** indicates p<0.01 compared to WT chow fed, ## indicates p<0.01 compared to WT high fat fed. These data are from n=5 mice in each experimental group, ++ indicates p<0.01 compared to MNK2KO high fat fed.

5.2.2 Studies of tissue from WT and Mnk2-KO mice.

Evidence from Chapter 4 showed that male Mnk1/2-DKO mice showed no overt differences in the weight of muscle, left lobe of the liver, abdominal adipose or scapular adipose with respect to their bodyweight, which was significantly lower (Fig. 4. 17). These mice did however exhibit a trend towards increased heart size and significantly increased weight of the right lobe of the liver (Fig. 4.17B, D). This is mostly in agreement with observations from the group that generated these mice [45]. However based on the distinct differences in weight gain in Mnk2-KO mice it was of interest to examine select organs from these mice, especially those related to metabolism.

5.2.2.1 Determination of organ size in relation to bodyweight from male and female WT and Mnk2-KO mice.

The striking differences observed in the weight gain between the sexes of Mnk2-KO mice deserved further investigation with regard to organ size. WT and Mnk2-KO mice were fed either normal chow or high fat diets for 12 weeks post weaning (~15weeks of age) and were euthanized (as described in Chapter 2, section 2.5.4). Organs were dissected and weighed and then the data were expressed as a % of total bodyweight.

Chow-fed male Mnk-2KO mice exhibit significantly increased heart weight in comparison to WT mice (Fig. 5.2A), which is similar to that seen in Mnk1/2-DKO mice (Fig. 4.17B). Feeding mice with a high fat diet results in significant decreases in heart weight/body weight in both WT and Mnk2-KO mice (Fig. 5.2A). This is perhaps expected as diet-induced obesity leads to increased deposition of interstitial fat and since these mice are still developing increased fat around organs, this may lead to retardation of organ growth. Unlike Mnk1/2-DKO mice, Mnk2-KO mice have decreased gastrocnemius skeletal muscle mass compared to WT mice, when fed normal chow diets (Fig. 5.2B). WT mice fed high fat diets exhibit significantly decreased muscle mass whilst Mnk2-KO mice show no decreases when compared to chow-fed Mnk2-KO mice but remain smaller than WT chow-fed mice (Fig. 5.2B). The decrease in muscle mass of WT mice fed high fat diets could be explained by increased intramyocellular fat accumulation and a reduction in muscle growth. However it is harder to explain why there is significantly lower muscle mass in chow-fed Mnk2-KO mice, but, the lack of further decrease with high fat diet feeding may suggest there is less intramyocellular fat accumulation, which is supported by the lack of weight gain in these mice (Fig. 5.1A, C).

The liver is formed of multiple lobes, Cantlie's line defines the left and right lobe of the liver, which are further divided into sub-lobes [308]. In the Mnk1/2-DKO mice the right lobe

of the liver had a significantly increased mass (Fig. 4.17D); however, chow-fed Mnk2-KO mice show no difference compared to WT mice (Fig. 5.2C, D). A decrease in mass of both the left and right lobes of the liver occur with high fat diet feeding in both WT and Mnk2-KO mice, although the left lobe of the liver is decreased significantly more in high fat fed Mnk2-KO mice than WT high fat fed mice (Fig. 5.2C). As with all the other organs, it is likely that high fat feeding leads to increased interstitial fat deposition and cellular TG accumulation leading to decreased organ size with respect to bodyweight .

Female chow-fed Mnk2-KO mice also exhibit increased heart size compared to WT mice (Fig. 5.3A). High fat feeding causes a decrease in heart size in WT mice as with males, but female Mnk2-KO high fat fed mice show significantly decreased heart size compared to matched WT mice (Fig. 5.3A). This may be indicative of the increased weight gain seen in female high fat fed Mnk2-KO mice (Fig. 5.1B, D). The muscle of chow-fed female Mnk2-KO mice shows a similar pattern to male mice in that Mnk2-KO mice show significantly lower muscle mass (Fig. 5.3B). However, and interestingly, muscle mass increases significantly in female Mnk2-KO mice fed a high fat diet and does not decrease in WT mice fed high fat diets (Fig. 5.3B). There does not appear to be an obvious explanation for this. Liver mass also follows a similar pattern to males; both the left and right lobes if the liver decrease in both WT and Mnk2-KO mice fed high fat diets accept this is more pronounced in Mnk2-KO mice (Fig. 5.3C, D). This is likely due to the increased bodyweight gain in female Mnk2-KO mice fed high fat diets (Fig. 5.1B, D).

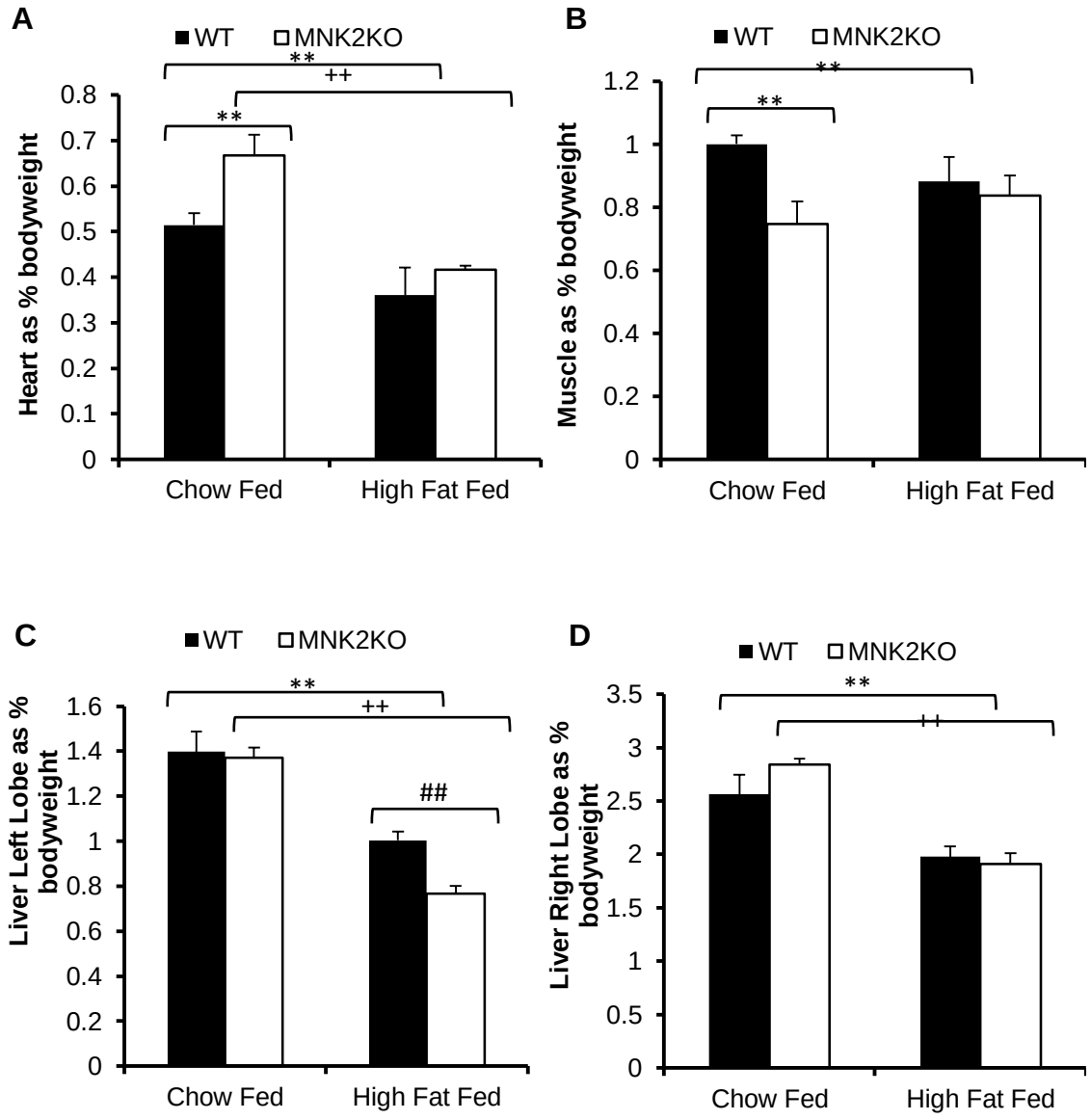

Figure 5.2. Organ weight data for male WT C57/BL6 and MNK2KO mice fed either normal chow diets or high fat (45% fat) diets. WT chow fed n=9, WT HF fed n=5, MNK2KO chow fed n=4, MNK2KO HF fed n= 5. A) Weight of heart from each experimental group expressed as a % of bodyweight, Students' t-test was used to analyse the data ** indicates $p<0.01$ compared to WT chow fed, ++ indicates $p<0.01$ compared to MNK2KO chow fed. B) Weight of the gastrocnemius skeletal muscle from each experimental group expressed as a % of bodyweight, Students' t-test was used to analyse the data **

indicates $p<0.01$ compared to WT chow fed. C) Weight of the left lobe of the liver from each experimental group expressed as a % of bodyweight, Students' t-test was used to analyse the data ** indicates $p<0.01$ compared to WT chow fed, ++ indicates $p<0.01$ compared to MNK2KO chow fed, ## indicates $p<0.01$ compared to WT high fat fed. D) Weight of the right lobe of the liver from each experimental group expressed as a % of bodyweight, Students' t-test was used to analyse the data ** indicates $p<0.01$ compared to WT chow fed, ++ indicates $p<0.01$ compared to MNK2KO chow fed.

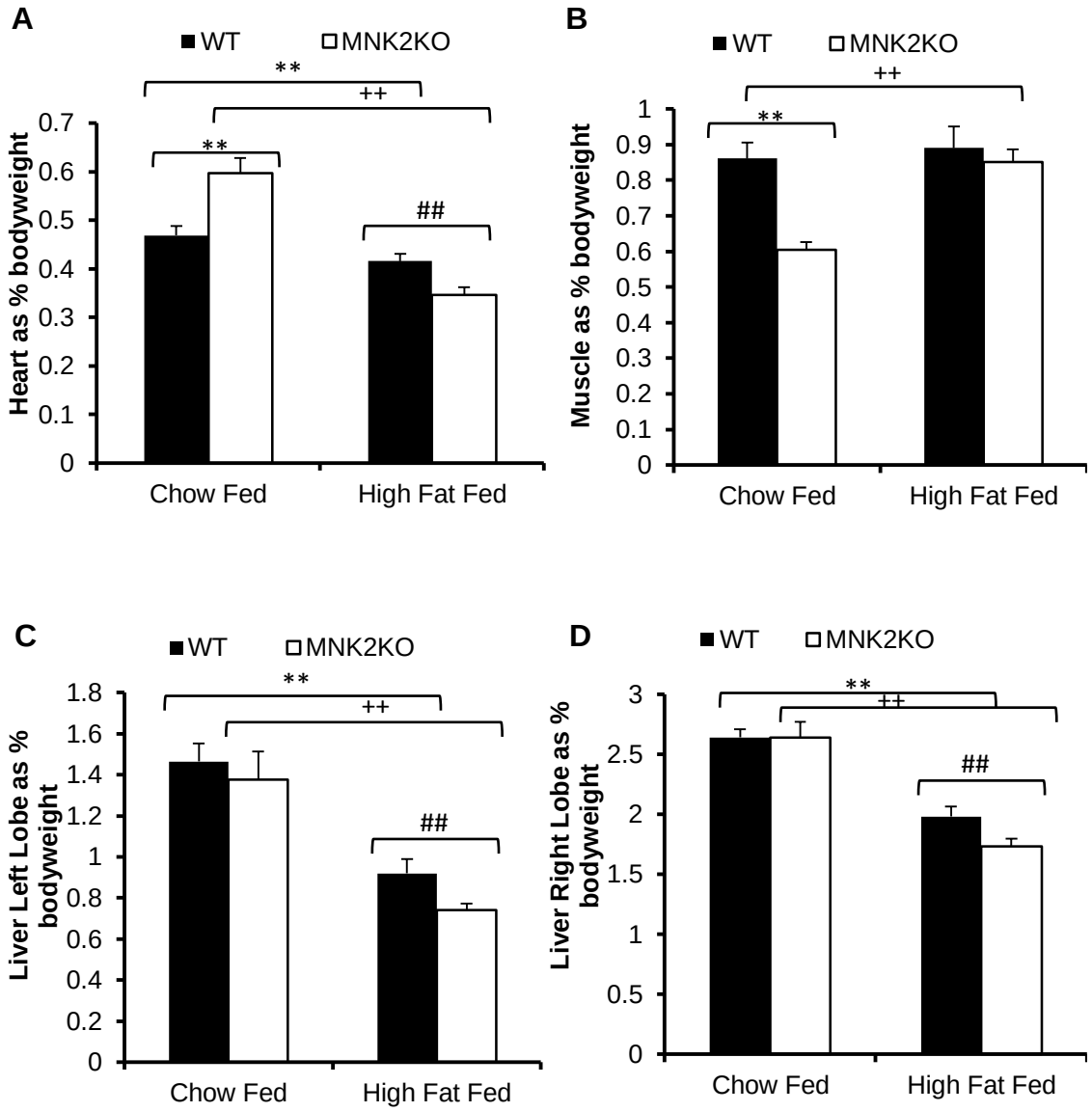

Figure 5.3. Organ weight data for female WT C57/BL6 and MNK2KO mice fed either normal chow diets or high fat (45% fat) diets. WT chow fed n=8, WT HF fed n=5, MNK2KO chow fed n=4, MNK2KO HF fed n= 5. A) Weight of heart from each experimental group expressed as a % of bodyweight, Students' t-test was used to analyse the data ** indicates $p<0.01$ compared to WT chow fed, ## indicates $p<0.01$ compared to WT high fat fed++ indicates $p<0.01$ compared to MNK2KO chow fed. B) Weight of the gastrocnemius skeletal muscle from each experimental group expressed as a % of bodyweight, Students' t-test was used to analyse the data ** indicates $p<0.01$ compared

to WT chow fed. C) Weight of the left lobe of the liver from each experimental group expressed as a % of bodyweight, Students' t-test was used to analyse the data ** indicates $p<0.01$ compared to WT chow fed, ++ indicates $p<0.01$ compared to MNK2KO chow fed, ## indicates $p<0.01$ compared to WT high fat fed. D) Weight of the right lobe of the liver from each experimental group expressed as a % of bodyweight, Students' t-test was used to analyse the data ** indicates $p<0.01$ compared to WT chow fed, ++ indicates $p<0.01$ compared to MNK2KO chow fed.

5.2.2.2 Microscopic analysis of gastrocnemius skeletal muscle from male WT and Mnk2-KO mice.

The gastrocnemius skeletal muscle of Mnk2-KO mice fed normal diets presented with significantly decreased mass (Fig. 5.2B), since this is a key site for insulin-stimulated glucose uptake, it was important to establish if there was any obvious reason for this phenotype. Samples of gastrocnemius muscle were fixed in formalin upon death and then embedded in paraffin followed by haematoxylin and eosin (H&E) staining to define cellular structure. This revealed no overt differences between experimental groups (Fig. 5.4A).

Following on from the histological analysis of skeletal muscle tissue, it was important to determine if there was any differences in IRS1 levels since the data presented in Chapter 4 would indicate that this may be the case. The evidence indicates that Mnk2 regulates the levels of IRS1 by phosphorylation and subsequently protects IRS1 from degradation (Figs. 4.14-4.16). Furthermore, there was also a modest change in the IRS1 mRNA levels (Fig. 4.14B). High fat diets have been strongly implicated in the negative regulation of IRS1 protein levels, which is a key cause of insulin resistance [309, 310], however as an apparent feedback loop, IRS1 mRNA levels increase [311]. The IRS1 mRNA levels in chow-fed Mnk2-KO mice are significantly higher (Fig. 5.4B), which is the opposite from the data seen in knockout cells (Fig. 4.14B) However; the IRS1 protein levels are clearly lower in Mnk2-KO chow-fed mice (Fig. 5.4C), which is consistent with the role of Mnk2 in stabilization of IRS1. High fat diet fed WT males express lower IRS1 protein (Fig. 5.4C) with higher mRNA levels as anticipated (Fig. 5.4B), which is similar to the pattern seen in Mnk2-KO high fat fed males.

These data suggest Mnk2-KO mice may exhibit skeletal muscle insulin resistance.

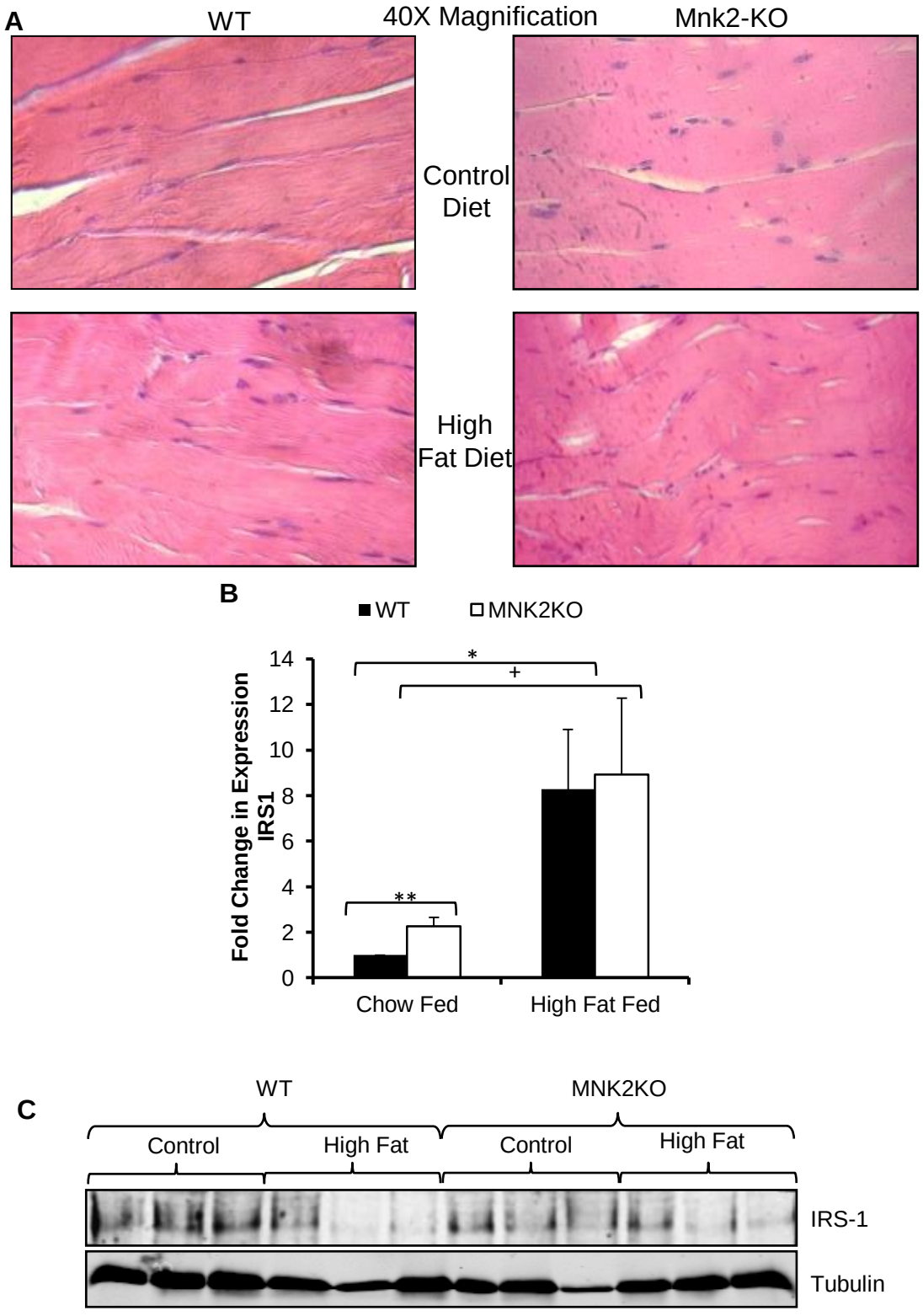

Figure 5.4. Analysis of the characteristics of muscle from WT and MNK2KO mice fed chow or high fat diets. A) Haematoxylin and eosin stained gastrocnemius skeletal muscle. B) qPCR analysis of IRS1 mRNA levels from gastrocnemius skeletal muscle, results were normalised to 18S rRNA and expressed as fold difference in expression compared to WT

chow fed. Students' t-test was used to analyse the data * indicates $p<0.05$ compared to WT chow fed, + indicates $p<0.05$ compared to MNK2KO chow fed. C) Western blot analysis of IRS1 protein levels in WT and MNK2KO mice from gastrocnemius skeletal muscle. Tubulin provides a loading control.

5.2.2.3 Microscopic analysis of the left lobe of the liver from male WT and Mnk2-KO mice.

In high fat fed Mnk2-KO mice the left lobe of the liver significantly decreased in mass compared with WT high fat fed mice, which had significantly lower liver mass than WT chow-fed mice (Fig. 5.2C). Thus, it was of interest to examine the properties of the liver in each group.

Histological analysis shows no obvious difference between WT and Mnk2-KO chow-fed mice (Fig. 5.5A). High fat diet feeding led to clear morphological changes in WT and slight changes in Mnk2-KO mice. In WT high fat fed mice there are distinctly more lipid droplets within liver cells, which is not the case in Mnk2-KO mice, which show visibly fewer droplets (arrows indicate examples (Fig. 5.5A)). These droplet are primarily TGs, which are generated from lipogenesis and dietary fat intake from fatty acids transported from the adipose to the liver. This is expected as a response to increased dietary fat intake. The reduction of droplets in Mnk2-KO high fat fed mice indicates either reduced lipogenesis in the liver, increased export in VLDL or reduced fatty acid input from adipose tissue.

The liver is a vital site of carbohydrate and lipid metabolism and so it was important to look at signalling pathways involved in these processes in each experimental group. Since IRS1 is the key mediator of insulin signalling the levels of mRNA were assessed, which showed some key differences. In chow-fed Mnk2-KO mice, there was significantly higher expression however interestingly this did not increase with high fat diet feeding as it did in the WT mice (Fig. 5.5B). The explanation for this could be that chow-fed Mnk2-KO mice are mildly insulin resistant leading to an increase in expression of IRS1 mRNA to compensate, as occurs in WT high fat fed mice; however why in high fat fed Mnk2-KO mice levels do not increase further is not clear. The effect of high fat diet feeding in WT mice does not lead to decreased protein levels as would be expected (Fig. 5.5C) and increase in correlation to mRNA levels (Fig.5 .5B). Furthermore in Mnk2-KO mice of both groups IRS1 protein levels are about the same as high fat fed mice. Perhaps 12 weeks of high fat diet feeding does not lead to hepatic insulin resistance and so IRS1 is acutely upregulated to compensate for adipose and skeletal muscle insulin resistance. Also Mnk2-KO chow-fed mice may also upregulate IRS1 in order to compensate for peripheral insulin resistance. To see if other components of the insulin signalling pathway were altered, p70S6K levels and its substrate S6 were assessed. p70S6K is a key regulator of IRS1 levels by phosphorylation of IRS1, which results in the degradation of IRS1; this is a negative feedback loop as p70S6K is activated by mTORC1, which itself is activated by insulin [229]. The data for the levels of p70S6K were not clear, but it appeared they increased with high fat diet feeding in both WT and Mnk2-KO groups (Fig. 5.5C),

suggesting the beginnings of insulin resistance. The levels of S6 phosphorylation also increased with high fat diet feeding, although the total levels of S6 also increased. Interestingly the levels of total S6 were higher in Mnk2-KO chow-fed mice and slightly lower in Mnk2-KO high fat fed mice.

To assess liver lipid biochemistry the levels of ATP citrate lyase (ATPCL) were analysed. As discussed in Chapter 1, section 1.4.2, ATPCL is the first point of lipogenesis from carbohydrates. As would be expected ATPCL is down regulated by high fat diet feeding in WT mice (Fig. 5.5C), since the mass increase in dietary lipids would switch off endogenous lipogenesis [10]. However, very interestingly, in chow-fed Mnk2-KO mice ATPCL is also largely decreased, which would indicate a dysfunction of hepatic lipid and carbohydrate metabolism in these mice, furthermore high fat diet feeding almost completely abolished ATPCL levels in Mnk2-KO mice (Fig. 5.5C).

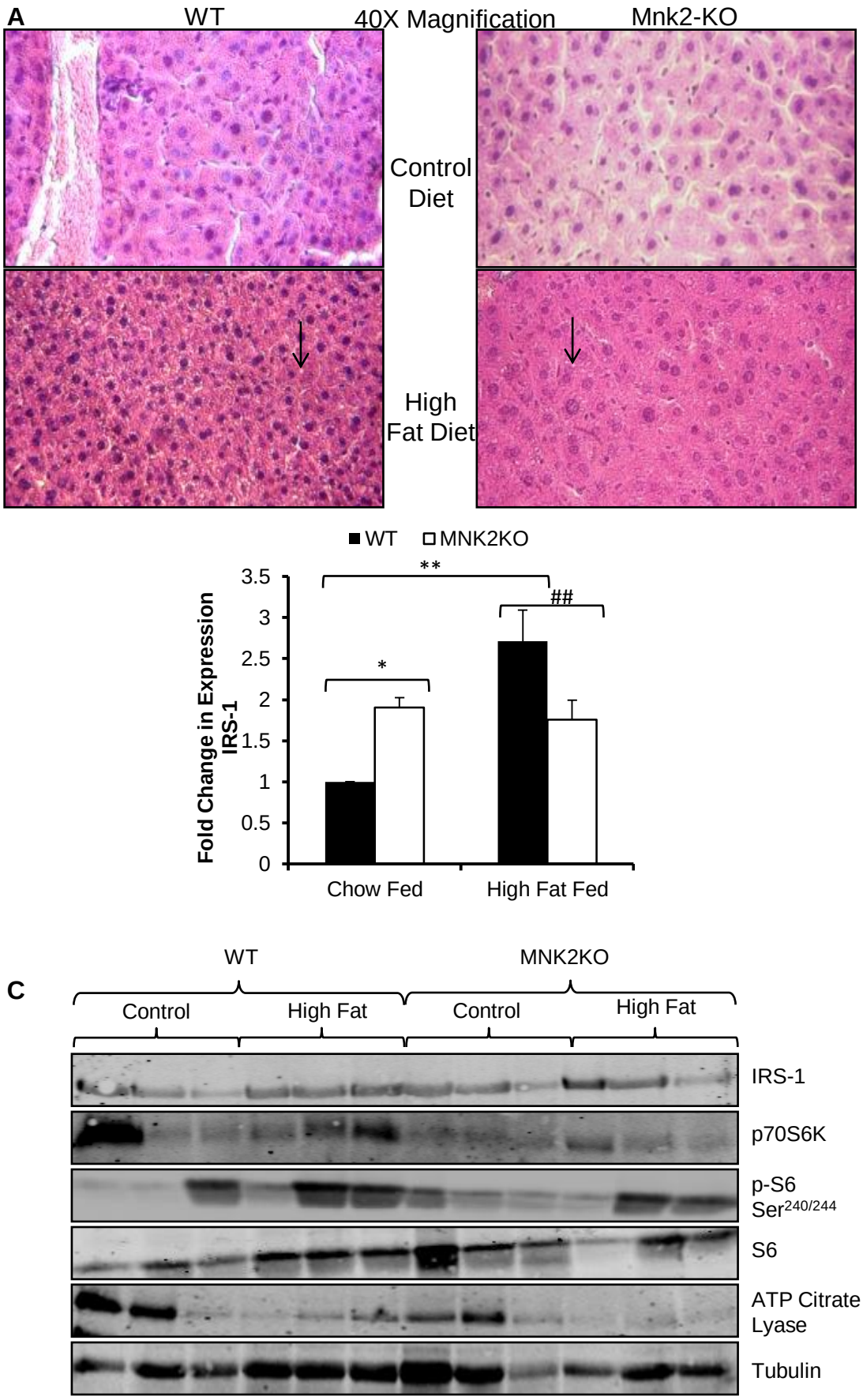

Figure 5.5 Analysis of the characteristics of the left lobe of the liver from WT and

MNK2KO mice fed chow or high fat diets. A) Haematoxylin and eosin stained left lobe of the liver. B) qPCR analysis of IRS1 mRNA levels from left lobe of the liver, results were normalised to 18S rRNA and expressed as fold difference in expression compared to WT chow fed. Students' t-test was used to analyse the data * indicates $p<0.05$ compared to WT chow fed, ** indicates $p<0.01$ compared to WT chow fed and ## indicates $p<0.01$ compared to WT high fat fed. C) Western blot analysis of IRS1, ATP citrate lyase, p70S6K kinase, phospho-ribosomal protein S6 $Ser^{240/244}$ and total S6 protein levels in WT and MNK2KO mice from left lobe of the liver. Tubulin provides a loading control.

5.2.3 Investigations into whole animal lipid homeostasis in WT and Mnk2-KO mice.

The results from skeletal muscle, bodyweight and the liver indicate Mnk2-KO mice had distinctive differences in their morphology on a macroscopic scale. The reductions in organ size, but lack of weight gain, as well as distinct differences in the biochemistry of their tissues are suggestive of differences in lipid distribution and metabolism. Most importantly, Mnk2 is highly expressed in abdominal adipose and scapular adipose of mice (Fig. 4.1B) and so knock-out mice would be expected to show changes in their lipid profiles.

5.2.3.1 Mnk2-KO mice exhibit an unusual fat distribution.

Dual-energy X-ray absorptiometry (DEXA) scans are being increasingly used in both clinical and research settings owing to the ability to rapidly and accurately quantify lean soft tissue, fat and bone density [312]. This method was employed to gain a greater understanding of the composition of Mnk2-KO mice. The results were very striking and readily show that Mnk2-KO mice have far greater subcutaneous fat (yellow)(Fig. 5.6) as well as infiltration of fat into the soft tissue leading to an increased fat volume of Mnk2-KO mice (Fig. 5.7C). This was completely unexpected since these mice weigh less than WT mice (Fig. 5.1A, C). However Mnk2-KO mice look distinctly slimmer than WT a mouse, which is reflected in the quantitative analysis of body volume, which shows significantly lower volume (Fig. 5.7A), furthermore, these mice exhibit significantly decreased length compared with WT mice (Fig. 5.7B). High fat feeding, as expected, led to significantly increased body volume of WT mice and Mnk2-KO although Mnk2-KO mice still have significantly lower body volume (Fig. 5.6A). There is also a significant increase in fat volume of both WT and Mnk2-KO mice (Figs. 5.6, 5.7C), which is again confusing since high fat-fed Mnk2-KO mice do not gain weight (Fig. 1A, C). This disparity may be explained by significantly reduced body volume (Fig. 5.7A) and tissue volume (Fig. 5.7D) in Mnk2-KO mice on either normal chow or high fat diets.

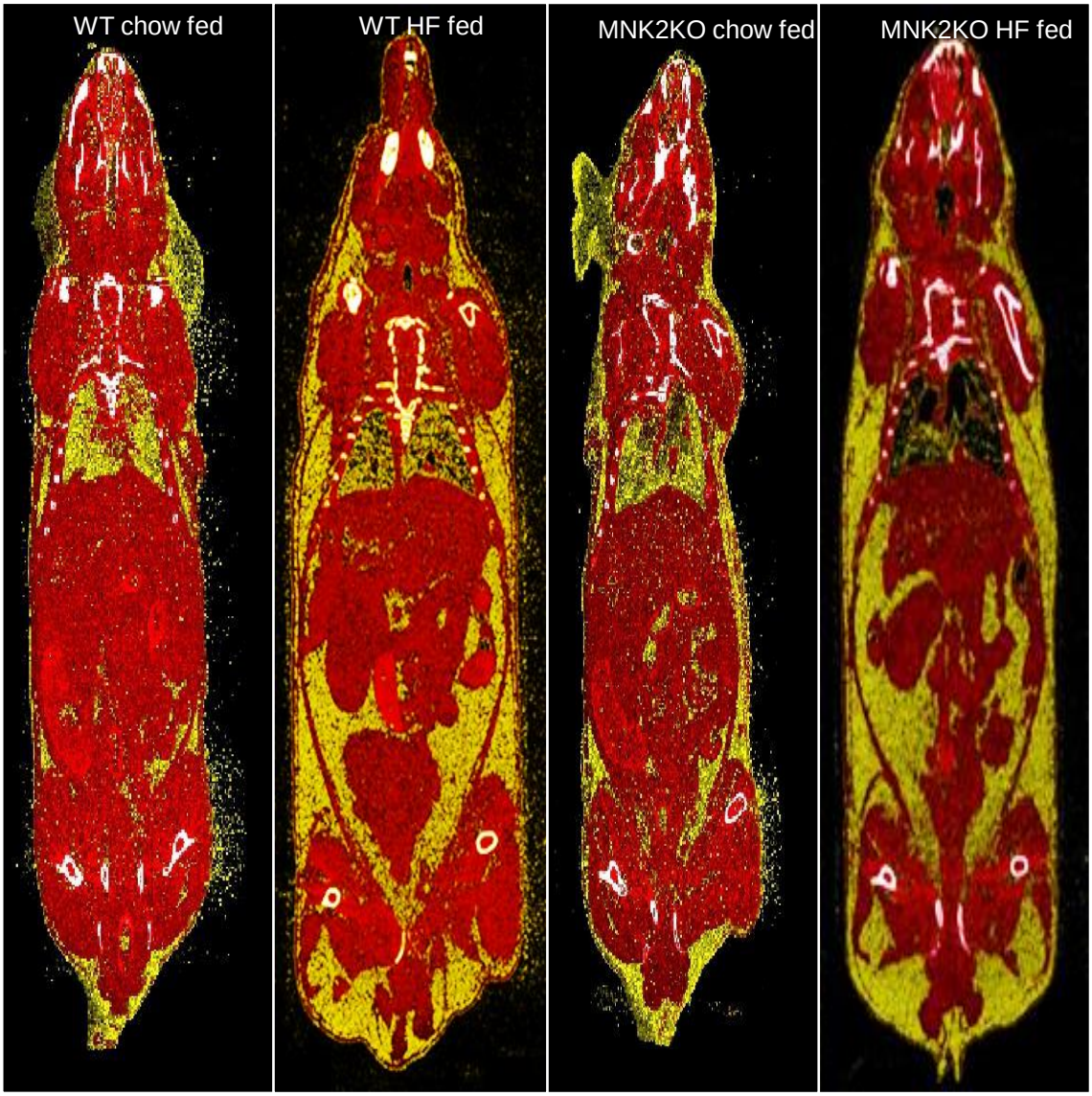

Figure 5.6. DEXA data for male WT C57/BL6 and MNK2KO mice fed either normal chow diets or high fat (45% fat) diets. DEXA images of examples of each WT and MNK2KO from chow fed and HF fed diets. Red indicates soft tissue, yellow indicates fat and white indicates bone.

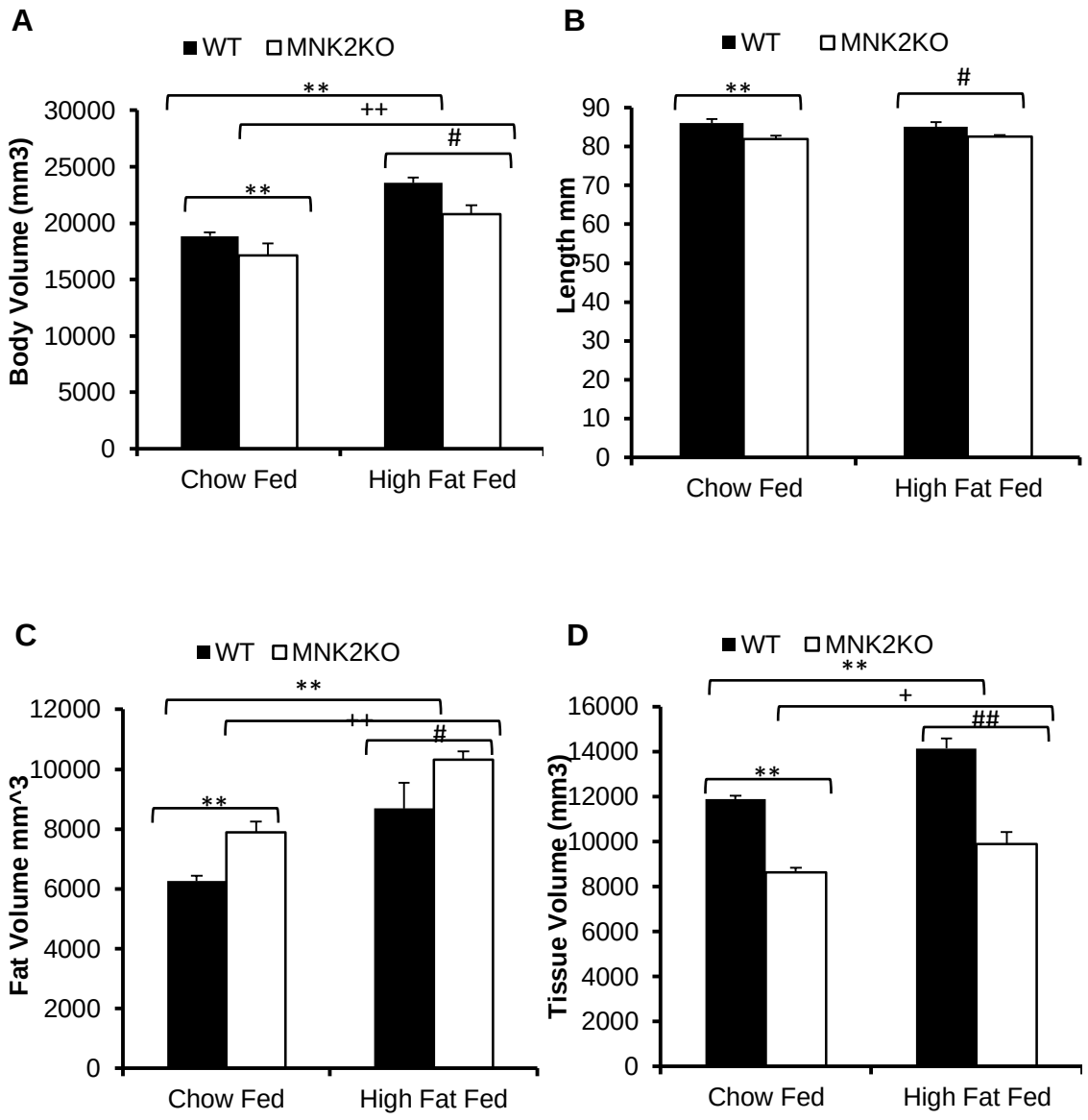

Figure 5.7 Quantitative analysis of DEXA data. WT chow fed n=6, MNK2KO chow fed n=7, WT HF fed n=5 and MNK2KO HF fed n= 5. A) Body volume measured as mm^3. B) Animal length measured as mm. C) Fat volume measured as mm^3. D) Tissue volume measured as mm^3. Students' t-test was used to analyse the data ** indicates $p<0.01$ compared to WT chow fed, ++ indicates $p<0.01$ compared to MNK2KO chow fed, # indicates $p<0.05$ compared to WT high fat fed, ## indicates $p<0.01$ compared to WT high fat fed.

5.2.3.2 Mnk2-KO mice display morphological and biochemical differences in key fat storage depots.

The apparent contradiction between the DEXA data and weight gain data suggested it was important to investigate further the properties of fat depots within Mnk2-KO mice. The scapular found in mice is important for non-shivering thermogenesis and is also found in human new-borns but has recently also been found in adult humans [313]. The abdominal adipose in mice is generally considered the equivalent of abdominal fat in humans, which is a depot that contributes to obesity [314]. These two fat depots were dissected from mice in each experimental group from male and female mice.

The scapular adipose from male Mnk2-KO fed normal diets was significantly heavier than WT mice and remained increased to a greater extent when fed high fat diets (Fig. 5.8A). However, female Mnk2-KO mice only had significantly greater levels of scapular adipose when fed high fat diets (Fig. 5.8C). This is important when considering the lack of weight gain in male high fat fed Mnk2-KO mice because scapular adipose functions as a “sink” for disposing of glucose and NEFAs as it rapidly generates energy due to its high mitochondrial content [315]. Interestingly, the presence of abdominal adipose is significantly reduced in chow-fed Mnk-2KO mice (Fig. 5.8B, D). This is important when considering whole animal lipid and glucose metabolism. However, when male Mnk2-KO mice are fed a high fat diet, there is still an increase in abdominal adipose although this is marginally lower (although not significant) than in WT mice (Fig. 5.8B). Female Mnk2-KO mice are distinctly different in this regard in that their abdominal adipose increases markedly with high fat diet feeding resulting in significantly greater amounts than high fat fed WT mice (Fig. 5.8D). This may account for the distinctive differences in weight gain when comparing high fat fed male and female Mnk2-KO mice (Fig. 5.1).

The distinct difference in scapular adipose weight in male Mnk2-KO mice required further investigation in order to try to establish the role of Mnk2 in this tissue. As with the skeletal muscle and liver, it was of interest to assess scapular adipose by H&E staining.

As with other highly metabolically active tissues, scapular adipose expresses IRS1. Since it has already been already shown that Mnk2 regulates the stability of IRS1 (Chapter 4), it was important to determine if scapular adipose showed any alterations in IRS1 levels. Surprisingly, the levels of both IRS1 mRNA and protein were increased in scapular adipose from Mnk2-KO mice fed normal chow diets (Fig. 5.9B, C). This would imply that scapular adipose in Mnk2-KO animals is better equipped to metabolize glucose. In WT and Mnk2-KO high fat fed mice, the IRS1 mRNA levels increased whilst protein levels decreased suggesting a degree of insulin resistance (Fig. 5.9B, C). This implies that if

there is a compensatory mechanism in chow-fed Mnk2-KO mice that boosts IRS1 levels, this mechanism is inactive when fed high fat diets.

The histological analysis of scapular adipose showed no overt differences between chow-fed WT and Mnk2-KO mice, however high fat diet feeding led to substantial increases in lipid droplets in Mnk2-KO mice compared with WT mice (Fig. 5.9A). Therefore, levels of adipocyte protein 2 (aP2, also known as fatty acid binding protein 4) were also checked. This protein plays a role in intracellular fatty acid trafficking [316]. Mnk2-KO mice fed normal chow diets exhibited increased levels of aP2 similar to those seen in high fat fed WT mice, but levels did not increase further with high fat diet feeding (Fig. 5.9C). Knockout of aP2 has been shown to ameliorate insulin resistance caused by diet induced obesity [317, 318] and this may therefore contribute to insulin resistance in chow-fed Mnk2-KO mice.

Mnk2 is also highly expressed in the abdominal adipose of mice (Fig. 4.1B) and given that there are distinct differences in scapular adipose it was pertinent to assess abdominal adipose in the same way. Histological analysis showed that the abdominal adipose from chow-fed Mnk2-KO mice exhibited adipocytes that were visibly larger than those from chow-fed WT mice (Fig. 5.10A). This is perhaps consistent with the DEXA data (Fig. 5.6, 5.7C), but does not follow with the weight data (Fig. 5.1A, C). High fat diet feeding results in hypertrophy of adipocytes from WT mice; however high fat fed Mnk-2KO mice do not show the same degree of hypertrophy (fig 5.10A). This is most evident when assessing the number of adipocytes in a given field; chow-fed Mnk2-KO mice have significantly fewer due to their moderate hypertrophy. High fat diet feeding causes a significant reduction in their numbers in both WT and Mnk2-KO mice although there is a trend towards a lesser reduction in high fat fed Mnk2-KO mice (Fig. 5.10B). These data indicated a potential difference in the balance of lipogenesis and lipolysis in Mnk2-KO mice, which is especially relevant given the differences in the amount of abdominal adipose in Mnk2-KO mice (Fig. 5.8B).

The evidence presented in Chapter 4 showed that Mnk1/2-DKO mice exhibit glucose intolerance, which may result from insulin resistance in abdominal adipose due to reduced IRS1 expression (Fig. 4.18B) Therefore, the mRNA levels of IRS1 were assessed in abdominal adipose. This showed that, on chow-fed diets, there was no difference between WT and Mnk2-KO mice; however upon high fat diet feeding IRS1 levels are significantly lower in Mnk2-KO mice whereas they do not change in WT mice (Fig. 5.11A). Analysis of the levels of IRS1 protein showed that high fat feeding in WT mice leads to reductions in the level of IRS1 protein, which could contribute to insulin resistance (Fig. 5.11C). As expected, chow-fed Mnk2-KO mice also show reduced levels of the protein, which given the evidence presented in Chapter 4, is consistent with Mnk2 positively regulating IRS1

stability. Interestingly, high fat feeding only leads to a slight reduction in IRS1 levels in Mnk2-KO mice but this is less than the decrease in the mRNA levels, which could suggest some stabilisation of IRS1 in high-fat fed Mnk2-KO mice (Fig. 5.11C). Further down the insulin signalling pathway, there is an increase in total and phosphorylated S6 in high fat fed WT and Mnk2-KO mice, with no discernible difference between WT and Mnk2-KO mice on either diet (Fig. 5.11C). This indicates no change in mTORC1 signalling.

Histological analysis of abdominal adipose revealed a difference in adipocyte size and number in Mnk2-KO mice and so the levels of mRNA for apolipoprotein E (ApoE) were assessed, because this protein has been linked to controlling adipocyte size [319, 320]. This analysis revealed that high fat diet feeding caused a reduction in ApoE levels in both Mnk2-KO mice and WT mice, which may be a protective mechanism to try to reduce hypertrophy (Fig. 5.11B). Further analysis revealed that chow-fed and high fat fed Mnk2-KO mice show reduced levels of phosphorylated and total levels of acetyl CoA carboxylase (ACC) (Fig. 5.11C). This was also seen in high fat fed WT animals and has previously been shown to occur in animals fed a high fat diet, since lipogenesis is no longer necessary when dietary fat intake is high [321, 322]. Furthermore insulin resistance caused by high fat diet feeding would lead to reduced ACC phosphorylation in response to insulin [138].

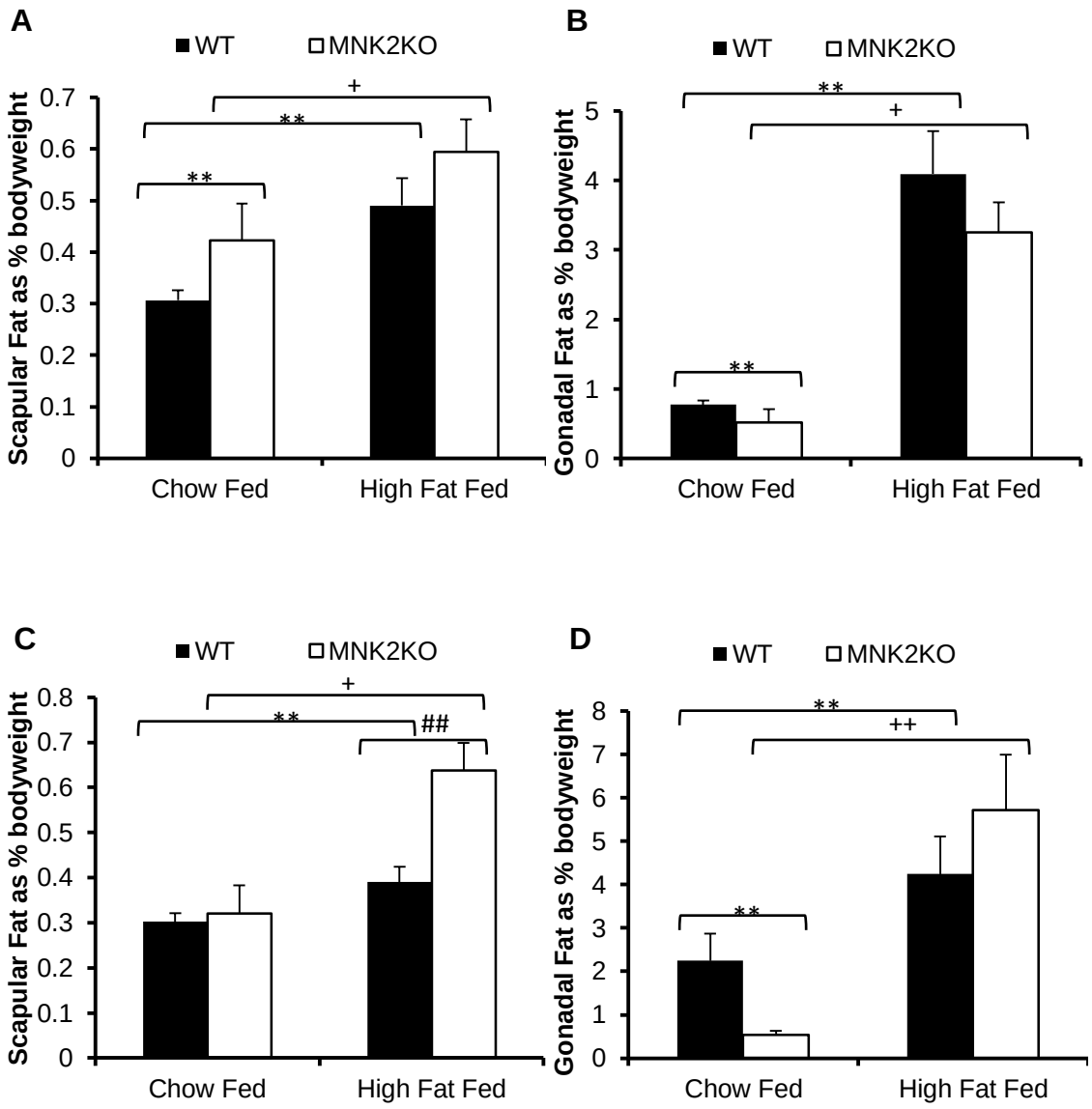

Figure 5.8. Organ weights of abdominal white adipose and scapular brown adipose from WT and MNK2KO mice fed chow or high fat diets WT chow fed n=6, MNK2KO chow fed n=4, WT HF fed n=5 and MNK2KO HF fed n= 5. A) Weight of scapular adipose tissue from male mice expressed as a % of bodyweight. B) Weight of abdominal adipose tissue from male mice expressed as a % of bodyweight. C) Weight of scapular adipose tissue from female mice expressed as a % of bodyweight. D) Weight of abdominal adipose tissue from female mice expressed as a % of bodyweight. Students' t-test was used to

analyse the data ** indicates $p<0.01$ compared to WT chow fed, + indicates $p<0.05$ compared to MNK2KO chow fed, ++ indicates $p<0.01$ compared to MNK2KO chow fed and ## indicates $p<0.01$ compared to WT high fat fed.

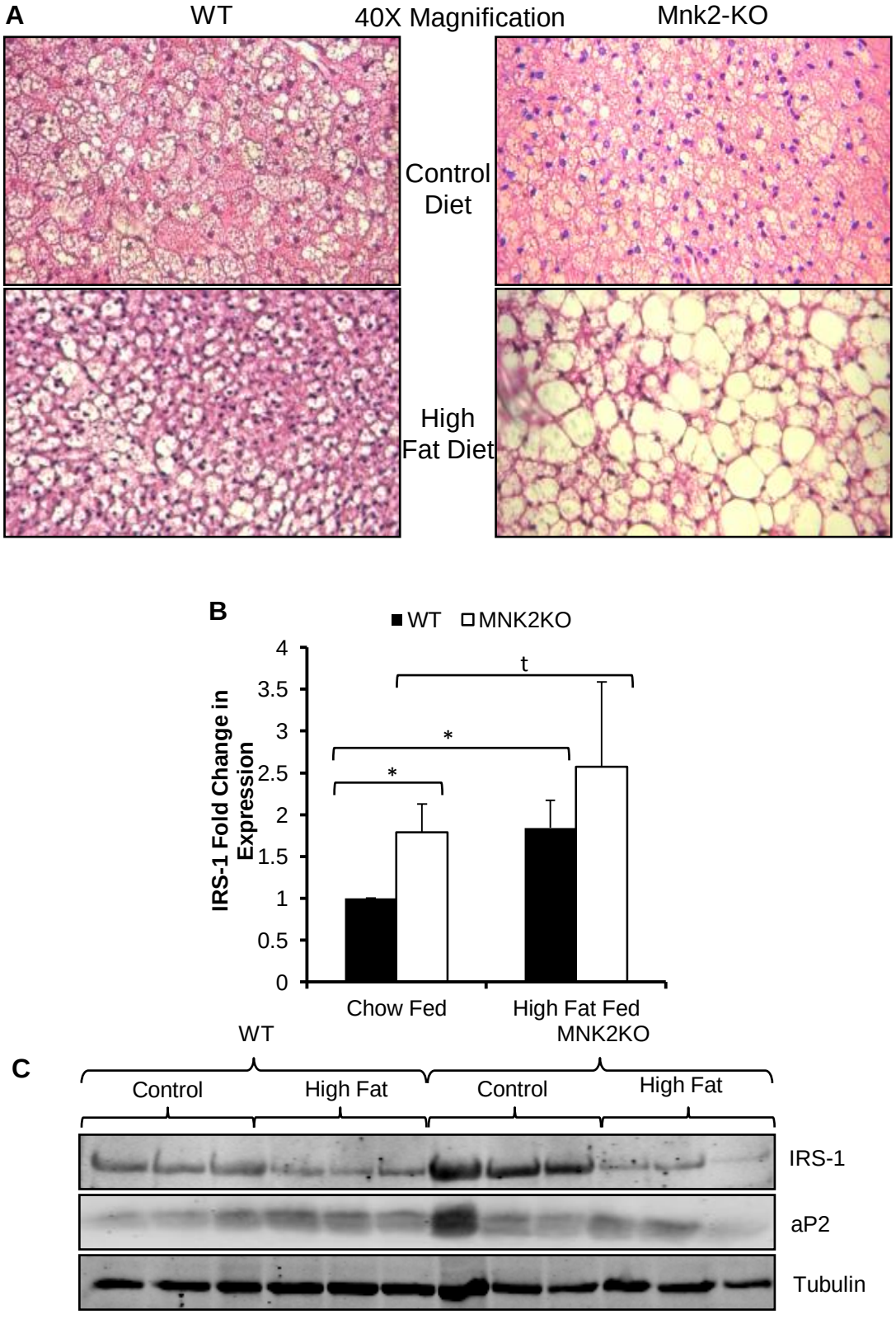

Figure 5.9. Analysis of the characteristics of scapular adipose in WT and MNK2KO mice fed chow or high fat diets. A) Haematoxylin and eosin stained scapular adipose. B) qPCR analysis of IRS1 mRNA levels from scapular adipose, results were normalised to 18S

rRNA and expressed as fold difference in expression compared to WT chow fed. Students' t-test was used to analyse the data * indicates $p<0.05$ compared to WT chow fed, T indicates $p<0.1$ compared to WT high fat fed. C) Western blot analysis of IRS1 and aP2 protein levels from scapular adipose. Tubulin provides a loading control.

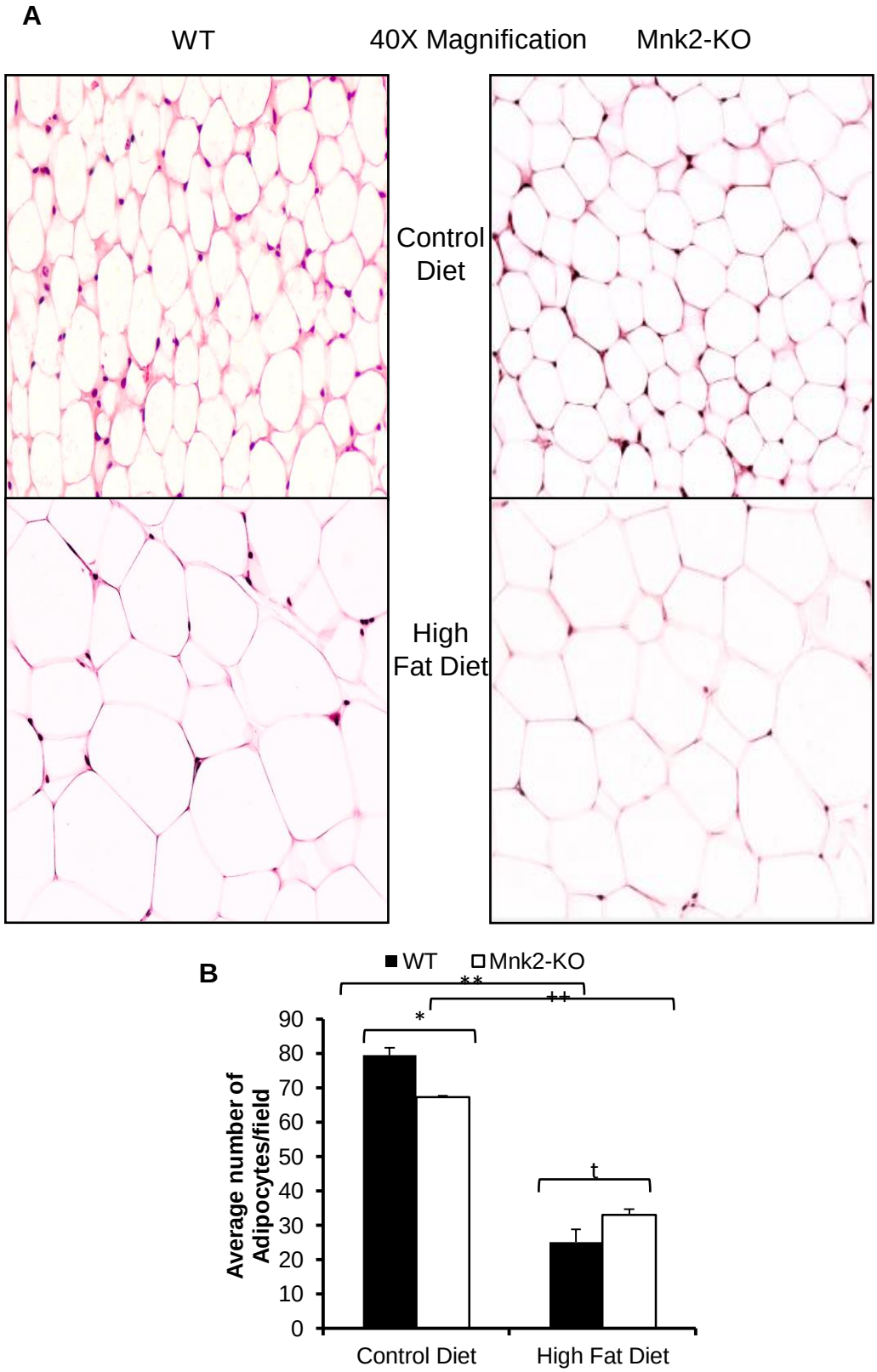

Figure 5.10. Analysis of the characteristics of abdominal adipose in WT and MNK2KO mice fed chow or high fat diets. A) Haematoxylin and eosin stained abdominal adipose. B) Adipocyte numbers from 10 consecutive fields from 3 different mice per experimental group. Students' t-test was used to analyse the data * indicates $p<0.05$ compared to WT

chow fed, ** indicates $p<0.01$ compared to WT chow fed, ++ indicates $p<0.01$ compared to MNK2KO chow fed and t indicates $p<0.1$ compared to WT high fat fed.

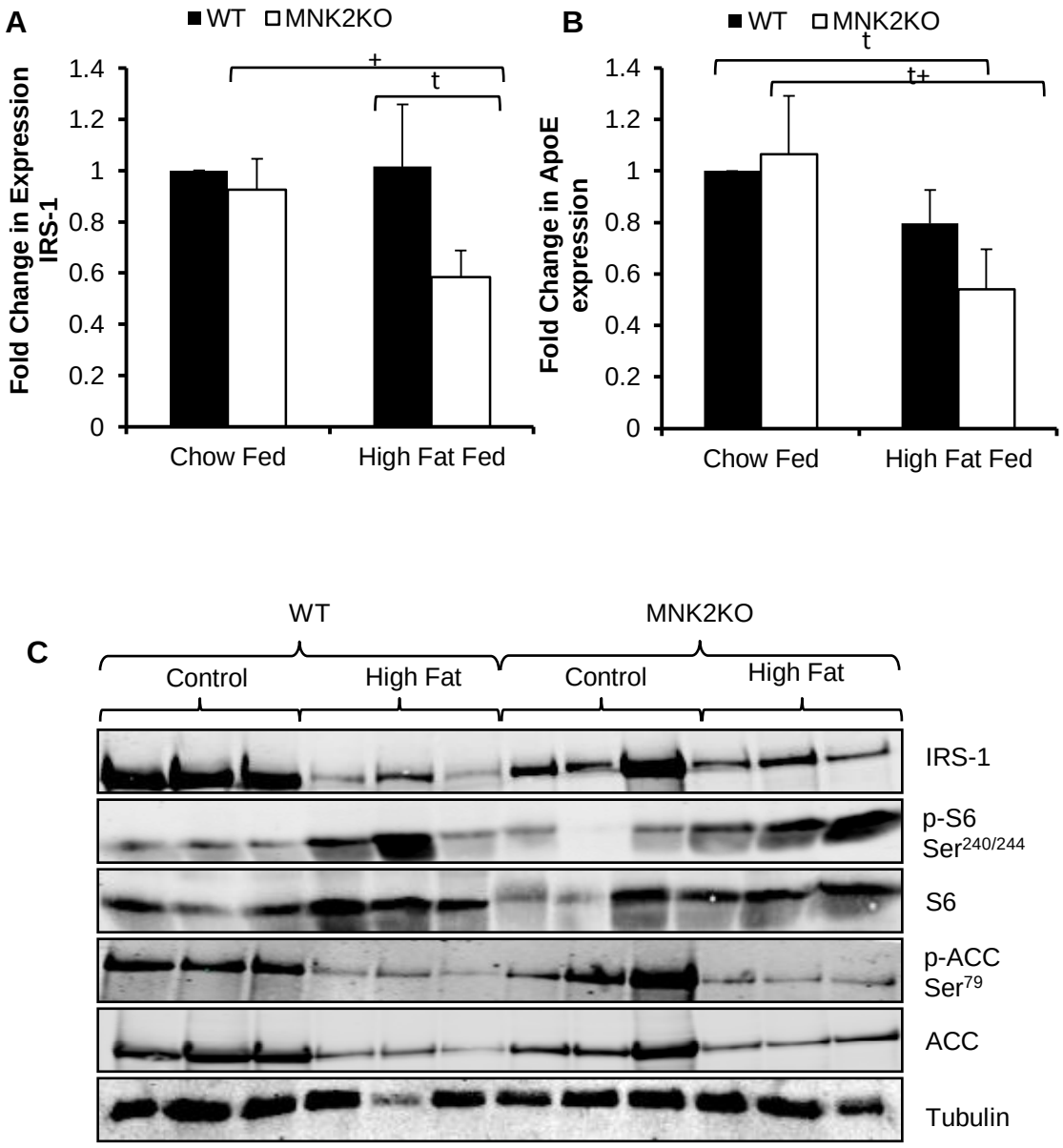

Figure 5.11. Analysis of the characteristics of abdominal adipose in WT and MNK2KO mice fed chow or high fat diets. A) qPCR analysis of IRS1 mRNA levels from abdominal adipose, results were normalised to 18S rRNA and expressed as fold difference in expression compared to WT chow fed. Students' t-test was used to analyse the data + indicates $p<0.05$ compared to MNK2KO chow fed and t indicates $p<0.1$ compared to WT high fat fed. B) qPCR analysis of ApoE mRNA levels from abdominal adipose, results were normalised to 18S rRNA and expressed as fold difference in expression compared to WT chow fed. Students' t-test was used to analyse the data t indicates $p<0.05$ compared to WT chow fed and t+ indicates $p<0.1$ compared to MNK2KO chow fed. C) Western blot analysis of IRS1, phospho-acetyl CoA carboxylase (ACC) Ser^{79}, total ACC,

phospho-S6 Ser240/244 and total S6 protein levels from abdominal adipose. Tubulin provides a loading control.

5.2.3.3 Mnk2-KO mice display altered levels of plasma lipid metabolites.

The data presented so far show that Mnk2-KO mice have an unusual phenotype with regards to their fat distribution and weight gain in response to normal and high fat diets. Plasma levels of lipid metabolites were therefore analysed (at the Cambridge NHS Hospitals Trust).

As discussed in Chapter 1 (section 1.4.5), leptin is a key adipokine that regulates food intake and insulin sensitivity. In Mnk2-KO chow-fed mice leptin was significantly elevated (Fig. 5.12A); this may be a consequence of increased subcutaneous fat levels in these mice (Fig. 5.6). With high fat diet feeding, there is a very substantial increase in plasma leptin levels in both WT and Mnk2-KO mice, as expected [153] (Fig. 5.12A).

The regulation of NEFAs, TGs and cholesterol is tightly mediated by the liver and adipose in response to insulin, nutrients, glucose and peripheral energy requirements. The levels of NEFAs in chow-fed Mnk2-KO mice were no different from those in WT mice. However, there was a significant increase in NEFAs in Mnk2-KO mice with high fat diet feeding, which was not seen in high fat fed WT mice (Fig. 5.12B). This may indicate an increase in NEFA spillover from the hydrolysis of TGs, a point that is supported by the observation that high fat fed Mnk2-KO mice have significantly increased TG levels (Fig. 5.12C). Interestingly chow-fed Mnk2-KO mice have reduced TG levels compared with chow-fed WT mice, which may be a result of the significantly lower levels of abdominal adipose (Fig. 5.8B). Furthermore, this suggests increased lipolysis of adipose tissue, followed by the repacking into VLDL by the liver and therefore the reduced size of adipocytes in high fat fed Mnk-2KO mice (Fig. 5.10B). The levels of total cholesterol are significantly lower in chow-fed Mnk2-KO mice and increase significantly with high fat diet feeding whilst there is only a trend in high fat fed WT mice for increased levels (Fig. 5.12D). The combination of increased NEFAs, TGs and cholesterol in high fat fed Mnk2-KO mice would suggest in combination with reduced levels of tissue IRS1 that these mice would be severely insulin resistant. The difference in plasma lipids is also reflected in the levels of the ketone body β-hydroxybutyrate, which are lower in chow-fed Mnk2-KO mice but substantially increased with high fat diet feeding (Fig. 5.12E). These results suggest that the reduction in stored fat in the adipose tissue reflects its use by the liver and possibly peripheral tissues as an energy source.

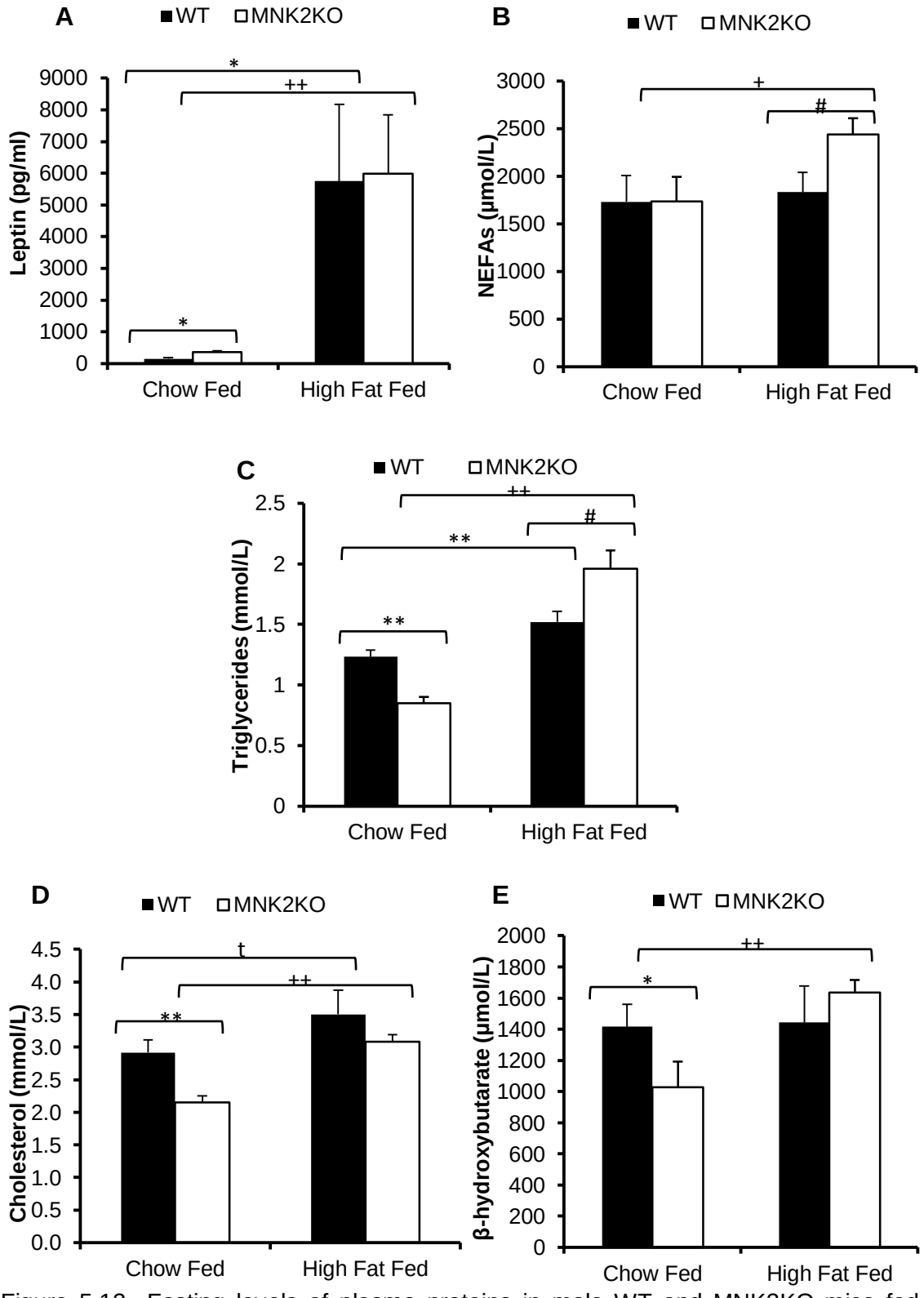

Figure 5.12 Fasting levels of plasma proteins in male WT and MNK2KO mice fed on either chow of high fat diets. For Leptin n= 4 WT chow fed, n=5 MNK2KO chow fed and high fat fed, n=5 WT high fat fed. For all other analyses n= 6 WT chow fed, n=6 MNK2KO chow fed, n=5 WT and MNK2KO high fat fed. A) Fasting leptin levels. B) Fasting non-esterified fatty acid (NEFA) levels C) Fasting triglyceride. D) Fasting Cholesterol. E)

Fasting β hydroxybutyrate levels n= 6 WT chow fed, n=7 MNK2KO chow fed, n=5 WT and MNK2KO high fat fed. Data was analyzed using Student's t-test; * indicates $p>0.05$ when compared to WT chow fed, ** indicates $p>0.01$ when compared to WT chow fed, ## indicates $p>0.01$ when compared to WT high fat fed, + indicates $p<0.05$ when compared to MNK2KO chow fed, ++ indicates $p<0.01$ when compared to MNK2KO chow fed.

5.2.4 Investigations into whole animal metabolism.

A simple and informative method to assess the basic behaviour and metabolism of mice is to place them into a metabolic cage. This apparatus measures food intake and overall activity of its residents.

5.2.4.1 Mnk2-KO mice exhibit differences in metabolic parameters.

The most obvious difference that could account for any differences in metabolism and weight gain is the amount of food consumed and thus energy intake. This was assessed in the chow-fed mice; the results show there is no difference between WT and Mnk2-KO mice (Fig. 5.13A). Due to the consistency of the high fat diet, which was easily crumbled in the food hopper, it was not appropriate to measure its intake and so the diet was placed into the cage in a small bowl instead.

The disparity between weight gain of high fat fed WT and Mnk2-KO mice could be explained by changes in activity. When the activity of Mnk2-KO mice was assessed a contradictory effect was seen, which showed a significant increase in activity on chow diets but significant decreases with the high fat diet (Fig. 5.13D). The WT mice were not different between diets. Assessment of the consumption of oxygen and production of CO_2 would be useful to identify substrate utilization in each experimental group and can also be used to generate energy expenditure profiles. Unfortunately due to a malfunction of this part of the metabolic cage although this was measured the data are invalid. A repeat of this experiment would be very important.

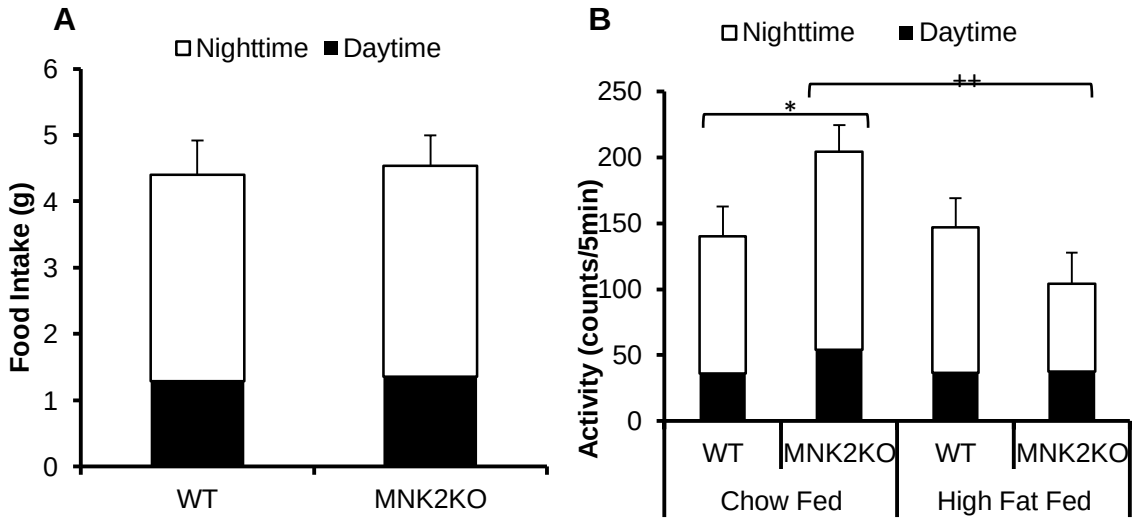

Figure 5.13. Metabolic assessment of WT and MNK2KO mice fed either chow or high fat diets. WT chow fed n=9, WT and MNK2KO high fat fed n=5 and MNK2KO chow fed n=8. A) Food intake was continuously measured using an extensiometric food weight transducer device (Panlab SLU, Spain). B) Physical activities of the mice were monitored by an infrared photocell beam interruption method (Panlab SLU, Spain). Student's t-test was used to analyse the results * indicates $p<0.05$ compared to WT chow fed and ++ indicates $p<0.01$ compared to MNK2KO chow fed.

5.2.4.2 Mnk2-KO mice display altered biochemistry of energy regulators in scapular adipose.

The scapular adipose is a major site of energy regulation in mice and so it is important to assess the biochemistry of this fat depot. Assessment of the uncoupling protein 1 (UCP1) was important because this protein is associated with increased substrate oxidation coupled with low ATP production [323]. This analysis revealed that UCP1 expression was significantly increased in high fat fed WT mice as expected (Fig. 5.14A) [323]. Interestingly, UCP1 expression was significantly increased in chow-fed Mnk2-KO mice, trending towards lower levels in high fat fed Mnk2-KO mice compared with WT high fat fed mice (Fig. 5.14A). It would be expected that increased UCP1 expression would lead to increased energy expenditure. However data from UCP1 knockout mice actually show the loss of UCP1 led to increased energy expenditure [324-326]. The reasons for this effect are not overtly clear. The expression of UCP1 is controlled by PPARγ and the PPARγ coactivator-1α (PGC1α) and so possible changes in expression in both PGC1α and PPARγ in scapular adipose were investigated [327]. Analysis of the mRNA levels of PGC1α were confusing since chow-fed Mnk2-KO mice had significantly decreased levels, which did not change with high fat diet feeding, whilst WT high fed mice also exhibited significantly reduced expression (Fig. 5.14B). This did not correlate with the changes in UCP1 expression (Fig. 5.14A). The levels of PPARγ protein exhibited the opposite pattern to PGC1α expression, such that there was an increase in expression levels in Mnk2-KO chow-fed, WT and Mnk2-KO high fat fed mice (Fig. 5.14C). Therefore, it is likely there are additional mechanisms controlling UCP1 expression such as transcript stability.

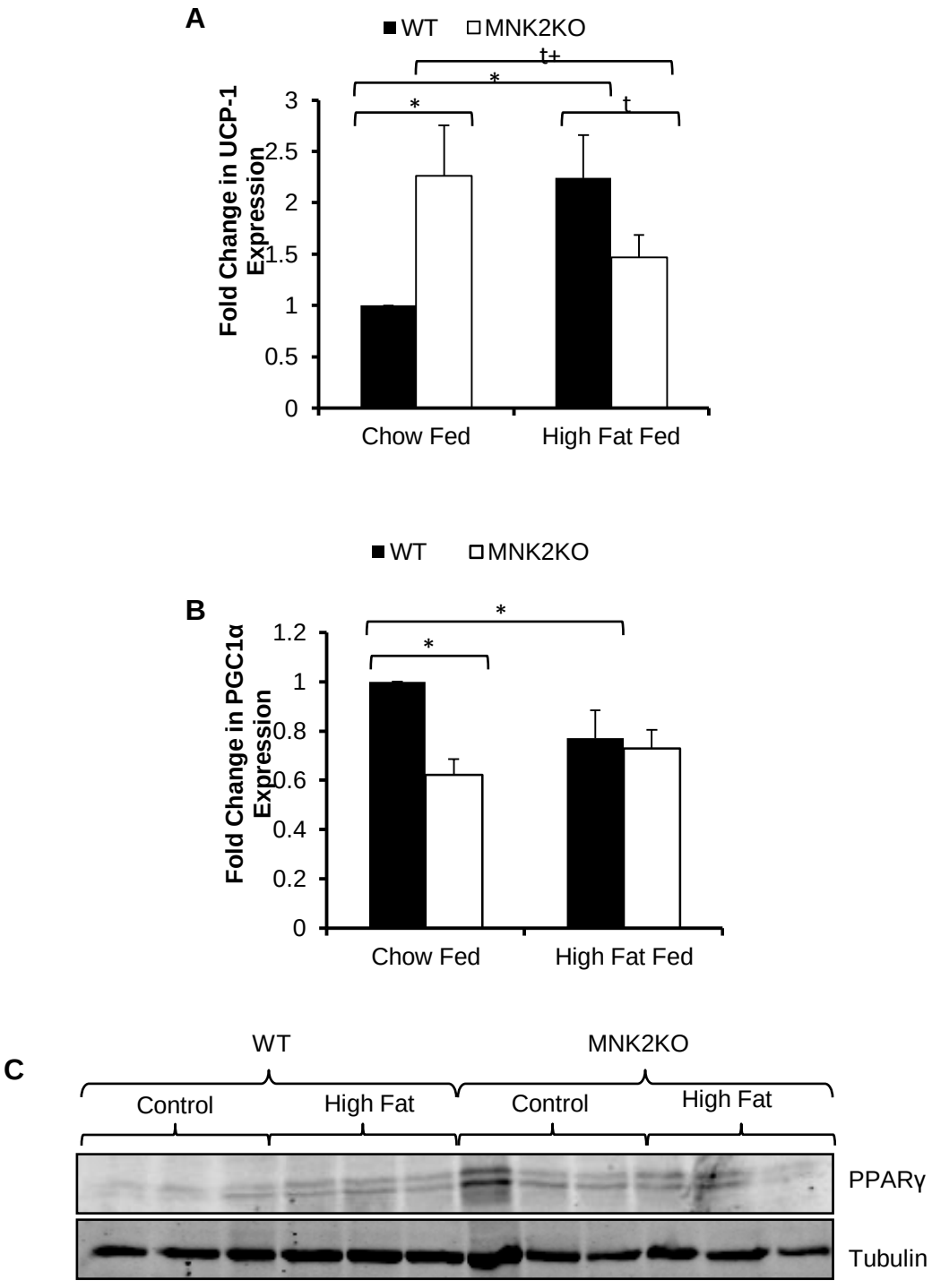

Figure 5.14. Analysis of the components of fat utilization of scapular adipose in WT and MNK2KO mice fed chow or high fat diets. A) qPCR analysis of UCP1 mRNA levels from scapular adipose, results were normalised to 18S rRNA and expressed as fold difference in expression compared to WT chow fed. Students' t-test was used to analyse the data * indicates $p<0.05$ compared to WT chow fed, t indicates $p<0.1$ compared to WT high fat fed and t+ indciates $p<.0.1$ compared to MNK2KO chow fed. B) qPCR analysis of PGC1α mRNA levels from scapular adipose, results were normalised to 18S rRNA and expressed

as fold difference in expression compared to WT chow fed. Students' t-test was used to analyse the data ** indicate $p<0.01$ compared to WT chow fed * indicates $p<0.05$ compared to WT chow fed. C) Western blot analysis of PPAR γ protein levels from scapular adipose. Tubulin provides a loading control.

5.2.5 Investigations into whole animal glucose homeostasis in WT and Mnk2-KO mice.

The standard assessment for glucose homeostasis is the glucose tolerance test. This test indicates the presence of insulin resistance and is very simple to conduct. Information from this test can be analysed in combination with the differences in insulin levels to determine the progression of insulin resistance towards fully developed T2DM.

5.2.5.1 Mnk2-KO mice show insulin resistance on chow-fed diets but resistant to diet induced insulin resistance.

To determine the relationship between fasting glucose and insulin in WT and Mnk2-KO mice fed normal and high fat diets, upon death total blood was removed by cardiac puncture (as described in Chapter 2, section 2.5.5). Normal fasting glucose levels are around 5-6.1 mmol/L in both mice and humans [107, 120], whilst fasted insulin levels vary considerably within the C57BL/6 strain [328, 329]. Fasting glucose levels for chow-fed Mnk2-KO mice were significantly increased compared with chow-fed WT mice (Fig. 5.15A), this was expected given the reduction in IRS1 levels in insulin-sensitive tissues as described throughout this chapter. Furthermore, WT high fat fed mice exhibited substantially increased fasted glucose levels indicative of severe insulin resistance, which again was expected based on the literature [329] and the data presented throughout this chapter. Very surprisingly high fat fed Mnk2-KO mice had significantly lower fasting glucose compared with WT high fat fed and trended towards a reduction compared to Mnk2-KO chow-fed mice to a level similar to WT chow-fed mice (Fig. 5.15A). This was completely unexpected and indicates high fat fed Mnk2-KO mice are protected from the detrimental effects of increased plasma NEFAs, TGs and cholesterol (Fig. 5.12B, C & D). This meant it was essential to determine the fasting levels of insulin and to calculate insulin resistance within the groups. This analysis revealed that chow-fed Mnk2-KO have significantly increased fasting insulin levels (Fig. 5.15B), likely in an attempt to compensate for reduced glucose clearance by target tissues. High fat diet feeding also led to a significant increase in fasting insulin levels in WT mice, again as would be expected to compensate for insulin resistance. Insulin levels were also increased in high fat fed Mnk2-KO mice, but this was not significant (Fig. 5.15B). A widely-used calculation to determine insulin resistance is the homeostatic model assessment of insulin resistance (HOMA-IR). This equation was developed to describe the relationship between fasting insulin and glucose; although originally developed for humans, it is accurate for use with mice and rats [329-331]. This calculation revealed that chow-fed Mnk2-KO mice are

insulin resistant but upon high fat diet feeding this does not change where as high fat fed WT mice are severely insulin resistant (Fig. 5.15C).

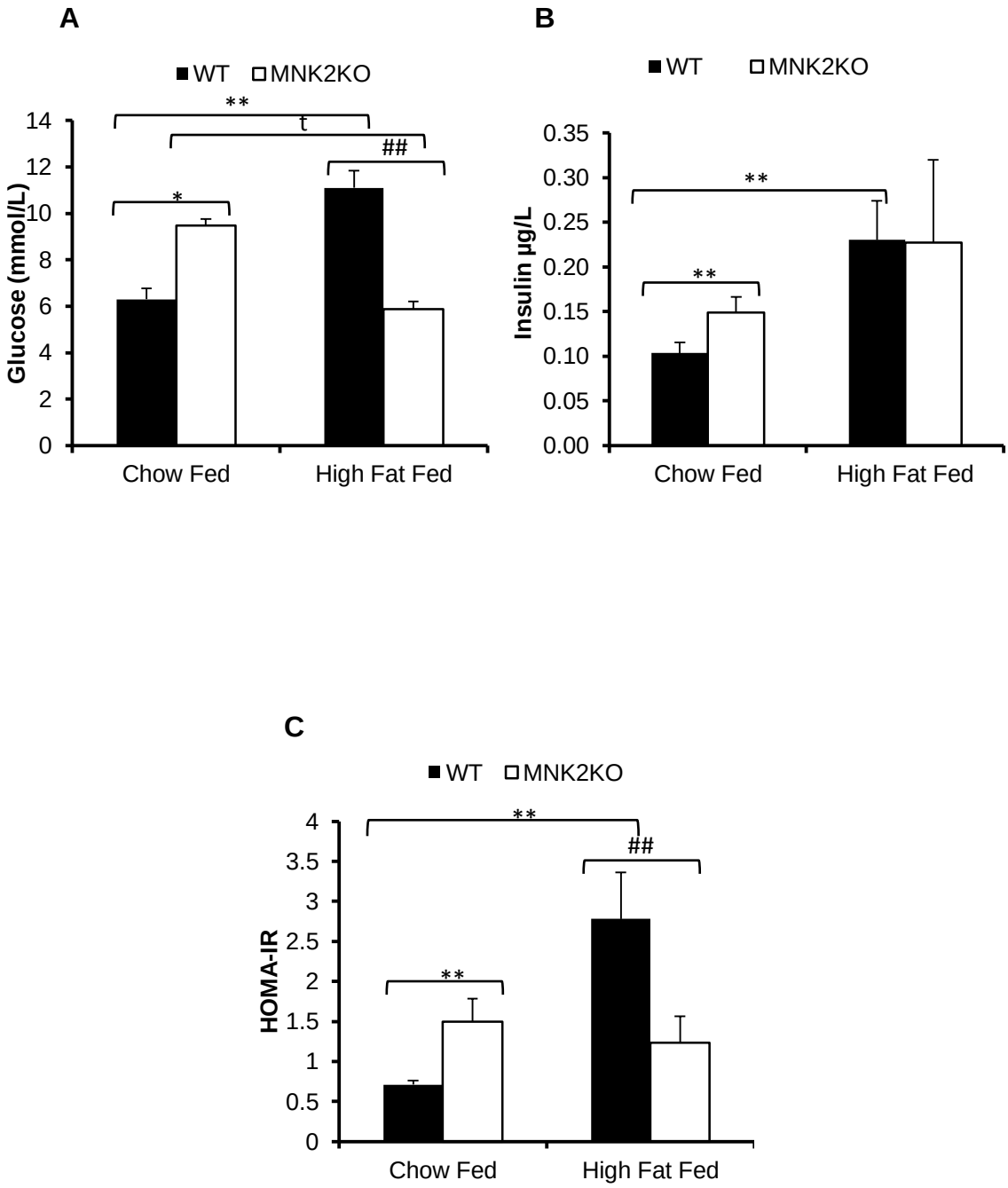

Figure 5.15 Fasting levels of plasma proteins in male WT and MNK2KO mice fed on either chow of high fat diets, n=5 WT and MNK2KO chow fed, n=4 WT and MNK2KO high fat fed. A) Fasting glucose levels. B) Fasting insulin levels. C) Fasting glucose and fasting insulin were used to calculate HOMA-IR using the normalization factor of 22.5 (fasting glucose X fasting insulin / 22.5). Data was analyzed by Student's t-test; ** indicates $p>0.01$ when compared to WT chow fed, ## indicates $p>0.01$ when compared to WT high fat fed, t indicates $p<0.1$ when compared to MNK2KO chow fed.

5.2.5.2 Mnk2-KO mice are protected from diet induced glucose intolerance.

In order to better understand the effect of Mnk2 knockout on glucose homeostasis the glucose tolerance test (GTT) approach was used. Mice were fasted overnight and an initial basal reading was taken before intraperitoneal injection of glucose and measurements across 2hrs (as described in Chapter 2, section 2.5.3).

Male chow-fed Mnk-2KO mice exhibited no difference in GTT; accept for elevated fasting glucose levels (Fig. 5.16A, B). However, high fat diet feeding revealed stark differences between WT and Mnk2-KO mice; as expected WT high fat fed mice had significantly elevated fasting glucose as well as poor glucose clearance (Fig. 5.16A, B). Mnk2-KO high fat fed mice exhibited significantly better glucose clearance than high fat fed WT mice, although not as good as chow-fed mice (Fig. 5.16A, B). This is consistent with the data presented in section 5.2.5.1, which provides strong evidence for a protective mechanism of Mnk2 knockout.

Female Mnk-2KO mice similar results as males. The only clear difference is that chow-fed female Mnk2-KO mice have significantly improved glucose tolerance compared to WT chow-fed mice, which although is significantly poorer with high fat diet feeding, is still better than high fat fed WT females (Fig. 5.16C, D).

The fact that the same glucose homeostasis phenotype is exhibited by both male and female high fat fed Mnk2-KO mice strongly supports the notion that an unidentified mechanism compensates for high fat diet induced insulin resistance.

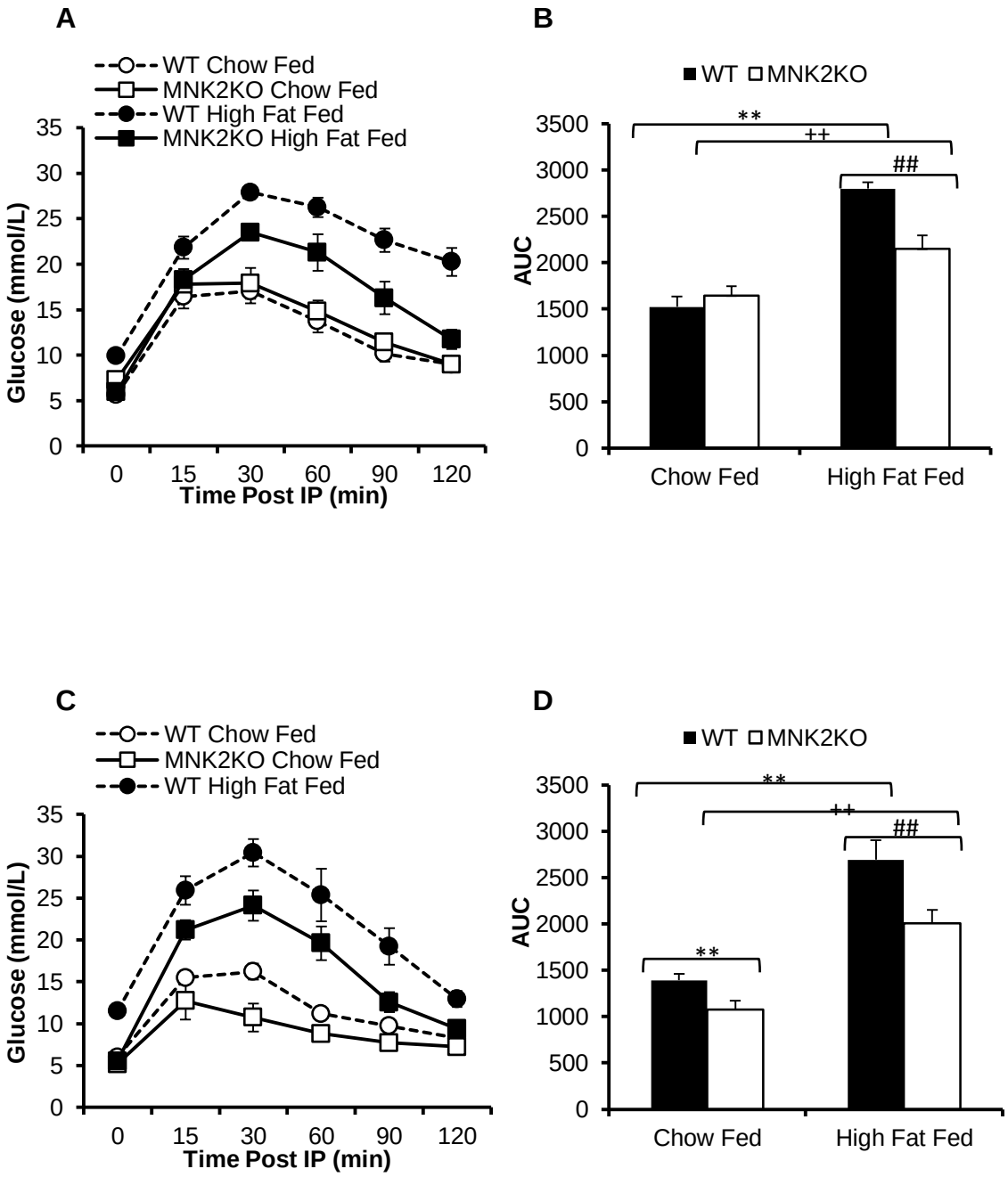

Figure 5.16. Assessment of glucose metabolism in WT and MNK2KO mice fed either chow or high at diets. A) Glucose tolerance tests in male mice, n=9 WT chow fed, n=10 MNK2KO chow fed, N=5 WT and MNK2KO high fat fed. Mice were fasted for 18 hours prior to the GTT, glucose was injected into the intraperitoneal cavity and at 15, 30, 60, 90 and 120 minutes blood glucose was sampled from the tail of each mouse. B) Area under the curve for male mice calculated using the trapezoid rule and Student's t-test used to analyze the data. C) Glucose tolerance tests in female mice, n= 5 WT chow fed, n=4 MNK2KO chow fed, n= WT and MNK2KO high fat fed. Mice were fasted for 18 hours prior to the GTT, glucose was injected into the intraperitoneal cavity and at 15, 30, 60, 90 and 120 minutes blood glucose was sampled from the tail of each mouse. D) Area under the

curve for female mice calculated using the trapezoid rule and Student's t-test used to analyze the data.

5.2.6 Mnk2-KO mice exhibit a beneficial inflammatory profile in response to high fat feeding.

The surprising finding that shows improved glucose tolerance in Mnk2-KO mice compared with WT mice fed high fat diets meant it was necessary to investigate the potential mechanism(s) for this. Since the lipid profile of Mnk2-KO mice suggested there would be very poor glucose tolerance, it was important to assess the inflammatory aspects of obesity-induced insulin resistance.

There is a wealth of evidence to suggest alterations in adipose T-cell populations in relation to the low grade inflammation associated with obesity (as discussed in Chapter 1, section 1.4.6). In order to investigate this, RT-qPCR was used to determine the levels of a number of different mRNAs associated with inflammation in the abdominal adipose of mice. Assessment of the pan T-cell marker CD3 revealed no discernible differences between experimental groups (Fig. 5.17A). The Th1 cell specific marker CXC chemokine receptor 3 (CXCR3) [332] was therefore examined to assess any changes in expression, which may be indicative of increased Th1 cell activation. This revealed some unexpected results; chow-fed Mnk2-KO mice had significantly higher levels of CXCR3, which were much greater than those in WT and Mnk2-KO high fat fed mice (Fig. 5.17B). WT high fat fed mice had significantly higher levels compared with chow-fed mice and Mnk2-KO high fat fed mice exhibited similar levels. It is interesting that high fat diet feeding in Mnk2-KO mice causes a complete reversal of this effect. A possible explanation for this phenomenon is the expression of a chemotactic factor for T cells called ‘regulated on activation normal T cell expressed and secreted’ (RANTES). This chemokine attracts T cells and macrophages resulting in infiltration into sites of inflammation [332, 333]. In Mnk2-KO chow-fed mice there are significantly higher levels of RANTES compared to WT chow-fed mice (Fig. 5.17C); however importantly this does not increase with high fat diet feeding as compared with WT high fat fed mice (Fig. 5.17C). Another chemokine associated with the inflammatory state of high fat diet feeding is monocyte chemoattractant protein 1 (MCP-1), which is linked to the infiltration of macrophages into abdominal adipose [334]. Again, there is an increase in expression in chow-fed Mnk2-KO mice, which does not increase with high fat diet feeding unlike in WT high fat fed mice (Fig. 5.17D). These data indicate Mnk2-KO mice fed normal diets have a low but significantly increased level of inflammation, which may account for the insulin resistance seen in these mice (Fig. 5.15C). Furthermore, this inflammation may be linked to the lower levels of abdominal adipose (Fig. 5.8A) and increased levels of subcutaneous fat (Fig. 5.6).

Increases in infiltration of Th1 cells and macrophages into abdominal adipose as a result of obesity are strongly correlated with increases in inflammatory cytokines produced by

these cells. There is strong evidence to support an increase in IFNγ protein and mRNA expression by Th1 cells, which is associated with increased TNFα expression and the increase in macrophage expression of TNFα [335, 336]. The expression of both IFNγ and TNFα was significantly increased in WT mice fed high fat diets but importantly this was not the case for high fat fed Mnk2-KO mice (Figs. 5.17E, F). This is further supported by reduced plasma levels of IFNγ (Fig. 5.18A). Additionally high fat fed Mnk2-KO mice exhibit increased plasma CXCL-1 levels (fig 5.18B), which may be beneficial due to a link with muscle fatty acid oxidation [337]. Another plasma cytokine that was elevated in Mnk2-KO mice was IL-6 (levels were below threshold in chow-fed mice and only detectable in 2 high fat fed WT and 3 high fat fed Mnk2-KO mice), which has both beneficial and damaging effects (as discussed in Chapter 1, section 1.5.5) (Fig. 5.18C). These data indicate a mechanism for improved glucose tolerance in high fat fed Mnk2-KO mice (Fig. 5.16).

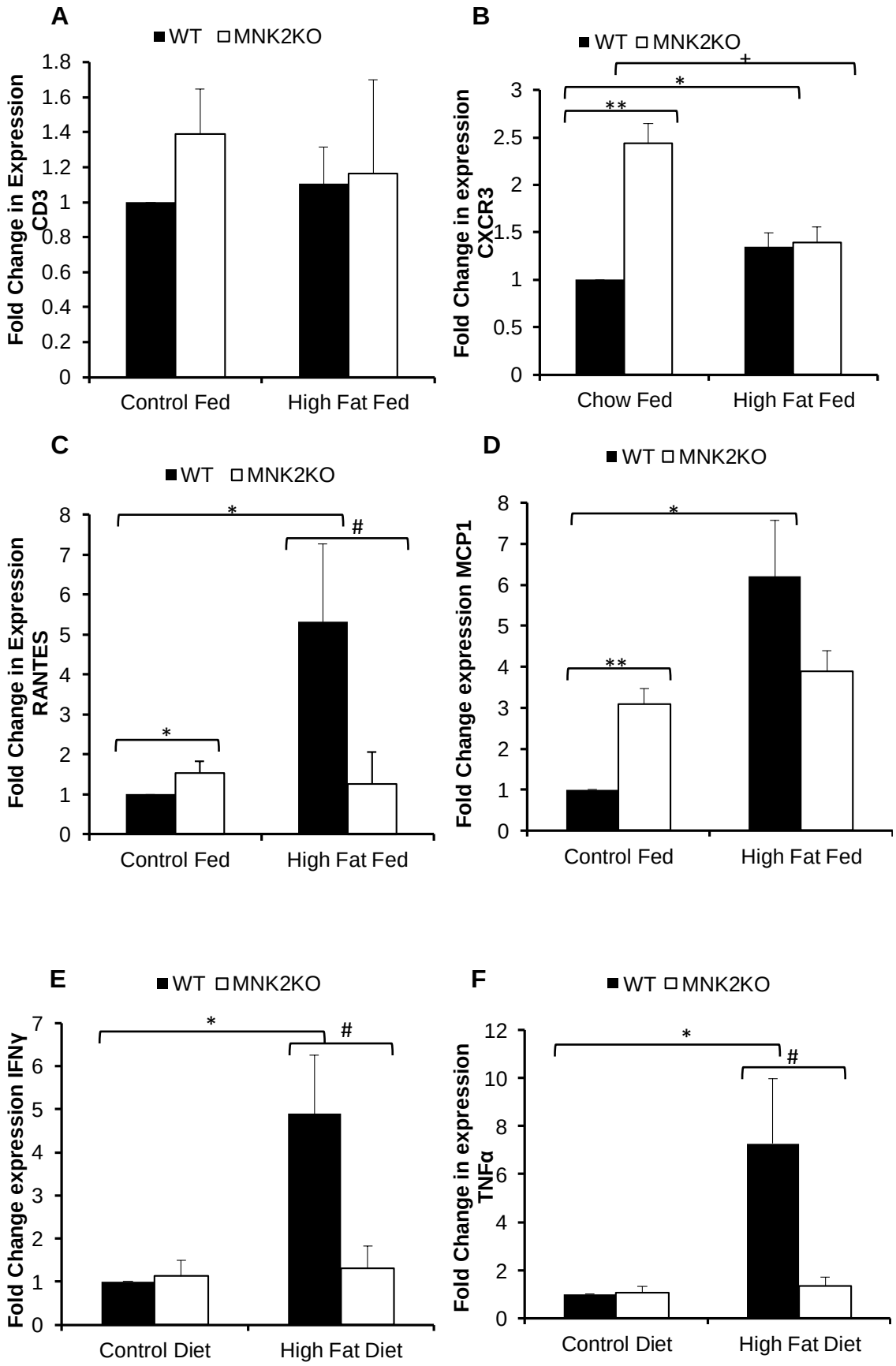

Figure 5.17. Analysis of the inflammatory characteristics of abdominal adipose in WT and MNK2KO mice fed chow or high fat diets. For CXCR3 n=3, for all experimental groups

and for all other analyses n=4. A) qPCR analysis of CD3 mRNA levels from abdominal adipose, results were normalised to 18S rRNA and expressed as fold difference in expression compared to WT chow fed. B) qPCR analysis of CXCR3 mRNA levels from abdominal adipose, results were normalised to 18S rRNA and expressed as fold difference in expression compared to WT chow fed. C) qPCR analysis of RANTES mRNA levels from abdominal adipose, results were normalised to 18S rRNA and expressed as fold difference in expression compared to WT chow fed. D) qPCR analysis of MCP-1 mRNA levels from abdominal adipose, results were normalised to 18S rRNA and expressed as fold difference in expression compared to WT chow fed. E) qPCR analysis of IFNγ mRNA levels from abdominal adipose, results were normalised to 18S rRNA and expressed as fold difference in expression compared to WT chow fed. F) qPCR analysis of TNFα mRNA levels from abdominal adipose, results were normalised to 18S rRNA and expressed as fold difference in expression compared to WT chow fed. Students' t-test was used to analyse the data * indicates $p<0.05$ compared to WT chow fed, ** indicates $p<0.01$ compared to WT chow fed, + indicated $p<0.05$ compared to MNK2KO chow fed and # indicates $p<0.05$ compared to WT high fat fed.

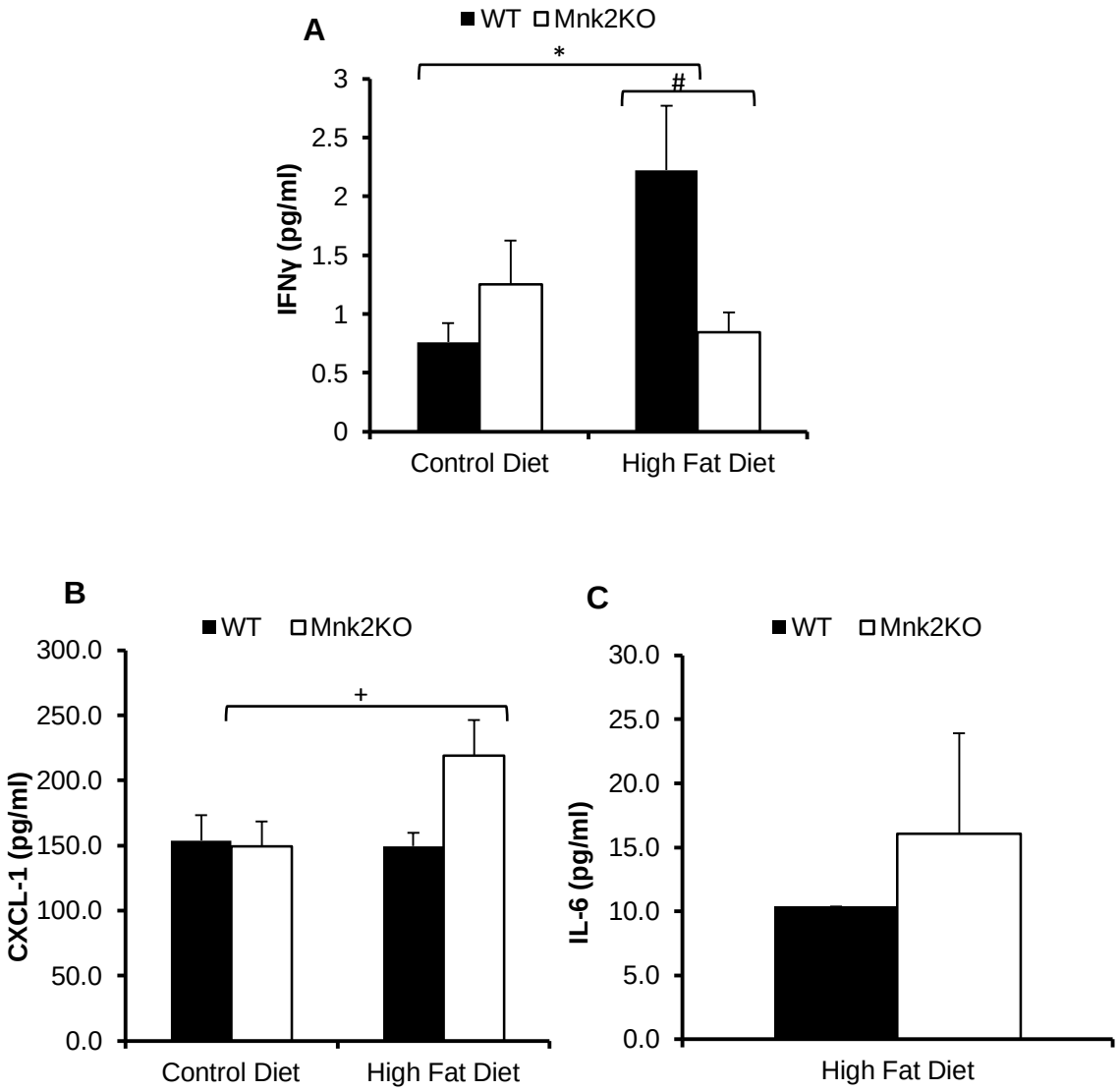

Figure 5.18. Analysis of the inflammatory characteristics in plasma of WT and MNK2KO mice fed chow or high fat diets. A) Fasting plasma levels of INFγ WT chow fed n=3, MNK2KO chow fed n=5, WT high fat fed n=5, MNK2KO high fat fed n=3. B) Fasting plasma levels of CXCL-1 WT chow fed n=6, MNK2KO chow fed n=7, WT high fat fed n=5, MNK2KO high fat fed n=4 C) Fasting plasma levels of IL-6 WT high fat fed n=2, MNK2KO high fat fed n=3. Students' t-test was used to analyse the data * indicates $p<0.05$ compared to WT chow fed, + indicated $p<0.05$ compared to MNK2KO chow fed and # indicates $p<0.05$ compared to WT high fat fed.

5.3 Discussion

The Mnks were discovered over 15 years ago [38, 39] and have since been widely researched within the context of tumorigenesis [31, 40, 78, 279]. However, apart from one report that suggested no overt phenotype in Mnk1/2-DKO mice [45], very little research has been conducted with regards to other functions of the Mnks. Patents concerning the use of Mnk agents to treat metabolic disease have been registered [106, 228]. The data presented in these patents led to the investigation into the role of the Mnks in metabolism. In this Chapter, the data show that knockout of only Mnk2 has a profound effect on both lipid and glucose metabolism. Challenging these mice with a high fat diet led to further distinctive differences compared with high fat fed WT mice. This raises important considerations in terms of obesity and T2DM.

The effect of high fat diet feeding in Mnk2-KO mice showed stark differences dependent on gender, with males gaining no weight and females gaining more weight compared with their WT counterparts. This disparity was not further investigated here but is of interest for future work. There were some consistencies between male and female mice when assessing the organs of these mice; Mnk2-KO mice exhibited increased heart size, reduced muscle mass and reduced abdominal adipose mass. Furthermore, when fed a high fat diet changes to muscle and fat mass may account for the reduced body weight in males and increased body weight in females. In males muscle mass and abdominal adipose mass did not increase to the extent seen in female mice. The interpretation of lack of weight gain by high fat fed male Mnk2-KO mice was further complicated when the DEXA data was analysed. This revealed an increased fat volume and reduced tissue volume in both chow and high fat diet fed Mnk2-KO mice, which is contradictory with regards to their lower weight. The explanation for this may be their reduced length, body volume, muscle mass and amount of abdominal adipose. The problem with DEXA analysis is that total fat volume is measured and cannot be divided into subcutaneous, retroperitoneal, abdominal and so forth. The images from the DEXA analysis appear to show that Mnk2-KO have more subcutaneous fat whilst dissection revealed less abdominal fat, however, there appeared to be more interstitial fat between the organs. This is important when considering the contributions of different fat depots to the consequences of obesity. Subcutaneous fat releases adipokines but is not as metabolically active as visceral fat [338]. Furthermore there is evidence subcutaneous fat can be protective, its removal does not improve glucose metabolism [339] whilst thiazolidinediones increase subcutaneous fat deposition with an improvement in insulin

sensitivity [340] and furthermore, transplantation of subcutaneous fat in place of visceral fat leads to improved glucose metabolism [341]. This could be one of the factors that contribute towards the improved glucose tolerance seen in high fat fed Mnk2-KO mice.

The original expectation was that Mnk2-KO mice would exhibit increased insulin resistance compared with WT mice due to the observations seen in Chapter 4. Both Mnks regulate IRS1 stability by reducing its degradation as a consequence of their phosphorylation of this protein. This meant that knockout of both Mnks leads to impaired glucose tolerance as seen in chow-fed Mnk1/2-DKO mice. This is likely attributable to reduced IRS1 expression in abdominal adipose. A similar result was seen in chow-fed Mnk2-KO mice but the decrease in IRS1 in Mnk2-KO high fat fed mice was not as great as in high fat fed WT mice. However, there were slightly reduced levels of IRS1 in the muscle of Mnk2-KO animals, which were reduced by high fat feeding to similar levels as high fat fed WT mice. In the liver mRNA levels of IRS1 did not correlate with protein levels, in chow-fed Mnk2-KO mice IRS1 mRNA was increased but not changed with high fat diet feeding whilst WT high fat fed mice had much higher levels. IRS1 protein appeared slightly greater in high fat fed Mnk2-KO mice compared with high fat fed WT mice despite lower mRNA levels. The mild insulin resistance and increased fasting glucose levels seen in chow-fed Mnk2-KO mice may be attributed to the amount of IRS1 in insulin sensitive tissues but the lack of any increases in insulin resistance with high fat diet feeding was not correlated with IRS1. These data imply that Mnk2-KO mice have a protective mechanism that allows them to maintain insulin sensitivity. The evidence from IRS1 knockout mice shows that, although they do develop insulin resistance, they do not exhibit T2DM and more importantly IRS2 knockout mice display T2DM due to reduced insulin secretion and severe hepatic insulin resistance [342, 343].

One of the major contributing factors to diet-induced insulin resistance and T2DM is the increase in plasma NEFAs, TGs and cholesterol [175]. In chow-fed Mnk2-KO mice there were distinctly lower levels of TGs and cholesterol, which probably reflects their reduced abdominal adipose mass and increased UCP1 expression, indicating a utilization of fat for energy. Interestingly, in high fat Mnk2-KO mice, the reduced abdominal adipose mass and number/size of adipocytes may lead to overspill of TGs, NEFAs and cholesterol, into circulation causing levels of these lipid metabolites to be much higher in high fat fed Mnk2-KO mice. Furthermore the data is indicative of a reduction in the storage of TGs in the liver as demonstrated by reduced droplets observed in H&E stains. This suggests that although there is an increase in fatty acids, which would be generated by lipolysis from adipose tissue, there is a reduction in TG storage in the liver. This indicates that there is an increase in TG export as VLDL and therefore explains the increased plasma TG levels

in high fat fed Mnk2-KO mice. The increased size of adipocytes from scapular adipose suggests the increased TGs are being deposited in this organ instead of the liver or even possibly the muscle. A diagram demonstrating this model can be seen Fig. 5.19. Further analysis of liver and muscle TG levels would be important to verify this. It would be expected that increased plasma TGs would contribute to insulin resistance and β cell dysfunction and thus that Mnk2-KO mice would present with T2DM. In fact, this is not the case perhaps because there is a reduction in UCP1 expression and increased β-hydroxybutyrate indicating more efficient fatty acid oxidation. This may also be helped by the increase in CXCL-1, which can activate fatty acid oxidation in muscle [322]. Furthermore, these data indicate that the altered lipid levels are not the major factor contributing to insulin resistance in the WT high fat fed mice when compared with the better performing Mnk2-KO mice.

The other major contributing factor to insulin resistance in diet-induced obesity is adipose inflammation [177, 183, 184]. As presented in Chapter 4, the Mnks and especially Mnk2, are highly expressed in the abdominal adipose and appear to have a major role in lipid metabolism; however the Mnks have also been strongly linked to enhancing the expression of inflammatory cytokines [41, 42, 44, 80]. The investigation into the levels of inflammatory cytokines and chemokines in high fat fed mice lead to what is probably the causative component that explains improved glucose tolerance in Mnk2-KO mice.

However, this is not simple because there are increases in RANTES, CXCR3 and MCP-1 in chow-fed Mnk2-KO mice. The expression of RANTES has previously been shown to be regulated by Mnk1 through modulating the translation of the transcription factor RANTES factor of late-activated T lymphocytes-1 (RFLAT-1) [283]. Activation of Mnk1 was associated with increased RFLAT-1 protein and RANTES. In Chapter 3 the activation of Mnk1 in response to PMA was significantly greater in Mnk2-KO cells compared to WT cells, it is possible the knockout of Mnk2 may lead to the moderate increase in RANTES seen in chow-fed Mnk2-KO mice due to increased activity of Mnk1. However the stimulus for inflammation caused by high fat diet feeding must require Mnk2 for RANTES expression and so there is no increase in high fat fed Mnk2-KO mice and this may also be the case for MCP1 and CXCR3, presenting an interesting avenue for further investigation.

The major finding of this work is that neither IFNγ nor TNFα is induced by high fat diet feeding in Mnk2-KO mice, which may be the most convincing evidence for the improved glucose tolerance in these mice. Very recently the expression of IFNγ has been shown to be reduced in Mnk1/2-DKO mice specifically from Th1 cells in response to myelin oligodendrocyte glycoprotein in a model of autoimmune encephalomyelitis, although the

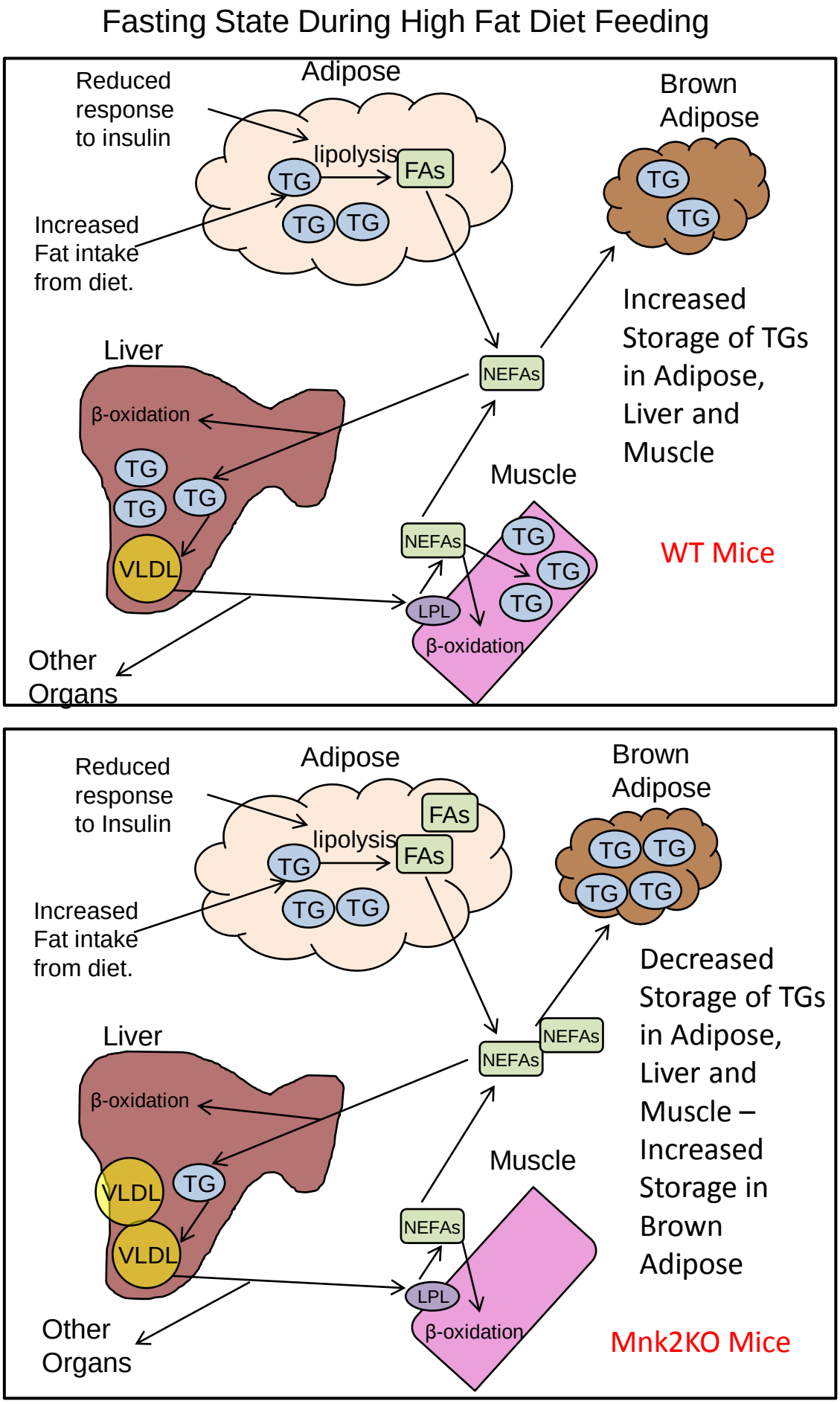

Figure 5.19. Model of Lipid Metabolism in WT and MNK2KO mice fed high fat diets.

Insulin resistance in white adipose tissue leads to increased lipolysis of triglycerides (TGs)

into fatty acids, which are released into the hepatic portal vein as non-esterified fatty acids (NEFAs), most of which enter the liver. In the liver NEFAs are re-esterified in TGs and exported as very low density lipoprotein (VLDL). VLDL interacts with lipoprotein lipase (LPL) at numerous organs and releases NEFAs, which are either taken up by the target tissue and stored as TGs or used for energy in β-oxidation.

authors do not show any direct evidence for the mechanism but allude to the potential role of eIF4E phosphorylation [281]. The translation of TNFα has been shown to be regulated by the Mnks through phosphorylation of hnRNPA1 and PSF.p54^{nrb} [41, 42], which suggests the loss of Mnk2, may result in reduced translation of TNFα and the subsequent degradation of TNFα mRNA leading to the results seen in this study. It would be very interesting to see if mice expressing the non-phosphorylatable S209A eIF4E mutant are also resistance to diet-induced insulin resistance and show reduced adipose inflammation. If this was the case then it indicates that Mnk-dependent eIF4E phosphorylation is the mechanism by which the Mnks contribute to diet-induced insulin resistance in a normal mouse.

Despite the differences in weight gain between male and female Mnk2-KO mice, a similar protection from insulin resistance was seen, suggesting inflammation is more important than the amount of fat. The reductions in inflammatory cytokines alone may well explain this protection based on evidence from IFNγ knockout mice, which show a very similar protection from diet-induced insulin resistance and exhibit similar reductions in RANTES, MCP-1 and TNFα [336]. TNFα null mice showed a moderate protection against diet-induced obesity [344] and there is a wealth of evidence supporting the role of TNFα in mediating insulin resistance (reviewed [188]).

The avenues for further research from the data presented here are numerous and potentially very interesting. The overt differences in weight gain between males and females should be investigated with regard to hormonal differences. One anticipates that detailed analysis of the intricate mechanisms by which Mnk2 controls particularly lipid metabolism will provide insights into the substrates of Mnk2 that are responsible for the differences seen. Finally, an in-depth investigation into the cell-type(s) responsible for the differences in the inflammatory profile seen in Mnk2-KO mice would be valuable. This is true in particular with regard to the potential for targeting Mnk activity for the treatment of inflammatory disease.

In summary, Mnk2KO mice are able to use glucose and lipids as energy sources in a novel fashion compared with WT mice, this means that, when fed normal chow diet, they use up lipids rapidly and subsequently have reduced visceral fat deposits but an increase in subcutaneous fat tissue. Consequently, when fed a high fat diet, their ability to use lipids as an energy resource and balance this with glucose utilization results in a protection against diet-induced obesity. Furthermore, the reduction in the expression of inflammatory mediators such as IFNγ and TNFα also helps to protect these mice from perturbed glucose tolerance and insulin resistance. This may indicate that specific Mnk2

inhibitors may be an appropriate and novel treatment for insulin resistance in obese patients.

Chapter 6

Final Discussion

Role of Mnk2a in rapamycin-induced eIF4E phosphorylation

The observations that rapamycin had potential for anti-cancer therapy led to the approval of derivatives of rapamycin (rapalogs) in the treatment of renal cell carcinoma [244]. The use of rapalogs in other cancers such as prostate cancer has proved less than desirable [259, 261, 345]. There is substantial evidence that rapamycin results in eIF4E phosphorylation in numerous cell types [29, 31, 262, 263], which represents a potential resistance mechanism to rapamycin since eIF4E phosphorylation has been linked to tumorigenesis [77-79]. Attempts to determine the pathway responsible for rapamycin-induced eIF4E phosphorylation have shown a role for PI3K and conflicting evidence for the role of PKB [29, 31, 263]. Furthermore, there is only one piece of data that investigates the Mnk isoform responsible and shows that both the Mnks are involved in rapamycin-induced eIF4E phosphorylation. This is despite evidence that neither ERK nor p38MAPK are activated, which are required for Mnk1 activity [29, 31].

In this study the evidence shows that inhibition of both the p110α and p110β subunits of PI3K is necessary to block rapamycin-induced eIF4E phosphorylation. This is consistent with evidence that shows the use of LY294002 and knockout of the p85α subunit of PI3K also blocks rapamycin-induced eIF4E phosphorylation [31]. PKB was shown to not be part of the signalling cascade responsible for rapamycin-induced eIF4E phosphorylation in this study.

Subsequent experiments demonstrated that Mnk2a was responsible for rapamycin-induced eIF4E phosphorylation in a mechanism that involved rapamycin-induced increases in Mnk2a activity independent of T-loop phosphorylation. Mass spectrometry analysis showed that two sites in Mnk2a exhibited changes in phosphorylation (although not quantitatively): Ser^{74} and Ser^{437} and subsequent mutagenesis experiments revealed that Ser^{437} was important for rapamycin-induced eIF4E phosphorylation. Interestingly the data suggested that dephosphorylation of Ser^{437} in a rapamycin induced fashion lead to increases in Mnk2a activity. These data also indicated that PP242 also increased Mnk2a activity indicating that this is a phenomenon related to mTORC1 inhibition irrespective of the mode of mTOR inhibition. This is very important when considering mTOR inhibitors as cancer therapies as increased Mnk2a activity may be oncogenic with regards to substrates other than eIF4E.

Regulation of insulin signalling by the Mnks

The majority of research involving the Mnks has focused on their best known substrate eIF4E and the link between its phosphorylation and tumorigenesis (reviewed [40, 79, 276]), whilst other research links the Mnks with inflammatory pathways and cytokine

translation [41, 42, 81, 282, 283]. There is evidence of only one other Mnk substrate that is not related to translation, which is Sprouty [74, 105]. There are however a couple of patents that relate the Mnks to glucose and lipid homeostasis [106, 228], which present evidence that the Mnks may modulate insulin sensitivity, albeit there is a distinct confliction as to the role the Mnks play.

Research presented here shows the Mnks are highly enriched in tissues related to glucose metabolism where both Mnk1 and Mnk2 are expressed in the skeletal muscle and fat depots whilst Mnk1 was the most enriched in the pancreas. Investigations using Mnk knockout cells revealed that loss of particularly Mnk2 resulted in a significant reduction in PKB activity, whilst the loss of both Mnks abrogated this further. PKB signalling to mTORC1 was disrupted to the greatest extent in Mnk1/2-DKO cells with some changes in Mnk1-KO and Mnk2-KO cells. There was a very strong effect of knockout of either of the Mnks on glucose uptake, which showed loss of the Mnks results in the inhibition of insulin-stimulated glucose. This was further corroborated with the use of Mnk inhibitors, which caused a reduction in insulin-stimulated glucose uptake, consistent with the Mnks regulating insulin signalling in a mechanism related to their kinase activity. Investigations into the mechanism by which the Mnks regulate insulin signalling revealed that PI3K activity was also reduced in Mnk1/2-DKO cells although the data from Mnk1-KO or Mnk2-KO cells was not as clear. Reduced PI3K activity in response to insulin was also seen in 3T3-L1 cells treated with Mnk inhibitors. These data indicated that the Mnks either acted directly on, or, upstream of PI3K.

IRS1 is highly regulated by phosphorylation (reviewed [229]) and therefore represented a potential target of the Mnks. Levels of IRS1 protein were distinctly lower in Mnk knockout, Mnk knockdown (siRNA treated WT cells) and Mnk inhibitor treated cells. Further investigation revealed that both Mnk1 and Mnk2 were able to phosphorylate IRS1 at 5 sites and subsequent experiments revealed these sites may be important for the stabilization of IRS1 by the Mnks.

The low levels of IRS1 in Mnk knockout cells suggested that tissues such as the muscle and white adipose from Mnk1/2-DKO mice would also show low levels of IRS1. This was not the case for skeletal muscle, but, adipose tissue appeared to have lower levels of IRS1 in Mnk1/2-DKO mice, although there was considerable mouse to mouse variation. The knockout of IRS1 in mice leads to systemic insulin resistance [342], whilst mice expressing a mutant of IRS1 that is resistant to degradation are protected from insulin resistance [309]. These observations led to the discovery, shown here, that Mnk1/2-DKO

mice are insulin resistant as revealed by a shift in glucose clearance when challenged with a glucose tolerance test.

These findings would indicate that insulin sensitivity might be improved by agents that increase the activity or expression of the Mnks. This is contradictive with regards to the data presented in a patent relating to Mnk inhibitors improving insulin sensitivity [106]. Analysis of Mnk2-KO mice revealed that IRS1 protein levels were reduced in both the skeletal muscle and white adipose tissue of chow-fed mice but they did not show insulin resistance as demonstrated by a normal glucose tolerance test. These observations reveal that the control of IRS1 levels by the Mnks is complex and requires further research to ascertain the role of Mnk1. The levels of Mnk1 are the greatest in the pancreas, whilst Mnk2 is not expressed in the pancreas, which is suggestive of a specific role for Mnk1 in this tissue. One explanation for the disparity seen with regards to insulin resistance when comparing Mnk2-KO and Mnk1/2-DKO mice is that the perturbed glucose tolerance of Mnk1/2-DKO mice is caused by changes to the levels of insulin. It would be very interesting to investigate if Mnk1 has any role in the pancreas with regards to insulin secretion or expression.

Role of Mnk2 in whole body glucose and lipid homeostasis

Perhaps the most interesting data presented here pertains to the effect of Mnk2 knockout on the metabolism of lipids and glucose and the effect high fat diet feeding has on these animals.

Evidence from one patent regarding the Mnks showed that an Mnk2DN mouse weighed more than WT mice whilst overexpression of Mnk2 in cells led to decreased TG storage and reduced lipogenesis [228]. The opposite was shown in another patent regarding and Mnk2 inhibitor, which showed insulin sensitizing properties and mice treated with the compound showed reduced bodyweight [106]. These observations are consistent with the data shown here where male Mnk2-KO mice weighed less than their WT counterparts even when challenged with a high fat diet. Furthermore both male and female Mnk2-KO mice were protected from diet-induced insulin resistance as shown in glucose tolerance tests and HOMA-IR calculations.

The lack of weight gain by male Mnk2-KO mice fed high fat diets is a desirable feature when considering the epidemic of obesity. It was therefore surprising when DEXA analysis revealed that even chow-fed Mnk2-KO mice exhibited increased subcutaneous fat and fat between the organs. Furthermore, Mnk2-KO mice fed high fat diets appeared to show similar increases in fat accumulation as high fat fed WT mice. Potential explanations for

the disparity between weight and the DEXA data came from the observations that Mnk2-KO are, overall, smaller than WT mice in terms of length and body volume whilst the amount of white fat was significantly lower in chow-fed Mnk2-KO mice and marginally reduced in high fat fed Mnk2-KO mice. Investigations into the histology and biochemistry of the fat depots revealed some interesting data. The brown adipose tissue of chow-fed and high fat fed Mnk2-KO mice weighed more with respect to bodyweight compared to WT mice, whilst the converse was true for white adipose tissue. The histology of both fats depots was also altered in Mnk2-KO mice; the brown adipose of high fat fed Mnk2-KO mice exhibited larger adipocytes. Chow-fed Mnk2-KO mice presented with larger adipocytes in white adipose that did not increase in size to the same extent as adipocytes from high fat fed WT mice. These observations indicate Mnk2 may have a role in fatty acid synthesis, lipolysis or adipogenesis and represents a novel area of research with regards to the physiological role of Mnk2. The data from plasma lipid metabolites shows chow-fed Mnk2-KO mice have lower levels of TGs, cholesterol and β-hydroxybutyrate, which is again a desirable phenotype. However in high fat fed Mnk2-KO mice plasma TGs, cholesterol, NEFAs and β-hydroxybutyrate increase significantly and to a greater extent than high fat fed WT mice. The explanation may be linked to the observations that Mnk2-KO mice fed chow diets had increased UCP-1 expression and reduced abdominal adipose mass, which may explain the lower levels of plasma lipids due to their use for energy. The increased plasma lipid levels in high fat fed Mnk2-KO mice may be a consequence of reduced storage of TGs in abdominal adipose and therefore spill-over into circulation.

Evidence currently suggests that diet-induced insulin resistance is caused by increased plasma NEFAs and TGs in combination with increased levels of inflammatory cytokines, and perturbed adipokine release (reviewed [157, 175, 177]). The mechanisms related to the protection of Mnk2-KO mice from diet-induced insulin resistance were not explained by differences in lipid metabolites as would be expected given the lack of weight gain. The analysis of inflammatory cytokines revealed that the protection from insulin resistance in high fat fed Mnk2-KO mice may be related to a reduced expression of inflammatory cytokines such as TNFα, IFNγ MCP-1 and RANTES. Furthermore, this suggests reducing the chronic inflammation associated with obesity is more beneficial than reducing plasma lipids. This is supported by the observation that high fat fed Mnk2-KO mice have higher levels of TGs and NEFAs than WT mice but exhibit improved insulin sensitivity.

Future directions for research involving the Mnks

There is still a distinct lack of information regarding the physiological roles of the Mnks and whilst this study presents an insight into novel functions of the Mnks there are still a number of unanswered questions with regards to distinct roles for the Mnks.

The increase in activity of Mnk2a in response to mTOR inhibition must be further investigated to determine the mechanism by which Ser^{437} modulates Mnk2a activity. Furthermore, it is important to identify substrates of Mnk2a that may be oncogenic whilst the role of eIF4E phosphorylation on translation of specific mRNAs still requires further investigation.

This study has revealed a novel substrate of the Mnks, IRS1 whose stability is regulated through phosphorylation. Future research would need to address if Mnk-dependent phosphorylation was required for signalling through IRS1 by testing whether the S-5-A IRS1 mutant exhibited reduced PKB activity and downstream signalling as seen in the Mnk knockout cells. Furthermore, the insulin levels in Mnk1/2-DKO and Mnk-1KO mice need to be assessed and a GTT needs to be conducted in Mnk1-KO mice. The role of Mnk1 in the pancreas is another exciting area of research, which may yield a physiological role for this kinase.

The role of Mnk2 in a whole animal model has been investigated here but there is still a lot of research required to identify how Mnk2 regulates fat distribution, adipocyte size, fatty acid synthesis and lipolysis, one or all of which may explain the phenotype presented by Mnk2-KO mice. Another interesting area of research with regards to Mnk2 would be to determine if translation of cytokines are regulated in diseases other than diet-induced obesity, representing another use of Mnk inhibitors in disease.

List of References

1 Leeds, D. (2006) Cellular Signalling Research. pp. vii-x, Nova Science Publishers, New York

2 Schwanhausser, B., Busse, D., Li, N., Dittmar, G., Schuchhardt, J., Wolf, J., Chen, W. and Selbach, M. (2011) Global quantification of mammalian gene expression control. Nature. **473**, 337-342

3 Van Der Kelen, K., Beyaert, R., Inze, D. and De Veylder, L. (2009) Translational control of eukaryotic gene expression. Critical reviews in biochemistry and molecular biology. **44**, 143-168

4 Alberts, B., Johnson, A., Lewis, J., Raff, M., Roberts, K. and Walter, P. (2002) Molecular Biology of the Cell. pp. 223-242, Garland Science, New York and London

5 Holt, C. E. and Bullock, S. L. (2009) Subcellular mRNA localization in animal cells and why it matters. Science. **326**, 1212-1216

6 Benne, R. and Sloof, P. (1987) Evolution of the mitochondrial protein synthetic machinery. Biosystems. **21**, 51-68

7 Gingras, A. C., Raught, B. and Sonenberg, N. (1999) eIF4 initiation factors: effectors of mRNA recruitment to ribosomes and regulators of translation. Annual review of biochemistry. **68**, 913-963

8 Hershey, J. W. B. and Merrick, W. C. (2000) Translational Control of Gene Expression. (Sonenberg, N., Hershey, J. W. B. and Mathews, M. B., eds.). pp. 45-56, Cold Spring Harbour Laboratory Press, New York

9 Aitken, C. E. and Lorsch, J. R. (2012) A mechanistic overview of translation initiation in eukaryotes. Nature structural & molecular biology. **19**, 568-576

10 Wang, Q., Li, S., Jiang, L., Zhou, Y., Li, Z., Shao, M., Li, W. and Liu, Y. (2010) Deficiency in hepatic ATP-citrate lyase affects VLDL-triglyceride mobilization and liver fatty acid composition in mice. J Lipid Res. **51**, 2516-2526

11 Fischer, P. M. (2009) Cap in hand: targeting eIF4E. Cell cycle. **8**, 2535-2541

12 von der Haar, T., Gross, J. D., Wagner, G. and McCarthy, J. E. (2004) The mRNA cap-binding protein eIF4E in post-transcriptional gene expression. Nature structural & molecular biology. **11**, 503-511

13 Coldwell, M. J., Sack, U., Cowan, J. L., Barrett, R. M., Vlasak, M., Sivakumaran, K. and Morley, S. J. (2012) Multiple isoforms of the translation initiation factor eIF4GII are generated via use of alternative promoters, splice sites and a non-canonical initiation codon. The Biochemical journal. **448**, 1-11

14 Valasek, L. S. (2012) 'Ribozoomin'--translation initiation from the perspective of the ribosome-bound eukaryotic initiation factors (eIFs). Current protein & peptide science. **13**, 305-330

15 Ramirez-Valle, F., Braunstein, S., Zavadil, J., Formenti, S. C. and Schneider, R. J. (2008) eIF4GI links nutrient sensing by mTOR to cell proliferation and inhibition of autophagy. The Journal of cell biology. **181**, 293-307

16 Richter, J. D. and Sonenberg, N. (2005) Regulation of cap-dependent translation by eIF4E inhibitory proteins. Nature. **433**, 477-480

17 Herbert, T. P. and Proud, C. G. (2007) Translational Control in Biology and Medicine. In Regulation of Translation Elongation and the Cotranslational Protein Targeting Pathway (Mathews, M. B., Sonenberg, N. and Hershey, J. W. B., eds.). pp. 602-608, Cold SpringHarbour Laboratory Press, New York

18 Taylor, D. J., Frank, J. and Kinzy, T. G. (2007) Translational Control in Biology and Medicine. In Structure and Function of the Eukaryotic Ribosome and Elongation Factors (Mathews, M. B., Sonenberg, N. and Hershey, J. W. B., eds.). pp. 71-72, Cold SpringHarbour Laboratory Press, New York

19 Browne, G. J. and Proud, C. G. (2002) Regulation of peptide-chain elongation in mammalian cells. European journal of biochemistry / FEBS. **269**, 5360-5368

20 Chavatte, L., Kervestin, S., Favre, A. and Jean-Jean, O. (2003) Stop codon selection in eukaryotic translation termination: comparison of the discriminating potential between human and ciliate eRF1s. The EMBO journal. **22**, 1644-1653

21 Inge-Vechtomov, S., Zhouravleva, G. and Philippe, M. (2003) Eukaryotic release factors (eRFs) history. Biology of the cell / under the auspices of the European Cell Biology Organization. **95**, 195-209

22 Yang, Q. and Guan, K. L. (2007) Expanding mTOR signaling. Cell Res. **17**, 666-681

23 Porta, C. and Figlin, R. A. (2009) Phosphatidylinositol-3-kinase/Akt signaling pathway and kidney cancer, and the therapeutic potential of phosphatidylinositol-3-kinase/Akt inhibitors. J Urol. **182**, 2569-2577

24 Sarbassov, D. D., Guertin, D. A., Ali, S. M. and Sabatini, D. M. (2005) Phosphorylation and regulation of Akt/PKB by the rictor-mTOR complex. Science. **307**, 1098-1101

25 Hay, N. and Sonenberg, N. (2004) Upstream and downstream of mTOR. Genes Dev. **18**, 1926-1945

26 Avruch, J., Long, X., Lin, Y., Ortiz-Vega, S., Rapley, J., Papageorgiou, A., Oshiro, N. and Kikkawa, U. (2009) Activation of mTORC1 in two steps: Rheb-GTP activation of catalytic function and increased binding of substrates to raptor. Biochemical Society transactions. **37**, 223-226

27 Crespo, J. L., Diaz-Troya, S. and Florencio, F. J. (2005) Inhibition of target of rapamycin signaling by rapamycin in the unicellular green alga Chlamydomonas reinhardtii. Plant Physiol. **139**, 1736-1749

28 Thoreen, C. C., Kang, S. A., Chang, J. W., Liu, Q., Zhang, J., Gao, Y., Reichling, L. J., Sim, T., Sabatini, D. M. and Gray, N. S. (2009) An ATP-competitive mammalian target of rapamycin inhibitor reveals rapamycin-resistant functions of mTORC1. J Biol Chem. **284**, 8023-8032

29 Bianchini, A., Loiarro, M., Bielli, P., Busa, R., Paronetto, M. P., Loreni, F., Geremia, R. and Sette, C. (2008) Phosphorylation of eIF4E by MNKs supports protein synthesis, cell cycle progression and proliferation in prostate cancer cells. Carcinogenesis. **29**, 2279-2288

30 Panja, D., Dagyte, G., Bidinosti, M., Wibrand, K., Kristiansen, A. M., Sonenberg, N. and Bramham, C. R. (2009) Novel translational control in Arc-dependent long term potentiation consolidation in vivo. J Biol Chem. **284**, 31498-31511

31 Wang, X., Yue, P., Chan, C. B., Ye, K., Ueda, T., Watanabe-Fukunaga, R., Fukunaga, R., Fu, H., Khuri, F. R. and Sun, S. Y. (2007) Inhibition of mammalian target of rapamycin induces phosphatidylinositol 3-kinase-dependent and Mnk-mediated eukaryotic translation initiation factor 4E phosphorylation. Molecular and cellular biology. **27**, 7405-7413

32 Fenton, T. R. and Gout, I. T. (2011) Functions and regulation of the 70kDa ribosomal S6 kinases. Int J Biochem Cell Biol. **43**, 47-59

33 Wang, X., Li, W., Williams, M., Terada, N., Alessi, D. R. and Proud, C. G. (2001) Regulation of elongation factor 2 kinase by p90(RSK1) and p70 S6 kinase. The EMBO journal. **20**, 4370-4379

34 Reinhardt, H. C., Hasskamp, P., Schmedding, I., Morandell, S., van Vugt, M. A., Wang, X., Linding, R., Ong, S. E., Weaver, D., Carr, S. A. and Yaffe, M. B. (2010) DNA damage activates a spatially distinct late cytoplasmic cell-cycle checkpoint network controlled by MK2-mediated RNA stabilization. Mol Cell. **40**, 34-49

35 Bollig, F., Winzen, R., Gaestel, M., Kostka, S., Resch, K. and Holtmann, H. (2003) Affinity purification of ARE-binding proteins identifies polyA-binding protein 1 as a potential substrate in MK2-induced mRNA stabilization. Biochem Biophys Res Commun. **301**, 665-670

36 Tiedje, C., Ronkina, N., Tehrani, M., Dhamija, S., Laass, K., Holtmann, H., Kotlyarov, A. and Gaestel, M. (2012) The p38/MK2-driven exchange between tristetraprolin and HuR regulates AU-rich element-dependent translation. PLoS Genet. **8**, e1002977

37 Roux, P. P. and Blenis, J. (2004) ERK and p38 MAPK-activated protein kinases: a family of protein kinases with diverse biological functions. Microbiol Mol Biol Rev. **68**, 320-344

38 Fukunaga, R. and Hunter, T. (1997) MNK1, a new MAP kinase-activated protein kinase, isolated by a novel expression screening method for identifying protein kinase substrates. The EMBO journal. **16**, 1921-1933

39 Waskiewicz, A. J., Flynn, A., Proud, C. G. and Cooper, J. A. (1997) Mitogen-activated protein kinases activate the serine/threonine kinases Mnk1 and Mnk2. The EMBO journal. **16**, 1909-1920

40 Hou, J., Lam, F., Proud, C. and Wang, S. (2012) Targeting Mnks for cancer therapy. Oncotarget. **3**, 118-131

41 Buxade, M., Morrice, N., Krebs, D. L. and Proud, C. G. (2008) The PSF.p54nrb complex is a novel Mnk substrate that binds the mRNA for tumor necrosis factor alpha. J Biol Chem. **283**, 57-65

42 Buxade, M., Parra, J. L., Rousseau, S., Shpiro, N., Marquez, R., Morrice, N., Bain, J., Espel, E. and Proud, C. G. (2005) The Mnks are novel components in the control of TNF alpha biosynthesis and phosphorylate and regulate hnRNP A1. Immunity. **23**, 177-189

43 Fortin, C. F., Mayer, T. Z., Cloutier, A. and McDonald, P. P. (2013) Translational control of human neutrophil responses by MNK1. J Leukoc Biol

44 Kjellerup, R. B., Kragballe, K., Iversen, L. and Johansen, C. (2008) Pro-inflammatory cytokine release in keratinocytes is mediated through the MAPK signal-integrating kinases. Experimental dermatology. **17**, 498-504

45 Ueda, T., Watanabe-Fukunaga, R., Fukuyama, H., Nagata, S. and Fukunaga, R. (2004) Mnk2 and Mnk1 are essential for constitutive and inducible phosphorylation of eukaryotic initiation factor 4E but not for cell growth or development. Molecular and cellular biology. **24**, 6539-6549

46 Sonenberg, N. and Gingras, A. C. (1998) The mRNA 5' cap-binding protein eIF4E and control of cell growth. Curr Opin Cell Biol. **10**, 268-275

47 Morley, S. J. (1994) Signal transduction mechanisms in the regulation of protein synthesis. Mol Biol Rep. **19**, 221-231

48 Raught, B. and Gingras, A. C. (1999) eIF4E activity is regulated at multiple levels. Int J Biochem Cell Biol. **31**, 43-57

49 Bonneau, A. M. and Sonenberg, N. (1987) Involvement of the 24-kDa cap-binding protein in regulation of protein synthesis in mitosis. J Biol Chem. **262**, 11134-11139

50 Rychlik, W., Russ, M. A. and Rhoads, R. E. (1987) Phosphorylation site of eukaryotic initiation factor 4E. J Biol Chem. **262**, 10434-10437

51 Morley, S. J., Dever, T. E., Etchison, D. and Traugh, J. A. (1991) Phosphorylation of eIF-4F by protein kinase C or multipotential S6 kinase stimulates protein synthesis at initiation. J Biol Chem. **266**, 4669-4672

52 Kaufman, R. J., Murtha-Riel, P., Pittman, D. D. and Davies, M. V. (1993) Characterization of wild-type and Ser53 mutant eukaryotic initiation factor 4E overexpression in mammalian cells. J Biol Chem. **268**, 11902-11909

53 Flynn, A. and Proud, C. G. (1995) Serine 209, not serine 53, is the major site of phosphorylation in initiation factor eIF-4E in serum-treated Chinese hamster ovary cells. J Biol Chem. **270**, 21684-21688

54 Kleijn, M., Scheper, G. C., Voorma, H. O. and Thomas, A. A. (1998) Regulation of translation initiation factors by signal transduction. European journal of biochemistry / FEBS. **253**, 531-544

55 Flynn, A. and Proud, G. (1996) Insulin-stimulated phosphorylation of initiation factor 4E is mediated by the MAP kinase pathway. FEBS Lett. **389**, 162-166

56 Flynn, A. and Proud, C. G. (1996) Insulin and phorbol ester stimulate initiation factor eIF-4E phosphorylation by distinct pathways in Chinese hamster ovary cells overexpressing the insulin receptor. European journal of biochemistry / FEBS. **236**, 40-47

57 Morley, S. J. and McKendrick, L. (1997) Involvement of stress-activated protein kinase and p38/RK mitogen-activated protein kinase signaling pathways in the enhanced phosphorylation of initiation factor 4E in NIH 3T3 cells. J Biol Chem. **272**, 17887-17893

58 Waskiewicz, A. J., Johnson, J. C., Penn, B., Mahalingam, M., Kimball, S. R. and Cooper, J. A. (1999) Phosphorylation of the cap-binding protein eukaryotic translation initiation factor 4E by protein kinase Mnk1 in vivo. Molecular and cellular biology. **19**, 1871-1880

59 Karandikar, M., Xu, S. and Cobb, M. H. (2000) MEKK1 binds raf-1 and the ERK2 cascade components. J Biol Chem. **275**, 40120-40127

60 Baud, V., Liu, Z. G., Bennett, B., Suzuki, N., Xia, Y. and Karin, M. (1999) Signaling by proinflammatory cytokines: oligomerization of TRAF2 and TRAF6 is sufficient for JNK and IKK activation and target gene induction via an amino-terminal effector domain. Genes Dev. **13**, 1297-1308

61 Derijard, B., Raingeaud, J., Barrett, T., Wu, I. H., Han, J., Ulevitch, R. J. and Davis, R. J. (1995) Independent human MAP-kinase signal transduction pathways defined by MEK and MKK isoforms. Science. **267**, 682-685

62 Voet, D., Voet, J. G. and Pratt, C. W. (2006) Fundamentals of Biochemistry Life at the Molecular Level. pp. 395-582, 744-784, John Wiley & Sons, Inc

63 Roskoski, R., Jr. (2012) ERK1/2 MAP kinases: structure, function, and regulation. Pharmacol Res. **66**, 105-143

64 Cuenda, A. and Rousseau, S. (2007) p38 MAP-kinases pathway regulation, function and role in human diseases. Biochim Biophys Acta. **1773**, 1358-1375

65 O'Loghlen, A., Gonzalez, V. M., Pineiro, D., Perez-Morgado, M. I., Salinas, M. and Martin, M. E. (2004) Identification and molecular characterization of Mnk1b, a splice variant of human MAP kinase-interacting kinase Mnk1. Exp Cell Res. **299**, 343-355

66 Slentz-Kesler, K., Moore, J. T., Lombard, M., Zhang, J., Hollingsworth, R. and Weiner, M. P. (2000) Identification of the human Mnk2 gene (MKNK2) through protein interaction with estrogen receptor beta. Genomics. **69**, 63-71

67 Goto, S., Yao, Z. and Proud, C. G. (2009) The C-terminal domain of Mnk1a plays a dual role in tightly regulating its activity. The Biochemical journal. **423**, 279-290

68 Jauch, R., Cho, M. K., Jakel, S., Netter, C., Schreiter, K., Aicher, B., Zweckstetter, M., Jackle, H. and Wahl, M. C. (2006) Mitogen-activated protein kinases interacting kinases are autoinhibited by a reprogrammed activation segment. The EMBO journal. **25**, 4020-4032

69 Nolen, B., Taylor, S. and Ghosh, G. (2004) Regulation of protein kinases; controlling activity through activation segment conformation. Mol Cell. **15**, 661-675

70 Jauch, R., Jakel, S., Netter, C., Schreiter, K., Aicher, B., Jackle, H. and Wahl, M. C. (2005) Crystal structures of the Mnk2 kinase domain reveal an inhibitory conformation and a zinc binding site. Structure. **13**, 1559-1568

71 Kornev, A. P., Haste, N. M., Taylor, S. S. and Eyck, L. F. (2006) Surface comparison of active and inactive protein kinases identifies a conserved activation mechanism. Proc Natl Acad Sci U S A. **103**, 17783-17788

72 Parra, J. L., Buxade, M. and Proud, C. G. (2005) Features of the catalytic domains and C termini of the MAPK signal-integrating kinases Mnk1 and Mnk2 determine their differing activities and regulatory properties. J Biol Chem. **280**, 37623-37633

73 Scheper, G. C., Morrice, N. A., Kleijn, M. and Proud, C. G. (2001) The mitogen-activated protein kinase signal-integrating kinase Mnk2 is a eukaryotic initiation factor 4E kinase with high levels of basal activity in mammalian cells. Molecular and cellular biology. **21**, 743-754

74 DaSilva, J., Xu, L., Kim, H. J., Miller, W. T. and Bar-Sagi, D. (2006) Regulation of sprouty stability by Mnk1-dependent phosphorylation. Molecular and cellular biology. **26**, 1898-1907

75 Scheper, G. C. and Proud, C. G. (2002) Does phosphorylation of the cap-binding protein eIF4E play a role in translation initiation? European journal of biochemistry / FEBS. **269**, 5350-5359

76 Knauf, U., Tschopp, C. and Gram, H. (2001) Negative regulation of protein translation by mitogen-activated protein kinase-interacting kinases 1 and 2. Molecular and cellular biology. **21**, 5500-5511

77 Furic, L., Rong, L., Larsson, O., Koumakpayi, I. H., Yoshida, K., Brueschke, A., Petroulakis, E., Robichaud, N., Pollak, M., Gaboury, L. A., Pandolfi, P. P., Saad, F. and Sonenberg, N. (2010) eIF4E phosphorylation promotes tumorigenesis and is associated with prostate cancer progression. Proc Natl Acad Sci U S A. **107**, 14134-14139

78 Ueda, T., Sasaki, M., Elia, A. J., Chio, II, Hamada, K., Fukunaga, R. and Mak, T. W. (2010) Combined deficiency for MAP kinase-interacting kinase 1 and 2 (Mnk1 and Mnk2) delays tumor development. Proc Natl Acad Sci U S A. **107**, 13984-13990

79 Wendel, H. G., Silva, R. L., Malina, A., Mills, J. R., Zhu, H., Ueda, T., Watanabe-Fukunaga, R., Fukunaga, R., Teruya-Feldstein, J., Pelletier, J. and Lowe, S. W. (2007) Dissecting eIF4E action in tumorigenesis. Genes Dev. **21**, 3232-3237

80 Grund, E. M., Spyropoulos, D. D., Watson, D. K. and Muise-Helmericks, R. C. (2005) Interleukins 2 and 15 regulate Ets1 expression via ERK1/2 and MNK1 in human natural killer cells. J Biol Chem. **280**, 4772-4778

81 Joshi, S., Kaur, S., Redig, A. J., Goldsborough, K., David, K., Ueda, T., Watanabe-Fukunaga, R., Baker, D. P., Fish, E. N., Fukunaga, R. and Platanias, L. C. (2009) Type I interferon (IFN)-dependent activation of Mnk1 and its role in the generation of growth inhibitory responses. Proc Natl Acad Sci U S A. **106**, 12097-12102

82 Meraro, D., Gleit-Kielmanowicz, M., Hauser, H. and Levi, B. Z. (2002) IFN-stimulated gene 15 is synergistically activated through interactions between the myelocyte/lymphocyte-specific transcription factors, PU.1, IFN regulatory factor-8/IFN consensus sequence binding protein, and IFN regulatory factor-4: characterization of a new subtype of IFN-stimulated response element. J Immunol. **168**, 6224-6231

83 Terenzi, F., Hui, D. J., Merrick, W. C. and Sen, G. C. (2006) Distinct induction patterns and functions of two closely related interferon-inducible human genes, ISG54 and ISG56. J Biol Chem. **281**, 34064-34071

84 Chen, Y. J., Tan, B. C., Cheng, Y. Y., Chen, J. S. and Lee, S. C. (2010) Differential regulation of CHOP translation by phosphorylated eIF4E under stress conditions. Nucleic acids research. **38**, 764-777

85 Pyronnet, S., Imataka, H., Gingras, A. C., Fukunaga, R., Hunter, T. and Sonenberg, N. (1999) Human eukaryotic translation initiation factor 4G (eIF4G) recruits mnk1 to phosphorylate eIF4E. The EMBO journal. **18**, 270-279

86 Parra-Palau, J. L., Scheper, G. C., Wilson, M. L. and Proud, C. G. (2003) Features in the N and C termini of the MAPK-interacting kinase Mnk1 mediate its nucleocytoplasmic shuttling. J Biol Chem. **278**, 44197-44204

87 Scheper, G. C., Parra, J. L., Wilson, M., Van Kollenburg, B., Vertegaal, A. C., Han, Z. G. and Proud, C. G. (2003) The N and C termini of the splice variants of the human mitogen-activated protein kinase-interacting kinase Mnk2 determine activity and localization. Molecular and cellular biology. **23**, 5692-5705

88 Bellsolell, L., Cho-Park, P. F., Poulin, F., Sonenberg, N. and Burley, S. K. (2006) Two structurally atypical HEAT domains in the C-terminal portion of human eIF4G support binding to eIF4A and Mnk1. Structure. **14**, 913-923

89 Groves, M. R., Hanlon, N., Turowski, P., Hemmings, B. A. and Barford, D. (1999) The structure of the protein phosphatase 2A PR65/A subunit reveals the conformation of its 15 tandemly repeated HEAT motifs. Cell. **96**, 99-110

90 Morino, S., Imataka, H., Svitkin, Y. V., Pestova, T. V. and Sonenberg, N. (2000) Eukaryotic translation initiation factor 4E (eIF4E) binding site and the middle one-third of eIF4GI constitute the core domain for cap-dependent translation, and the C-terminal one-third functions as a modulatory region. Molecular and cellular biology. **20**, 468-477

91 Li, Y., Yue, P., Deng, X., Ueda, T., Fukunaga, R., Khuri, F. R. and Sun, S. Y. (2010) Protein phosphatase 2A negatively regulates eukaryotic initiation factor 4E phosphorylation and eIF4F assembly through direct dephosphorylation of Mnk and eIF4E. Neoplasia. **12**, 848-855

92 Dobrikov, M. I., Dobrikova, E. Y. and Gromeier, M. (2013) Dynamic regulation of the translation initiation helicase complex by mitogenic signal transduction to eukaryotic translation initiation factor 4G. Molecular and cellular biology. **33**, 937-946

93 Dobrikov, M., Dobrikova, E., Shveygert, M. and Gromeier, M. (2011) Phosphorylation of eukaryotic translation initiation factor 4G1 (eIF4G1) by protein kinase C{alpha} regulates eIF4G1 binding to Mnk1. Molecular and cellular biology. **31**, 2947-2959

94 Shveygert, M., Kaiser, C., Bradrick, S. S. and Gromeier, M. (2010) Regulation of eukaryotic initiation factor 4E (eIF4E) phosphorylation by mitogen-activated protein kinase occurs through modulation of Mnk1-eIF4G interaction. Molecular and cellular biology. **30**, 5160-5167

95 Orton, K. C., Ling, J., Waskiewicz, A. J., Cooper, J. A., Merrick, W. C., Korneeva, N. L., Rhoads, R. E., Sonenberg, N. and Traugh, J. A. (2004) Phosphorylation of Mnk1 by caspase-activated Pak2/gamma-PAK inhibits phosphorylation and interaction of eIF4G with Mnk. J Biol Chem. **279**, 38649-38657

96 Hu, S. I., Katz, M., Chin, S., Qi, X., Cruz, J., Ibebunjo, C., Zhao, S., Chen, A. and Glass, D. J. (2012) MNK2 inhibits eIF4G activation through a pathway involving serine-arginine-rich protein kinase in skeletal muscle. Sci Signal. **5**, ra14

97 Palanisamy, V., Jakymiw, A., Van Tubergen, E. A., D'Silva, N. J. and Kirkwood, K. L. (2012) Control of cytokine mRNA expression by RNA-binding proteins and microRNAs. J Dent Res. **91**, 651-658

98 Chrestensen, C. A., Schroeder, M. J., Shabanowitz, J., Hunt, D. F., Pelo, J. W., Worthington, M. T. and Sturgill, T. W. (2004) MAPKAP kinase 2 phosphorylates tristetraprolin on in vivo sites including Ser178, a site required for 14-3-3 binding. J Biol Chem. **279**, 10176-10184

99 Tran, H., Maurer, F. and Nagamine, Y. (2003) Stabilization of urokinase and urokinase receptor mRNAs by HuR is linked to its cytoplasmic accumulation induced by activated mitogen-activated protein kinase-activated protein kinase 2. Molecular and cellular biology. **23**, 7177-7188

100 Rousseau, S., Morrice, N., Peggie, M., Campbell, D. G., Gaestel, M. and Cohen, P. (2002) Inhibition of SAPK2a/p38 prevents hnRNP A0 phosphorylation by MAPKAP-K2 and its interaction with cytokine mRNAs. The EMBO journal. **21**, 6505-6514

101 Shav-Tal, Y. and Zipori, D. (2002) PSF and p54(nrb)/NonO--multi-functional nuclear proteins. FEBS Lett. **531**, 109-114

102 Spruill, L. S. and McDermott, P. J. (2006) Regulation of c-jun mRNA expression in adult cardiocytes by MAP kinase interacting kinase-1 (MNK1). FASEB J. **20**, 2133-2135

103 Fiorini, M., Alimandi, M., Fiorentino, L., Sala, G. and Segatto, O. (2001) Negative regulation of receptor tyrosine kinase signals. FEBS Lett. **490**, 132-141

104 Mason, J. M., Morrison, D. J., Basson, M. A. and Licht, J. D. (2006) Sprouty proteins: multifaceted negative-feedback regulators of receptor tyrosine kinase signaling. Trends Cell Biol. **16**, 45-54

105 Edwin, F., Anderson, K. and Patel, T. B. (2010) HECT domain-containing E3 ubiquitin ligase Nedd4 interacts with and ubiquitinates Sprouty2. J Biol Chem. **285**, 255-264

106 Aicher, B., Coulter, T. S., Jaekel, S., Kelter, A., Murfin, S., Reuter, T. and S., T. (2007) Thienopyrimidines Having MnkL/Mnk2 Inhibiting Activity for the Pharmaceutical Compositions In Patent Cooperation Treaty (Organization, W. I. P.)

107 Guyton, A. C. and Hall, J. E. (2006) Medical Physiology. pp. 808-815, 829-851 859-874, 881-887, 961-976, Elsevier Saunders

108 Wright, E. M., Loo, D. D., Panayotova-Heiermann, M., Lostao, M. P., Hirayama, B. H., Mackenzie, B., Boorer, K. and Zampighi, G. (1994) 'Active' sugar transport in eukaryotes. J Exp Biol. **196**, 197-212

109 Bell, G. I., Kayano, T., Buse, J. B., Burant, C. F., Takeda, J., Lin, D., Fukumoto, H. and Seino, S. (1990) Molecular biology of mammalian glucose transporters. Diabetes Care. **13**, 198-208

110 Kellett, G. L., Brot-Laroche, E., Mace, O. J. and Leturque, A. (2008) Sugar absorption in the intestine: the role of GLUT2. Annu Rev Nutr. **28**, 35-54

111 Carruthers, A., DeZutter, J., Ganguly, A. and Devaskar, S. U. (2009) Will the original glucose transporter isoform please stand up! Am J Physiol Endocrinol Metab. **297**, E836-848

112 Mueckler, M. (1994) Facilitative glucose transporters. European journal of biochemistry / FEBS. **219**, 713-725

113 Hebert, D. N. and Carruthers, A. (1992) Glucose transporter oligomeric structure determines transporter function. Reversible redox-dependent interconversions of tetrameric and dimeric GLUT1. J Biol Chem. **267**, 23829-23838

114 Berg, J. M., Tymoczko, J. L. and Stryer, L. (2002) Biochemistry. pp. 1249-1274, W.H. Freeman

115 Philp, A., Hargreaves, M. and Baar, K. (2012) More than a store: regulatory roles for glycogen in skeletal muscle adaptation to exercise. Am J Physiol Endocrinol Metab. **302**, E1343-1351

116 Gerich, J. E., Meyer, C., Woerle, H. J. and Stumvoll, M. (2001) Renal gluconeogenesis: its importance in human glucose homeostasis. Diabetes Care. **24**, 382-391

117 Mithieux, G. (2005) The new functions of the gut in the control of glucose homeostasis. Curr Opin Clin Nutr Metab Care. **8**, 445-449

118 Watford, M. (2005) Is the small intestine a gluconeogenic organ. Nutr Rev. **63**, 356-360

119 Mitrakou, A. (2011) Kidney: its impact on glucose homeostasis and hormonal regulation. Diabetes Res Clin Pract. **93 Suppl 1**, S66-72

120 Tirosh, A., Shai, I., Tekes-Manova, D., Israeli, E., Pereg, D., Shochat, T., Kochba, I. and Rudich, A. (2005) Normal fasting plasma glucose levels and type 2 diabetes in young men. N Engl J Med. **353**, 1454-1462

121 Thorens, B. (2008) Glucose sensing and the pathogenesis of obesity and type 2 diabetes. Int J Obes (Lond). **32 Suppl 6**, S62-71

122 Schuit, F. C., Huypens, P., Heimberg, H. and Pipeleers, D. G. (2001) Glucose sensing in pancreatic beta-cells: a model for the study of other glucose-regulated cells in gut, pancreas, and hypothalamus. Diabetes. **50**, 1-11

123 Radziuk, J. and Pye, S. (2001) Hepatic glucose uptake, gluconeogenesis and the regulation of glycogen synthesis. Diabetes Metab Res Rev. **17**, 250-272

124 Roach, P. J., Depaoli-Roach, A. A., Hurley, T. D. and Tagliabracci, V. S. (2012) Glycogen and its metabolism: some new developments and old themes. The Biochemical journal. **441**, 763-787

125 Bouskila, M., Hirshman, M. F., Jensen, J., Goodyear, L. J. and Sakamoto, K. (2008) Insulin promotes glycogen synthesis in the absence of GSK3 phosphorylation in skeletal muscle. Am J Physiol Endocrinol Metab. **294**, E28-35

126 Ivy, J. L. and Kuo, C. H. (1998) Regulation of GLUT4 protein and glycogen synthase during muscle glycogen synthesis after exercise. Acta Physiol Scand. **162**, 295-304

127 Froissart, R., Piraud, M., Boudjemline, A. M., Vianey-Saban, C., Petit, F., Hubert-Buron, A., Eberschweiler, P. T., Gajdos, V. and Labrune, P. (2011) Glucose-6-phosphatase deficiency. Orphanet J Rare Dis. **6**, 27

128 Virtanen, K. A., Lonnroth, P., Parkkola, R., Peltoniemi, P., Asola, M., Viljanen, T., Tolvanen, T., Knuuti, J., Ronnemaa, T., Huupponen, R. and Nuutila, P. (2002) Glucose uptake and perfusion in subcutaneous and visceral adipose tissue during insulin stimulation in nonobese and obese humans. J Clin Endocrinol Metab. **87**, 3902-3910

129 World Health Organization (2006) Definition and Diagnosis of Diabetes Mellitus and Intermediate Hyperglycemia. WHO Press http://www.who.int/diabetes/publications/diagnosis_diabetes2006/en/index.html

130 Diabetes, U.K. (2010) Diabetes in the UK 2010: Key statistics on diabetes. Diabetes UK http://www.diabetes.org.uk/Documents/Reports/Diabetes_in_the_UK_2010.pdf

131 Currie, C. J., Peters, J. R. and Evans, M. (2010) Dispensing patterns and financial costs of glucose-lowering therapies in the UK from 2000 to 2008. Diabet Med. **27**, 744-752

132 Nicholson, G. and Hall, G. M. (2011) Diabetes mellitus: new drugs for a new epidemic. Br J Anaesth. **107**, 65-73

133 Bailey, C. J. (2007) Treating insulin resistance: future prospects. Diab Vasc Dis Res. **4**, 20-31

134 Golay, A. and Ybarra, J. (2005) Link between obesity and type 2 diabetes. Best Pract Res Clin Endocrinol Metab. **19**, 649-663

135 MHRA. (2010) Rosiglitazone (Avandia) Questions and Answers for Patients September 2010. http://www.mhra.gov.uk/home/groups/pl-p/documents/websiteresources/con093790.pdf

136 Ali, S. and Fonseca, V. (2012) Overview of metformin: special focus on metformin extended release. Expert Opin Pharmacother. **13**, 1797-1805

137 Zechner, R., Zimmermann, R., Eichmann, T. O., Kohlwein, S. D., Haemmerle, G., Lass, A. and Madeo, F. (2012) FAT SIGNALS--lipases and lipolysis in lipid metabolism and signaling. Cell Metab. **15**, 279-291

138 Wakil, S. J. and Abu-Elheiga, L. A. (2009) Fatty acid metabolism: target for metabolic syndrome. J Lipid Res. **50 Suppl**, S138-143

139 Potapova, I. A., El-Maghrabi, M. R., Doronin, S. V. and Benjamin, W. B. (2000) Phosphorylation of recombinant human ATP:citrate lyase by cAMP-dependent protein kinase abolishes homotropic allosteric regulation of the enzyme by citrate and increases the enzyme activity. Allosteric activation of ATP:citrate lyase by phosphorylated sugars. Biochemistry. **39**, 1169-1179

140 Berwick, D. C., Hers, I., Heesom, K. J., Moule, S. K. and Tavare, J. M. (2002) The identification of ATP-citrate lyase as a protein kinase B (Akt) substrate in primary adipocytes. J Biol Chem. **277**, 33895-33900

141 Ye, J. and DeBose-Boyd, R. A. (2011) Regulation of cholesterol and fatty acid synthesis. Cold Spring Harb Perspect Biol. **3**

142 Chakrabarti, P., English, T., Karki, S., Qiang, L., Tao, R., Kim, J., Luo, Z., Farmer, S. R. and Kandror, K. V. (2011) SIRT1 controls lipolysis in adipocytes via FOXO1-mediated expression of ATGL. J Lipid Res. **52**, 1693-1701

143 Bassendine, M. F., Sheridan, D. A., Felmlee, D. J., Bridge, S. H., Toms, G. L. and Neely, R. D. (2011) HCV and the hepatic lipid pathway as a potential treatment target. J Hepatol. **55**, 1428-1440

144 Jones, A. L., Hradek, G. T., Hornick, C., Renaud, G., Windler, E. E. and Havel, R. J. (1984) Uptake and processing of remnants of chylomicrons and very low density lipoproteins by rat liver. J Lipid Res. **25**, 1151-1158

145 Minokoshi, Y., Kim, Y. B., Peroni, O. D., Fryer, L. G., Muller, C., Carling, D. and Kahn, B. B. (2002) Leptin stimulates fatty-acid oxidation by activating AMP-activated protein kinase. Nature. **415**, 339-343

146 Bingham, T. C., Parathath, S., Tian, H., Reiss, A., Chan, E., Fisher, E. A. and Cronstein, B. N. (2012) Cholesterol 27-hydroxylase but not apolipoprotein apoE contributes to A2A adenosine receptor stimulated reverse cholesterol transport. Inflammation. **35**, 49-57

147 Seufert, J. (2004) Leptin effects on pancreatic beta-cell gene expression and function. Diabetes. **53 Suppl 1**, S152-158

148 Kadowaki, T., Yamauchi, T., Waki, H., Iwabu, M., Okada-Iwabu, M. and Nakamura, M. (2011) Adiponectin, adiponectin receptors, and epigenetic regulation of adipogenesis. Cold Spring Harb Symp Quant Biol. **76**, 257-265

149 Gibbons, G. F., Wiggins, D., Brown, A. M. and Hebbachi, A. M. (2004) Synthesis and function of hepatic very-low-density lipoprotein. Biochemical Society transactions. **32**, 59-64

150 Fisher, E. A., Feig, J. E., Hewing, B., Hazen, S. L. and Smith, J. D. (2012) High-density lipoprotein function, dysfunction, and reverse cholesterol transport. Arterioscler Thromb Vasc Biol. **32**, 2813-2820

151 Xiao, C., Hsieh, J., Adeli, K. and Lewis, G. F. (2011) Gut-liver interaction in triglyceride-rich lipoprotein metabolism. Am J Physiol Endocrinol Metab. **301**, E429-446

152 Rayner, D. V. and Trayhurn, P. (2001) Regulation of leptin production: sympathetic nervous system interactions. J Mol Med (Berl). **79**, 8-20

153 Galic, S., Oakhill, J. S. and Steinberg, G. R. (2010) Adipose tissue as an endocrine organ. Mol Cell Endocrinol. **316**, 129-139

154 Phillips, S. A. and Kung, J. T. (2010) Mechanisms of adiponectin regulation and use as a pharmacological target. Curr Opin Pharmacol. **10**, 676-683

155 Turer, A. T. and Scherer, P. E. (2012) Adiponectin: mechanistic insights and clinical implications. Diabetologia. **55**, 2319-2326

156 Diez, J. J. and Iglesias, P. (2003) The role of the novel adipocyte-derived hormone adiponectin in human disease. Eur J Endocrinol. **148**, 293-300

157 Harwood, H. J., Jr. (2012) The adipocyte as an endocrine organ in the regulation of metabolic homeostasis. Neuropharmacology. **63**, 57-75

158 Steppan, C. M., Bailey, S. T., Bhat, S., Brown, E. J., Banerjee, R. R., Wright, C. M., Patel, H. R., Ahima, R. S. and Lazar, M. A. (2001) The hormone resistin links obesity to diabetes. Nature. **409**, 307-312

159 Fukuhara, A., Matsuda, M., Nishizawa, M., Segawa, K., Tanaka, M., Kishimoto, K., Matsuki, Y., Murakami, M., Ichisaka, T., Murakami, H., Watanabe, E., Takagi, T., Akiyoshi, M., Ohtsubo, T., Kihara, S., Yamashita, S., Makishima, M., Funahashi, T., Yamanaka, S., Hiramatsu, R., Matsuzawa, Y. and Shimomura, I. (2005) Visfatin: a protein secreted by visceral fat that mimics the effects of insulin. Science. **307**, 426-430

160 Stofkova, A. (2010) Resistin and visfatin: regulators of insulin sensitivity, inflammation and immunity. Endocr Regul. **44**, 25-36

161 Kim, K. H., Lee, K., Moon, Y. S. and Sul, H. S. (2001) A cysteine-rich adipose tissue-specific secretory factor inhibits adipocyte differentiation. J Biol Chem. **276**, 11252-11256

162 Liu, F., Fan, H. Q., Qiu, J., Wang, B., Zhang, M., Gu, N., Zhang, C. M., Fei, L., Pan, X. Q., Guo, M., Chen, R. H. and Guo, X. R. (2008) A paradox: insulin inhibits expression and secretion of resistin which induces insulin resistance. World J Gastroenterol. **14**, 95-100

163 Fukuhara, A., Matsuda, M., Nishizawa, M., Segawa, K., Tanaka, M., Kishimoto, K., Matsuki, Y., Murakami, M., Ichisaka, T., Murakami, H., Watanabe, E., Takagi, T., Akiyoshi, M., Ohtsubo, T., Kihara, S., Yamashita, S., Makishima, M., Funahashi, T., Yamanaka, S., Hiramatsu, R., Matsuzawa, Y. and Shimomura, I. (2007) Retraction. Science. **318**, 565

164 Chang, Y. H., Chang, D. M., Lin, K. C., Shin, S. J. and Lee, Y. J. (2011) Visfatin in overweight/obesity, type 2 diabetes mellitus, insulin resistance, metabolic syndrome and cardiovascular diseases: a meta-analysis and systemic review. Diabetes Metab Res Rev. **27**, 515-527

165 Imai, S. (2011) Dissecting systemic control of metabolism and aging in the NAD World: the importance of SIRT1 and NAMPT-mediated NAD biosynthesis. FEBS Lett. **585**, 1657-1662

166 Coppack, S. W. (2001) Pro-inflammatory cytokines and adipose tissue. Proc Nutr Soc. **60**, 349-356

167 Sewter, C. P., Digby, J. E., Blows, F., Prins, J. and O'Rahilly, S. (1999) Regulation of tumour necrosis factor-alpha release from human adipose tissue in vitro. J Endocrinol. **163**, 33-38

168 Department of Health (2013) Reducing Obesity and Improving Diet. www.gov.uk/government/policies/reducing-obesity-and-improving-diet

169 Haslam, D. W. and James, W. P. (2005) Obesity. Lancet. **366**, 1197-1209

170 Grundy, S. M., Brewer, H. B., Jr., Cleeman, J. I., Smith, S. C., Jr. and Lenfant, C. (2004) Definition of metabolic syndrome: Report of the National Heart, Lung, and Blood Institute/American Heart Association conference on scientific issues related to definition. Circulation. **109**, 433-438

171 Marantz, P. R., Bird, E. D. and Alderman, M. H. (2008) A call for higher standards of evidence for dietary guidelines. Am J Prev Med. **34**, 234-240

172 Bleich, S., Cutler, D., Murray, C. and Adams, A. (2008) Why is the developed world obese? Annu Rev Public Health. **29**, 273-295

173 Tchernof, A. and Despres, J. P. (2013) Pathophysiology of human visceral obesity: an update. Physiol Rev. **93**, 359-404

174 Marques, B. G., Hausman, D. B. and Martin, R. J. (1998) Association of fat cell size and paracrine growth factors in development of hyperplastic obesity. Am J Physiol. **275**, R1898-1908

175 Item, F. and Konrad, D. (2012) Visceral fat and metabolic inflammation: the portal theory revisited. Obes Rev. **13 Suppl 2**, 30-39

176 Harford, K. A., Reynolds, C. M., McGillicuddy, F. C. and Roche, H. M. (2011) Fats, inflammation and insulin resistance: insights to the role of macrophage and T-cell accumulation in adipose tissue. Proc Nutr Soc. **70**, 408-417

177 Johnson, A. R., Milner, J. J. and Makowski, L. (2012) The inflammation highway: metabolism accelerates inflammatory traffic in obesity. Immunol Rev. **249**, 218-238

178 Zhao, Y. F., Feng, D. D. and Chen, C. (2006) Contribution of adipocyte-derived factors to beta-cell dysfunction in diabetes. Int J Biochem Cell Biol. **38**, 804-819

179 Ouchi, N., Parker, J. L., Lugus, J. J. and Walsh, K. (2011) Adipokines in inflammation and metabolic disease. Nat Rev Immunol. **11**, 85-97

180 Fausto, N. (2005) Tweaking liver progenitor cells. Nat Med. **11**, 1053-1054

181 Hotamisligil, G. S. (2006) Inflammation and metabolic disorders. Nature. **444**, 860-867

182 Feuerer, M., Herrero, L., Cipolletta, D., Naaz, A., Wong, J., Nayer, A., Lee, J., Goldfine, A. B., Benoist, C., Shoelson, S. and Mathis, D. (2009) Lean, but not obese, fat is enriched for a unique population of regulatory T cells that affect metabolic parameters. Nat Med. **15**, 930-939

183 Duffaut, C., Galitzky, J., Lafontan, M. and Bouloumie, A. (2009) Unexpected trafficking of immune cells within the adipose tissue during the onset of obesity. Biochem Biophys Res Commun. **384**, 482-485

184 Lumeng, C. N. and Saltiel, A. R. (2011) Inflammatory links between obesity and metabolic disease. J Clin Invest. **121**, 2111-2117

185 Kahn, B. B. and Flier, J. S. (2000) Obesity and insulin resistance. J Clin Invest. **106**, 473-481

186 Shoelson, S. E., Herrero, L. and Naaz, A. (2007) Obesity, inflammation, and insulin resistance. Gastroenterology. **132**, 2169-2180

187 Steinberg, G. R., Michell, B. J., van Denderen, B. J., Watt, M. J., Carey, A. L., Fam, B. C., Andrikopoulos, S., Proietto, J., Gorgun, C. Z., Carling, D., Hotamisligil, G. S., Febbraio, M. A., Kay, T. W. and Kemp, B. E. (2006) Tumor necrosis factor alpha-induced skeletal muscle insulin resistance involves suppression of AMP-kinase signaling. Cell Metab. **4**, 465-474

188 Nieto-Vazquez, I., Fernandez-Veledo, S., Kramer, D. K., Vila-Bedmar, R., Garcia-Guerra, L. and Lorenzo, M. (2008) Insulin resistance associated to obesity: the link TNF-alpha. Arch Physiol Biochem. **114**, 183-194

189 Marra, F. and Bertolani, C. (2009) Adipokines in liver diseases. Hepatology. **50**, 957-969

190 Myers, M. G., Cowley, M. A. and Munzberg, H. (2008) Mechanisms of leptin action and leptin resistance. Annu Rev Physiol. **70**, 537-556

191 Rabe, K., Lehrke, M., Parhofer, K. G. and Broedl, U. C. (2008) Adipokines and insulin resistance. Mol Med. **14**, 741-751

192 Kraegen, E. W. and Cooney, G. J. (2008) Free fatty acids and skeletal muscle insulin resistance. Curr Opin Lipidol. **19**, 235-241

193 Boden, G., She, P., Mozzoli, M., Cheung, P., Gumireddy, K., Reddy, P., Xiang, X., Luo, Z. and Ruderman, N. (2005) Free fatty acids produce insulin resistance and activate the proinflammatory nuclear factor-kappaB pathway in rat liver. Diabetes. **54**, 3458-3465

194 Burks, D. J. and White, M. F. (2001) IRS proteins and beta-cell function. Diabetes. **50 Suppl 1**, S140-145

195 Kharroubi, I., Ladriere, L., Cardozo, A. K., Dogusan, Z., Cnop, M. and Eizirik, D. L. (2004) Free fatty acids and cytokines induce pancreatic beta-cell apoptosis by different mechanisms: role of nuclear factor-kappaB and endoplasmic reticulum stress. Endocrinology. **145**, 5087-5096

196 Saltiel, A. R. and Kahn, C. R. (2001) Insulin signalling and the regulation of glucose and lipid metabolism. Nature. **414**, 799-806

197 Proud, C. G. (2006) Regulation of protein synthesis by insulin. Biochemical Society transactions. **34**, 213-216

198 Boyd, D. B. (2003) Insulin and cancer. Integr Cancer Ther. **2**, 315-329

199 Dunaif, A. (1997) Insulin resistance and the polycystic ovary syndrome: mechanism and implications for pathogenesis. Endocr Rev. **18**, 774-800

200 Ward, C. W. and Lawrence, M. C. (2009) Ligand-induced activation of the insulin receptor: a multi-step process involving structural changes in both the ligand and the receptor. Bioessays. **31**, 422-434

201 Boute, N., Pernet, K. and Issad, T. (2001) Monitoring the activation state of the insulin receptor using bioluminescence resonance energy transfer. Mol Pharmacol. **60**, 640-645

202 Mardilovich, K., Pankratz, S. L. and Shaw, L. M. (2009) Expression and function of the insulin receptor substrate proteins in cancer. Cell Commun Signal. **7**, 14

203 Thirone, A. C., Huang, C. and Klip, A. (2006) Tissue-specific roles of IRS proteins in insulin signaling and glucose transport. Trends Endocrinol Metab. **17**, 72-78

204 Fantin, V. R., Wang, Q., Lienhard, G. E. and Keller, S. R. (2000) Mice lacking insulin receptor substrate 4 exhibit mild defects in growth, reproduction, and glucose homeostasis. Am J Physiol Endocrinol Metab. **278**, E127-133

205 Sun, X. J., Wang, L. M., Zhang, Y., Yenush, L., Myers, M. G., Jr., Glasheen, E., Lane, W. S., Pierce, J. H. and White, M. F. (1995) Role of IRS-2 in insulin and cytokine signalling. Nature. **377**, 173-177

206 Valverde, A. M., Lorenzo, M., Pons, S., White, M. F. and Benito, M. (1998) Insulin receptor substrate (IRS) proteins IRS-1 and IRS-2 differential signaling in the insulin/insulin-like growth factor-I pathways in fetal brown adipocytes. Mol Endocrinol. **12**, 688-697

207 Siddle, K. (2011) Signalling by insulin and IGF receptors: supporting acts and new players. J Mol Endocrinol. **47**, R1-10

208 Inoue, G., Cheatham, B., Emkey, R. and Kahn, C. R. (1998) Dynamics of insulin signaling in 3T3-L1 adipocytes. Differential compartmentalization and trafficking of insulin receptor substrate (IRS)-1 and IRS-2. J Biol Chem. **273**, 11548-11555

209 Asano, T., Fujishiro, M., Kushiyama, A., Nakatsu, Y., Yoneda, M., Kamata, H. and Sakoda, H. (2007) Role of phosphatidylinositol 3-kinase activation on insulin action and its alteration in diabetic conditions. Biol Pharm Bull. **30**, 1610-1616

210 Esposito, D. L., Li, Y., Cama, A. and Quon, M. J. (2001) Tyr(612) and Tyr(632) in human insulin receptor substrate-1 are important for full activation of insulin-stimulated phosphatidylinositol 3-kinase activity and translocation of GLUT4 in adipose cells. Endocrinology. **142**, 2833-2840

211 Mellor, P., Furber, L. A., Nyarko, J. N. and Anderson, D. H. (2012) Multiple roles for the p85alpha isoform in the regulation and function of PI3K signalling and receptor trafficking. The Biochemical journal. **441**, 23-37

212 Cantley, L. C. (2002) The phosphoinositide 3-kinase pathway. Science. **296**, 1655-1657

213 Bayascas, J. R. (2008) Dissecting the role of the 3-phosphoinositide-dependent protein kinase-1 (PDK1) signalling pathways. Cell cycle. **7**, 2978-2982

214 Bozulic, L. and Hemmings, B. A. (2009) PIKKing on PKB: regulation of PKB activity by phosphorylation. Curr Opin Cell Biol. **21**, 256-261

215 Hers, I., Vincent, E. E. and Tavare, J. M. (2011) Akt signalling in health and disease. Cell Signal. **23**, 1515-1527

216 Leto, D. and Saltiel, A. R. (2012) Regulation of glucose transport by insulin: traffic control of GLUT4. Nat Rev Mol Cell Biol. **13**, 383-396

217 Jedrychowski, M. P., Gartner, C. A., Gygi, S. P., Zhou, L., Herz, J., Kandror, K. V. and Pilch, P. F. (2010) Proteomic analysis of GLUT4 storage vesicles reveals LRP1 to be an important vesicle component and target of insulin signaling. J Biol Chem. **285**, 104-114

218 Lodhi, I. J., Chiang, S. H., Chang, L., Vollenweider, D., Watson, R. T., Inoue, M., Pessin, J. E. and Saltiel, A. R. (2007) Gapex-5, a Rab31 guanine nucleotide exchange factor that regulates Glut4 trafficking in adipocytes. Cell Metab. **5**, 59-72

219 Bogan, J. S., Hendon, N., McKee, A. E., Tsao, T. S. and Lodish, H. F. (2003) Functional cloning of TUG as a regulator of GLUT4 glucose transporter trafficking. Nature. **425**, 727-733

220 Sano, H., Kane, S., Sano, E., Miinea, C. P., Asara, J. M., Lane, W. S., Garner, C. W. and Lienhard, G. E. (2003) Insulin-stimulated phosphorylation of a Rab GTPase-activating protein regulates GLUT4 translocation. J Biol Chem. **278**, 14599-14602

221 Zaid, H., Antonescu, C. N., Randhawa, V. K. and Klip, A. (2008) Insulin action on glucose transporters through molecular switches, tracks and tethers. The Biochemical journal. **413**, 201-215

222 Geraghty, K. M., Chen, S., Harthill, J. E., Ibrahim, A. F., Toth, R., Morrice, N. A., Vandermoere, F., Moorhead, G. B., Hardie, D. G. and MacKintosh, C. (2007) Regulation of multisite phosphorylation and 14-3-3 binding of AS160 in response to IGF-1, EGF, PMA and AICAR. The Biochemical journal. **407**, 231-241

223 Huang, J., Imamura, T., Babendure, J. L., Lu, J. C. and Olefsky, J. M. (2005) Disruption of microtubules ablates the specificity of insulin signaling to GLUT4 translocation in 3T3-L1 adipocytes. J Biol Chem. **280**, 42300-42306

224 Inoue, M., Chang, L., Hwang, J., Chiang, S. H. and Saltiel, A. R. (2003) The exocyst complex is required for targeting of Glut4 to the plasma membrane by insulin. Nature. **422**, 629-633

225 Chen, X. W., Leto, D., Xiong, T., Yu, G., Cheng, A., Decker, S. and Saltiel, A. R. (2011) A Ral GAP complex links PI 3-kinase/Akt signaling to RalA activation in insulin action. Mol Biol Cell. **22**, 141-152

226 Chen, X. W., Leto, D., Xiao, J., Goss, J., Wang, Q., Shavit, J. A., Xiong, T., Yu, G., Ginsburg, D., Toomre, D., Xu, Z. and Saltiel, A. R. (2011) Exocyst function is regulated by effector phosphorylation. Nat Cell Biol. **13**, 580-588

227 Jewell, J. L., Oh, E., Ramalingam, L., Kalwat, M. A., Tagliabracci, V. S., Tackett, L., Elmendorf, J. S. and Thurmond, D. C. (2011) Munc18c phosphorylation by the insulin

receptor links cell signaling directly to SNARE exocytosis. The Journal of cell biology. **193**, 185-199

228 Steuernagel, A., Eulenberg, K., Broenner, G., Ciossek, T., Rudolph, B., Rudolph, D., Belgore, F., Jaekel, S. and Christoph., M. (2011) Mnk kinase homologous proteins involved in the regulation of energy homeostasis and organelle metabolism. (Organization, W. I. P.), United States of America

229 Gual, P., Le Marchand-Brustel, Y. and Tanti, J. F. (2005) Positive and negative regulation of insulin signaling through IRS-1 phosphorylation. Biochimie. **87**, 99-109

230 Brooks, R. A. (1977) A quantitative theory of the Hounsfield unit and its application to dual energy scanning. J Comput Assist Tomogr. **1**, 487-493

231 Joshi, B., Cai, A. L., Keiper, B. D., Minich, W. B., Mendez, R., Beach, C. M., Stepinski, J., Stolarski, R., Darzynkiewicz, E. and Rhoads, R. E. (1995) Phosphorylation of eukaryotic protein synthesis initiation factor 4E at Ser-209. J Biol Chem. **270**, 14597-14603

232 Wang, X., Flynn, A., Waskiewicz, A. J., Webb, B. L., Vries, R. G., Baines, I. A., Cooper, J. A. and Proud, C. G. (1998) The phosphorylation of eukaryotic initiation factor eIF4E in response to phorbol esters, cell stresses, and cytokines is mediated by distinct MAP kinase pathways. J Biol Chem. **273**, 9373-9377

233 Graff, J. R., Konicek, B. W., Carter, J. H. and Marcusson, E. G. (2008) Targeting the eukaryotic translation initiation factor 4E for cancer therapy. Cancer Res. **68**, 631-634

234 Ruggero, D., Montanaro, L., Ma, L., Xu, W., Londei, P., Cordon-Cardo, C. and Pandolfi, P. P. (2004) The translation factor eIF-4E promotes tumor formation and cooperates with c-Myc in lymphomagenesis. Nat Med. **10**, 484-486

235 Wendel, H. G., De Stanchina, E., Fridman, J. S., Malina, A., Ray, S., Kogan, S., Cordon-Cardo, C., Pelletier, J. and Lowe, S. W. (2004) Survival signalling by Akt and eIF4E in oncogenesis and cancer therapy. Nature. **428**, 332-337

236 Averous, J. and Proud, C. G. (2006) When translation meets transformation: the mTOR story. Oncogene. **25**, 6423-6435

237 Vezina, C., Kudelski, A. and Sehgal, S. N. (1975) Rapamycin (AY-22,989), a new antifungal antibiotic. I. Taxonomy of the producing streptomycete and isolation of the active principle. J Antibiot (Tokyo). **28**, 721-726

238 Calne, R. Y., Collier, D. S., Lim, S., Pollard, S. G., Samaan, A., White, D. J. and Thiru, S. (1989) Rapamycin for immunosuppression in organ allografting. Lancet. **2**, 227

239 Brown, E. J., Albers, M. W., Shin, T. B., Ichikawa, K., Keith, C. T., Lane, W. S. and Schreiber, S. L. (1994) A mammalian protein targeted by G1-arresting rapamycin-receptor complex. Nature. **369**, 756-758

240 Heitman, J., Movva, N. R. and Hall, M. N. (1991) Targets for cell cycle arrest by the immunosuppressant rapamycin in yeast. Science. **253**, 905-909

241 Thoreen, C. C. and Sabatini, D. M. (2009) Rapamycin inhibits mTORC1, but not completely. Autophagy. **5**, 725-726

242 Huang, J. and Manning, B. D. (2008) The TSC1-TSC2 complex: a molecular switchboard controlling cell growth. The Biochemical journal. **412**, 179-190

243 Proud, C. G. (2007) Signalling to translation: how signal transduction pathways control the protein synthetic machinery. The Biochemical journal. **403**, 217-234

244 Battelli, C. and Cho, D. C. (2011) mTOR inhibitors in renal cell carcinoma. Therapy. **8**, 359-367

245 Feldman, M. E., Apsel, B., Uotila, A., Loewith, R., Knight, Z. A., Ruggero, D. and Shokat, K. M. (2009) Active-site inhibitors of mTOR target rapamycin-resistant outputs of mTORC1 and mTORC2. PLoS Biol. **7**, e38

246 Chresta, C. M., Davies, B. R., Hickson, I., Harding, T., Cosulich, S., Critchlow, S. E., Vincent, J. P., Ellston, R., Jones, D., Sini, P., James, D., Howard, Z., Dudley, P., Hughes, G., Smith, L., Maguire, S., Hummersone, M., Malagu, K., Menear, K., Jenkins, R., Jacobsen, M., Smith, G. C., Guichard, S. and Pass, M. (2010) AZD8055 is a potent, selective, and orally bioavailable ATP-competitive mammalian target of rapamycin kinase inhibitor with in vitro and in vivo antitumor activity. Cancer Res. **70**, 288-298

247 Kaighn, M. E., Narayan, K. S., Ohnuki, Y., Lechner, J. F. and Jones, L. W. (1979) Establishment and characterization of a human prostatic carcinoma cell line (PC-3). Invest Urol. **17**, 16-23

248 Ghosh, A., Wang, X., Klein, E. and Heston, W. D. (2005) Novel role of prostate-specific membrane antigen in suppressing prostate cancer invasiveness. Cancer Res. **65**, 727-731

249 Alimirah, F., Chen, J., Basrawala, Z., Xin, H. and Choubey, D. (2006) DU-145 and PC-3 human prostate cancer cell lines express androgen receptor: implications for the androgen receptor functions and regulation. FEBS Lett. **580**, 2294-2300

250 van Bokhoven, A., Varella-Garcia, M., Korch, C., Johannes, W. U., Smith, E. E., Miller, H. L., Nordeen, S. K., Miller, G. J. and Lucia, M. S. (2003) Molecular characterization of human prostate carcinoma cell lines. Prostate. **57**, 205-225

251 Aghaei, M., Karami-Tehrani, F., Panjehpour, M., Salami, S. and Fallahian, F. (2012) Adenosine induces cell-cycle arrest and apoptosis in androgen-dependent and -independent prostate cancer cell lines, LNcap-FGC-10, DU-145, and PC3. Prostate. **72**, 361-375

252 Tai, S., Sun, Y., Squires, J. M., Zhang, H., Oh, W. K., Liang, C. Z. and Huang, J. (2011) PC3 is a cell line characteristic of prostatic small cell carcinoma. Prostate. **71**, 1668-1679

253 Kochuparambil, S. T., Al-Husein, B., Goc, A., Soliman, S. and Somanath, P. R. (2011) Anticancer efficacy of simvastatin on prostate cancer cells and tumor xenografts is associated with inhibition of Akt and reduced prostate-specific antigen expression. J Pharmacol Exp Ther. **336**, 496-505

254 Vlietstra, R. J., van Alewijk, D. C., Hermans, K. G., van Steenbrugge, G. J. and Trapman, J. (1998) Frequent inactivation of PTEN in prostate cancer cell lines and xenografts. Cancer Res. **58**, 2720-2723

255 Kremer, C. L., Klein, R. R., Mendelson, J., Browne, W., Samadzedeh, L. K., Vanpatten, K., Highstrom, L., Pestano, G. A. and Nagle, R. B. (2006) Expression of mTOR signaling pathway markers in prostate cancer progression. Prostate. **66**, 1203-1212

256 McMenamin, M. E., Soung, P., Perera, S., Kaplan, I., Loda, M. and Sellers, W. R. (1999) Loss of PTEN expression in paraffin-embedded primary prostate cancer correlates with high Gleason score and advanced stage. Cancer Res. **59**, 4291-4296

257 Shukla, S., Maclennan, G. T., Hartman, D. J., Fu, P., Resnick, M. I. and Gupta, S. (2007) Activation of PI3K-Akt signaling pathway promotes prostate cancer cell invasion. Int J Cancer. **121**, 1424-1432

258 Fang, J., Ding, M., Yang, L., Liu, L. Z. and Jiang, B. H. (2007) PI3K/PTEN/AKT signaling regulates prostate tumor angiogenesis. Cell Signal. **19**, 2487-2497

259 Armstrong, A. J., Netto, G. J., Rudek, M. A., Halabi, S., Wood, D. P., Creel, P. A., Mundy, K., Davis, S. L., Wang, T., Albadine, R., Schultz, L., Partin, A. W., Jimeno, A., Fedor, H., Febbo, P. G., George, D. J., Gurganus, R., De Marzo, A. M. and Carducci, M. A. (2010) A pharmacodynamic study of rapamycin in men with intermediate- to high-risk localized prostate cancer. Clin Cancer Res. **16**, 3057-3066

260 Amato, R. J., Jac, J., Mohammad, T. and Saxena, S. (2008) Pilot study of rapamycin in patients with hormone-refractory prostate cancer. Clin Genitourin Cancer. **6**, 97-102

261 Morgan, T. M., Koreckij, T. D. and Corey, E. (2009) Targeted therapy for advanced prostate cancer: inhibition of the PI3K/Akt/mTOR pathway. Curr Cancer Drug Targets. **9**, 237-249

262 Marzec, M., Liu, X., Wysocka, M., Rook, A. H., Odum, N. and Wasik, M. A. (2011) Simultaneous inhibition of mTOR-containing complex 1 (mTORC1) and MNK induces apoptosis of cutaneous T-cell lymphoma (CTCL) cells. PLoS One. **6**, e24849

263 Sun, S. Y., Rosenberg, L. M., Wang, X., Zhou, Z., Yue, P., Fu, H. and Khuri, F. R. (2005) Activation of Akt and eIF4E survival pathways by rapamycin-mediated mammalian target of rapamycin inhibition. Cancer Res. **65**, 7052-7058

264 Zang, C., Eucker, J., Liu, H., Muller, A., Possinger, K. and Scholz, C. W. (2012) Concurrent inhibition of PI3-Kinase and mTOR induces cell death in diffuse large B cell lymphomas, a mechanism involving down regulation of Mcl-1. Cancer Lett

265 Dilling, M. B., Germain, G. S., Dudkin, L., Jayaraman, A. L., Zhang, X., Harwood, F. C. and Houghton, P. J. (2002) 4E-binding proteins, the suppressors of eukaryotic initiation factor 4E, are down-regulated in cells with acquired or intrinsic resistance to rapamycin. J Biol Chem. **277**, 13907-13917

266 O'Reilly, K. E., Rojo, F., She, Q. B., Solit, D., Mills, G. B., Smith, D., Lane, H., Hofmann, F., Hicklin, D. J., Ludwig, D. L., Baselga, J. and Rosen, N. (2006) mTOR inhibition induces upstream receptor tyrosine kinase signaling and activates Akt. Cancer Res. **66**, 1500-1508

267 Brunn, G. J., Williams, J., Sabers, C., Wiederrecht, G., Lawrence, J. C., Jr. and Abraham, R. T. (1996) Direct inhibition of the signaling functions of the mammalian target of rapamycin by the phosphoinositide 3-kinase inhibitors, wortmannin and LY294002. The EMBO journal. **15**, 5256-5267

268 Ballou, L. M., Selinger, E. S., Choi, J. Y., Drueckhammer, D. G. and Lin, R. Z. (2007) Inhibition of mammalian target of rapamycin signaling by 2-(morpholin-1-yl)pyrimido[2,1-alpha]isoquinolin-4-one. J Biol Chem. **282**, 24463-24470

269 Jackson, S. P., Schoenwaelder, S. M., Goncalves, I., Nesbitt, W. S., Yap, C. L., Wright, C. E., Kenche, V., Anderson, K. E., Dopheide, S. M., Yuan, Y., Sturgeon, S. A., Prabaharan, H., Thompson, P. E., Smith, G. D., Shepherd, P. R., Daniele, N., Kulkarni, S., Abbott, B., Saylik, D., Jones, C., Lu, L., Giuliano, S., Hughan, S. C., Angus, J. A., Robertson, A. D. and Salem, H. H. (2005) PI 3-kinase p110beta: a new target for antithrombotic therapy. Nat Med. **11**, 507-514

270 El Haibi, C. P., Sharma, P. K., Singh, R., Johnson, P. R., Suttles, J., Singh, S. and Lillard, J. W., Jr. (2010) PI3Kp110-, Src-, FAK-dependent and DOCK2-independent migration and invasion of CXCL13-stimulated prostate cancer cells. Molecular cancer. **9**, 85

271 Ling, J., Morley, S. J. and Traugh, J. A. (2005) Inhibition of cap-dependent translation via phosphorylation of eIF4G by protein kinase Pak2. The EMBO journal. **24**, 4094-4105

272 von Der Haar, T., Ball, P. D. and McCarthy, J. E. (2000) Stabilization of eukaryotic initiation factor 4E binding to the mRNA 5'-Cap by domains of eIF4G. J Biol Chem. **275**, 30551-30555

273 Chrestensen, C. A., Eschenroeder, A., Ross, W. G., Ueda, T., Watanabe-Fukunaga, R., Fukunaga, R. and Sturgill, T. W. (2007) Loss of MNK function sensitizes fibroblasts to serum-withdrawal induced apoptosis. Genes to Cells. **12**, 1133-1140

274 Shenberger, J. S., Zhang, L., Hughlock, M. K., Ueda, T., Watanabe-Fukunaga, R. and Fukunaga, R. (2007) Roles of mitogen-activated protein kinase signal-integrating kinases 1 and 2 in oxidant-mediated eIF4E phosphorylation. Roles of mitogen-activated protein kinase signal-integrating kinases 1 and 2 in oxidant-mediated eIF4E phosphorylation. **39**, 1828-1842

275 Polak, P. and Hall, M. N. (2006) mTORC2 Caught in a SINful Akt. Dev Cell. **11**, 433-434

276 Hay, N. (2010) Mnk earmarks eIF4E for cancer therapy. Proc Natl Acad Sci U S A. **107**, 13975-13976

277 Fan, S., Ramalingam, S. S., Kauh, J., Xu, Z., Khuri, F. R. and Sun, S. Y. (2009) Phosphorylated eukaryotic translation initiation factor 4 (eIF4E) is elevated in human cancer tissues. Cancer Biol Ther. **8**, 1463-1469

278 Chrestensen, C. A., Eschenroeder, A., Ross, W. G., Ueda, T., Watanabe-Fukunaga, R., Fukunaga, R. and Sturgill, T. W. (2007) Loss of MNK function sensitizes fibroblasts to serum-withdrawal induced apoptosis. Genes Cells. **12**, 1133-1140

279 Muta, D., Makino, K., Nakamura, H., Yano, S., Kudo, M. and Kuratsu, J. (2011) Inhibition of eIF4E phosphorylation reduces cell growth and proliferation in primary central nervous system lymphoma cells. J Neurooncol. **101**, 33-39

280 Andersson, K. and Sundler, R. (2006) Posttranscriptional regulation of TNFalpha expression via eukaryotic initiation factor 4E (eIF4E) phosphorylation in mouse macrophages. Cytokine. **33**, 52-57

281 Gorentla, B. K., Krishna, S., Shin, J., Inoue, M., Shinohara, M. L., Grayson, J. M., Fukunaga, R. and Zhong, X. P. (2013) Mnk1 and 2 are dispensable for T cell development and activation but important for the pathogenesis of experimental autoimmune encephalomyelitis. J Immunol. **190**, 1026-1037

282 Joshi, S., Sharma, B., Kaur, S., Majchrzak, B., Ueda, T., Fukunaga, R., Verma, A. K., Fish, E. N. and Platanias, L. C. (2011) Essential role for Mnk kinases in type II interferon (IFNgamma) signaling and its suppressive effects on normal hematopoiesis. J Biol Chem. **286**, 6017-6026

283 Nikolcheva, T., Pyronnet, S., Chou, S. Y., Sonenberg, N., Song, A., Clayberger, C. and Krensky, A. M. (2002) A translational rheostat for RFLAT-1 regulates RANTES expression in T lymphocytes. J Clin Invest. **110**, 119-126

284 Cohen, D. (2010) Rosiglitazone: what went wrong? BMJ. **341**, c4848

285 Hernandez, R., Teruel, T. and Lorenzo, M. (2001) Akt mediates insulin induction of glucose uptake and up-regulation of GLUT4 gene expression in brown adipocytes. FEBS Lett. **494**, 225-231

286 Vincent, E. E., Elder, D. J., Thomas, E. C., Phillips, L., Morgan, C., Pawade, J., Sohail, M., May, M. T., Hetzel, M. R. and Tavare, J. M. (2011) Akt phosphorylation on Thr308 but not on Ser473 correlates with Akt protein kinase activity in human non-small cell lung cancer. Br J Cancer, 1755-1761

287 Dan, H. C., Sun, M., Yang, L., Feldman, R. I., Sui, X. M., Ou, C. C., Nellist, M., Yeung, R. S., Halley, D. J., Nicosia, S. V., Pledger, W. J. and Cheng, J. Q. (2002) Phosphatidylinositol 3-kinase/Akt pathway regulates tuberous sclerosis tumor suppressor complex by phosphorylation of tuberin. J Biol Chem. **277**, 35364-35370

288 Manning, B. D., Tee, A. R., Logsdon, M. N., Blenis, J. and Cantley, L. C. (2002) Identification of the tuberous sclerosis complex-2 tumor suppressor gene product tuberin as a target of the phosphoinositide 3-kinase/akt pathway. Mol Cell. **10**, 151-162

289 Nascimento, E. B., Snel, M., Guigas, B., van der Zon, G. C., Kriek, J., Maassen, J. A., Jazet, I. M., Diamant, M. and Ouwens, D. M. (2010) Phosphorylation of PRAS40 on Thr246 by PKB/AKT facilitates efficient phosphorylation of Ser183 by mTORC1. Cell Signal. **22**, 961-967

290 Gingras, A. C., Gygi, S. P., Raught, B., Polakiewicz, R. D., Abraham, R. T., Hoekstra, M. F., Aebersold, R. and Sonenberg, N. (1999) Regulation of 4E-BP1 phosphorylation: a novel two-step mechanism. Genes Dev. **13**, 1422-1437

291 Gout, I., Minami, T., Hara, K., Tsujishita, Y., Filonenko, V., Waterfield, M. D. and Yonezawa, K. (1998) Molecular cloning and characterization of a novel p70 S6 kinase, p70 S6 kinase beta containing a proline-rich region. J Biol Chem. **273**, 30061-30064

292 Brewer, P. D., Romenskaia, I., Kanow, M. A. and Mastick, C. C. (2011) Loss of AS160 Akt Substrate Causes Glut4 Protein to Accumulate in Compartments That Are Primed for Fusion in Basal Adipocytes. Journal of Biological Chemistry. **286**, 26287-26297

293 Blot, V. and McGraw, T. E. (2008) Use of quantitative immunofluorescence microscopy to study intracellular trafficking: studies of the GLUT4 glucose transporter. Methods Mol Biol. **457**, 347-366

294 Blot, V. and McGraw, T. E. (2008) Molecular mechanisms controlling GLUT4 intracellular retention. Mol Biol Cell. **19**, 3477-3487

295 Bain, J., Plater, L., Elliott, M., Shpiro, N., Hastie, C. J., McLauchlan, H., Klevernic, I., Arthur, J. S., Alessi, D. R. and Cohen, P. (2007) The selectivity of protein kinase inhibitors: a further update. The Biochemical journal. **408**, 297-315

296 Sun, X. J., Goldberg, J. L., Qiao, L. Y. and Mitchell, J. J. (1999) Insulin-induced insulin receptor substrate-1 degradation is mediated by the proteasome degradation pathway. Diabetes. **48**, 1359-1364

297 Greene, M. W., Morrice, N., Garofalo, R. S. and Roth, R. A. (2004) Modulation of human insulin receptor substrate-1 tyrosine phosphorylation by protein kinase Cdelta. The Biochemical journal. **378**, 105-116

298 Luo, M., Langlais, P., Yi, Z., Lefort, N., De Filippis, E. A., Hwang, H., Christ-Roberts, C. Y. and Mandarino, L. J. (2007) Phosphorylation of human insulin receptor substrate-1 at Serine 629 plays a positive role in insulin signaling. Endocrinology. **148**, 4895-4905

299 Boura-Halfon, S. and Zick, Y. (2009) Serine kinases of insulin receptor substrate proteins. Vitam Horm. **80**, 313-349

300 Weigert, C., Kron, M., Kalbacher, H., Pohl, A. K., Runge, H., Haring, H. U., Schleicher, E. and Lehmann, R. (2008) Interplay and effects of temporal changes in the phosphorylation state of serine-302, -307, and -318 of insulin receptor substrate-1 on insulin action in skeletal muscle cells. Mol Endocrinol. **22**, 2729-2740

301 Balasubramanyam, M., Sampathkumar, R. and Mohan, V. (2005) Is insulin signaling molecules misguided in diabetes for ubiquitin-proteasome mediated degradation? Mol Cell Biochem. **275**, 117-125

302 Ueki, K., Kondo, T. and Kahn, C. R. (2004) Suppressor of cytokine signaling 1 (SOCS-1) and SOCS-3 cause insulin resistance through inhibition of tyrosine phosphorylation of insulin receptor substrate proteins by discrete mechanisms. Molecular and cellular biology. **24**, 5434-5446

303 Rui, L., Yuan, M., Frantz, D., Shoelson, S. and White, M. F. (2002) SOCS-1 and SOCS-3 block insulin signaling by ubiquitin-mediated degradation of IRS1 and IRS2. J Biol Chem. **277**, 42394-42398

304 Pederson, T. M., Kramer, D. L. and Rondinone, C. M. (2001) Serine/threonine phosphorylation of IRS-1 triggers its degradation: possible regulation by tyrosine phosphorylation. Diabetes. **50**, 24-31

305 Xu, X., Keshwani, M., Meyer, K., Sarikas, A., Taylor, S. and Pan, Z. Q. (2012) Identification of the degradation determinants of insulin receptor substrate 1 for signaling cullin-RING E3 ubiquitin ligase 7-mediated ubiquitination. J Biol Chem. **287**, 40758-40766

306 Wang, Y., Nishina, P. M. and Naggert, J. K. (2009) Degradation of IRS1 leads to impaired glucose uptake in adipose tissue of the type 2 diabetes mouse model TALLYHO/Jng. J Endocrinol. **203**, 65-74

307 Capecchi, M. R. (2001) Generating mice with targeted mutations. Nat Med. **7**, 1086-1090

308 Zuidema, G. D. (1997) The John Hopkins Atlas of Human Functional Anatomy. p. 137, The John Hopkins University Press

309 Morino, K., Neschen, S., Bilz, S., Sono, S., Tsirigotis, D., Reznick, R. M., Moore, I., Nagai, Y., Samuel, V., Sebastian, D., White, M., Philbrick, W. and Shulman, G. I. (2008) Muscle-specific IRS-1 Ser->Ala transgenic mice are protected from fat-induced insulin resistance in skeletal muscle. Diabetes. **57**, 2644-2651

310 Yaspelkis, B. B., 3rd, Kvasha, I. A. and Figueroa, T. Y. (2009) High-fat feeding increases insulin receptor and IRS-1 coimmunoprecipitation with SOCS-3, IKKalpha/beta phosphorylation and decreases PI-3 kinase activity in muscle. Am J Physiol Regul Integr Comp Physiol. **296**, R1709-1715

311 MacLaren, R., Cui, W., Simard, S. and Cianflone, K. (2008) Influence of obesity and insulin sensitivity on insulin signaling genes in human omental and subcutaneous adipose tissue. J Lipid Res. **49**, 308-323

312 St-Onge, M. P., Wang, J., Shen, W., Wang, Z., Allison, D. B., Heshka, S., Pierson, R. N., Jr. and Heymsfield, S. B. (2004) Dual-energy x-ray absorptiometry-measured lean soft tissue mass: differing relation to body cell mass across the adult life span. J Gerontol A Biol Sci Med Sci. **59**, 796-800

313 Nedergaard, J., Bengtsson, T. and Cannon, B. (2007) Unexpected evidence for active brown adipose tissue in adult humans. Am J Physiol Endocrinol Metab. **293**, E444-452

314 Casteilla, L., Penicaud, L., Cousin, B. and Calise, D. (2008) Choosing an adipose tissue depot for sampling: factors in selection and depot specificity. Methods Mol Biol. **456**, 23-38

315 Kajimura, S., Seale, P., Kubota, K., Lunsford, E., Frangioni, J. V., Gygi, S. P. and Spiegelman, B. M. (2009) Initiation of myoblast to brown fat switch by a PRDM16-C/EBP-beta transcriptional complex. Nature. **460**, 1154-1158

316 Zimmerman, A. W. and Veerkamp, J. H. (2002) New insights into the structure and function of fatty acid-binding proteins. Cell Mol Life Sci. **59**, 1096-1116

317 Hertzel, A. V., Smith, L. A., Berg, A. H., Cline, G. W., Shulman, G. I., Scherer, P. E. and Bernlohr, D. A. (2006) Lipid metabolism and adipokine levels in fatty acid-binding protein null and transgenic mice. Am J Physiol Endocrinol Metab. **290**, E814-823

318 Cabre, A., Lazaro, I., Girona, J., Manzanares, J. M., Marimon, F., Plana, N., Heras, M. and Masana, L. (2008) Plasma fatty acid binding protein 4 is associated with atherogenic dyslipidemia in diabetes. J Lipid Res. **49**, 1746-1751

319 Gao, J., Katagiri, H., Ishigaki, Y., Yamada, T., Ogihara, T., Imai, J., Uno, K., Hasegawa, Y., Kanzaki, M., Yamamoto, T. T., Ishibashi, S. and Oka, Y. (2007) Involvement of apolipoprotein E in excess fat accumulation and insulin resistance. Diabetes. **56**, 24-33

320 Huang, Z. H., Gu, D. and Mazzone, T. (2009) Role of adipocyte-derived apoE in modulating adipocyte size, lipid metabolism, and gene expression in vivo. Am J Physiol Endocrinol Metab. **296**, E1110-1119

321 Swierczynski, J., Goyke, E., Wach, L., Pankiewicz, A., Kochan, Z., Adamonis, W., Sledzinski, Z. and Aleksandrowicz, Z. (2000) Comparative study of the lipogenic potential of human and rat adipose tissue. Metabolism. **49**, 594-599

322 Petersen, P. S., Jin, C., Madsen, A. N., Rasmussen, M., Kuhre, R., Egerod, K. L., Nielsen, L. B., Schwartz, T. W. and Holst, B. (2011) Deficiency of the GPR39 receptor is associated with obesity and altered adipocyte metabolism. FASEB J. **25**, 3803-3814

323 Fromme, T. and Klingenspor, M. (2011) Uncoupling protein 1 expression and high-fat diets. Am J Physiol Regul Integr Comp Physiol. **300**, R1-8

324 Liu, X., Rossmeisl, M., McClaine, J., Riachi, M., Harper, M. E. and Kozak, L. P. (2003) Paradoxical resistance to diet-induced obesity in UCP1-deficient mice. J Clin Invest. **111**, 399-407

325 Kozak, L. P. and Anunciado-Koza, R. (2008) UCP1: its involvement and utility in obesity. Int J Obes (Lond). **32 Suppl 7**, S32-38

326 Anunciado-Koza, R., Ukropec, J., Koza, R. A. and Kozak, L. P. (2008) Inactivation of UCP1 and the glycerol phosphate cycle synergistically increases energy expenditure to resist diet-induced obesity. J Biol Chem. **283**, 27688-27697

327 Bostrom, P., Wu, J., Jedrychowski, M. P., Korde, A., Ye, L., Lo, J. C., Rasbach, K. A., Bostrom, E. A., Choi, J. H., Long, J. Z., Kajimura, S., Zingaretti, M. C., Vind, B. F., Tu, H., Cinti, S., Hojlund, K., Gygi, S. P. and Spiegelman, B. M. (2012) A PGC1-alpha-dependent myokine that drives brown-fat-like development of white fat and thermogenesis. Nature. **481**, 463-468

328 Ding, Y. L., Wang, Y. H., Huang, W., Liu, G., Ross, C., Hayden, M. R. and Yang, J. K. (2010) Glucose intolerance and decreased early insulin response in mice with severe hypertriglyceridemia. Exp Biol Med (Maywood). **235**, 40-46

329 Andrikopoulos, S., Blair, A. R., Deluca, N., Fam, B. C. and Proietto, J. (2008) Evaluating the glucose tolerance test in mice. Am J Physiol Endocrinol Metab. **295**, E1323-1332

330 Hermans, M. P., Levy, J. C., Morris, R. J. and Turner, R. C. (1999) Comparison of insulin sensitivity tests across a range of glucose tolerance from normal to diabetes. Diabetologia. **42**, 678-687

331 Mather, K. (2009) Surrogate measures of insulin resistance: of rats, mice, and men. Am J Physiol Endocrinol Metab. **296**, E398-399

332 Qin, S., Rottman, J. B., Myers, P., Kassam, N., Weinblatt, M., Loetscher, M., Koch, A. E., Moser, B. and Mackay, C. R. (1998) The chemokine receptors CXCR3 and CCR5 mark subsets of T cells associated with certain inflammatory reactions. J Clin Invest. **101**, 746-754

333 Kitade, H., Sawamoto, K., Nagashimada, M., Inoue, H., Yamamoto, Y., Sai, Y., Takamura, T., Yamamoto, H., Miyamoto, K., Ginsberg, H. N., Mukaida, N., Kaneko, S. and Ota, T. (2012) CCR5 plays a critical role in obesity-induced adipose tissue inflammation and insulin resistance by regulating both macrophage recruitment and M1/M2 status. Diabetes. **61**, 1680-1690

334 Kanda, H., Tateya, S., Tamori, Y., Kotani, K., Hiasa, K., Kitazawa, R., Kitazawa, S., Miyachi, H., Maeda, S., Egashira, K. and Kasuga, M. (2006) MCP-1 contributes to macrophage infiltration into adipose tissue, insulin resistance, and hepatic steatosis in obesity. J Clin Invest. **116**, 1494-1505

335 Strissel, K. J., DeFuria, J., Shaul, M. E., Bennett, G., Greenberg, A. S. and Obin, M. S. (2010) T-cell recruitment and Th1 polarization in adipose tissue during diet-induced obesity in C57BL/6 mice. Obesity (Silver Spring). **18**, 1918-1925

336 Rocha, V. Z., Folco, E. J., Sukhova, G., Shimizu, K., Gotsman, I., Vernon, A. H. and Libby, P. (2008) Interferon-gamma, a Th1 cytokine, regulates fat inflammation: a role for adaptive immunity in obesity. Circ Res. **103**, 467-476

337 Pedersen, L., Olsen, C. H., Pedersen, B. K. and Hojman, P. (2012) Muscle-derived expression of the chemokine CXCL1 attenuates diet-induced obesity and improves fatty acid oxidation in the muscle. Am J Physiol Endocrinol Metab. **302**, E831-840

338 Porter, S. A., Massaro, J. M., Hoffmann, U., Vasan, R. S., O'Donnel, C. J. and Fox, C. S. (2009) Abdominal subcutaneous adipose tissue: a protective fat depot? Diabetes Care. **32**, 1068-1075

339 Klein, S., Fontana, L., Young, V. L., Coggan, A. R., Kilo, C., Patterson, B. W. and Mohammed, B. S. (2004) Absence of an effect of liposuction on insulin action and risk factors for coronary heart disease. N Engl J Med. **350**, 2549-2557

340 Miyazaki, Y., Mahankali, A., Matsuda, M., Mahankali, S., Hardies, J., Cusi, K., Mandarino, L. J. and DeFronzo, R. A. (2002) Effect of pioglitazone on abdominal fat distribution and insulin sensitivity in type 2 diabetic patients. J Clin Endocrinol Metab. **87**, 2784-2791

341 Tran, T. T., Yamamoto, Y., Gesta, S. and Kahn, C. R. (2008) Beneficial effects of subcutaneous fat transplantation on metabolism. Cell Metab. **7**, 410-420

342 Tamemoto, H., Kadowaki, T., Tobe, K., Yagi, T., Sakura, H., Hayakawa, T., Terauchi, Y., Ueki, K., Kaburagi, Y., Satoh, S. and et al. (1994) Insulin resistance and growth retardation in mice lacking insulin receptor substrate-1. Nature. **372**, 182-186

343 Withers, D. J., Gutierrez, J. S., Towery, H., Burks, D. J., Ren, J. M., Previs, S., Zhang, Y., Bernal, D., Pons, S., Shulman, G. I., Bonner-Weir, S. and White, M. F. (1998) Disruption of IRS-2 causes type 2 diabetes in mice. Nature. **391**, 900-904

344 Uysal, K. T., Wiesbrock, S. M. and Hotamisligil, G. S. (1998) Functional analysis of tumor necrosis factor (TNF) receptors in TNF-alpha-mediated insulin resistance in genetic obesity. Endocrinology. **139**, 4832-4838

345 Amato, R. J., Shingler, W., Naylor, S., Jac, J., Willis, J., Saxena, S., Hernandez-McClain, J. and Harrop, R. (2008) Vaccination of renal cell cancer patients with modified vaccinia ankara delivering tumor antigen 5T4 (TroVax) administered with interleukin 2: a phase II trial. Clin Cancer Res. **14**, 7504-7510